Exploration of the Mechanisms of Adjuvanticity for Toll-like Receptor Agonists

By

Alex C. D. Salyer

Submitted to the Graduate Degree program in Medicinal Chemistry

and the Graduate Faculty of the University of Kansas

in partial fulfillment of the requirements for the degree of

Doctor of Philosophy

Dissertation Committee:

_____   _____

Chairperson (Apurba Dutta)   Co-chairperson (Sunil A. David)

_____   _____

Michael F. Rafferty   Blake R. Peterson

_____

Russel Middaugh

Date defended: 08/25/2017

The Thesis Committee for Alex C. D Salyer certifies

that this is the approved version of the following thesis:

Exploration of the Mechanisms of Adjuvanticity for Toll-like Receptor Agonists

Dissertation Committee:

Chairperson (Apurba Dutta)

Co-chairperson (Sunil A. David)

Michael F. Rafferty

Blake R. Peterson

Russel Middaugh

Date approved: 08/30/2017

Abstract

Small-molecule agonists have been identified for Toll-like Receptors (TLR) 2, TLR4, TLR7 and TLR8 thus far, and chemotypes other than those of canonical ligands are yet to be explored for a number of innate immune receptors. The discovery of novel immunostimulatory molecules would enhance the repertoire of tools available for interrogating innate immune effector mechanisms, and provide additional venues for vaccine adjuvant development. It is with this in mind that we aimed to identify novel immunostimulatory compounds by high-throughput screening, characterize transcriptomal 'signatures' of innate immune stimulation and explore mechanisms of adjuvanticity for TLR2, TLR2/7 and TLR8 agonists.

A multiplexed, reporter gene-based high-throughput assay capable of detecting agonists of TLR2, TLR3, TLR4, TLR5, TLR7, TLR8, TLR9, nucleotide-binding oligomerization domain-like receptors (NOD) 1 and NOD2 was utilized in screening 123,943 compounds, in which amphotericin B (AmpB) and nystatin were identified as prominent hits. The polyene antifungal agents act as TLR2- and TLR4-agonists. The TLR4-stimulatory activity of AmpB was similar to that of monophosphoryl lipid A, suggestive of TRIF-biased signaling. The adjuvantic activity of AmpB, at a dose of 100 micrograms, was comparable to several other candidate adjuvants in rabbit models of immunization. (Chapter 2)

We sought to identify transcriptomal signatures of innate immune stimulating molecules using next-generation RNA sequencing with the goal of being able to utilize such signatures in identifying novel immunostimulatory compounds with adjuvantic activity. We observed that the

CC family of chemokines, particularly CC chemokines 1, 2, 3, 4, 7, 8, 17, 18, 20, and 23, were broadly upregulated by most TLR and nucleotide-binding domain and leucine-rich repeat–containing receptors (NLR) stimuli, while the CXC chemokine family appeared to show distinctions in upregulation. Extracellular receptors such as TLR2, TLR4 and TLR5 induced the transcription of CXC chemokines including CXCL5, CXCL6 and CXCL8, whereas intracellular receptors such as TLR7 and TLR8 upregulated CXC chemokines 11 and 12. A comparison of a variety of TLR agonists in a standardized rabbit immunization model indicated prominent adjuvantic activity for TLR2 agonists. Strong chemokine induction by TLR2 agonists was observed in human peripheral blood mononuclear cells. In addition, human foreskin fibroblasts stimulated with TLR2/6 agonists, but not TLR1/2 agonists resulted in chemokine production, which was consistent with strong expression of TLR2 and TLR6, but not of TLR1, in fibroblasts. TLR2/6 stimulated fibroblasts demonstrated functional chemotactic responses to human T cell and natural killer cells subsets. (Chapter 3)

We hypothesized that an ESAT-6-based subunit vaccine adjuvanted with a TLR2/7 hybrid would induce balanced T helper (Th) 1/Th2 responses capable of conferring protection against *M. tuberculosis*. We therefore covalently linked a potent TLR2 agonist with a dual TLR7/8 agonist, and observed that the resulting TLR2/7 hybrid molecules remained active, though less potent, against TLR2 and TLR7. The TLR2/7 hybrid was equipotent to the two individual TLR agonists in a standardized rabbit immunization model, but induced higher 'quality' antibodies as measured by surface plasmon resonance. Linear epitope mapping revealed that the hybrid induced immunoreactivity to more contiguous epitopes in a model antigen. The hybrid molecule was able

to induce increases in ESAT-6-specific interferon-γ spot-forming units in the lungs of mice, and reduce the mycobacterial burden in the lungs following *M. tuberculosis* challenge. (Chapter 4)

Part-structures of the 2-aminobenzimidazole scaffold were examined with a view to identifying structural requisites corresponding to the smallest possible fragment of the benzimidazole core that would allow for retention of TLR8-agonistic activity. TLR8-specific agonistic activity was retained in 1-pentyl-4-phenyl-1*H*-imidazol-2-amine. The crystal structure of this compound bound to TLR8 ectodomain displayed binding interactions that are common to other TLR8 agonists. This compound showed markedly attenuated proinflammatory properties in *ex vivo* human blood models. Structure-activity relationship (SAR) studies revealed that 4-(2-(benzyloxy)phenyl)-1-pentyl-1*H*-imidazol-2-amine inhibited TLR signaling in a variety of TLR reporter cell lines, as well as in pharmacologically-relevant human blood model systems. A kinase screen of this compound showed relative specificity for calmodulin kinases. (Chapter 5)

The effects of TLR8 agonists on innate immune function suggest that these compounds could potentially be useful as vaccine adjuvants in neonatal vaccines. We examined how TLR8 agonists influence processing of soluble antigens by antigen presenting cells. TLR8-active compounds were unique in inducing pyroptosis-like death in monocytes, leading to the formation of $CD14^+$ extracellular vesicles (ECV) of 100-400 nm diameter. ECV formation was dependent on myeloid differentiation primary response gene 88 (MyD88), interleukin-1 receptor-associated kinases (IRAK) 1 and 4, and p38 mitogen-activated protein kinase (MAPK). The monocyte-derived ECVs contain near-intact soluble antigens, and stimulate antigen-specific recall responses in autologous

CD4$^+$ T lymphocytes. The formation of antigen-loaded, monocyte-derived ECVs may be a distinct mechanism underlying the adjuvantic activities of TLR8 agonists. (Chapter 6)

The results presented here highlight the applicability of high-throughput screens for the identification of novel innate immune stimuli, and identified transcriptomal profiles to aid in determining adjuvanticity of new compounds, as well as aiding in target identification. The insight gained into mechanisms of adjuvanticity for the TLR2, TLR2/7, and TLR8 agonists highlights the utility of TLR agonists as vaccine adjuvants, and justifies the continued study of small-molecule innate immune stimuli for applications in vaccines.

Acknowledgements

There have been many people who have helped and guided me along my studies as a graduate student who I am immensely grateful for. First, I would like to thank my advisor, Prof. Sunil David. None of this would have been possible without his wisdom and guidance. His never ending passion for science and enthusiasm for learning was an inspiration for which I cannot thank him enough. I am also thankful for all of my lab mates who never fell short of finding ways to brighten my days and encourage me over the last several years. While they are too numerous to mention all of them, I would like to thank Dr. Nikunj Shukla and Dr. Euna Yoo for their mentorship and friendship throughout their time in the lab.

Next, I would like to thank my committee, Dr. Apurba Dutta, Dr. Blake Peterson, Dr. Michael Rafferty, and Dr. Russ Middaugh for all of their help and the time they put into helping me prepare for the next steps in my life.

I would not be where I am today without the never-ending love and support of my friends and family. I want to specifically thank Olivia Recht, Brian Kress, and Brad Kress for always being there when I needed them. My family has always encouraged me to pursue my dreams and helped in more ways than they realize to get me here, and I cannot find the words to express how thankful I am for them. For the sake of brevity, I will only mention my dad Chris, mom Alisa, stepdad Devin, and sister Mackenzie.

Alex Salyer

08/01/2017

Table of Contents

Abbreviations

AmpB	Amphotericin B
APC	Antigen-presenting Cell
BCG	Bacille Calmette-Guérin
CAMK	Calmodulin-dependent Protein Kinase
CCR	Chemokine Receptor
cDC	Conventional Dendritic Cell
CLR	C-type Lectin Receptor
CMV	Cytomegalovirus
CpG	Deoxycytidyl-deoxyguanosine
CXCL	Chemokine Ligand
DC	Dendritic Cell
DDA	Dimethyldioctadecyl-ammonium bromide
DIPEA	Diisopropylethylamine
DMF	Dimethylformamide
DMSO	Dimethylsulfoxide
dsRNA	Double Stranded RNA
EC_{50}	Half Maximal Effective Concentration
ECV	Extracellular Vesicle
ELISA	Enzyme-linked Immunosorbent Assay
ERK	Extracellular Signal–regulated Kinases
ESI	Electrospray Ionization
FDA	Food And Drug Administration
FSC	Forward Scatter
HEK	Human Embryonic Kidney
HFF	Human Foreskin Fibroblast
HLA	Human Leukocyte Antigen
hPBMC	Human Peripheral Blood Mononuclear Cell
IFN	Interferon
Ig	Immunoglobulin
IL	Interleukin
IRAK	Interleukin-1 Receptor-Associated Kinase
IRF	IFN Regulatory Factor
LC	Liquid Chromatography
LPS	Lipopolysaccharide
LRR	Leucine-Rich Repeats
LTA	Lipoteichoic Acid
MAPK	Mitogen Activated Protein Kinase
MCP	Monocyte Chemoattractant Protein
MHC	Major Histocompatibility Complex
MIP	Macrophage Inflammatory Protein

MPL	Monophosphoryl Lipid A
MS	Mass Spectroscopy
MyD88	Myeloid Differentiation Primary Response Gene 88
NALP	NACHT, LRR And PYD Domains-containing Protein
NBS	*N*-Bromosuccinimide
NF-kB	Nuclear Factor-κB
NIAID	National Institute Of Allergy and Infectious Disease
NK	Natural Killer
NLR	NOD-like Receptor
NMR	Nuclear Magnetic Resonance
NOD	Nucleotide Oligomerization Domain
ODN	Oligodeoxynucleotides
PAMP	Pathogen-associated Molecular Pattern
PBS	Phosphate-buffered Saline
pDC	Plasmacytoid Dendritic Cell
PMN	Polymorphonuclear leukocyte
pp65	Cytomegalovirus Protein Pp65
PRR	Pattern Recognition Receptor
RIG	Retinoic Acid Inducible Gene
RLR	RIG-I-like Receptor
sAP	Secreted Alkaline Phosphatase
SAR	Structure-activity Relationship
SSC	Side Scatter
TB	Tuberculosis
Th1	T Helper 1
Th17	T Helper 17
Th2	T Helper 2
TIR	Toll/IL-1 Receptor
TIRAP	MAL/TIR Domain-containing Adaptor Protein
TLR	Toll-like Receptor
TNF	Tumor Necrosis Factor
TRIF	TIR-Domain-containing Adapter-Inducing Interferon-B
TrkA	Tropomyosin Receptor Kinase A
TSSK3	Testis-specific Serine Kinase-3

Chapter 1.

Introduction

Chapter 1.1 Pattern Recognition Receptors of the Innate Immune System

The immune system is an incredibly intricate machine capable of discriminating subtle differences in foreign molecules, and then marshalling effector mechanisms to eliminate invading pathogens, with minimal damage to the host. Many of the initial responses to colonization or invasion by pathogens, or to the presence of non-self molecules are derived from the innate wing of the immune system. The innate immune system is characterized in a broad sense as being rapidly activated, not antigen specific, and without memory. In the absence of memory, the innate immune system relies on germline-encoded pattern recognition receptors (PRRs) to identify conserved microbial patterns, referred to as pathogen-associated molecular patterns (PAMPs), that are common across diverse families of microbial and viral pathogens. The innate immune system not only acts as an early defense against invading pathogens, but also serves to direct the subsequent adaptive immune responses, which are highly specific and endowed with long-term memory.

There are four major families of PRRs in the human: the Toll-like receptors (TLRs), nucleotide-binding oligomerization domain (NOD)-like receptors (NLRs), RIG-like receptors (RLRs), and C-type lectin receptors (CLRs).[1] PRRs serve as sentinels for the immune system against both extracellular and intracellular pathogens and, as such, these receptors are distributed throughout the cell, including the cell surface, within the cytosol, and within the endosomal pathway. The biology of the TLRs will be discussed below.

There are 10 functional TLRs in humans. All of the TLRs are approximately 90 kDa transmembrane proteins that are located on the cell plasma membrane, or within endosomal vesicles.[2] Structurally, TLRs contain a Toll-interleukin receptor (TIR) domain for signal

transduction, a single alpha helix spanning the membrane, and an extracellular leucine-rich repeat (LRR) domain for ligand binding. The global structural similarities notwithstanding, the TLRs can be divided into 5 subfamilies based on sequence similarity: TLR2, TLR3, TLR4, TLR5, and TLR9 subfamilies.[2] The subsequent chapters will focus on the two largest of the subfamilies: the TLR2 and TLR9 subfamilies.

Chapter 1.1.1 TLR2 Subfamily

The TLR2 subfamily is the largest of the subfamilies and contains TLRs -1, -2, -6, and -10. All four of the members are expressed on the cell surface and detect extracellular PAMPs. They share approximately 60% sequence identity overall, and almost 90% sequence identity in the TIR domains.[3] This family is unique among the TLRs in that TLR2 can heterodimerize with TLR1 and TLR6, while all of the other TLRs are known only to signal through homodimerization.[4] TLR2 utilizes two distinct co-receptors depending on the TLR binding partner; the TLR1/2 heterodimer utilizes CD14, while the TLR2/6 heterodimer functions with the transmembrane protein CD36 for cargo and receptor internalization.[5] Despite the differences in co-receptors, the TLR1/2 and TLR2/6 complexes signal through the same adaptor molecules following ligand recognition. Upon ligand binding, the adaptor protein myeloid differentiation primary response gene 88 (MyD88) is recruited to the TIR domains of the TLRs, and ultimately results in signal transduction to the transcription factor nuclear factor kappa-light-chain-enhancer of activated B cells (NF-κB), which leads to innate immune activation. The TLR2 family additionally recruits the adaptor protein MAL/TIR domain-containing adaptor protein (TIRAP), which is unique to the TLR2 and TLR4 subfamilies, and is critical to MyD88-independent signal transduction to NF-κB.[6-7]

The TLR2 family has evolved to sense a wide variety of PAMPs commonly associated with cell-wall-derived lipopeptides from numerous gram-negative and gram-positive bacteria, and also mycoplasma.[8] TLR1/2 heterodimers sense triacylated species common in gram-negative bacteria and synthetic molecules such as PAM_3CSK_4,[9-10] while TLR2/6 heterodimers recognize diacylated lipopeptides found in gram-positive bacteria, mycoplasmas and synthetic molecules such as PAM_2CSK_4.[4]

Despite the diversity in TLR2 binding partners, the downstream adaptive immune responses are remarkably similar within a given animal model. It is to be noted, however, that the mouse, which is the primary animal model used in immunology, appears to diverge from the human with respect to adaptive immune responses following TLR2 stimulation, and has left the nature of T helper (Th) cell polarization up for debate. Investigators who have utilized the mouse as a model system tend identify TLR2 agonists as biasing towards humoral immunity through Th2 polarization via the identification of Th2 markers such as interleukin (IL)-4, IL-5, and the mouse antibody isotype IgG1.[11-13] Additionally, the immunological outcomes of TLR2 stimulation in mice further point to Th2 driven immunity by exacerbation of *Leishmania major* infection, which is thought to be controlled through Th1 driven cellular immunity, following immunization with the TLR2/6 adjuvant PAM_2CSK_4, while the same adjuvant leads to protection from Th2 controlled *Brugia malayi* infection.[12]

Many others have found the opposite in human responses to TLR2 agonists, and tend to associate TLR2 stimulation with Th1 polarization. They have demonstrated the presence of the Th1 markers IL-2, IL-12, and interferon (IFN)-γ in human PBMCs following TLR2 stimulation, and an absence

of IL-4.[14-17] This builds upon previously reported IL-12 induction from isolated human dendritic cells stimulated with TLR2 agonists.[18] While there is not yet clarity in defining TLR2 agonists by T helper polarization, this remains an active area of research and will be discussed in greater detail in chapters 3 and 4.

Chapter 1.1.2 TLR9 Subfamily

The TLR9 subfamily is composed of the endosomal receptors TLR7, -8, and -9. Within this family, TLR7 and TLR8 are most closely related with 42% identity and 73% similarity in their amino acid sequences.[19-20] The TLR9 subfamily shares many of the signaling molecules with the TLR2 family, including the co-receptor CD14 and the adaptor protein MyD88,[21] but differs significantly in ligand specificity and adaptive immune polarization. The TLR9 subfamily is further distinguished from the TLR2 family through additional signal transduction to the Interferon Regulatory Factors (IRFs), which exert transcription control of Type I and Type II IFNs.

All three members of this family recognize various forms of genetic material; TLR7 and TLR8 both recognize single stranded RNA, while TLR9 senses unmethylated deoxycytidyl-deoxyguanosine (CpG) motifs in DNA.[2] Additionally, small molecules targeting TLR7 and -8 have been identified by many research groups, including ours, and will be given significant attention in chapters 4-6.[22-29] While TLR7 and -8 share similarities in ligand recognition, they differ substantially in subsequent cytokine responses. TLR7 stimulation results in activation of the transcription factors IRF3 and IRF7, which lead to the secretion of the Type I interferons IFN-β and IFN-α, respectively.[30] TLR8 on the other, hand drives robust Type II interferon responses, namely IFN-γ, mediated through IRF1.[31]

Small molecule agonists of TLR9 have remained more elusive and there are currently no published small molecule TLR9 agonists. Despite the lack of small molecule TLR9 agonists, three broad classes of TLR9 active CpG DNAs have been identified based on distinct cellular activation and cytokine induction profiles.[32-33] Class A CpG oligodeoxynucleotides (ODN) elicit strong natural killer (NK) cell and plasmacytoid dendritic cell (pDC) responses characterized by the induction of Type I interferons, while Class B CpG ODNs are potent activators of B lymphocytes. The final class of CpG ODNs described are the Class C ODNs.[34-35] Members of this class share the qualities of both Class A and B ODNs by eliciting both B cell activation and pDC-mediated Type I IFN production.[32]

Chapter 1.2 TLR Cellular Expression

As TLRs are sensors for various pathogens and their engagement serves to catalyze subsequent innate and adaptive immune responses, they have broad expression in both hematopoietic and nonhematopoietic cell lineages. Antigen presenting cells (APC) such as monocytes, macrophages, and dendritic cells (DC) show broad, but not identical, TLR expression patterns. Monocytes and macrophages, in particular, show expression of many of the TLRs, but are not homogeneous in composition, with tissue specific expression of the various TLRs.[2] DCs on the other hand have very specific TLR expression patterns, with pDC exclusively expressing TLR7 and -9, while the two major circulating conventional DC (cDC) populations, $CD1c^+$ and $CD141^+$, express TLR1, -2, -3, -4, -5, -6, and -8, based on western blotting and PCR.[36-37] However, there is evidence based on costimulatory marker upregulation that both populations of cDCs respond to TLR7 agonists, while only the $CD1c^+$ respond to TLR8 agonists.[38-39] Lymphocytic populations also bear TLRs, with NK cells expressing TLR2, -3, -4, -5, -7, and -9 [40-41] and B cells expressing TLR1, -2, -4, -6,

-7, and -9.[42] Lastly, T lymphocytes, including both CD4^{+} and CD8^{+}, show expression of TLR3, -4, -7, and -9.[43]

Cells of non-hematopoietic lineages also express TLRs. While not as well studied as leukocytes, epithelial cells express TLRs and likely contribute to innate immune responses. Expression of the TLRs varies dramatically in the mucosal membranes and is detected at both the mRNA and protein levels.[44] The airway epithelium is perhaps the best studied of the epithelial cell types, and show strong expression of both TLR2 and TLR4.[45-46] Stimulation of TLRs in airway epithelial cells enables engagement of innate immune responses to invading pathogens by directing the expression of mucin glycoproteins, a major component of mucus, well as human beta-defensins-1 and -4.[47-48] Epithelial cell TLRs can further amplify the early immune responses through the secretion of many inflammatory mediators and chemokines including tumor necrosis factor-alpha (TNF-α), IL-5, IL-6, IL-8, macrophage inflammatory protein (MIP)-1α, and MIP-1β. This, in turn, leads to the recruitment and influx of leukocytes such as DCs, macrophages, monocytes, NK cells, and polymorphonuclear cells (PMNs), enabling the clearance of pathogens and facilitating subsequent pathogen-specific adaptive immune responses.[49-50] Epithelial TLRs, especially TLR2 and TLR4, are also believed to play a critical role in the induction and maintenance of asthma and allergy through similar mechanisms as the pathogen-specific responses, mentioned above, but with Th2 skewed responses, leading to disease.[48, 51]

Chapter 1.3 Vaccines and Vaccine Adjuvants

Vaccines have proven to be one of the greatest tools available in medicine to prevent infectious diseases.[52-53] Vaccines have several important functions within the healthcare setting. First, they

protect healthy individuals, including those who do not have fully competent immune systems, from disease, but also protect those who are unable to receive vaccinations through the process of "herd immunity". Herd immunity is achieved when a majority of the population, usually between 75-94%, depending on the pathogen, have immunity and prevent colonization of the pathogen within the population, which, in turn, protects individuals that are unable to acquire immunity against that pathogen.[54]

The practice of vaccination or inoculation was first shown to be effective by Edward Jenner in 1798 when he inoculated an 8-year-old boy with pus derived from a cowpox lesion, and then infected the boy with the smallpox virus. The boy was ultimately protected from the smallpox virus. Vaccines now represent a twenty-four-billion-dollar market covering a wide range of pathogens. However, there is still a great unmet need for vaccines to a number of pathogens, such as malaria, tuberculosis, HIV, and several flaviviruses, as well as the need for improvement of existing vaccines such as the annual influenza vaccine and the acellular pertussis vaccine that remain suboptimal.[55-56]

Chapter 1.3.1 Live Attenuated and Inactivated Vaccines

Early vaccines were initially derived from whole inactivated or live attenuated pathogens. One of the best success stories utilizing both of these strategies has been the near-eradication of the poliovirus using the live attenuated oral poliovirus vaccine and the inactivated poliovirus vaccine.[57] The oral poliovirus vaccine contains all three serotypes of poliovirus that have been attenuated by serial passage though African green monkey kidney cells, which resulted in significantly reduced pathogenicity.[58] Following administration of this replication-competent

vaccine, the patient develops a sub-clinical infection in the mucosal membranes, allowing the host immune system to develop natural humoral and mucosal immunity to the virus.[59] As such, this vaccine is widely used in the developing world due to low cost of manufacturing, ease of oral administration, and the strong induction of humoral and mucosal immunity. The live-attenuated polio vaccine is associated with rare vaccine-associated diseases, such as vaccine-associated paralytic poliomyelitis, which is clinically indistinguishable from the poliomyelitis caused by wild-type virus.[60] Most industrialized countries, including the United States, have adopted the inactivated poliovirus vaccine, which differs from the attenuated oral vaccine in that the three poliovirus serotypes are inactivated by formalin. While the inactivated poliovirus vaccine is significantly safer than the attenuated vaccine, the inactivated vaccine does suffer from reduced efficacy at eliciting protective immunity in the lower intestinal tract, relative to the attenuated vaccine, and does not prevent intestinal shedding of the virus. The inactivated vaccines does however provide protection equal to that of the oral vaccine in pharyngeal membranes.[61]

Chapter 1.3.2 Subunit Vaccines and Adjuvants

The tradeoffs between safety and efficacy in the two types of poliovirus vaccines are also relevant in several other live-attenuated vaccines. Current trends in vaccine development have focused on use of highly purified protein antigens, and such vaccines are termed subunit vaccines. Examples are Hepatitis B, *Haemophilus influenza* type B, pertussis, and human papillomavirus vaccines. Although exceedingly safe, the highly purified antigens are frequently poorly immunogenic, and rely heavily on adjuvants to enhance immunogenicity and steer adaptive immune responses to the antigen.[62-63].

The role of adjuvants in subunit vaccines is pivotal. Once referred to as "immunologist's dirty little secret" by Charles Janeway,[64] adjuvants now represent a major area of inquiry in immunology and vaccinology. Only a small number of adjuvants are currently approved by the FDA. The most commonly used vaccine adjuvants to date are the aluminum salts (commonly referred to as 'alum'), which can be found in the vaccines such as those against diphtheria, hepatitis B, pertussis, and *Haemophilus influenza* type B.[62] The adjuvantic activity of the aluminum salts were originally described by Glenny and coworkers in 1926, in which they suggested antigen alone was too rapidly eliminated to induce robust immune responses, and required precipitation with alum in order to slow the rate of elimination of antigen.[65] Many groups have built upon the work of Glenny and have expanded the understanding of the mechanisms of action for the aluminum salts, which can be summarized as increasing antigen uptake by DCs, recruiting leukocytes to the injection site, activating the innate immune system through the indirect engagement of the NLPR3 inflammasome.[66] Alum is believed to indirectly activate the inflammasome by inducing necrosis and causing the release of uric acid, a danger signal. However, there are currently no known receptors that are engaged directly by alum.[67-68] Additionally, Wang and coworkers observed that alum stimulated a population of Grl^+, $IL-4^+$ eosinophils in the spleens of mice that primed B cells leading to Th2 polarization of the adaptive immune responses.[69]

While alum-adjuvanted vaccines are generally safe and well tolerated with over one billion doses administered world-wide,[70] they are not without limitations. Aluminum salt-adjuvanted vaccines polarize Th2 immunity, providing limited benefit in vaccines targeting intracellular pathogens that rely on either Th1 or Th17 driven immunity for protection and clearance. This was highlighted by Warfel *et. al.* in comparing the whole-cell pertussis vaccine to the alum adjuvanted acellular

pertussis vaccine in baboons.[71] In this study the authors demonstrate that baboons vaccinated with acellular, alum adjuvanted Infanrix® (GlaxoSmithKline) were able to prevent major disease upon challenge with *B. pertussis* in a similar manner to the whole-cell vaccine, but failed to prevent either colonization of the bacterium or prevent transmission to naïve animals. They also noted that both natural infections and vaccinations with the whole-cell vaccine resulted in memory Th1 and Th17 cells, while the acellular vaccine yielded Th1 and Th2 responses. The acellular pertussis vaccine was able to protect animals from major disease, but it showed potential limitations in enabling "herd immunity".[71]

The more recent FDA-approved vaccine adjuvants have focused more closely on biasing adaptive immune responses towards Th1 responses. AS04, the first adjuvant to gain approval against human papilloma virus types 16 and 18, builds upon the adjuvantic activity of alum immunogenicity through the absorption of the TLR4 agonist monophosphoryl lipid A (MPLA) to alum.[72-73] Didierlaurent and colleagues demonstrated that the adjuvantic activity of AS04 was driven primarily by the TLR4 component and resulted in enhancement of DC and monocyte antigen uptake and cytokine secretion both at the site of injection and draining lymph node, while the alum component of AS04 served to prolong the APC stimulation observed at the injection site.[74] They also demonstrated that AS04 does not directly stimulate T cells through either CD69 upregulation or IFN-γ secretion, but only appeared to drive APC activation with strong expression of TNF-α, IL-6, and caspase 1-dependent IL-1β.[74]

The latest generation of adjuvants to gain approval are the oil-in-water emulsions MF59 (squalene in water) and AS03 (squalene and α-tocopherol in water) from Novartis and GlaxoSmithKline,

respectively. Despite being referred to as antigen delivery systems, these adjuvant systems are able to modulate immune responses. Early work on establishing mechanisms of action for these adjuvant systems demonstrated that neither of the systems worked through the formation of micro-depots, but rather through leukocyte recruitment to the site of injection and the draining lymph nodes.[75-76] The oil-in-water emulsions differ from many TLR agonists, such as MPLA in AS04, in that they act by inducing chemokines, such as CCL2 and CCL3, in APCs, which increase the number of leukocytes that migrate to the site of injection and increase antigen internalization. However, they do not induce strong co-stimulatory molecule upregulation in APCs or activate T cells directly.[77-79] Within the leukocyte populations that respond to these adjuvants, monocytes serve as the primary antigen-internalizing cells at the site of injection, and also appear to transport the antigen to draining lymph nodes for B cells and DC presentation of the antigen to cognate T cells.[78-79]

The adjuvants currently under development are generally comprised of ligands of novel targets such as the TLRs. AS04 contains the only TLR ligand currently approved by the FDA. However, there are several pure TLR agonists in clinical trials and many more, including some of compounds described in this work, in preclinical development. Some of the compounds in current clinical trials include TLR9 active CpG DNA (phase III), TLR5/NLRC4 ligand flagellin (phase II), and TLR4 active glucopyranosyl lipid A (phase I).[80] Given the important roles that TLRs occupy in bridging the innate and adaptive immune systems, targeting these innate immune receptors have been a fruitful area of research in the development of novel vaccine adjuvants. Depending on the TLR engaged, downstream responses include leukocyte recruitment, APC activation and maturation, as

well as lymphocyte activation. More detail on the specifics of TLR-mediated immune activation will be provided in the subsequent chapters.

The premise of the work presented here is to advance the knowledge of TLR mechanisms of adjuvantic action across the TLR2 and TLR9 subfamilies of receptors, and establish robust assays for assessing innate immune stimulation. Chapters 2 and 3 are dedicated to high-throughput screening for novel TLR stimuli and transcriptional profiling of established TLR ligands to enable the identification of patterns characteristic of innate immune stimulation. The subsequent chapters (4-6) describe our efforts to evaluate the mechanisms of TLR adjuvanticity.

Chapter 2.

Identification of Amphotericin B as a TLR2/4 Agonist in a Poly-TLR/NLR High-throughput Screening
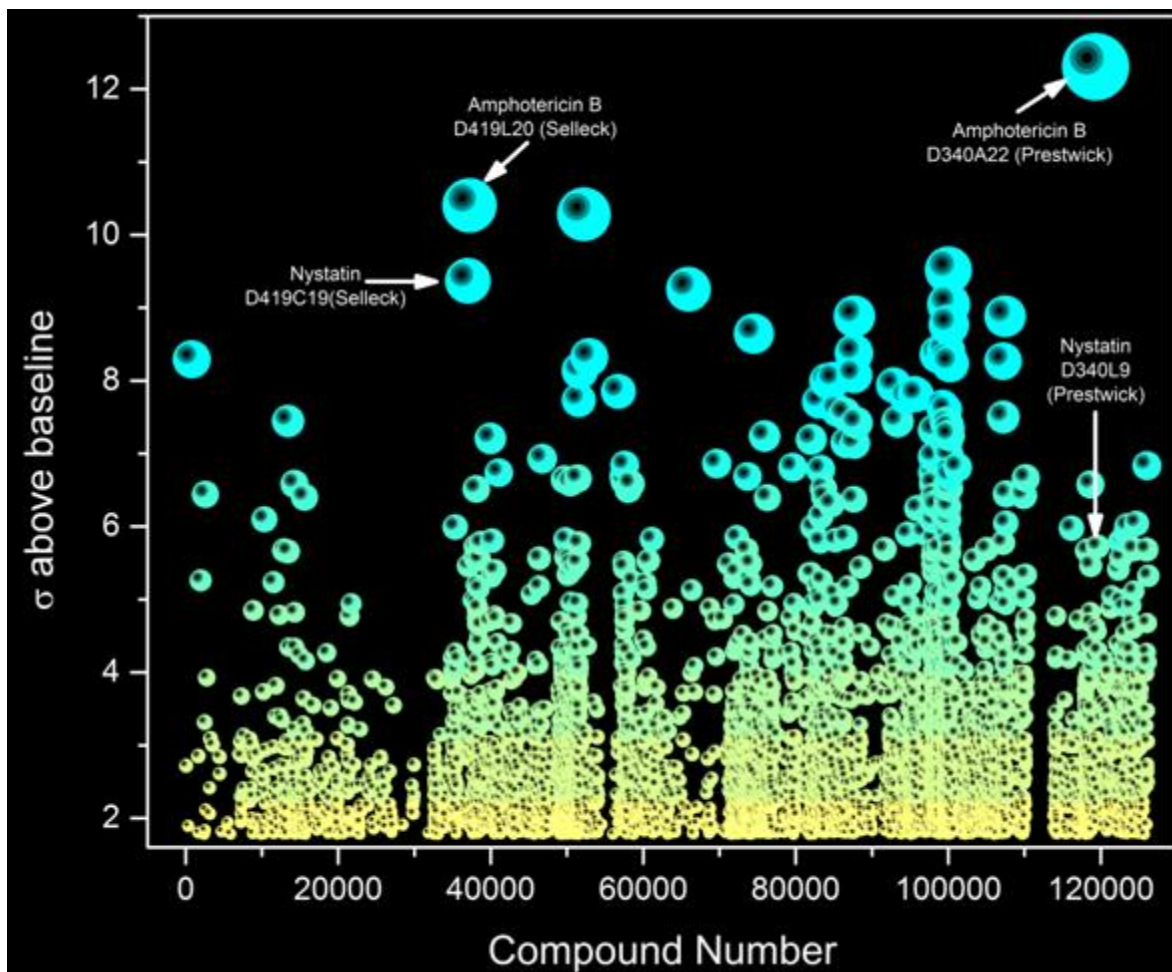
2.1 Introduction

We set out to identify novel innate immune-active chemical entities and expand the repertoire of potential vaccine adjuvants to combat the large number of devastating infectious diseases for which no effective vaccines currently exist. The major causes of mortality in pediatric populations in the developing world are attributable to lower respiratory infections, infectious diarrhea, malaria and measles,[81] all of which are preventable illnesses. However, a significant impediment in the effective delivery of vaccines in the developing world is the requirement for most vaccines of multiple, booster doses for successful immunization. Methods of safely enhancing immunogenicity of vaccines would be an important step toward realizing the bold,[82-83] but faltering[84] vision of the Children's Vaccine Initiative: an affordable, heat-stable, orally administered, multiple-antigen, single immunization to be given at birth. As mentioned in Chapter 1, in contrast to older vaccines which utilized inactivated whole organisms or attenuated live vaccines,[85-86] there is an increasing emphasis in contemporary vaccines on the use of subunit vaccines which have the distinct advantages of ease of production, quality control, and safety; however, such subunit antigens are largely soluble proteins and tend to be poorly immunogenic, necessitating the use of adjuvants to induce robust immune responses.

Our focus on the discovery and development of safe and effective vaccine adjuvants has served as an impetus for a detailed exploration of structure-activity relationships (SAR) in a variety of innate immune stimuli, including small molecule agonists of TLR2,[87-89] TLR7,[28, 90-97] TLR8,[25-26, 97-100] NOD1,[101] as well as C-C chemokine receptor type 1 (CCR1).[102] Other than canonical ligands or derivatives thereof, defined small molecule agonists are yet to be discovered for a large number of PRRs such as TLR3 and TLR9, and it was of interest to us to embark on high-throughput screens

with a view to identifying novel immunostimulatory chemotypes. Desiring a strategy that would permit the identification of immunostimulatory molecular classes acting on a very broad range of PRRs, we designed and evaluated a multiplexed, reporter gene-based high-throughput assay. Among the most prominent of 'hits' in screening 123,943 compounds were the polyene antifungal agents amphotericin B (AmpB) and nystatin. Deconvolution and dose-response profiles of the polyenes demonstrated TLR2- and TLR4-agonistic activity. Cytokine and chemokine induction profiles of AmpB closely resembled that of MPLA, suggesting a Toll–interleukin-1 receptor domain–containing adaptor inducing interferon-β (TRIF)-biased signaling. AmpB as an adjuvant was comparable to several other candidate adjuvants in rabbit models of immunization. These results point to its potential applicability as an adjuvant for human vaccines.

2.2 Results and Discussion

Small-molecule agonists have been identified for TLR7,[90-91, 96, 103-111] TLR8,[26, 97, 99-100, 112-113] TLR4,[114-117] and TLR2.[118-119] Chemotypes representing structural families other than those of canonical ligands are yet to be explored for a number of TLRs such as TLR3, TLR5 and TLR9, as well as other PRRs. The discovery of novel immunostimulatory molecules of defined receptor specificities would enhance the repertoire of tools available for interrogating innate immune effector mechanisms, and provide additional venues for vaccine adjuvant development. Our primary goal was, therefore, to identify novel PRR agonists. We envisioned that an efficient strategy would be to design and implement an assay that would permit the identification of immunostimulatory molecular classes acting on a very broad range of PRRs and, having cast a wide net, as it were, to then deconvolute signals and assign receptor specificities.

We tested this premise by first examining the responses of a human monocyte-derived THP-1 reporter cell line; similar constructs have been successfully utilized to identify agonists of TLR4.[114, 116] These cells responded robustly to TLR2 and TLR4, and feebly to TLR5, TLR8, NOD1 and NOD2 stimuli; agonists of TLR3, TLR7 and TLR9, however, failed to elicit any response (Fig. 1).
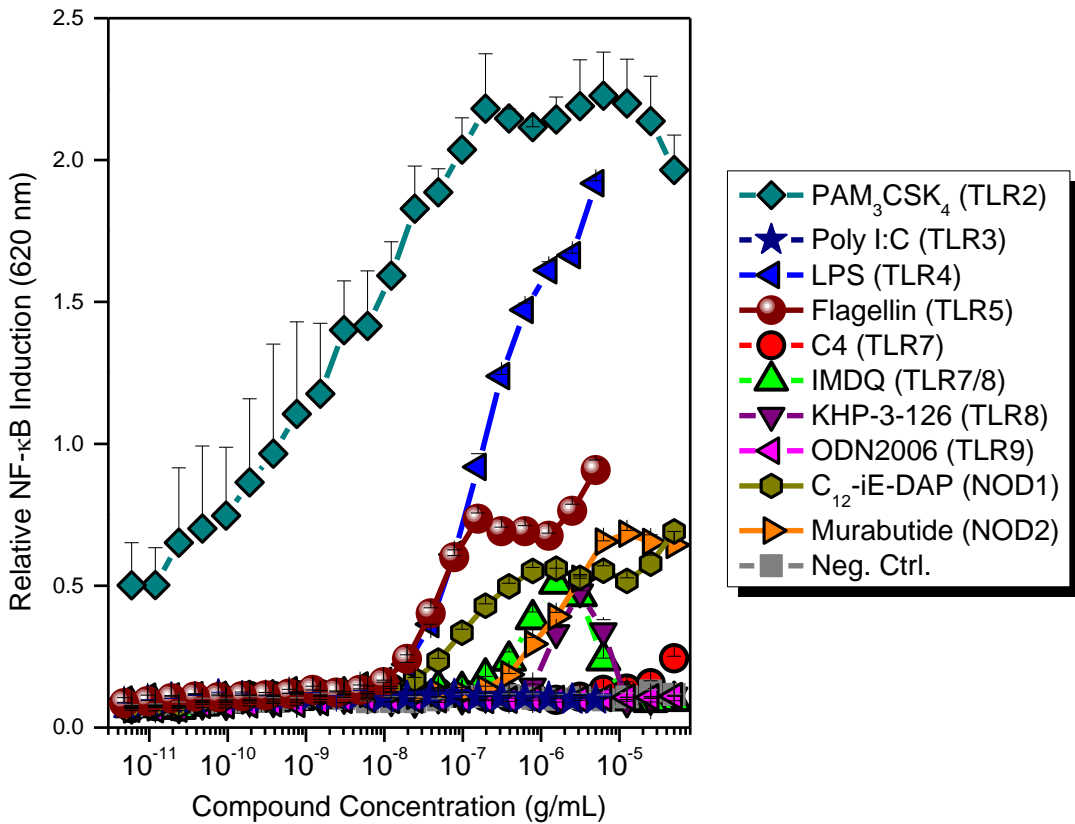
Figure 1. Responses of THP1-Blue™ NF-κB reporter cells to various TLR and NLR agonists.
Dose-response profiles indicate strong responses to PAM$_3$CSK$_4$ (TLR2 agonist) and LPS (TLR4 agonist), and the absence of responsiveness to Poly I:C (TLR3 agonist), C4 (TLR7 agonist), and ODN2006 (TLR9 agonist). Attenuated responses were observed for flagellin (TLR5 agonist), KHP-3-126 (TLR8 agonist), C$_{12}$-iE-DAP (NOD1 agonist) and Murabutide (NOD2 agonist).

We therefore set out to develop a 'Universal Reporter' cell line by constructing hybridomas derived from the fusion of CD14$^+$ primary human monocytes with human embryonic kidney cells (HEK) expressing only the NF-κB-inducible secreted embryonic alkaline phosphatase (sAP) reporter gene (HEK-Blue™ Null cells).[102] Although we were able to isolate, expand and characterize the ploidy of the heterokaryons, these cells were unstable, rapidly regressing back to an embryonic, CD14$^-$ phenotype (data not shown).

We reasoned that multiplexing (combining) individual reporter cell lines (HEK2, HEK3, HEK4, HEK5, HEK7, HEK8, HEK9, NOD1, NOD2 and HEK-Null) would also achieve our objective of simultaneously detecting signals from a wide range of PRRs. Utilizing this multiplexing approach, we conducted a pilot high-throughput screen of 34,848 compounds (Fig. 2A). Z' factors[120] were optimized by varying several parameters (relative proportion of each reporter cell line, total cell density per well, incubation period, liquid handling protocols and plating methods). Responses in this assay were first characterized using both a 'Master Mix' (mixture of individual ligands, Fig. 3), as well as individual stimuli (a metric for deconvolution) in each of the ninety-nine test plates (Fig. 2B). Although excellent Z' values were observed to individual stimuli (Fig. 2C), the relatively high baselines in unstimulated control wells (median: 1.5 AU, Fig. 2C), necessitated a cutoff value of 2.0 AU, which could potentially limit the dynamic range of the assay and possibly compromise the detection of weak signals.

Figure 2. Pilot HTS Screen.

A. *Composite heat map of 99 384-well plates used for the pilot screen using the full complement of 10 multiplexed reporter cell lines.*

**B**. *Heat map of Plate 39 showing the organization of controls in the first two columns. Wells designated 'N' correspond to negative controls. Wells 1-11 correspond, respectively, to PAM$_2$CSK$_4$, Poly(I:C), LPS, MPLA, Flagellin, C4 (TLR7 agonist), IMDQ (Dual TLR7/8 agonist), KHP-3-126 (TLR8 agonist), ODN-2006, C$_{12}$-iE-DAP, and Murabutide at 5 µg/mL. Well 12 corresponds to a 'Master-Mix' combining all stimuli at 0.45 µg/mL of the individual ligands.*

C. *Distribution of baseline values and signals (a subset is shown for visual clarity). Means and standard deviations were computed for replicates from 99 plates from which Z' factors were calculated. Shown also are Gaussian fits of the histograms.*
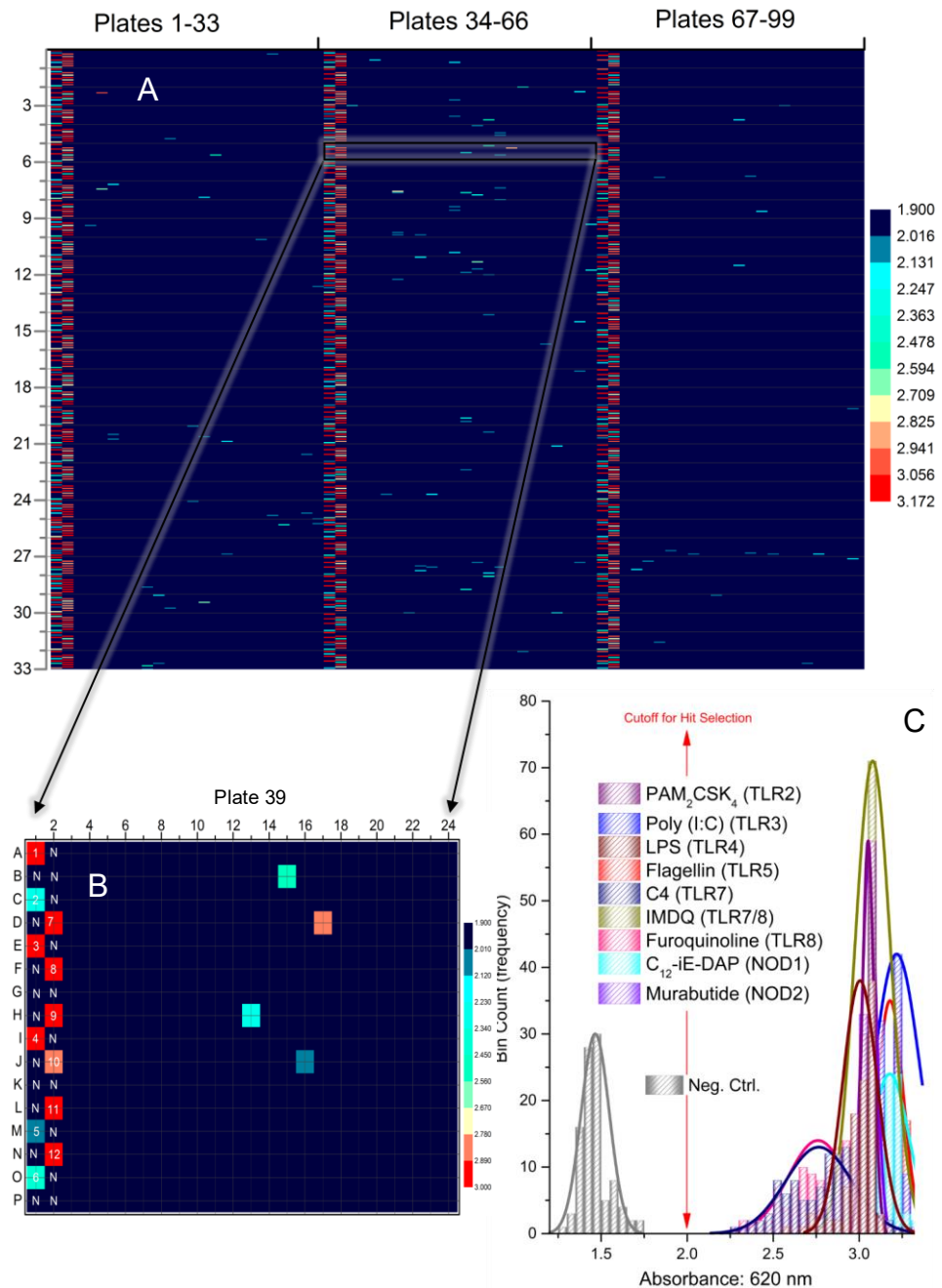
We examined the possibility of improving signal-to-noise (S/N) ratios and dynamic range of the assay by eliminating possible redundancy in signaling in the individual reporter cell lines. We tested the responses of each individual reporter cell line to well-characterized innate immune stimuli. We observed considerable redundancy and degeneracy within these reporter cells (Fig. 4A).
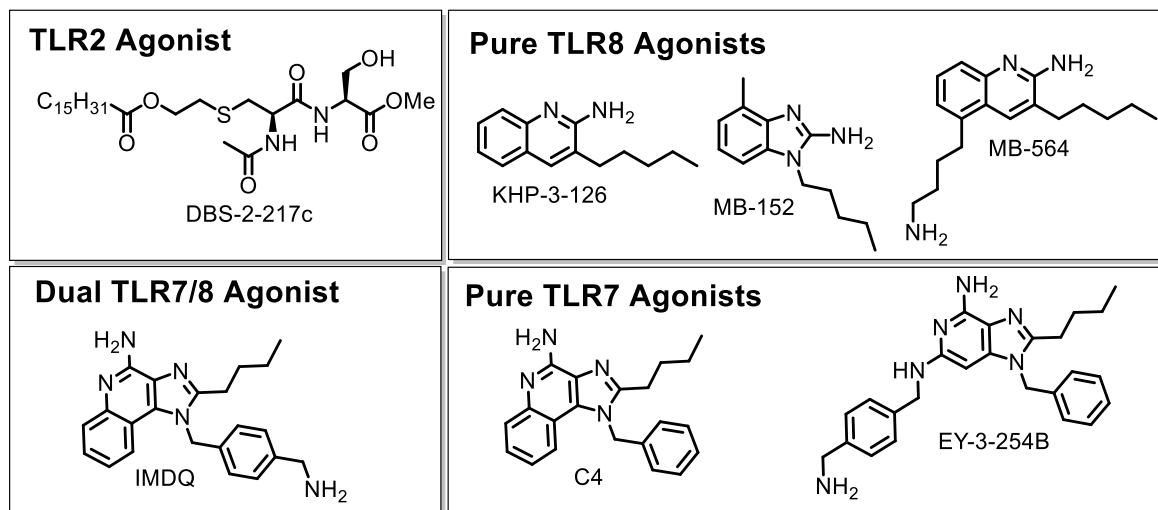
**Figure 3. Structures of positive controls used in the HTS.**

Virtually all of the reporter cell lines responded to Poly(I:C), a TLR3 ligand which also signals via the RIG-I-like receptors, RIG-I, Melanoma Differentiation-Associated protein 5 (MDA5), or the RIG-I-like RNA helicase LGP2.[121-123] HEK2 cells responded, as expected, to canonical TLR2 ligands (PAM$_2$CSK$_4$,[124] LTA,[125] and the monoacyl human TLR2-specific lipopeptide, DBS-2-217C), but also to flagellin and C$_{12}$-iE-DAP,[101] TLR5 and NOD1 agonists, respectively; HEK5 cells responded, in reciprocal fashion, to flagellin and the TLR2 agonists, as well as C$_{12}$-iE-DAP. Flagellin also activates, apparently ectopically, HEK3, HEK4, HEK7, HEK8, HEK9 and NOD1 cells, presumably by alternate sensing via Naip5.[126-127] HEK7 cells responded to pure TLR7 agonists C4,[91] EY-3-254B[111] and to the dual TLR7/8 agonist IMDQ[92, 96] (in addition to, as
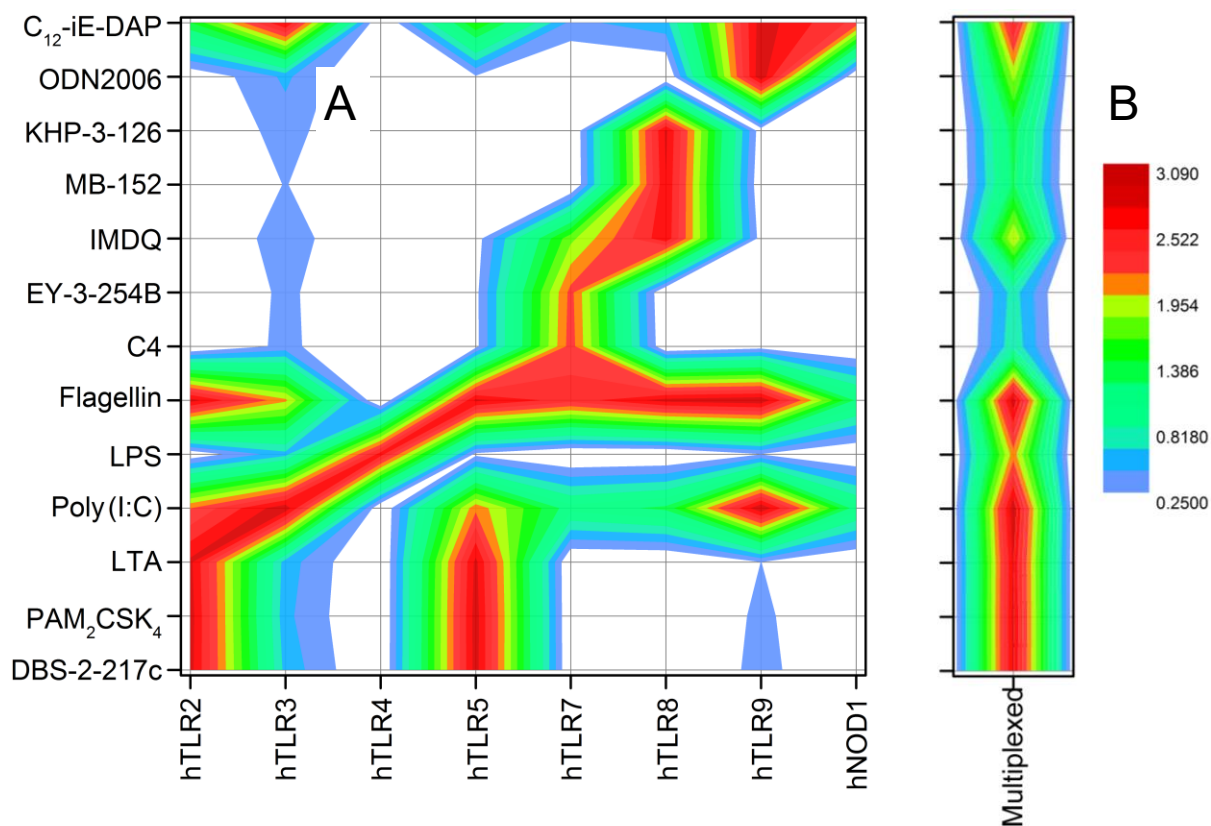
Figure 4. ***Responses of individual reporter cell lines to innate immune stimuli***. ***A.*** *Heat map of responses of individual reporter cell lines to a variety of TLR/NLR stimuli (see Fig 3 for structures of compounds), showing redundancy in PRR engagement.* ***B.*** *Multiplexing TLR2, TLR4, TLR7, TLR8, and TLR9 cells is sufficient and necessary for robust detection of signals.*

mentioned earlier, poly(I:C) and flagellin), as well as to C_{12}-iE-DAP. HEK8 cells showed responses to TLR8 agonists KHP-3-126,[26] MB-152,[100] and to the dual TLR7/8 agonist IMDQ; poly(I:C), flagellin and C_{12}-iE-DAP also elicited NF-κB induction in these cells. An analysis of the redundancies indicated that a subset comprising HEK2, HEK4, HEK7, HEK8 and HEK9, when multiplexed, responded to all of the innate immune stimuli (Fig. 4B), while showing a markedly reduced baseline absorbance of 0.25 AU.

This multiplexed platform was implemented in screening to screen 123,943 compounds and, as in the pilot screen, the inclusion of individual controls in each of the 354 assay plates (Fig. 2B) allowed the examination of S/N ratios and Z' factors for individual stimuli, which ranged from 0.74 (HEK7) to > 0.85 for poly(I:C) and flagellin (Fig. 5). A cutoff value of 4σ above in-plate absorbance mean yielded 552 provisional hits (Fig. 6). Among the most prominent of signals were those originating from the polyene antifungal agents AmpB and nystatin; both these compounds were identified as prominent hits in the Selleck as well as the Prestwick libraries (Fig. 6).
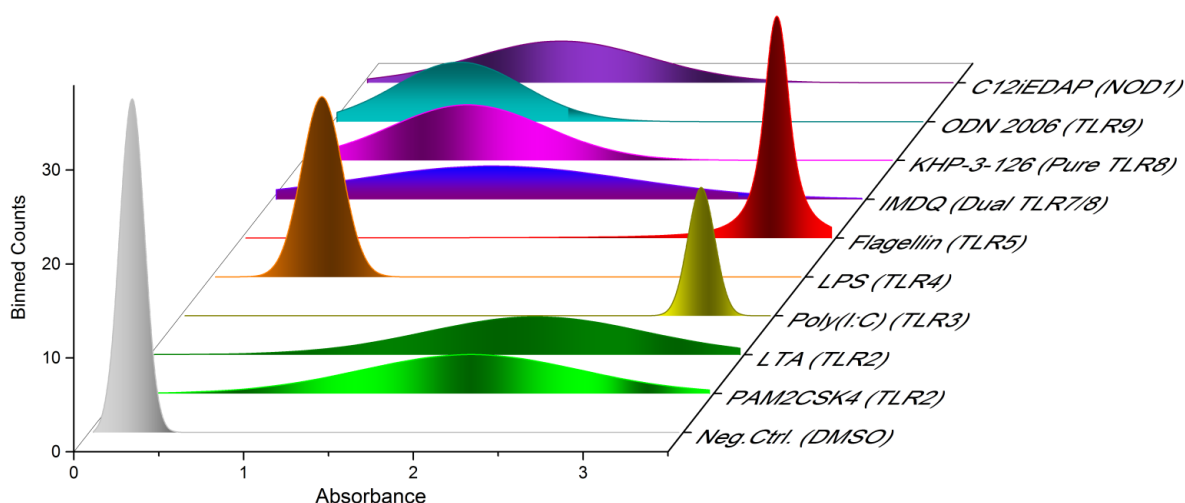

Figure 5. Distribution of negative and individual positive controls obtained in the modified multiplexed HTS screen.
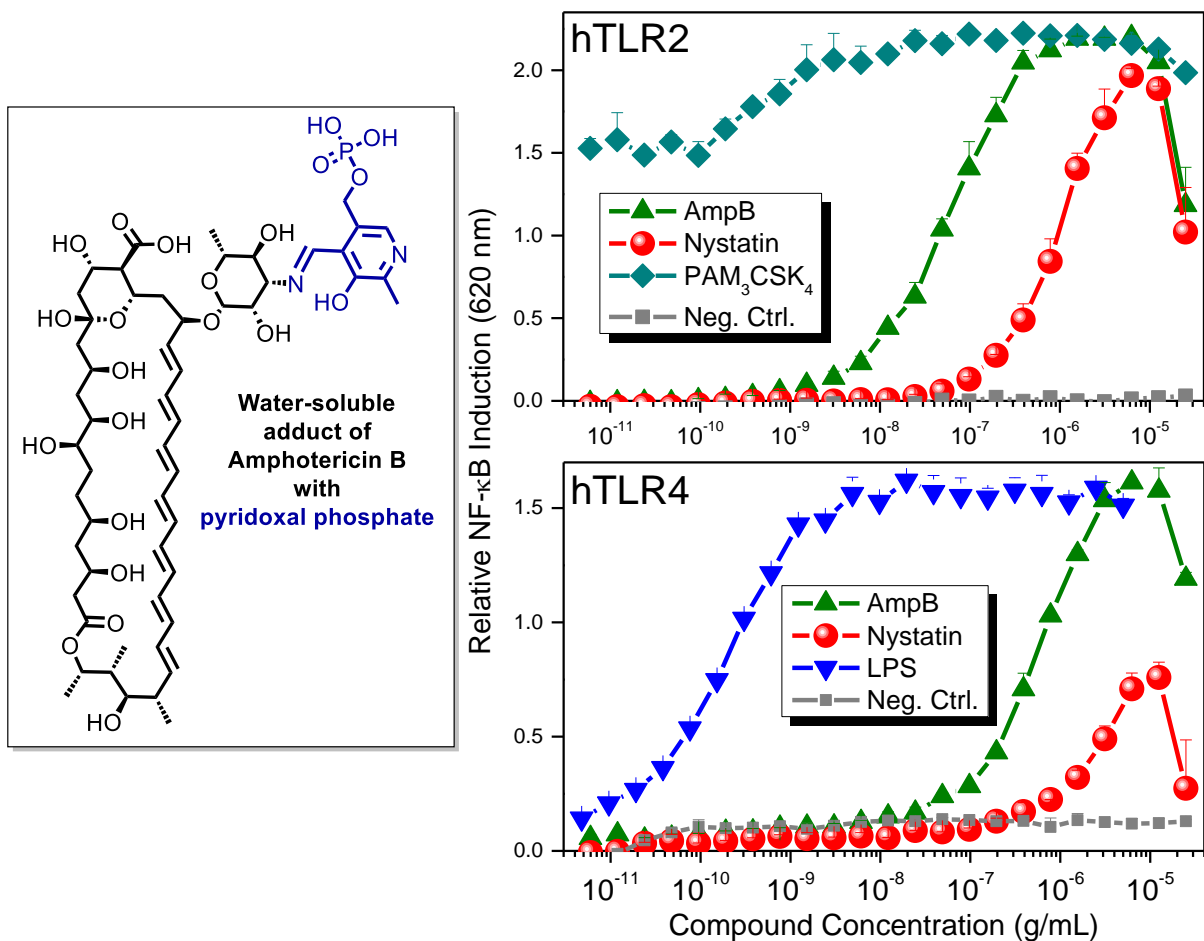
Simultaneous deconvolution and dose-response profiles in individual reporter cell lines (HEK2, HEK3, HEK4, HEK5, HEK7, HEK8, HEK9, NOD1 and HEK-Null) were performed for all provisional hits. AmpB and nystatin showed dose-dependent NF-κB induction in human TLR2- and TLR4-specific reporter cell lines (Fig. 7), consistent with previous reports demonstrating TLR2 and TLR4 activation by these antifungal agents.[128-130]

AmpB has remained the frontline chemotherapeutic agent for serious systemic fungal infections for more than a half-century.[131-132] AmpB is, as the name suggests, amphoteric which, compounded by its pronounced amphipathic nature (due to the asymmetric distribution of polar hydroxyl groups on one face of the molecule and a markedly hydrophobic, conjugated polyene on the other), has a marked propensity to self-associate with a critical aggregation concentration of ~ 0.2 µg/mL. Consequently, the drug is very sparingly soluble in water (< 1 µg/mL).[133] AmpB was more potent than nystatin (Fig. 7), is an FDA-approved drug for parenteral use (which nystatin is not), and we had previously reported a practical and convenient method for obtaining highly water-soluble (>100 mg/mL) formulations of AmpB using pyridoxal phosphate (vitamin B_6) as a complexing
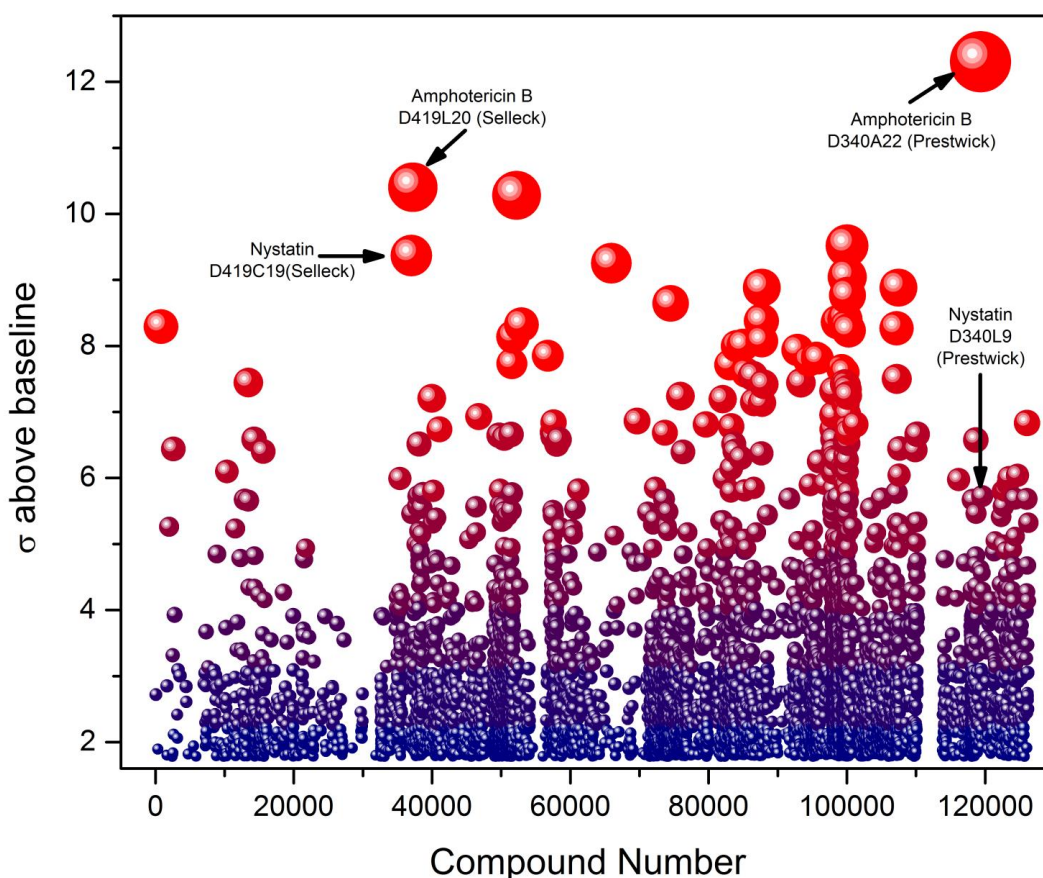

Figure 6. HTS data on 123,943 compounds showing prominent signals originating from AmpB and nystatin. *Hits were defined as signals > 4 σ (in-plate standard deviations for test compounds above negative control means).*

*Figure 7. Deconvolution and dose-response of AmpB and nystatin showing human TLR2 and TLR4-agonistic activities.*

agent.[134] For these reasons, we chose to evaluate the adjuvantic properties of AmpB.

Given the dose-dependent TLR2- and TLR4-agonistic properties[128-130] of AmpB (Fig. 7), we compared cytokine and chemokine induction by AmpB to the TLR2-specifi c diacyl and triacyl lipopeptides PAM2CSK4 and PAM3CSK4 (which signal via TLR2/6 and TLR2/1 heterodimerization , respectively[135-136]), MPLA, a TLR4 agonist which is a component of the FDA-approved AS04 adjuvant, [137-139] as well as LPS, a highly proinflammatory TLR4 agonist, in human PBMCs.
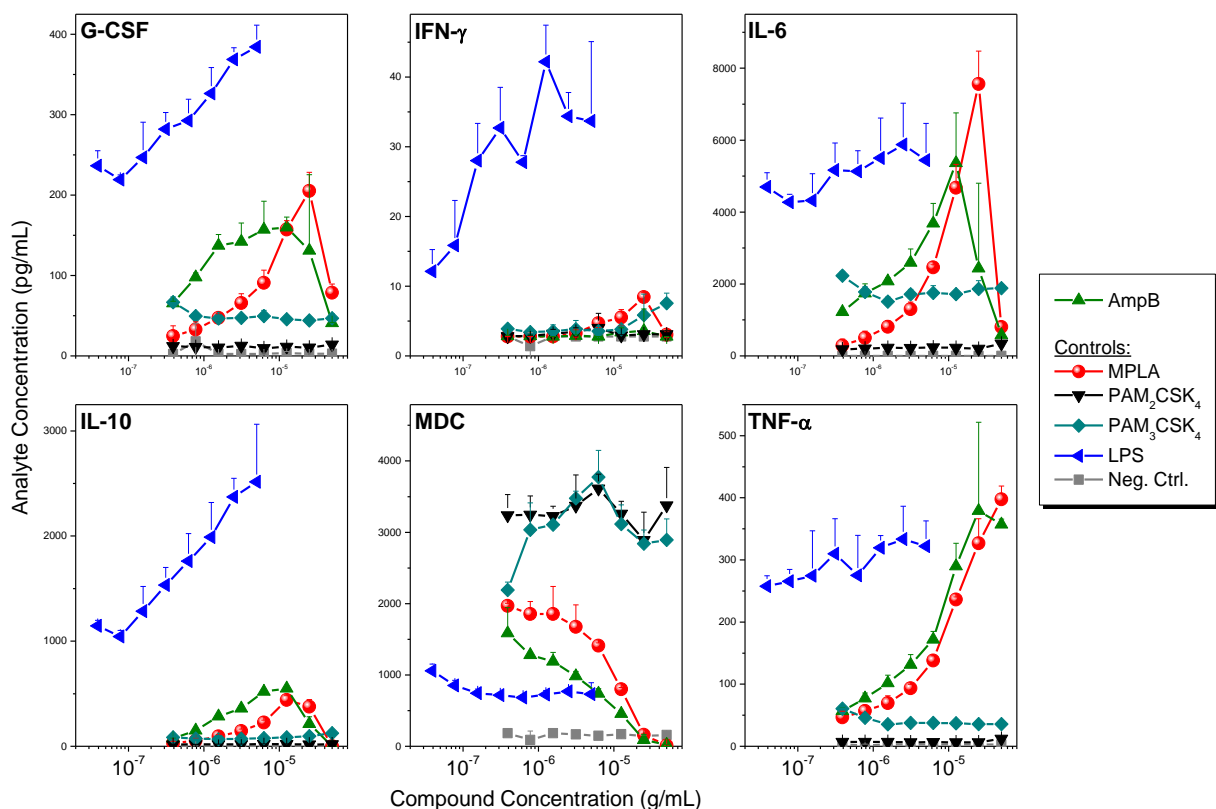
Figure 8. Cytokine and chemokine induction of AmpB in human PBMCs. *Aliquots of human PBMCs (10^5 cells in 100 µL/well) were stimulated for 16 h with graded concentrations (two-fold dilutions starting at 25 µg/mL) of test compounds. Supernatants were isolated by centrifugation, and were assayed in triplicates (from individual donors) using analyte-specific multiplexed cytokine/chemokine bead array assays. The cytokine profile of AmpB closely resembles that of MPLA, suggestive of TRIF-biased signaling.*

A high degree of congruence in the pattern of cytokine and chemokine induction between AmpB and MPLA was observed (Fig. 8), suggesting a TRIF-biased signaling for AmpB, as has been observed for MPLA.[140-142] In particular, both AmpB and MPLA, relative to LPS, induce significant levels of Myd88-dependent TNF-α and IFN-γ secretion[140] only at high concentrations, whereas both AmpB and MPLA strongly induce MDC (Fig. 8) and RANTES responses at low concentrations, consistent with TRIF-dominant signaling of AmpB.[140-142] A possible clinical correlate of a dominant TRIF-biased TLR4 activation by AmpB, which is associated with
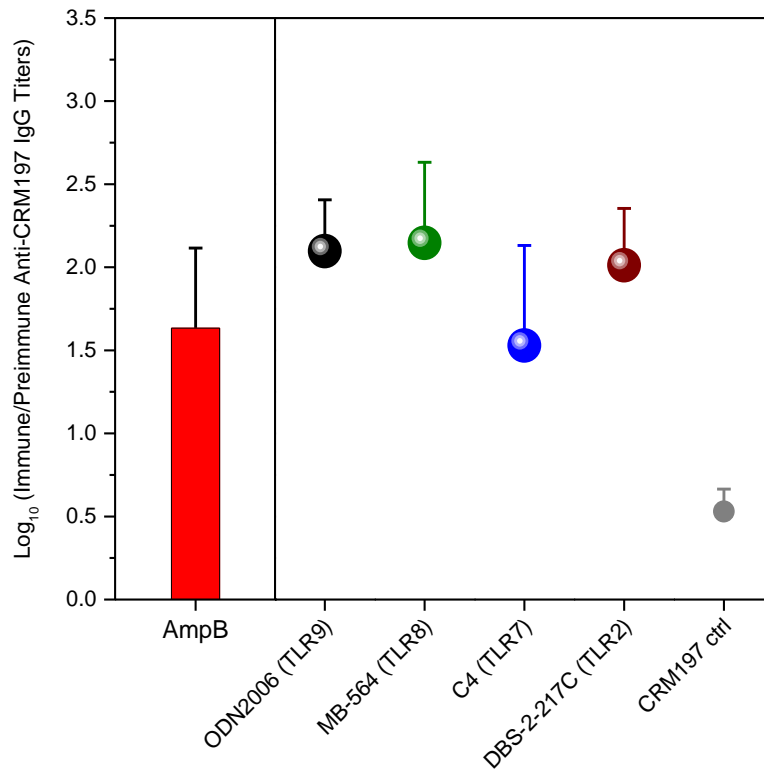
Figure 9. Adjuvanticity of AmpB in a standardized rabbit model of immunization. *Cohorts of adult female New Zealand white rabbits (n = 4) were immunized intramuscularly in the flank region with 10 μg of CRM197 in 0.2 mL of saline (unadjuvanted control) or 10 μg of CRM197 in 0.2 mL of saline plus 100 μg of AmpB-pyridoxal phosphate adduct without any other excipients. Other TLR-active candidate adjuvants were used as comparators. Preimmune test-bleeds were obtained on day 0, and animals were immunized on days 1, 15, and 28. A final bleed was obtained on day 38. CRM197-specific ELISAs were performed using automated liquid handling methods and are depicted as $\log_{10}$ (immune/preimmune) titers.*

relatively low levels of proinflammatory mediator in circulation, is the occurrence of infusion-related febrile reactions[131, 143] at therapeutic doses of up to 1 mg/kg per day; in contrast, febrile reactions and hemodynamic derangements in humans occur at much lower doses of LPS infusion (4 ng/kg).[144-146]

The in vitro signatures of a TRIF-biased cytokine induction profile that portend low, if any, local or systemic reactogenicity, coupled with the fact that parenteral AmpB has been in the clinic for several decades prompted the evaluation of its adjuvanticity in highly standardized rabbit models (51, 62) that we have been using to benchmark candidate vaccine adjuvants using CRM197 (10 µg/dose) as antigen (92). CRM197 is a non-toxic mutant of diphtheria toxin, containing a single amino acid substitution (G52E), and is used as a carrier protein in conjugate vaccines for polysaccharide antigens, which are frequently T cell-dependent antigens, requiring T cell helpfor humoral responses.[147] The adjuvantic effects of the highly water-soluble and stable AmpB-pyridoxal phosphate complex (100 µg/dose) was compared to that of ODN 2006 (TLR9), MB-564 (TLR8), C4 (TLR7) and DBS-2-217c (TLR2), all of which are also fully water-soluble and were also used at 100 µg/dose. AmpB as an adjuvant elicited comparable anti-CRM197 IgG titers relative to the other candidate adjuvants (Fig. 9) in rabbits with no detectable local inflammation.

2.3 Conclusions

As mentioned earlier, AmpB has had a long track-record in the clinic, with a well-documented adverse effect profile; the very low doses of AmpB required for adjuvanting vaccines emphasizes its potential use as an adjuvant for human vaccines. Furthermore, the development of a novel multiplexed innate immune detection platform described herein has led to the identification of several immunostimulatory chemotypes, structure-activity relationship studies of which are currently in progress, and will be reported elsewhere.

2.4 Materials and Methods

Compounds for HTS screens

Curated compound collections from the University of Kansas High Throughput Screening laboratory which include Life Chemicals (15,040), ChemBridge (43,736), ChemDiv (56,232), Selleck Bioactives (1649), TimTec (5000), and FDA Repurposed Library (2,286) were used. Compound transfers from source (80 nL of 10 mM stocks) to assay plates were performed using an Echo 550 acoustic liquid handler (Labcyte, Sunnyvale, CA). For most libraries, a target final concentration of 10 μM of compound (in a final volume of 80 μL for the multiplexed reporter gene-based assay described below) was achieved; the FDA Repurposed Library compounds were plated to obtain final concentrations of 2.5 μM. Assay plates were hermetically sealed and stored at -80 $^\circ$C until used. AmpB and nystatin were purchased from Sigma-Aldrich (St. Louis, MO). Synthetic MPLA, lipoteichoic acid (LTA) from *S. aureus*, PAM$_2$CSK$_4$, Poly(I:C), ultrapure LPS from *E. coli* K12, flagellin from *S. typhimurium*, ODN-2006 (Vaccigrade), C12-*i*E-DAP, and Murabutide were procured from InvivoGen (San Diego, CA). The structures of small molecule PRR agonists synthesized by us are shown in Fig. 3. Responses to a variety of TLR and NLR agonists were first examined using THP1-Blue™ NF-κB reporter cells (InvivoGen, San Diego, CA).

Multiplexed human TLR-2/-3/-4/-5/-7/-8/-9/Null and NOD-1/NOD-2 reporter gene assays (NF-κB induction)

Human TLR-2/-3/-4/-5/-7/-8/-9/Null and NOD-1/NOD-2-specific reporter cells (InvivoGen, San Diego, CA; referred to hereafter as HEK2, HEK3 ... HEK9 cells) were used for the multiplexed screen.[91, 101-102] HEK293 cells stably co-transfected with the appropriate hTLR (or NOD) and

secreted alkaline phosphatase (sAP) genes were maintained in HEK-Blue™ Selection medium (InvivoGen, San Diego, CA). Expression of sAP under control of NF-κB/AP-1 promoters is inducible by appropriate TLR/NOD agonists, and extracellular sAP in the supernatant is proportional to NF-κB induction.

For the pilot screen, all ten individual reporter cells were used. Cells were harvested by trypsinization from T75 tissue culture flasks, washed once with pyrogen-free phosphate-buffered saline (PBS), and resuspended in HEK-Blue Detection Media at a density of 10^6 cells/mL. Combining equal proportions of the ten different cell lines yielded a density of ~10^5 cells/mL of each cell type. The first two columns of each assay plate were reserved for controls (see Fig 2B); alternate wells received DMSO or HEK-Blue Detection Media alone (unstimulated, negative controls), or individual, TLR/NOD-specific stimuli (see legend to Fig 2B). Structures of small-molecule TLR/NOD-specific compounds are shown in Fig. 3. 80 µl/well of the multiplexed cell mixture was added to 384-well, flat-bottomed, cell culture-treated assay plates, and incubated overnight in cell culture incubators. sAP was assayed spectrophotometrically using an alkaline phosphatase-specific chromogen (present in HEK-detection medium as supplied by InvivoGen) at 620 nm using a SpectraMax M2 multimode microplate reader (Molecular Devices, Sunnyvale, CA). Z' factors[120] were computed for each TLR/NOD-specific signal from 99 assay plates (Fig. 2C). The modified multiplexed assay used in the final screen included a subset comprising human TLR2, TLR4, TLR7, TLR8 and TLR9-specific reporter cells. The following individual stimuli were used to quantify signal-to-noise characteristics: PAM$_2$CSK$_4$ (TLR2), DBS-2-217c (TLR2), lipoteichoic acid (LTA, TLR2), Poly(I:C) (TLR3), LPS (TLR4), flagellin (TLR5), C4 (pure TLR7),[91] EY-3-254B (pure TLR7),[111] IMDQ (TLR7/8),[92, 96] KHP-3-126 (pure TLR8),[26] MB-152

(pure TLR8),[100] ODN-2006 (TLR9), C_{12}-iE-DAP (NOD1), and Murabutide (NOD2). Performance metrics for the controls used in the final screen are shown in Fig 5.

All hits (n = 552), defined as signals $\geq$ 4 σ (in-plate standard deviations for test compounds above negative control means), were deconvoluted in full dose-response assays in human TLR-2/-3/-4/-5/-7/-8/-9 and NOD-1/NOD-2-specific reporter cells in liquid handler-assisted assay formats as described by us previously.[91, 101-102]

Synthesis of pyridoxal phosphate adducts of AmpB and nystatin

AmpB (20.0 mg) was dissolved in 2 mL of dimethylformamide, to which was added a solution of 20 mg of pyridoxal phosphate in 2 mL of water (adjusted to pH 7.4 with Na_2CO_3). The mixture was lyophilized, and the resultant fully water-soluble adduct was characterized by liquid chromatography-mass spectrometry as described previously.[133]

Immunoassays for cytokines

Fresh human peripheral blood mononuclear cells (PBMCs) were isolated from human blood obtained by venipuncture (approved by the University of Minnesota institutional review board, Protocol ID: 1506-32702H). Written informed consent was obtained as per University guidelines. PBMCs were isolated using Vacutainer® CPT™ Cell Preparation Tubes (Beckton-Dickinson, New Jersey, NJ). Aliquots of human PBMCs (10^5 cells in 100 μL/well) were stimulated for 16 h with graded concentrations (two-fold dilutions starting at 25 μg/mL) of test compounds. Supernatants were isolated by centrifugation, and were assayed in triplicates (from individual donors) using analyte-specific multiplexed cytokine/chemokine bead array assays (Milliplex

HCYTOMAG-60K, EMD Millipore, Billerica, MA) as reported by us previously [100]. The analytes examined include: sCD40L, VEGF, TNF-β, TNF-α, TGF-α, RANTES, PDGF-AB/BB, PDGF-AA, MIP-1β, MIP-1α, MDC (CCL22), MCP-3, MCP-1, IP-10, IL-17A, IL-15, IL-13, IL-12 (p70), IL-12 (p40), IL-10, IL-9, IL-8, IL-7, IL-6, IL-5, IL-4, IL-3, IL-2, IL-1ra, IL-1β, IL-1α, IFN-γ, IFN-α2, GRO, GM-CSF, G-CSF, Fractalkine, Flt-3 ligand, FGF-2, Eotaxin, EGF.

Rabbit immunization and CRM197-specific immunoassays

All experiments were performed at Harlan Laboratories (Indianapolis, IN) in accordance with institutional guidelines (Protocol Number: 150416HBS73DAYSTD). The Harlan IACUC Committee approved this study. Small bore needles (24-gauge) were used to minimize distress to the animals during intramuscular administration. Following termination of the study, animals were first anesthetized using ketamine (0.5 mL of 100 mg/mL for average 6 lb. rabbit) and xylazine (0.5 mL of 20 mg/mL for average 6 lb. rabbit), and then euthanized by carbon dioxide inhalation. All antigen/adjuvant preparations were entirely aqueous; no liposomal or emulsifying agents were used. Cohorts of adult female New Zealand White rabbits (n = 4) were immunized intramuscularly in the flank region with (a) 10 µg of CRM197[148] in 0.2 mL saline (unadjuvanted control), or (b) 10 µg of CRM197 in 0.2 mL saline plus 100 µg of either AmpB or TLR agonist. Pre-immune test-bleeds were first obtained via venipuncture of the marginal vein of the ear. Animals were immunized on Days 1, 15 and 28. A final test-bleed was performed via the marginal vein of the ear on Day 38. Sera were stored at −80 °C until used. CRM197-specific ELISAs were performed in 384-well format using automated liquid handling methods as described by us elsewhere [96]. A Precision 2000 liquid handler (Bio-Tek, Winooski, VT) was used for all serial dilution and reagent addition steps, and a Bio-Tek ELx405 384-well plate washer was employed for plate washes.

Nunc-ImmunoMaxiSorp (384-well) plates were coated with 80 µL of CRM197 (10 µg/mL) in 100 mM carbonate buffer, pH 9.0 overnight at 4 °C. After 3 washes in 100 mM phosphate-buffered saline (PBS) pH 7.4, containing 0.1% Tween-20, the plates were blocked with 3% bovine serum albumin (in PBS, pH 7.4) for 1 h at rt. Serum samples (in quadruplicate) were serially diluted in a separate 384-well plate using the liquid handler; 40 µL of the serum dilutions were transferred using the liquid handler, and the plate incubated at 37 °C for 1 h. The assay plate was washed three times, and 40 µl of 1: 10,000 diluted appropriate anti-rabbit immunoglobulin (IgG, γ-chain) conjugated with horseradish peroxidase was added to all wells. Following an incubation step at 37 °C for 1 h, and three washes, tetramethylbenzidine substrate was added at concentrations recommended by vendor (Sigma). The chromogenic reaction was terminated at 30 min by the addition of 2M H_2SO_4. Plates were then read at 450 nm using a SpectraMax M2 device (Molecular Devices, Sunnyvale, CA).

Chapter 3.

# Transcriptomal Signatures of Innate Immune Stimuli and Accessory Immunostimulation of Fibroblasts by TLR2 Agonists
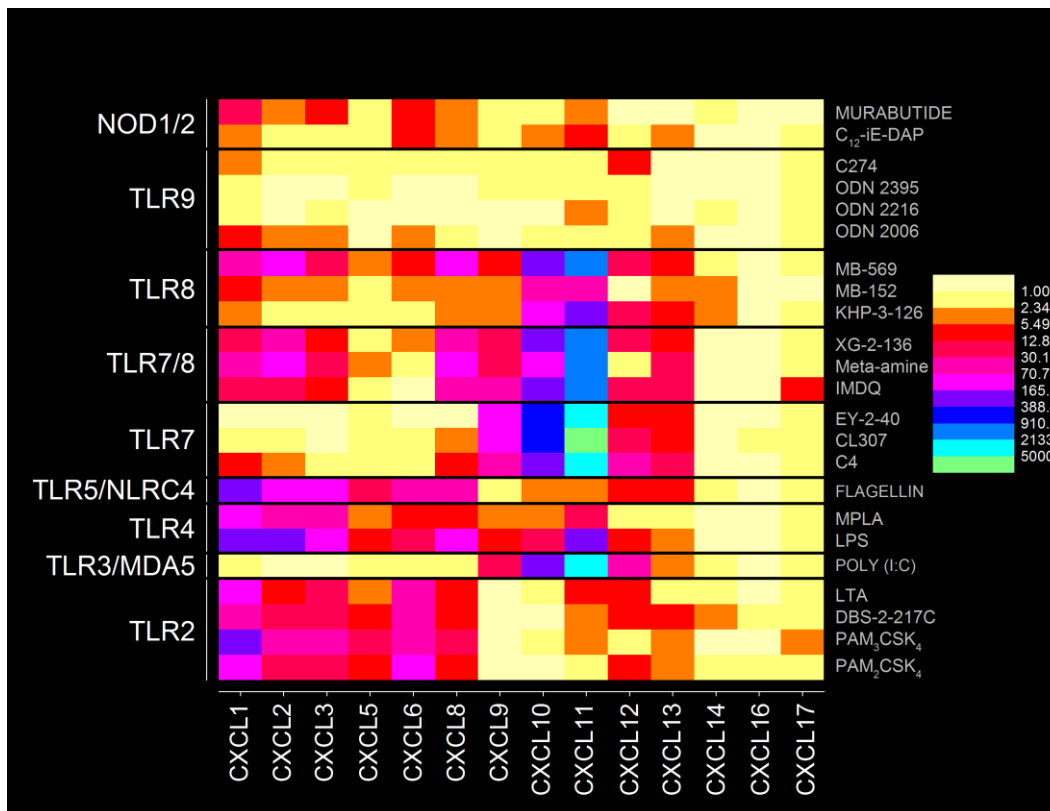
3.1 Introduction

Following the success of high-throughput screening using transfected reporter cells (Chapter 2), we sought methods of better identifying and authenticating novel innate immune stimuli for examination as vaccine adjuvants. Given the enormous diversity of signals recognized by the TLRs, which are present both in the extracellular and intracellular compartments, and the potential for Th cell polarization by TLRs, we sought to address three questions: (i) are there any 'signatures' that are diagnostic of innate immune activation, regardless of the innate immune sensor involved, (ii) which of the many TLR ligands that we have characterized induce strong humoral responses to subunit antigens, and (iii) the mechanistic basis for the superior adjuvantic activity of such ligands. Whole transcriptome next-generation RNA sequencing of human peripheral blood mononuclear cells exposed to 23 compounds encompassing almost the entire repertoire of TLR ligands indicate prominent upregulation of CC and CXC chemokines, independent of the chemotype. In a standardized rabbit model of immunization with a diphtheria toxin mutein CRM197.[148-149] we observed that TLR2 agonists outperformed all other TLR-active compounds. Non-hematopoietic cells such as fibroblasts express TLR2, and therefore respond uniquely to TLR2 stimuli, resulting in the induction of chemokines, and manifesting in the chemotaxis of several major human lymphocytic subsets. These results point to the utility of chemokine induction as a 'signature' of adjuvantic activity, and provides mechanistic insight into the potential utility of harnessing TLR2 agonists as vaccine adjuvants.

3.2 Results and Discussion

A main goal of this work was to examine if there are any transcriptional signatures common to the broad range of TLR/NLR-active compounds that we have evaluated as vaccine adjuvants. These

compounds are shown in Fig. 1, and include both canonical and novel small-molecule agonists of TLR2 (PAM$_2$CSK$_4$, PAM$_3$CSK$_4$, DBS-2-217C, and lipoteichoic acid), TLR3/MDA5 (Poly I:C), TLR4 (LPS from *E. coli*, MPLA), TLR5/NLRC4 (flagellin), TLR7 (C4, CL307, EY-2-40), TLR8 (KHP-3-126, MB-569, MB-152), dual TLR7/TLR8 (XG-2-136, Meta-amine and IMDQ), TLR9 (ODNs 2006, 2216, 2395, and C274), NOD1 (C12-iE-DAP) and NOD2 (Murabutide). We had previously characterized the transcriptional responses to a small subset of innate immune stimulatory compounds using microarrays.[150]
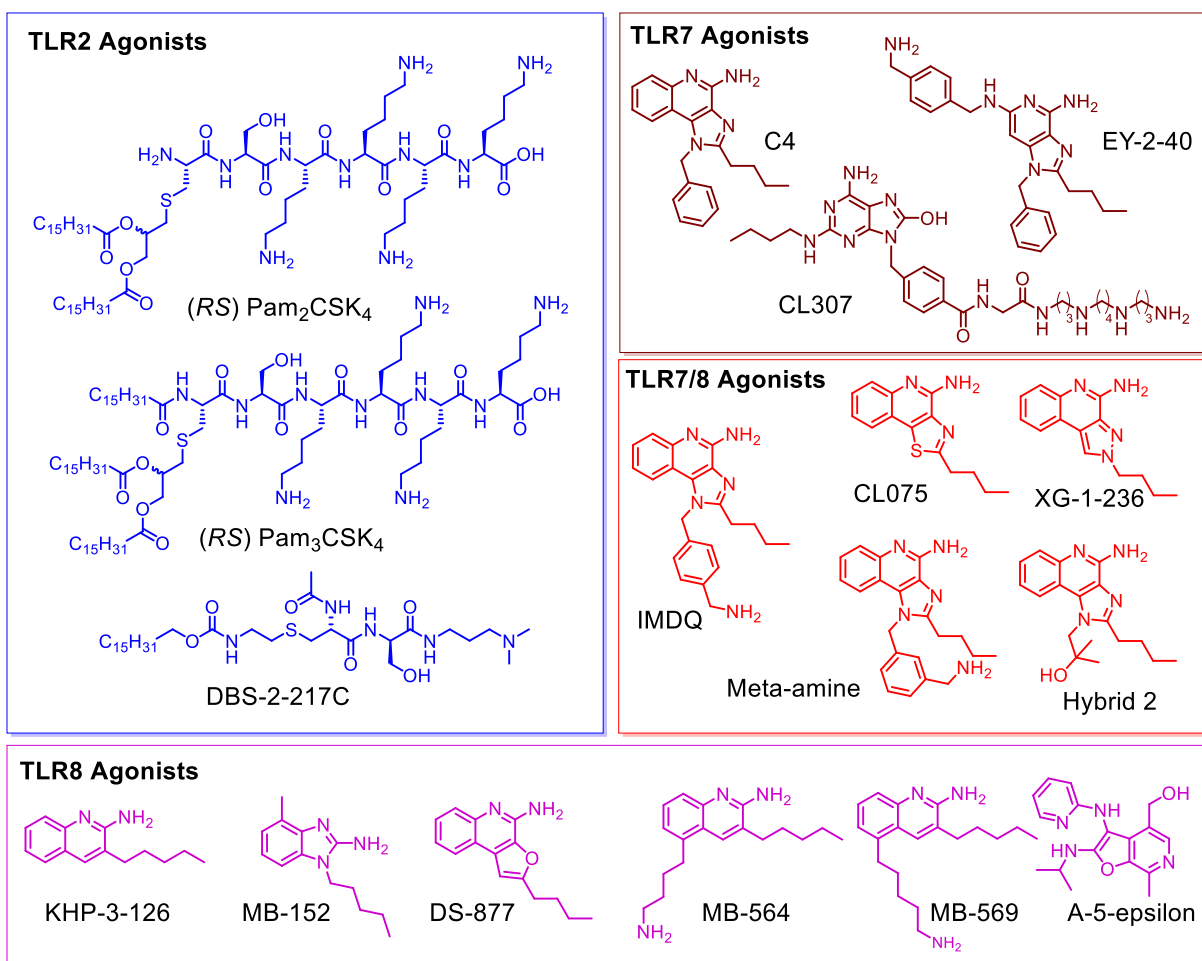
Figure 1. Structures of TLR agonists arranged by receptor target. *TLR2 agonists are shown in blue, pure TLR7 agonists are shown in maroon, dual TLR7/8 agonists are shown in red, and pure TLR8 agonists are shown in magenta.*

In this study, we utilized next-generation sequencing of total RNA isolated from human PBMCs stimulated with for 3.5 h with 1 µg/mL of each of the agonists to assess early transcriptional responses. A total of 26,363 annotated genes for each of the 23 test samples were compared in duplicate against unstimulated (or vehicle-alone, mock-stimulated) control samples.

As we had previously reported, diagnostic transcriptional signatures such as proinflammatory cytokine (TLR4), interferon, and interferon-inducible genes (TLR7) were strongly upregulated in
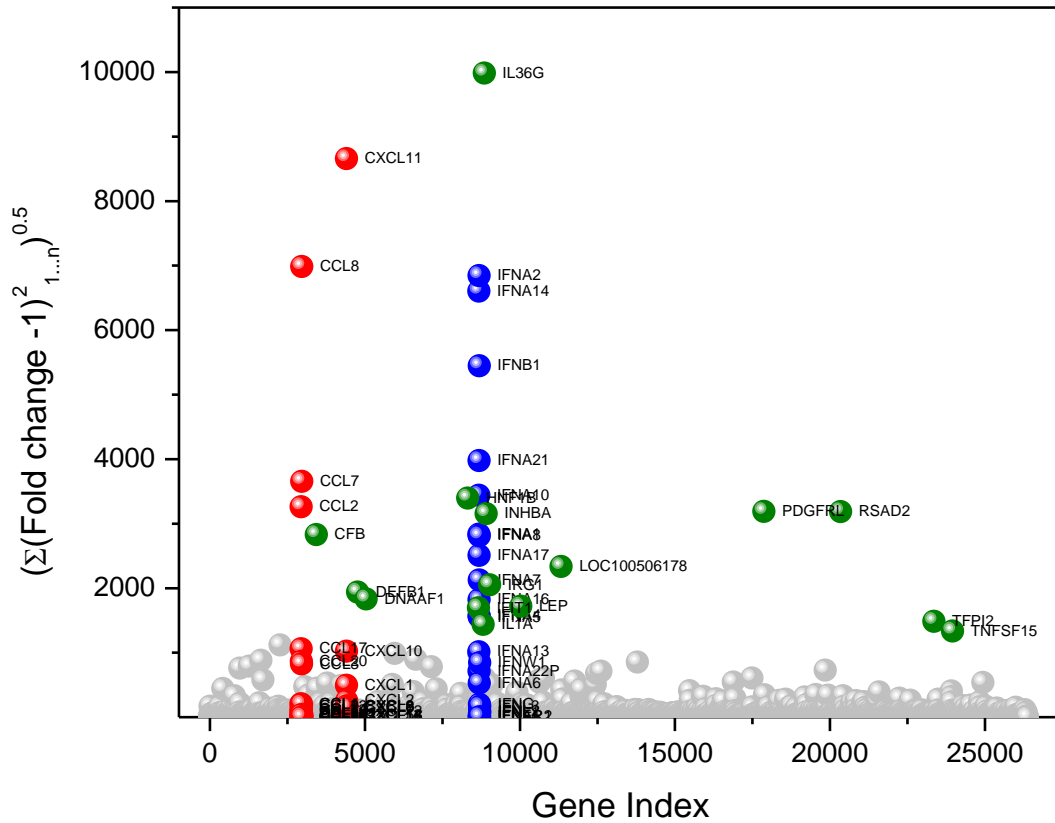

Figure 2. All TLR and NLR agonists upregulate genes associated primarily with three gene families. Root mean square deviations of fold change highlight the upregulation of three gene families: CC chemokines (red), CXC chemokines (red), and interferons (blue). Genes that were upregulated outside of these families are shown in green.

the samples. In order to discern global signatures in an unbiased manner, we compared root mean square deviations of fold change (from control values) in expression of each of the genes across the 24 test samples (Fig. 2). We observed pronounced deviations in three gene families: the CXC and CC chemokines, and Type I interferons (Fig. 2); additionally, we noted significant change in a subset of genes including *TNFSF15* (TNF superfamily ligand, member 15), *TFPI2* (tissue factor pathway inhibitor 2), *RSAD2* (radical S-adenosyl methionine domain containing 2), *PDGFRL* (platelet derived growth factor receptor like), *LEP* (leptin), *IL6* (interleukin-6), *IL12B* (interleukin-12B), *IL1A* (interleukin-1α) *IL36G* (interleukin-36γ), *IRG1* (immunoresponsive gene 1), *INHBA* (inhibin beta A subunit), *IFIT1* (interferon induced protein with tetratricopeptide repeats 1), *DNAAF1* (dynein axonemal assembly factor 1), *DEFB1* (defensin β-1), *CFB* (complement factor B), and *LOC100506178* (uncharacterized).

We next quantified changes in the CC and CXC chemokines, as well as IFN genes for each of the agonists. Strong signals for the CC chemokines 1, 2, 3, 4, 7, 8, 17, 18, 20, and 23 were observed for TLR2, TLR3, TLR4, TLR5, TLR7, TLR7/8, TLR8, NOD1, and NOD2 agonists (Fig. 3). The signals for TLR9 were significantly weaker, likely on account of the oligonucleotides requiring longer incubation periods as we had previously observed.[150]
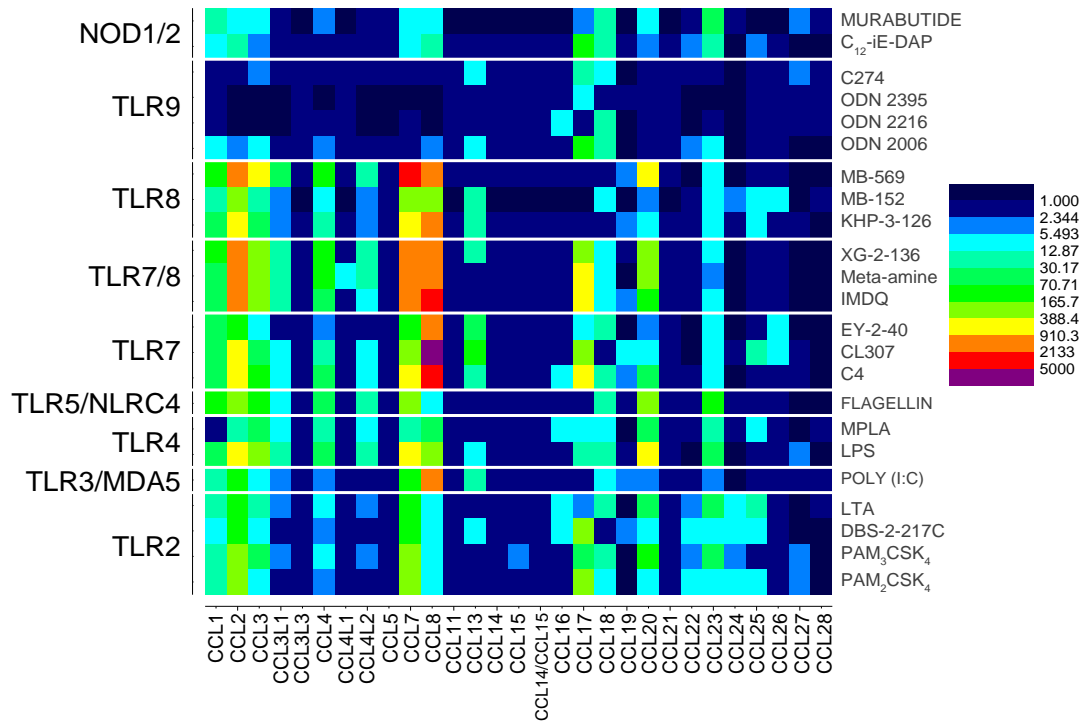
Figure 3. 'Signatures' of innate immune stimulation in CC chemokines. *Many of the TLRs and NLRs upregulated the CC chemokines 1, 2, 3, 4, 7, 8, 17, 18, 20, and 23.*
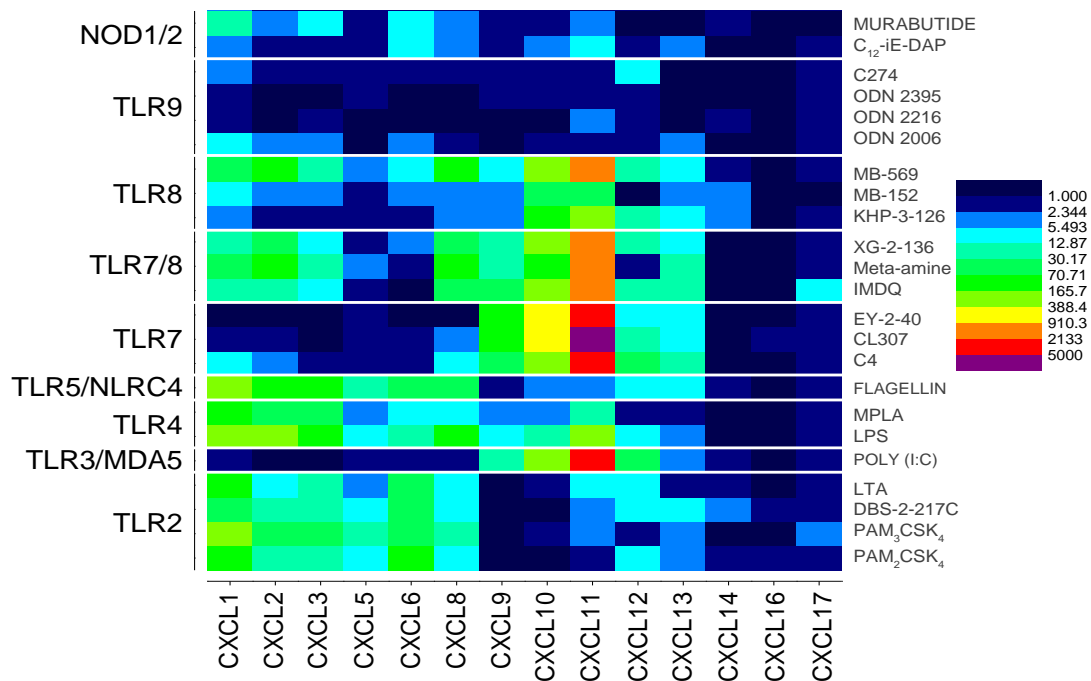
Figure 4. Discrimination between extracellular and intracellular innate immune receptors by CXC chemokine profiles. *The extracellular TLRs 2, 4, and 5 showed strong upregulation of CXCL5, CXCL6 and CXCL8, while the endolyososomal TLRs 3, 7, and 8 were characterized by upregulation of CXCL11 and CXCL12.*
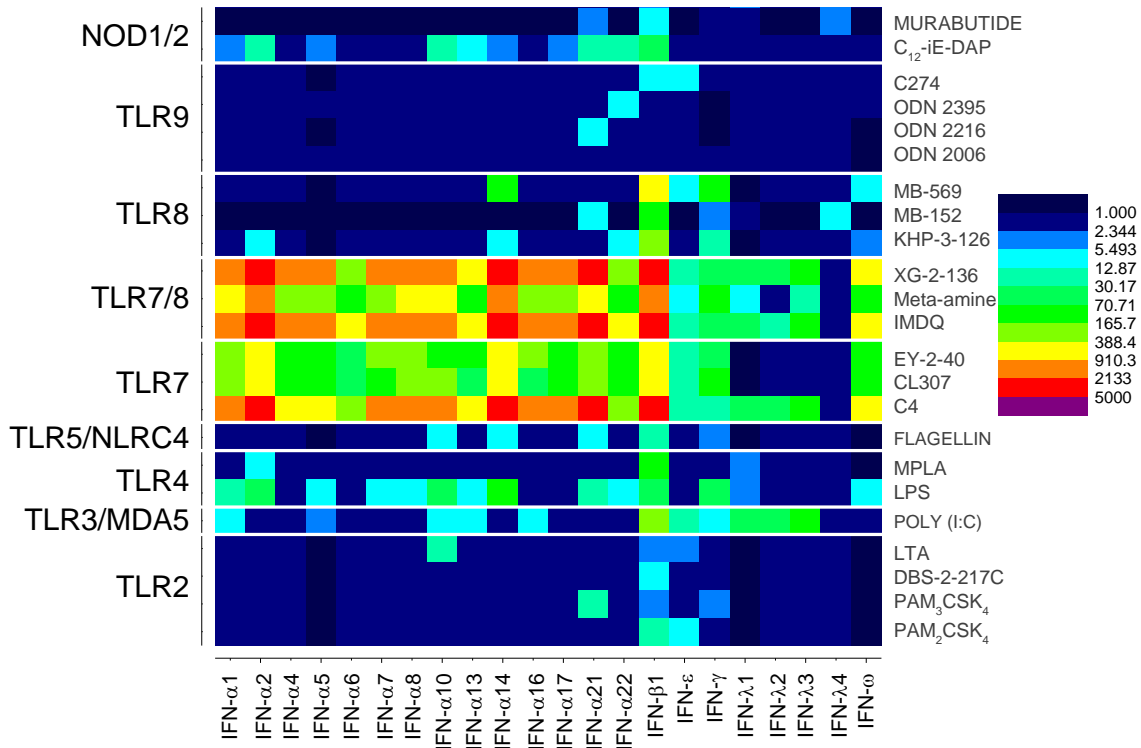
Figure 5. TLR7 upregulation of IFN-α and IFN-ω. *Pure TLR7 and dual TLR7/8 agonists dramatically upregulated all IFN-α genes and IFN-ω.*

A clear demarcation of extracellular versus intracellular TLR/NLR activation was apparent in the analysis of gene expression levels for the CXC chemokines. The engagement of the extracellular TLRs 2, 4, and 5 resulted in strong upregulation of CXCL5, CXCL6 and CXCL8 genes. In contrast, stimulation of the intracellular receptors TLR3, 7, and 8 manifested in upregulation of CXCL11 and CXCL12 (Fig. 4). Signals for CXCL1, CXCL2, and CXCL3 were also observed to be strongly enhanced but, like the CC chemokines, were found to be common for almost all agonists (Fig. 4). Interferon-α responses, as expected were almost exclusively restricted to TLR7 (and TLR7/8 activation), and it is noteworthy that interferon-ω signals were also evoked by TLR7 engagement (Fig. 5).

These data point to the potential utility of chemokine readouts as surrogate markers of innate immune activation, irrespective of the nature of stimulation. Indeed, both alum,[151-152] as well as MF59, a squalene-in-water emulsion containing the surfactants polysorbate 80 and sorbitan trioleate[153-154] are FDA-approved vaccine adjuvants that do not activate any of the TLRs, but induce chemokine secretion in hematopoietic cells.[155]

We next compared the adjuvantic activity of the various classes of TLR agonists in a standardized rabbit model of immunization with 10 µg/dose of CRM197 and 100 µg/dose of adjuvant, and a
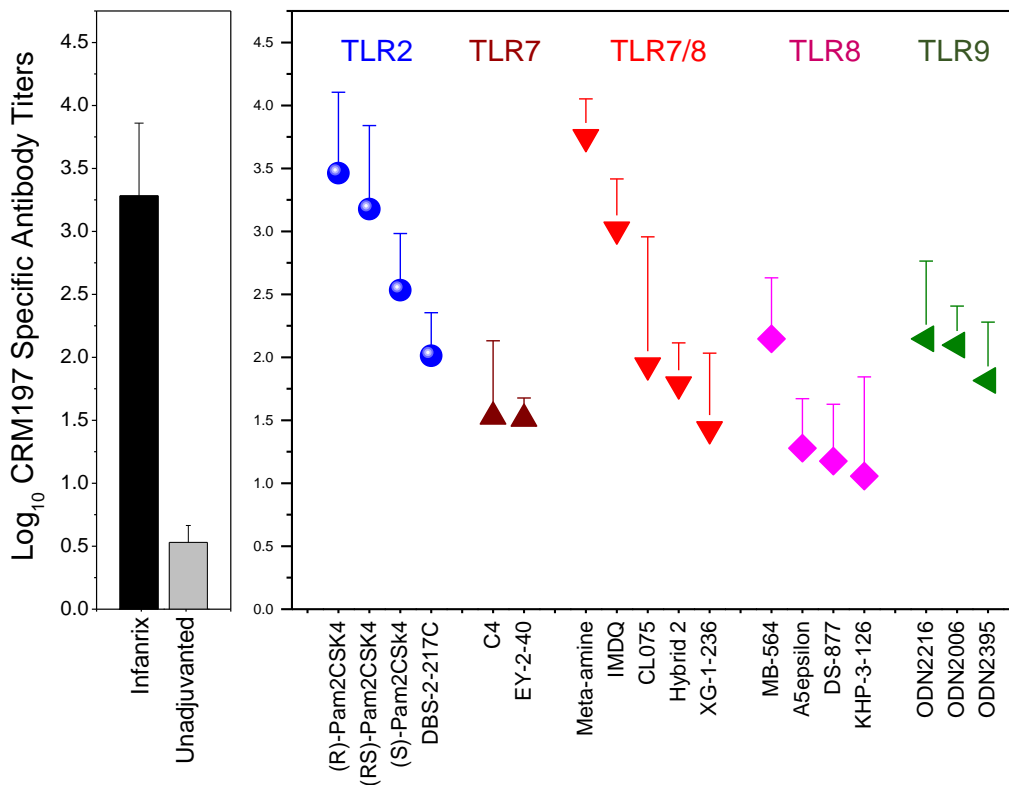
Figure 6. TLR agonists in rank order of adjuvantic potency in a rabbit immunization model, organized by target receptor. *TLR agonists were compared head-to-head in a standardized rabbit immunization model with CRM197 as antigen. TLR2 agonists are shown in blue, TLR7 agonists are shown in maroon, dual TLR7/8 agonists are shown in red, pure TLR8 agonists are shown in magenta, and TLR9 agonists are shown in green.*

full human dose of Infanrix® was used as a comparator (Fig. 6). Animals (n=4/cohort) received two boosts following a priming dose, spaced 15 days apart. As anticipated, the potent dual TLR7/8 agonists IMDQ and meta-amine,[92] were found to possess prominent adjuvantic activity (Fig. 6). Somewhat unexpectedly, we observed that almost all of the TLR2 agonists were also strongly adjuvantic, with the adjuvantic potency correlating with *in vitro* potency: (*R*)-PAM$_2$CSK$_4$ > (*RS*)-PAM$_2$CSK$_4$ > (*S*)-PAM$_2$CSK$_4$[89]; the mono-acyl DBS-2-217C is human TLR2-specific agonist,[156] and therefore, as expected found to be weaker (Fig. 6).

We sought to understand why TLR2-active compounds displayed strong adjuvantic activity. Transcriptomal profiling (Figs. 3 and 4) pointed to strong CXCL and CCL chemokine induction which we confirmed in human PBMCs (data not shown). However, it has been suggested that adventitial cells such as fibroblasts have immunoregulatory functions, and should therefore be considered as sentinel cells.[157-158] Human fibroblasts from disparate anatomical sites have been shown to synthesize CC and CXC chemokines.[159-164] Using multiplexed cytokine and chemokine assays, we initially examined the effect of almost the entire set of TLR agonists on cytokine and chemokine secretion in human foreskin fibroblasts (HFFs) and in human bronchial adenocarcinoma A549 cells, and found that, in both cell lines, the TLR2-active compounds PAM$_2$CSK$_4$ and DBS-2-217C induced both CC and CXC chemokines, including CXCL6/GCP2, CCL20/MIP-3α, CCL8/IL-8, CCL2/MCP-1 and MCP-3/CCL7; shown in Fig 7A is the dose-dependent induction of CXCL6, CCL20 and CCL8 in HFFs.
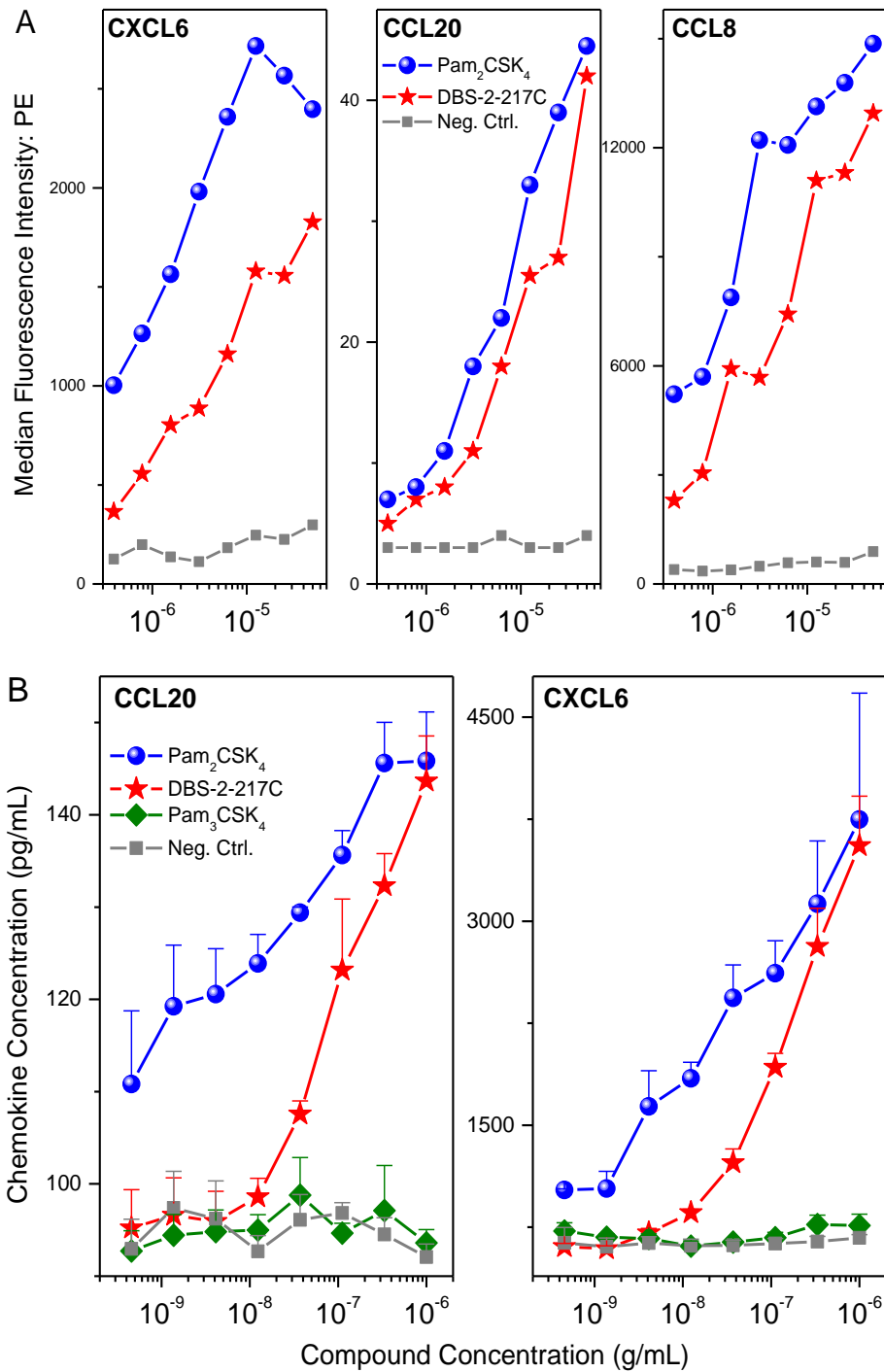
Figure 7. TLR2 agonists induce chemokines in human foreskin fibroblasts*. A. TLR2 agonists were screened for activity in HFFs using multiplexed cytokine (MagPix™) assays and showed CXCL6, CCL20 and CCL8 induction. **B.** CCL20 and CXCL6 induction by TLR2 agonists in HFFs were confirmed by ELISA. The TLR2/6 agonist Pam2CSK4 induced chemokine responses in HFFs, but the TLR1/2 agonists Pam3CSK4 failed to induce chemokine responses in HFFs.*
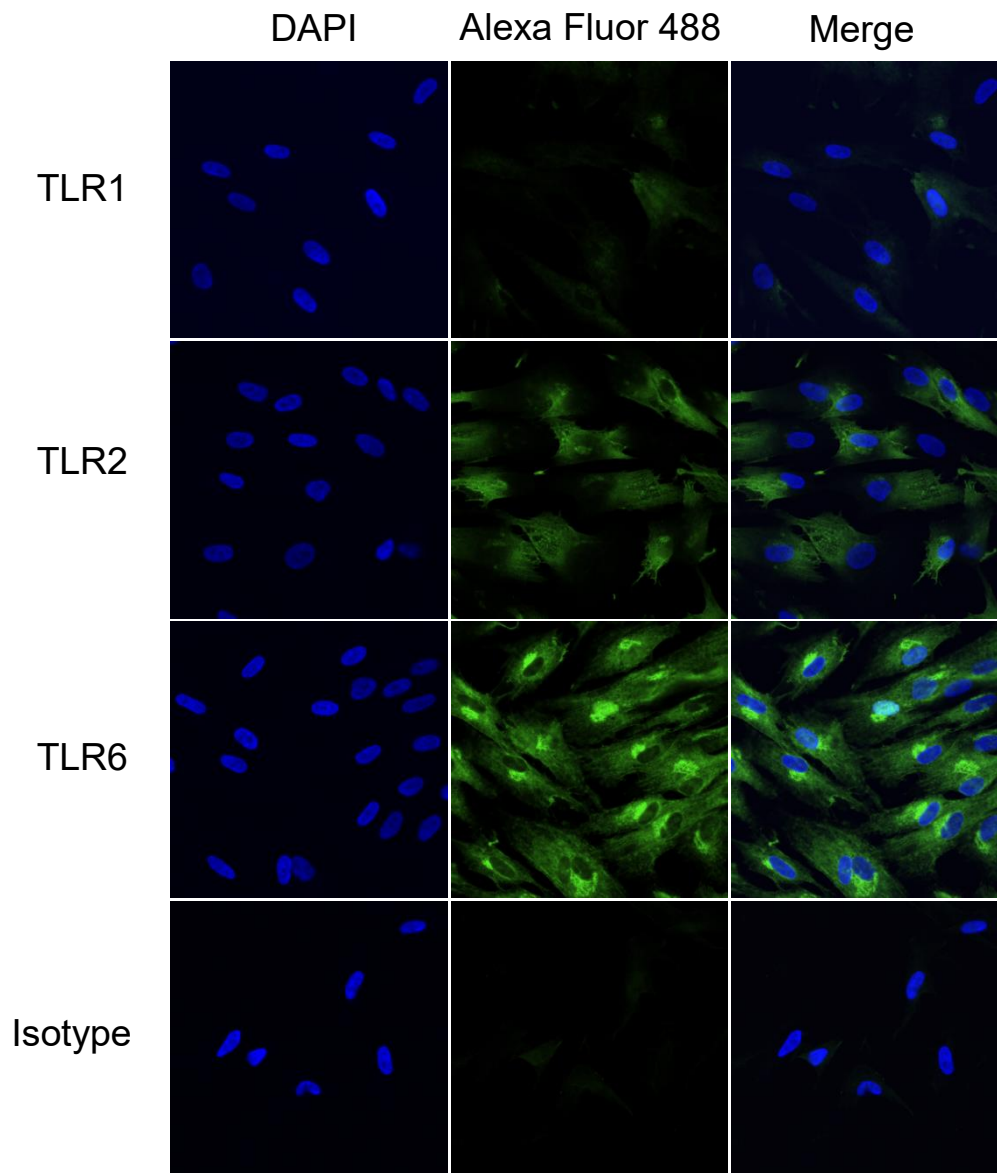
Figure 8. TLR2 and TLR6 are expressed in human foreskin fibroblasts. *HFFs stained for TLRs 1, 2, and 6 were signal amplified using tyramide signal amplification. HFFs showed strong staining for TLR2 and TLR6, but stain very weakly for TLR1.*

Seeking to confirm the data using alternative immunoassay platforms, we extended the range of TLR2 agonists. We noted an unexpected selectivity in that only the diacyl and monoacyl TLR2/6 agonists PAM_2CSK_4 and DBS-2-217C, but not the triacyl TLR1/2 agonist PAM_3CSK_4,[165-166] elicited chemokine responses in fibroblasts (Fig. 7B); in contrast, human PBMCs as well as A549

cells responded to TLR1/2 and TLR2/6 agonists (data not shown). In human airway epithelium, for example, TLR1 expression has been observed preferentially on the luminal surface of the tracheal epithelium, while TLR2 and TLR6 appear to be distributed predominantly on basolateral surfaces.[167] We hypothesized that the apparent selectivity could be a consequence of differential TLR expression in fibroblasts. We therefore examined the expression of TLR1, TLR2, and TLR6
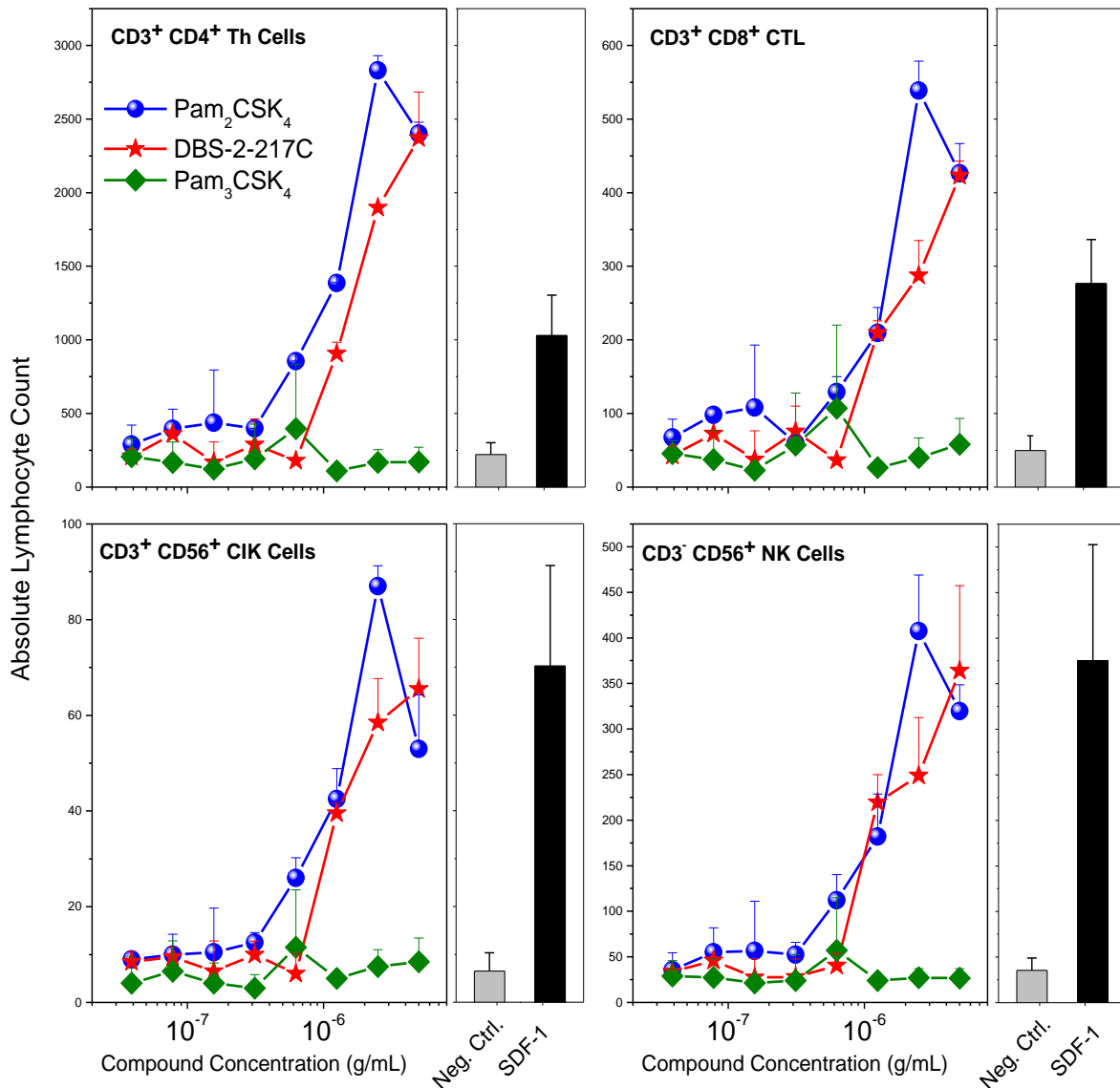
Figure 9. PBMC chemotactic responses to TLR2/6- stimulated human foreskin fibroblasts. *TLR2/6 stimulated HFFs produced functional chemotactic responses from lymphocytic populations. The TLR1/2 agonist failed to induce chemotaxis.*

in fibroblasts, employing tyramide signal amplification[168-169] for enhancing sensitivity of detection. We observed strong expression in fibroblasts of TLR2 and TLR6, but very faint levels of TLR1 (Fig. 8), which is consistent with responses elicited by the TLR2/6 agonists PAM_2CSK_4 and DBS-2-217C, and not by the TLR1/2 agonist PAM_3CSK_4.

In order to verify that TLR2/6 occupancy and the consequent secretion of CC and CXC chemokines in fibroblasts have functional outcomes, we measured the chemotaxis of human PBMCs toward fibroblasts stimulated with TLR2/6 and TLR1/2 ligands. Human SDF-1 was used as a positive control in these experiments. We observed dose-dependent migration of PBMCs toward fibroblasts stimulated with TLR2/6, but not TLR1/2 ligands (Fig. 9).

Flow cytometric assessment of absolute counts of migrated PBMCs showed that T lymphocytic subsets ($CD4^+$ Th cells, $CD8^+$ CTLs, and $CD3^+$ $CD56^+$ cytokine-induced killer cells), but not B lymphocytes ($CD19^+$) underwent chemotaxis (Fig. 9). The induction of chemotactic gradients by adventital cells and consequent migration of immune cells to the site of injection may likely contribute to the strong adjuvantic properties of TLR2/6 agonists.

3.3 Conclusions

A dominant CC chemokine signature (CC chemokines 1, 2, 3, 4, 7, 8, 17, 18, 20, and 23) appears to be a common transcriptional outcome of virtually all immunostimulatory classes of molecules, whereas the CXC chemokine patterns allow for the distinction of extracellular (CXCL5, CXCL6 and CXCL8) vis-à-vis intracellular (CXL11 and CXCL12) TLR/NLR activation. These findings are likely to be useful both in prospectively examining novel compounds for adjuvantic activity,

and in understanding structure-activity relationships in such molecules. TLR2/6 agonists distinguish themselves in being able to activate adventitial cells such as fibroblasts; local secretion of chemokines at the site of immunization, and consequent chemotaxis of immune-competent cells to areas where the local concentrations of immunogens are expected to be initially high likely contribute to the potent adjuvantic properties in these compounds.

3.4 Materials and Methods

Reagents

The following TLR ligands: PAM$_2$CSK$_4$, PAM$_3$CSK$_4$, lipoteichoic acid (LTA), LPS from *P. gingivalis* and *E. coli* 055:B4, Poly (I:C) (high molecular weight), flagellin, CL307, ODN2216, ODN2006, and ODN2395 were purchased (InvivoGen, San Diego, CA). The TLR agonists DBS-2-217C,[156] C4, IMDQ, Meta-amine,[91] EY-2-40,[111] XG-1-236,[97] MB-564, MB-569,[113] MB-152,[100] and KHP-3-126[112] were synthesized using the routes previously described by us. C274[170] was graciously provided by Dynavax Technologies (Berkeley, CA).

Culture of human blood and cell lines

Whole human blood was collected in heparinized vacutainers, and PBMCs were collected and isolated in CPT Vacutainers™ (Becton Dickinson, Franklin Lakes, NJ) from healthy volunteers providing written informed consent in accordance with the University of Minnesota Institutional Review Board approved protocol (IRB Protocol 1506M74641). PBMCs were cultured in RPMI 1640 supplemented with 10% fetal bovine serum, 2 mM penicillin, and 50 µg/mL streptomycin (complete RPMI). Human foreskin fibroblasts (HFFs, ATCC Catalog No. SCRC-1041) were cultured in DMEM supplemented with 10% fetal bovine serum, 2 mM penicillin, and 50 µg/mL

streptomycin (complete DMEM). Cells were cultured in 96-well plates at 37ºC for 3.5-16 h as indicated for that experiment.

Adjuvanticity studies in rabbits

All immunizations were performed in accordance with University of Minnesota IACUC guidelines (Protocol 1601-33398A) by Envigo (Huntington, UK). Cohorts of 4 female New Zealand white rabbits were immunized intramuscularly in the flank with 10 µg antigen (diphtheria toxin mutant CRM197, List Biological Laboratories, Campbell, CA)[147-148] and 100 µg adjuvant in 0.2 mL saline, or antigen alone as published previously by us [171]. Prebleeds were collected for each animal from the marginal vein in the ear. Immunizations were carried out on days 1, 15, and 28 with blood collections on days 25 and 38. Sera was isolated immediately following blood collection and stored at -80ºC until utilized. CRM197-specific antibody titers were evaluated by ELISA as previously reported by us.[171]

Next-generation sequencing of PBMCs

PBMCs were stimulated in 96-well plates for 3.5 h with 1 µg/mL TLR/NLR agonist. Total RNA was isolated using RNeasy 96 kits according to the manufacturer's instructions (Qiagen, Hilden, Germany). Samples were stored in RNase free 96-well PCR plates at -80ºC until used. RNA quality and concentration were determined using Agilent RNA 6000 Nano Kits (Agilent Technologies, Santa Clara, CA) and libraries were generated using Clontech SMARTer Standards Total-RNA Pico Kits (Clontech Laboratories, Inc., Mountain View, CA). Libraries contained inserts of approximately 200 base pairs and averaged quality scores over Q30. Individual TruSeq libraries were pooled into 2 and sequenced across 3 lanes. Next-generation sequencing was carried

out by the University of Minnesota Genomics Center using a HiSeq 2500 (Illumina, San Diego, CA) in high output mode for 13 x 10^6 reads per sample for 50 base pair paired ends using v4 chemistry. Data were calculated as fold change over unstimulated control samples using the EDGE test.[172-173] RNA Seq data is available at the Sequence Read Archive (BioProject ID: PRJNA390780; http://www.ncbi.nlm.nih.gov/bioproject/390780).

Multiplexed cytokine analysis in PBMCs and HFFs

Cytokine and chemokine responses PBMC and HFF were measured using methods previously reported by us[113, 174-175] with the following Milliplex kits: HCYTMAG-60K-PX41, HCYPMAG-63K, and HCYP2MAG-62K (EMD Millipore, Billerica MA). PBMCs or HFFs were seeded at a density of 10^5 cells per well and stimulated for 16 h with graded concentrations of stimuli or mock-stimulated with vehicle (DMSO). Supernatants were collected by Precision 2000 liquid handlers (Bio-Tek, Winooski, VT) and diluted 1:3 for each kit. The data was acquired on a MagPix® instrument and the data analyzed using Milliplex Analyst (EMD Millipore, Billerica MA).

ELISAs for HFF chemokine secretion

HFFs were cultured in 96-well plates at 10^5 cells per well in complete DMEM with graded concentrations of TLR ligands for 16 h at 37ºC. Plates were centrifuged to collect supernatants. Supernatants were diluted 1:5 for CXCL6 ELISAs (Abcam, Cambridge, MA., Catalog number AB155431) and 1:2 for CCL20 ELISAs (Abcam, Cambridge, MA., Catalog number AB100599). The manufacturer's procedures were followed for both types of ELISA and acquired on a SpectraMax M2 (Molecular Devices, Sunnyvale, CA). Concentrations were quantified from four-parameter logistic fits of standard curves for each analyte.

Imaging for TLR1, -2, and -6 in HFFs

HFFs were plated at 10^4 per well in a tissue culture-treated 96-well plate and incubated overnight. Each well was washed 3 times in PBS and then fixed for 10 min at room temperature in 4% paraformaldehyde followed by blocking with 10% goat serum in PBS (recommended blocking buffer for the Tyramide Superboost kit described below) for 1 h at room temperature. Polyclonal anti-TLR1, -2, and -6 antibodies (Abcam, Cambridge, MA., Catalog numbers AB189337, AB191458, AB37072, respectively) were utilized at 1:100 dilutions in 100 µL blocking buffer to stain cells for 1 h at room temperature, followed by 1 h of incubation with goat-anti-rabbit-HRP antibody conjugate. Tyramide signal amplification was carried out for 5 min according to the Tyramide SuperBoost kit's manufacturer (Invitrogen, Carlsbad, CA., Catalog number B40922). Samples were counterstained with 100 ng of DAPI and imaged at the University of Minnesota Imaging Center using a Nikon A1R confocal microscope with a 60X water immersion objective with a numerical aperture of 1.20.

PBMC Chemotaxis with HFFs

HFFs were plated at 10^6 per well in an IncuCyte ClearView 96-well reservoir plate (Essen Bioscience, Ann Arbor, MI) in complete DMEM and cultured for 16 hours. Following incubation, the cells were stimulated with graded concentrations of TLR agonists for 24 h. An IncuCyte ClearView chemotaxis plate was coated with 0.5 mg/mL Matrigel (Corning Life Sciences, Corning, NY., Catalog number 354248) in complete RPMI on ice. Matrigel polymerization was carried out for 30 minutes at 37ºC, and then the chemotaxis plate was cooled to room temperature for 1 h. PBMCs were plated in 60 µL of complete RPMI in the top well of the chemotaxis plate. The top of the chemotaxis plate was placed on the reservoir plate containing HFFs and cultured

for 16 h at 37ºC. After the incubation, the bottom reservoir plate was stained with CD3-PE and CD56-APC (eBioscience, San Diego, CA., Catalog numbers 12-0037-42 and 17-0566-42, respectively), CD4-V450, CD8-V500, CD14-FITC, and CD19-PE-Cy7 (Becton Dickinson, Franklin Lakes, NJ., Catalog numbers 560345, 560774, 555397, 557835, respectively). Erythrocytes were lysed and leukocytes fixed by transferring 200 µL of PBMCs to 800 µL of warm Lyse/Fix buffer (Becton Dickinson, Franklin Lakes, NJ) in a 96-deep well plate by liquid handler for 10 min at 37ºC. The fixing process was carried out one additional time before washing with 800 µL complete RPMI. Samples were resuspended in 200 µL of complete RPMI, and acquired on a FACSVerse flow cytometer (Becton Dickinson, Franklin Lakes, NJ) for 250,000 gated events. Absolute counts were recorded by an inline flow sensor for lymphocytes (FSC, SSC), T cells (CD3$^+$ CD56$^-$), Th cells CD3$^+$ CD4$^+$ CD8$^-$ CD56$^-$), CTLs (CD3$^+$ CD4$^-$ CD8$^+$ CD56$^-$), NK cells (CD3$^-$ CD56$^+$), B cells (CD3$^-$ CD19$^+$ CD56$^-$), cytokine-induced killer cells (CIK) (CD3$^+$ CD56$^+$), and monocytes (CD14$^+$).

Chapter 4.

Protective Responses against *Mycobacterium tuberculosis* Induced by ESAT-6 Immunization with a Toll-like Receptor 2/7 Hybrid Agonist
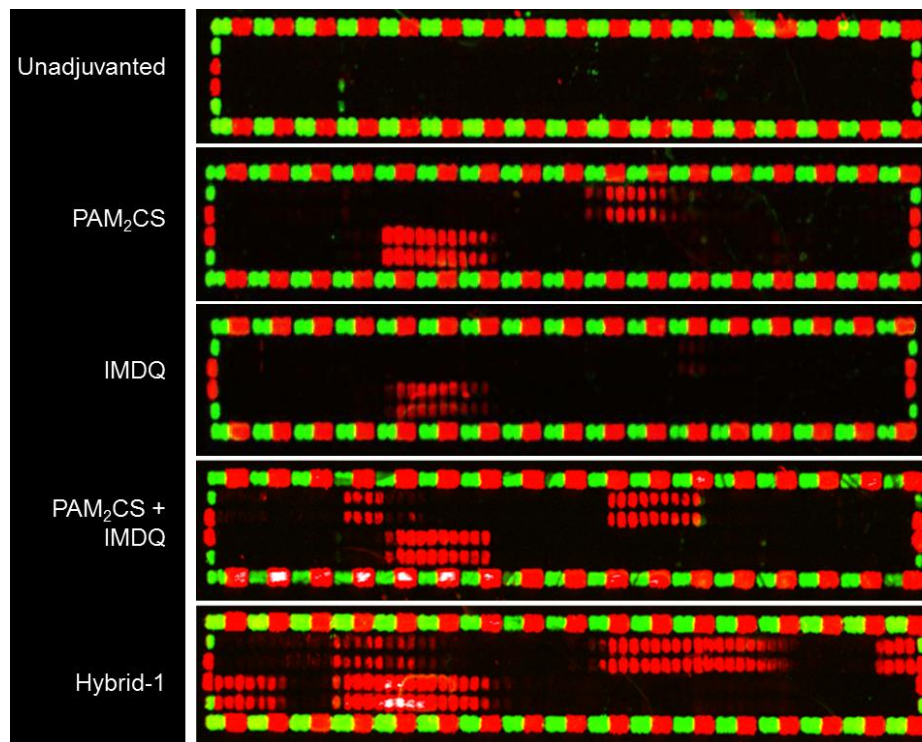
4.1 Introduction

Tuberculosis (TB) is one of the most prevalent infections worldwide, with an estimated one-third of the world's population infected and 1.3 million TB-related deaths per year.[176] The threat posed by TB has been compounded in recent years by the emergence of multidrug-resistant tuberculosis for which few promising candidate drugs have been identified in the development pipeline.[177] As with the majority of transmissible infectious diseases, vaccination may be a cost-effective and practical strategy to reduce the global burden of TB.

The live attenuated *M. bovis*-derived Bacille Calmette-Guérin (BCG) is the only currently approved vaccine for TB. While BCG was shown to be effective in preventing up to 70% of miliary TB and TB meningitis when administered within several days of birth,[178] the efficacy of BCG appears to be highly variable in preventing pulmonary TB in adult populations, with clinical trials ranging from 0-80% success.[179-182] The limitations of the BCG vaccine and a renewed need for vaccines providing durable protection against pulmonary disease have spurred the exploration of new vaccine constructs, many of which are subunit vaccines.[176] As mentioned in Chapter 1, modern subunit vaccines utilize highly purified immunogens of defined composition, facilitating the ease of production and quality control. However, such immunogens are often poorly immunogenic and fail to induce strong, protective memory responses, necessitating the inclusion of vaccine adjuvants to induce robust, long-lived immunological memory.[183-185]

Despite the widespread use of BCG in developing countries aimed at reducing the burden of extra-pulmonary disease, the correlates of protection for TB in humans are poorly understood.[186-187] It is believed that TB-specific CD4$^+$ T helper cell-mediated immune responses (Th1),[188-189] and not

antibody-mediated humoral immunity is essential for the control of TB. There is, however, evidence that TB directly engages TLR2[190] which, as was discussed previously (Chapter 3), is still under investigation to determine the nature of T cell polarization (Th1 or Th2), and could potentially result in Th2 polarization during natural infections.[191]

We hypothesized that mimicking the TLR2 engagement observed for TB, and additionally enhancing the immunostimulation by the addition of Th1-biasing TLR7/8 agonist, could yield a hybrid poly-TLR vaccine adjuvant for TB possessing TLR2/7/8 activity. Furthermore, of the several hundred compounds that we have examined to date, we have found that TLR2 agonists,[87-88, 192-193] as well as TLR7/8 agonists,[39, 91, 93, 96-97, 194-195] were highly potent in immunogenicity screens in rabbits. We therefore elected to focus on 'hybrids' of TLR2 and TLR7 agonists. Proof-of-concept studies with such a TLR2/7 hybrid molecule indicated potent adjuvantic activity. Epitope mapping experiments showed that the hybrid adjuvant induced immunoreactivity to more contiguous peptide epitopes in a model antigen. Immunization of mice with the *M. tuberculosis* antigen ESAT-6 adjuvanted with a water-soluble analogue of the hybrid elicited reductions in pulmonary mycobacterial loads.

4.2 Results and Discussion

Poly-TLR adjuvants have been explored recently in studies which showed that combining a TRIF-biased TLR4 agonist (MPLA)[196] and a TLR7 agonist (imidazoquinoline) enhanced antibody and T cell responses.[197] Concurrent engagement of a TRIF-coupled TLR in combination with an

endosomal TLR appears to be pivotal in synergistically upregulating IL-12p70 production in dendritic cells; this synergy is lost when the two individual stimuli are delivered 24 hours apart.[198] These and other studies[199-201] suggest that particular combinations of TLR agonists are more effective than others and, importantly, highlight the need for efficient, simultaneous delivery of the individual innate immune stimuli to the antigen-presenting cell.

Recently, Gutjahr and coworkers demonstrated synergistic activity using a covalently linked TLR2 and TLR7 agonists.[202] We therefore set out to build upon the studies of poly-TLRs conducted by other groups,[199-201] and we selected a best-in-class imidazoquinoline (compound **1**, IMDQ), which possess potent TLR7/8 activity, and the TLR2 agonist PAM$_2$CS (compound **6**) to covalently link together and form a hybrid poly-TLR agonist, as is shown in Scheme 1).

Scheme 1
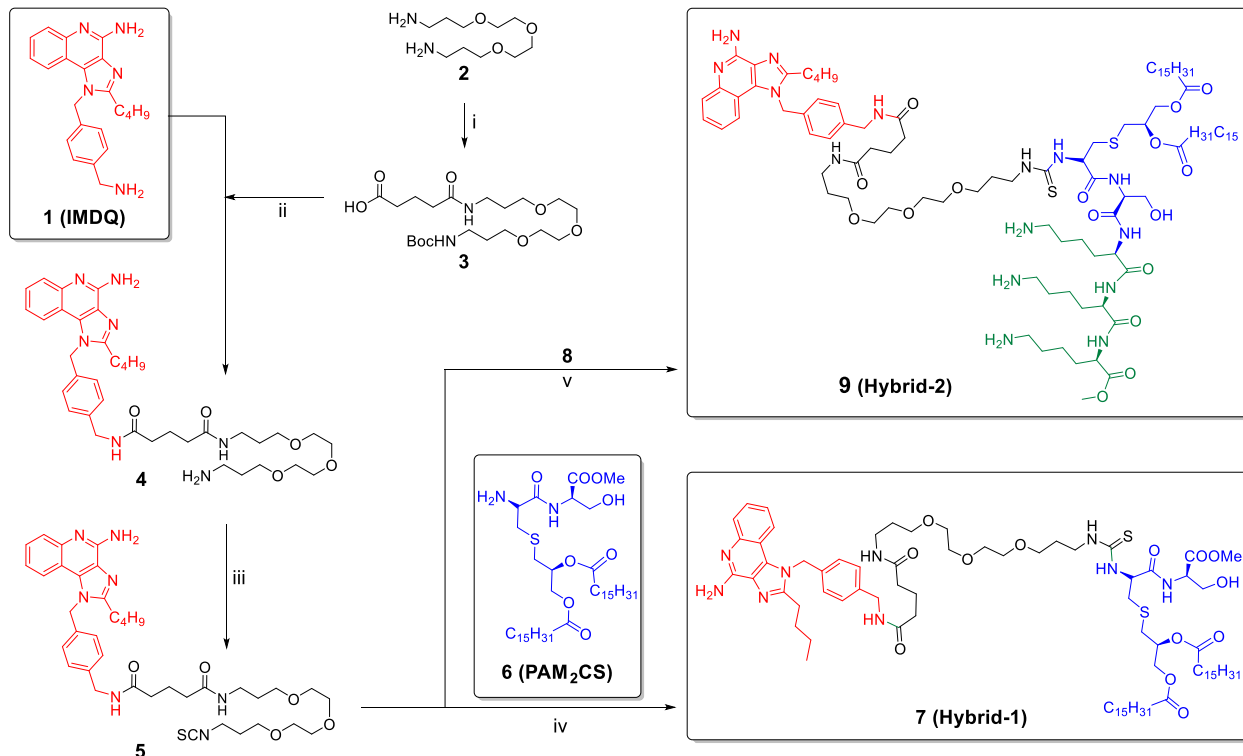
Reagents and conditions: i. (a) 0.9 equivalent (Boc)$_2$O, (b) Glutaric anhydride, Et$_3$N, THF; ii. (a) Et$_3$N, HBTU, DMF, (b) 4M HCl/dioxane; iii. CS$_2$, Et$_3$N, (Boc)$_2$O, DMAP, CH$_2$Cl$_2$; iv. Pyridine, 45 ^{o}C; v. (a) Pyridine, 45 ^{o}C (b) SnCl$_4$, CH$_2$Cl$_2$.

Initially, a Boc-protected polyoxyethylene linker with a free carboxylic acid was appended to the benzylic amine of IMDQ using an amide-bond coupling reagent HBTU. Following Boc-deprotection, the resulting primary amine was reacted sequentially with carbon disulfide and di-*tert*-butyl dicarbonate in the presence of catalytic amounts of DMAP to yield the isothiocyanate compound **5**. Compound **5** was directly reacted with PAM₂CS under mildly basic conditions to yield compound **7** (Hybrid-1). The water soluble analog Hybrid-2 was synthesized from compound **5** and a tris-Boc-protected trilysine analog of PAM₂CS (synthesized as shown in Scheme 2) under identical conditions, involving an additional mild Boc-deprotection protocol using Tin(II) choride (synthesis was conducted by Dr. Nikunj Shukla).

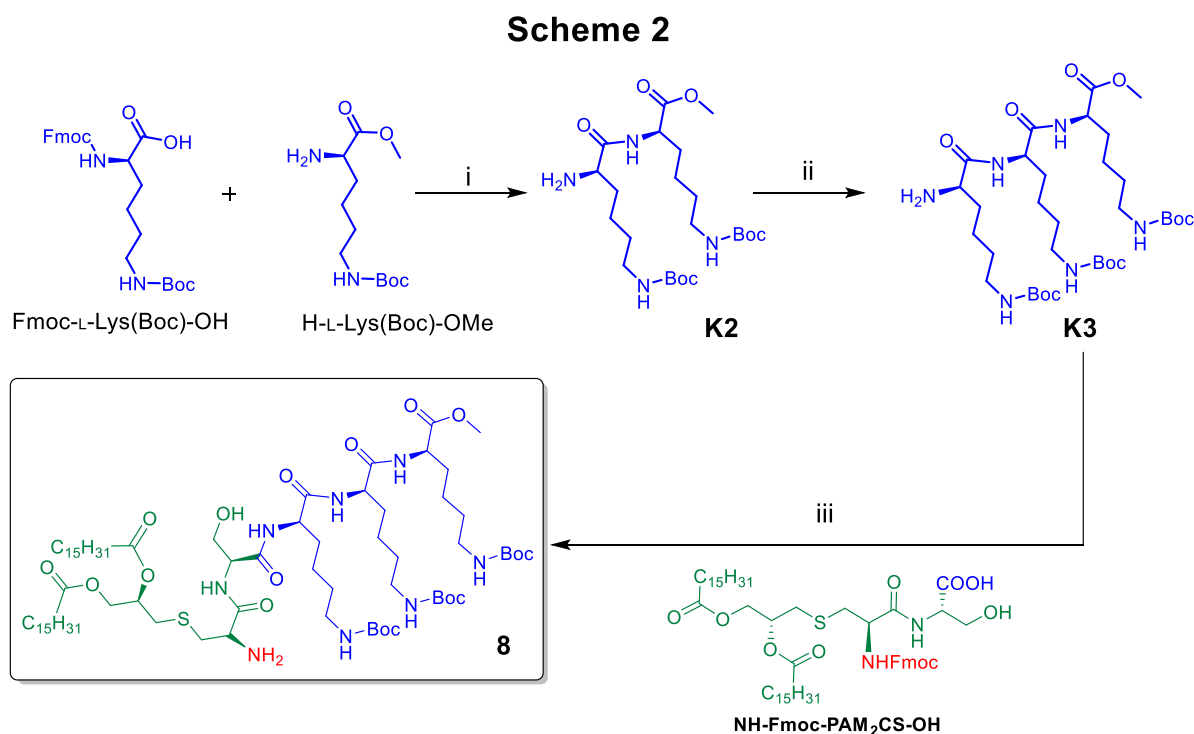## Scheme 2

Figure S1. Reagents and Conditions for compound 8: i. (a) HBTU, pyridine, DMF (b) Piperidine; ii. (a) Fmoc-L-Lys(Boc)-OH, HBTU, pyridine, DMF; (b) Piperidine; iii. (a) HBTU, pyridine, DMF; (b) Piperidine.

Following the successful conjugation of IMDQ and PAM2CS, we examined the TLR activity profiles of Hybrid-1 and Hybrid-2 in human-specific TLR reporter cell lines to ensure that there was retention of TLR2 and TLR7 activity. The TLR2-active PAM2CS has an EC_{50} (half-maximal effective concentration) of 1 nM in TLR2 reporter cells, and IMDQ exhibits EC_{50} values of 10 nM and 300 nM in TLR7 and TLR8 reporter cells, respectively (Fig. 1).[87, 91] Hybrid-1 retained activity
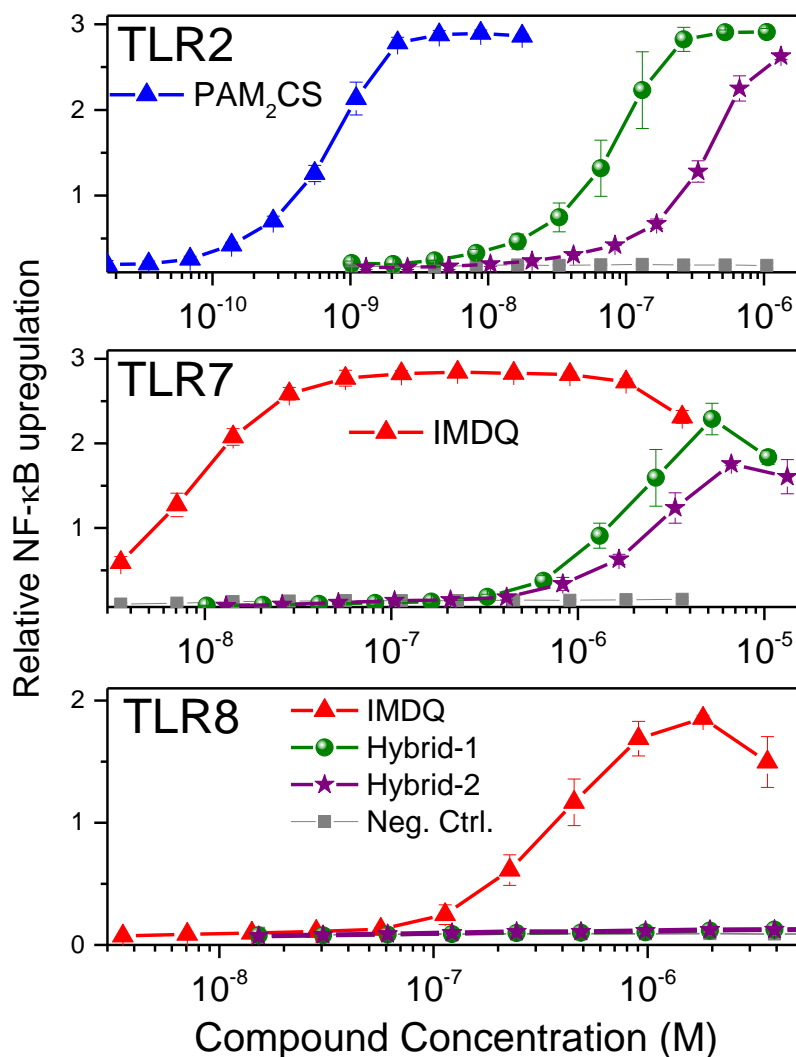

Figure 1. TLR activity profile of Hybrid-1 in human-specific TLR reporter assays. *Hybrid-1 and Hybrid-2 were active in TLR2- and TLR7-specific human TLR reporter cells, but with a loss of potency at both targets relative to the parent compounds, IMDQ and PAM₂CS. All activity was lost in TLR8 for both hybrids. Mean and standard deviations of quadruplicates are shown.*

in TLR2 and TLR7, but with reduced potencies of 100 nM and 10 μM, respectively; Hybrid-2 was slightly less potent than Hybrid-1 with potencies of 300 nM and 20 μM in TLR2 and TLR7, respectively. The losses in activity at TLR2 and TLR7 for the hybrid compounds could be derived from the substantial increases in the size of the molecules resulting in reduced membrane permeability and possible steric hindrance at the receptors. Previously, we had shown that the benzylic amine of IMDQ was required for TLR8 activity[92] and, as expected, utilizing this amine of IMDQ for the conjugation to the TLR2 agonists resulted in the complete loss of all TLR8 activity in the conjugates (Fig. 1).

IMDQ and PAM$_2$CS were previously shown to be potent adjuvants individually during the course of their respective structure-activity relationship studies, but the TLR agonists were not evaluated during those studies in combination for synergistic adjuvanticity. We therefore examined the TLR agonists individually and in combination for adjuvanticity in a standardized rabbit immunization model. Each cohort of rabbits was primed and boosted twice at 15 day intervals with 10 μg of bovine α-lactalbumin antigen and 100 μg of adjuvant. As we anticipated, IMDQ and PAM$_2$CS both elicited high anti-α-lactalbumin-specific IgG titers individually (Fig. 2A). A 1:1 mixture of IMDQ and PAM$_2$CS also resulted in high antibody titers, but with more variability than the individual TLR agonists. Hybrid-1 was equipotent to either of the individual TLR agonists with respect to humoral responses, but showed increased variability similar to the mixture of IMDQ and PAM$_2$CS (Fig. 2A).

We were not able to determine clear differences between the various TLR agonists by only examining α-lactalbumin-specific antibody titers (Fig. 2A), so we examined the quality of the
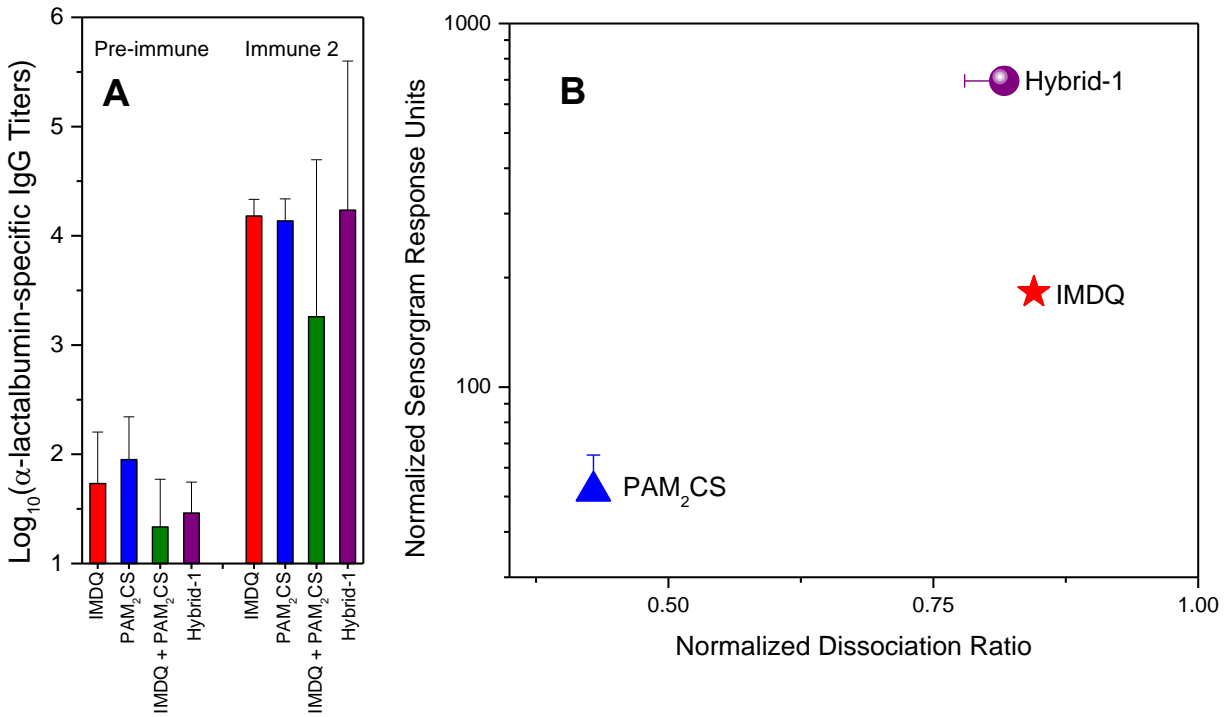
Figure 2. Hybrid-1 induced strong humoral responses in rabbits immunized with α-lactalbumin. A. Cohorts of 3 rabbits were primed and boosted twice at 15 day intervals with 10 µg/dose of bovine α-lactalbumin and 100 µg/dose adjuvant. Sera was isolated from the rabbits prior to immunization (Pre-immune) and on day 38 (Immune 2). IMDQ, PAM₂CS, and Hybrid-1, along with the mixture of IMDQ and PAM₂CS, were equally adjuvantic at 100 µg/dose in rabbits. B. Bovine α-lactalbumin was immobilized on SPR chips to determine the quality of the Immune 2 sera elicited by the various TLR agonists. Evaluation of the antibody quality revealed that Hybrid-1 induced high quality antibodies to bovine α-lactalbumin with high dissociation ratios and sensorgram responses. Mean and standard deviations of the three rabbits in each cohort are shown.

antibodies generated by each adjuvant using surface plasmon resonance (SPR). The protein antigen α-lactalbumin was immobilized on the chip and the various immune sera were washed over the immobilized antigen. Dissociation ratios were calculated from the ratio of the responses at 15 seconds and 500 seconds. Sera from Hybrid-1 yielded high dissociation ratios and sensorgram responses relative to either PAM₂CS or IMDQ (Fig. 2B). IMDQ adjuvanted animals yielded

antibodies of intermediate quality relative to Hybrid-1 with high dissociation ratios, but lower sensorgram responses, while PAM$_2$CS resulted in antibodies with the lowest dissociation ratios and sensorgram responses. Hybrid-1 appeared to drive the highest quality of antibody to the model antigen α-lactalbumin.

We continued to examine the antibodies generated against α-lactalbumin by the TLR2/7 hybrid against the mixture of IMDQ and PAM$_2$CS by conducting linear epitope mapping of the immune sera. Thirteen-mer peptides with overlaps of 12 amino acids covering the entire sequence of α-lactalbumin were printed in duplicate on chips. Alternating Flag and hemagglutinin control peptides were printed in a boarder surrounding the α-lactalbumin peptides. Chips were then incubated with immune sera followed by fluorescent secondary antibodies to evaluate linear epitopes to α-lactalbumin. Five representative fluorescence images are shown in Fig. 3A, with control Fusion Tag (Flag, DYKDDDDKGG) peptides in green and hemagglutinin peptides (YPYDVPDYAG) in red bordering the peptide arrays. Sera from rabbits immunized with α-lactalbumin alone failed to show any signals above baseline, while sera from all cohorts adjuvanted with Hybrid-1 or IMDQ and PAM$_2$CS, either individually, or in combination, recognized linear peptide epitopes (Fig. 3A). A comparison of Hybrid-1 adjuvanted samples with the mixture of IMDQ and PAM$_2$CS revealed that Hybrid-1 induced immunoreactivity to more contiguous epitopes of α-lactalbumin, with epitope spreading observed through amino acids 50-58 and 62-75 relative to sera from rabbits adjuvanted with the IMDQ and PAM$_2$CS mixture (Fig. 3B). The induction of epitope spreading by vaccine adjuvants has been shown to be important in eliciting cross-protective responses to viruses, such as influenza and the human papillomavirus.[203-204]
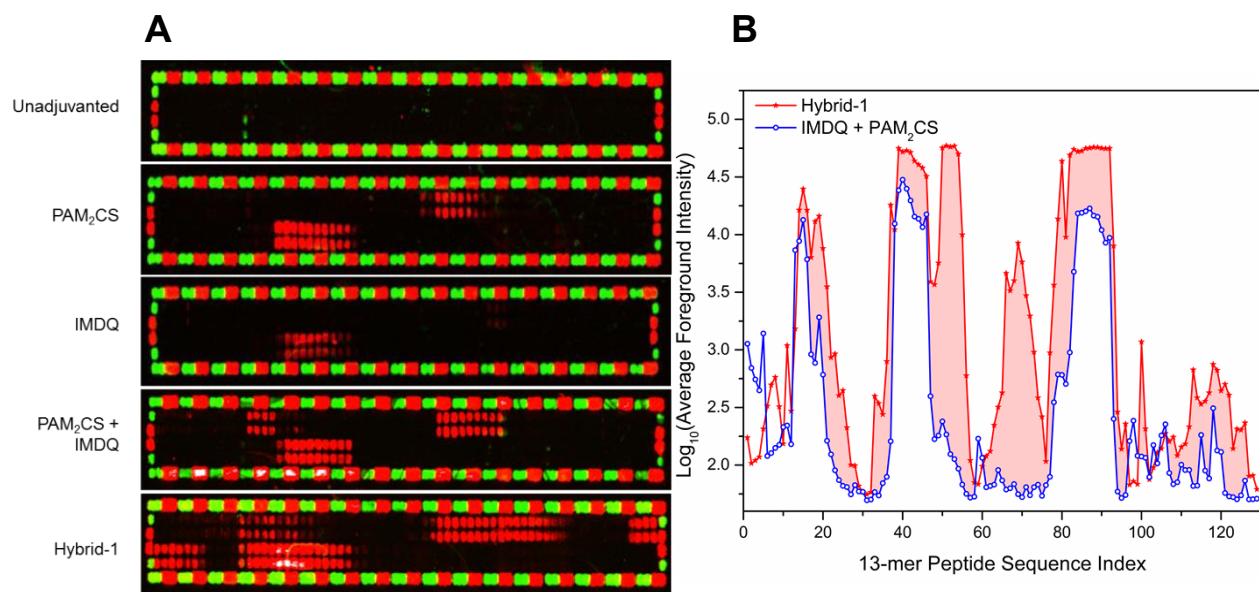
Figure 3. Hybrid-1 induced linear epitope spreading. A. 13-mer overlapping peptides covering the full sequence of α-lactalbumin were printed on chips in duplicates with boarders of Flag and hemagglutinin peptides as controls. Immune Sera from the 3 rabbits in each cohort was incubated with the chips. Green and red fluorescent borders for each chip represent control Flag peptide and hemagglutinin peptide, respectively. Representative raw fluorescence images are shown for sera from IMDQ, PAM₂CS, Hybrid-1, mixtures of IMDQ and PAM₂CS, and unadjuvanted control immunized rabbits. B. Rabbits immunized with α-lactalbumin reacted to more linear epitopes when adjuvanted with Hybrid-1 compared to any of the other cohorts. Representative data from 1 rabbit immunized with Hybrid-1, and 1 rabbit immunized with the mixture of IMDQ and PAM₂CS are shown.

Epitope spreading has also been observed in *M. tuberculosis* antigens,[205] but remains of unknown value for TB vaccines, as there have been no successful subunit vaccines approved for TB.

The high quality of the antibodies generated with the TLR2/7 hybrid molecule (Fig. 2) and the exposure of cryptic epitopes (Fig. 3) pointed to the potential superiority of the covalently linked TLR stimuli at inducing humor responses. One possibility for the superior humoral responses elicited by the covalently linked TLR2/7 hybrid over the mixture of TLR ligands is direct

activation of both TLR2 and TLR7 within the same cell. While TLR2 and TLR7 possess distinct localization patterns on the plasma membrane and within endosomes, respectively,[206] there is growing evidence of TLR2 internalization and trafficking to endosomes following ligation.[207-209] Given the superior activity of the TLR2/7 hybrids at eliciting humoral responses in rabbits using a model antigen, we sought to evaluate their potential as vaccine adjuvants using models more relevant to *M. tuberculosis*. MPLA formulated in dimethyldioctadecyl-ammonium bromide (DDA) liposomes was previously shown to induce protective adaptive immune responses when administered as an adjuvant with the secreted *M. tuberculosis* antigens ESAT-6 and Antigen-85.[210-213] Furthermore, previous work by others revealed the immunostimulation derived from this adjuvantic formulation induced balanced Th1/Th2 responses.[212-213] With this in mind, we aimed to determine if our TLR2/7 hybrid was able to mimic the immunostimulatory profile of the MPLA DDA liposome formulation, and ultimately induce protective responses to *M. tuberculosis*. Cohorts of three C57BL/6 mice were immunized three times at two-week intervals with 10 µg of ESAT-6 as antigen and 20 µg of adjuvant, which was found to be optimal from pilot experiments conducted by the lab of Dr. Marc Jenkins (data not shown). MPLA formulated in DDA liposomes was used as a reference control. We selected the water-soluble Hybrid-2 for these studies to eliminate potential confounding effects of AddaVax, which Hybrid-1 had to be formulated in.

Four weeks following the final immunization the axillary lymph nodes and spleens were harvested for ESAT-6-specific tetramer enrichment of T helper cells. Singlet cells were selected by FSC-A/FSC-W and SSC-A/SSC-W and, from the singlet cells, effector memory T helper cells were further defined as CD90.2$^+$ CD4$^+$ CD44$^+$. ESAT-6-specific effector memory T cells were identified by tetramer staining and categorized as T regulatory (Treg), Th1, Th17, and T follicular

Figure 4. ESAT-6-specific T cell analysis of polarization. A. Mice (n = 3 per cohort) were primed and boosted twice at two week intervals with 10 μg/dose of ESAT-6 antigen and 20 μg/dose adjuvant. Mice were sacrificed four weeks following the final immunization and the spleen and lymph nodes were harvested to examine ESAT-6-specific T cell populations. Singlet cells were selected by FSC-A/FSC-W and SSC-A/SSC-W. Effector memory T helper cells were further defined as CD90.2+
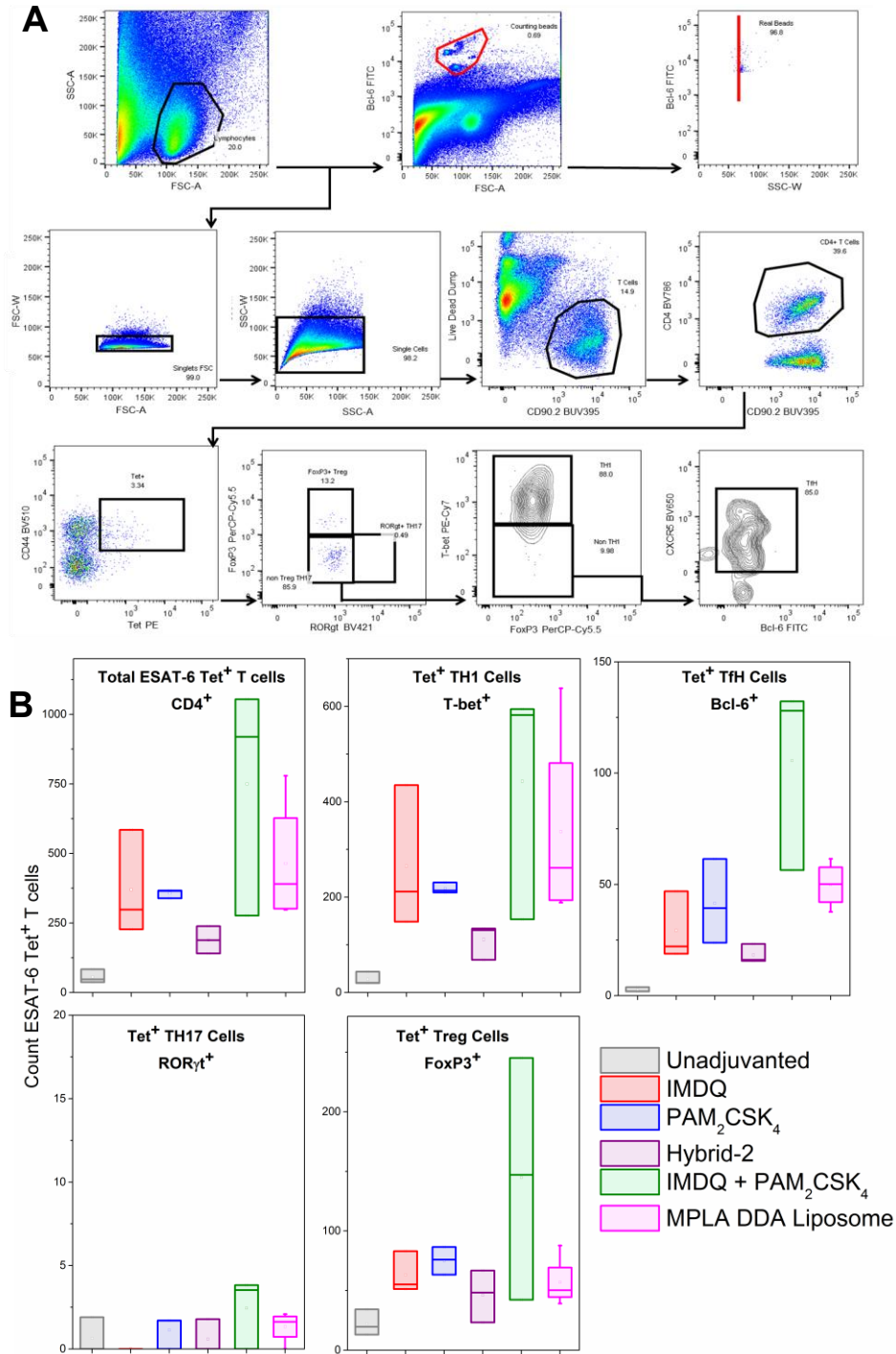
CD4+ CD44+. ESAT-6-specific effector memory T cells were identified by tetramer staining and categorized as T regulatory (Treg), Th1, Th17, and T follicular helper (Tfh) ce lls based on the expression of FoxP3, T-bet, RORγt, and Bcl-6, respectively. B. None of the adjuvants examined were significantly different from one another. Small cohort size limited the applicability of the data.

helper (Tfh) cells based on the expression of FoxP3, T-bet, RORγt, and Bcl-6, respectively (Fig. 4A). However, our efforts to gain insight into ESAT-6-specific T cells were hampered by small cohort sizes, and we were not able to observe statistically significant differences between the cohorts in any of the cell populations (Fig. 4B).
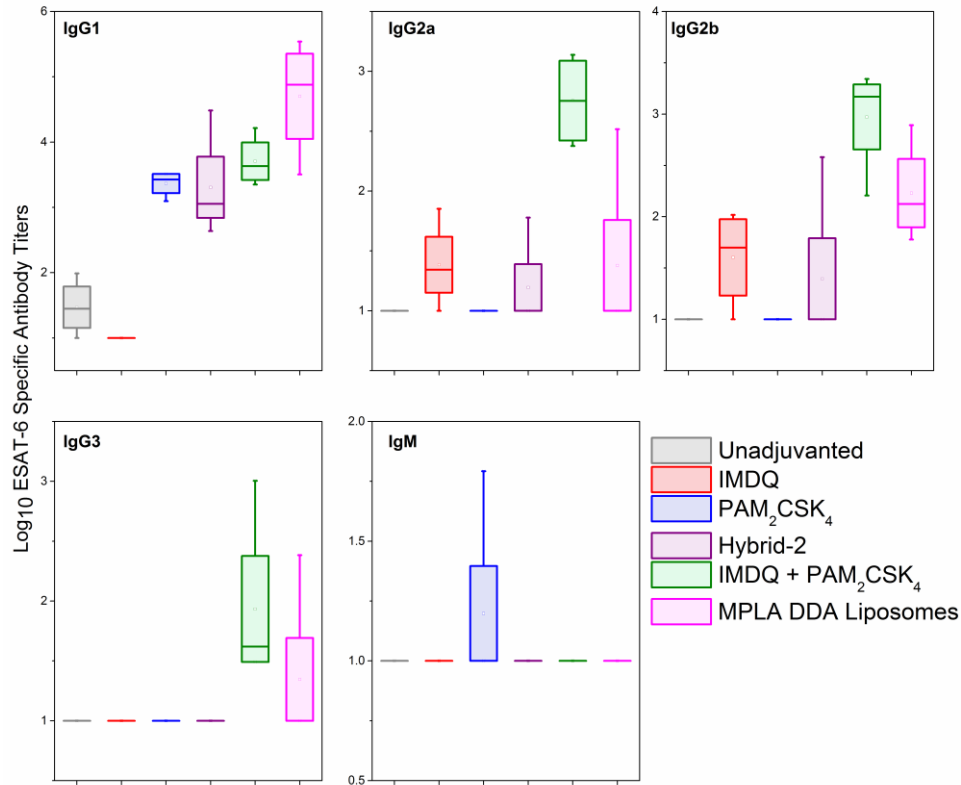
Figure 5. ESAT-6-specific antibody isotypes. *Blood was collected by cardiac puncture from the mice immunized with ESAT-6 and various adjuvants mentioned above, and was analyzed by ELISA for ESAT-6-specific antibody isotypes. The same limited cohort sizes and animal variability resulted in non-significant data.*

In parallel to the T cell analysis, we attempted to examine immune sera collected from the mice immunized above to examine ESAT-6-specific antibody isotypes for characterization of the Th1/Th2 polarization induced by the various TLR agonists. IgG1, IgG2a, IgG2b, IgG3, and IgM ESAT-6-specific titers were evaluated by ELISA. While there appeared to be distinctions between the Th2-driven IgG1 titers,[214] and the Th1-driven IgG2a and IgG2b titers,[215] the small cohort size

and variability between the individual mice within the cohorts resulted in data that failed to reach statistical significance (Fig. 5).
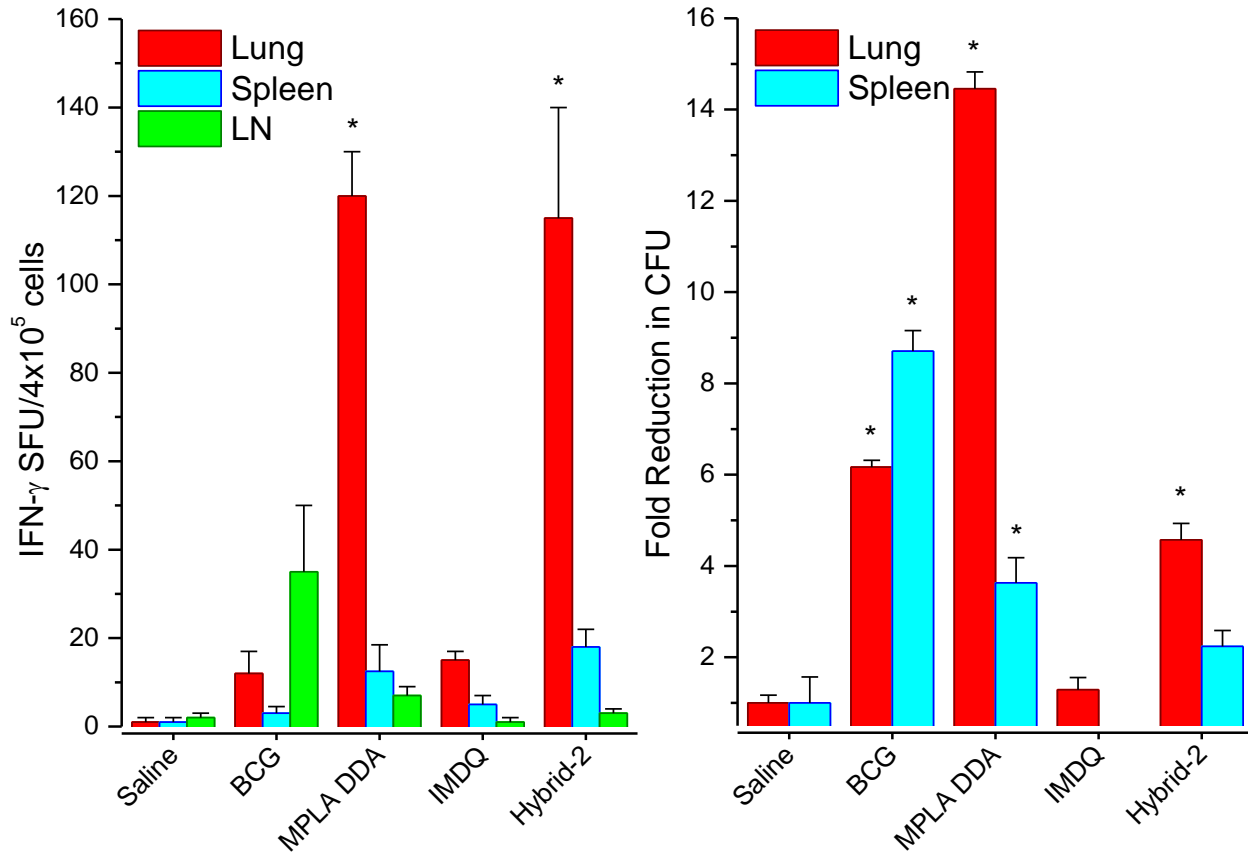
***Figure 6. Functional responses in mice immunized with ESAT-6.*** *Mice (n = 10 per cohort) were primed and boosted twice at two week intervals with 10 µg/dose of ESAT-6 antigen and 20 µg/dose adjuvant. **A.** Five mice from each cohort were sacrificed four weeks following the final boost. Lungs, spleen, and lymph nodes were harvested to examine ESAT-6-specific T cells in the tissues by ELISpot. MPLA DDA liposomes and Hybrid-2 both induced significant numbers of ESAT-6-specific IFN-γ SFUs in the lungs of mice. **B.** The remaining five mice per cohort were infected with approximately 100 bacilli of M. tuberculosis H37Rv each by aerosol. Four weeks following challenge, the mice were sacrificed and the lungs and spleens were analyzed for colony forming units (CFUs) of M. tuberculosis. BCG, MPLA DDA liposomes, and Hybrid-2 all reduced mycobacterial loads in the lungs of the mice. BCG and MPLA DDA liposomes additionally reduced CFUs in the spleen of the mice. IMDQ failed to show any reduction in mycobacterial loads. Mean and standard deviations are shown for each of the 5 mice. (* P<0.05)*

While we were unable to gain insight into ESAT-6-specific cellular and humoral immunity, because of small sample sizes, we opted to examine functional responses of Hybrid-2-adjuvanted ESAT-6 immunizations in a TB challenge study in collaboration with Dr. Angelo Izzo. Mice were immunized with 10 µg ESAT-6 and 20 µg adjuvant three times at two-week intervals. Four weeks following the final immunization the mice were either sacrificed to examine ESAT-6-specific IFN-γ spot-forming units (SFU) in lungs, spleen, and lymph nodes, or were challenged with aerosolized *M. tuberculosis* and sacrificed four weeks later to evaluate *M. tuberculosis* colony-forming units (CFU) in the lungs and spleen. BCG was used as a positive control and MPLA DDA liposomes were used as a reference control. Saline was used as a negative control. MPLA DDA liposomes increased the SFUs in the lungs to 120 SFUs per $4x10^5$ cells (Fig. 6A). The heavy bias to the lungs that was observed for the MPLA DDA liposomes was also observed for Hybrid-2. Hybrid-2 increased the SFUs in the lungs to identical levels as the MPLA DDA liposomes. BCG and IMDQ failed to elicit significant SFUs in any of the tissues.

There appeared to be a connection between the increases in SFUs in the lungs induced by MPLA DDA liposomes and Hybrid-2, but not BCG, with functional reductions in mycobacterial loads in the lungs following challenge with *M. tuberculosis* H37Rv (Fig. 6B). Hybrid-2 adjuvanted mice showed significant reductions in the lungs of 5-fold, while MPLA DDA liposomes reduced the CFUs in the lungs by 15-fold, with additional reductions in the spleen of 4-fold. BCG, on the other hand, showed balanced reductions in CFUs in both the lungs and spleen of mice, with reductions of 6-fold and 8-fold, respectively. The TLR7/8 agonist IMDQ failed to induce protective responses in the mice, and reduced the CFUs in neither the lungs nor the spleen (Fig. 6B). The reductions in

mycobacterial load in the lungs of mice adjuvanted with Hybrid-2 are comparable to that elicited by BCG, and merits further investigation.

4.3 Conclusions

In conclusion, poly-TLR agonists can be synthesized from the repertoire of existing small-molecule TLR agonists. The resulting hybrid molecules we synthesized retained TLR2/7 activity, but at the expense of all TLR8 activity. Using model antigens, Hybrid-1 was able to induce antibody titers equivalent to either individual TLR agonists, but at a higher quality. The water-soluble Hybrid-2 was able to elicit reductions in mycobacterial burdens when administered prophylactically with ESAT-6. However, our attempts to gain insight into the mechanisms of adjuvanticity were stymied by small cohort sizes and variability within the animals. More robust studies with larger cohorts will need to be conducted before correlations between protection and immunogenicity can be observed.

4.4 Materials and Methods

Chemistry Reagents

Synthesis was conducted by Dr. Nikunj Shukla. All of the solvents and reagents used were obtained commercially and used as such, unless noted otherwise. Moisture- or air-sensitive reactions were conducted under nitrogen atmosphere in oven-dried (120 ℃) glass apparatus. The solvents were removed under reduced pressure using standard rotary evaporators. Flash column chromatography was carried out using RediSep Rf 'Gold' high performance silica columns on CombiFlash® Rf instrument (Teledyne Isco Inc, Lincoln, NE) unless otherwise mentioned, while thin-layer chromatography was carried out on silica gel (200 μm) CCM pre-coated aluminum sheets. Purity for all final compounds was confirmed to be greater than 97% by LC-MS using a

Zorbax Eclipse Plus 4.6 mm x 150 mm, 5 μm analytical reverse phase C18 column with H_2O-CH_3CN gradient on either Shimadzu LC (Shimadzu Corp., Kyoto, Japan) or Agilent LC combined with an Agilent ESI-TOF mass spectrometer (Agilent Technologies, Santa Clara, CA; mass accuracy of 10 ppm) operating in the positive ion acquisition mode.

*Synthesis of Compound **1** (IMDQ)*

Compound **1** (1-(4-(aminomethyl)benzyl)-2-butyl-1*H*-imidazo[4,5-*c*]quinolin-4-amine) was synthesized as described previously.[91]

*Synthesis of Compound **4***

To a solution of compound **2** (purchased from Matrix Science, Columbia, SC; 500 mg, 2.3 mmol) in anhydrous dichloromethane was added, di-*tert*-butyl dicarbonate (454 mg, 2.08 mmol) and the reaction was stirred for 1 hour, followed by removal of the solvent under vacuum. The residue was then dissolved in anhydrous THF and triethylamine (52 mg, 5.2 mmol) and glutaric anhydride (445 mg, 3.9 mmol) were added. The reaction mixture was stirred for 2 hours followed by removal of the solvent under vacuum to obtain the crude residue which was purified using column chromatography (20% MeOH/dichloromethane) to yield compound **3** (400 mg, 41%). To a solution of **3** (125 mg, 0.23 mmol) in anhydrous DMF were added, triethylamine (60 mg, 0.59 mmol), HBTU (98 mg, 0.26 mmol) and the imidazoquinoline **1** (100 mg, 0.23 mmol). The reaction mixture was stirred for 12 hours followed by removal of the solvent under vacuum. The residue was purified using flash chromatography (20% MeOH/CH_2Cl_2) to obtain the *N*-Boc protected intermediate. *N*-Boc deprotection was carried out by stirring in 1 mL of 4M HCl/dioxane solution for 6 hours followed by removal of the solvent under vacuum to obtain hydrochloride salt of

compound **4**, *N*1-(4-((4-amino-2-butyl-1*H*-imidazo[4,5-*c*]quinolin-1-yl)methyl)benzyl)-*N*5-(3-(2-(2-(3-aminopropoxy)ethoxy)ethoxy)propyl)glutaramide (140 mg, 80%). ^{1}H NMR (500 MHz, MeOD) δ 7.96 (dd, J = 8.4, 0.7 Hz, 1H), 7.75 (dd, J = 8.4, 0.8 Hz, 1H), 7.63 (ddd, J = 8.4, 7.3, 1.2 Hz, 1H), 7.36 (ddd, J = 8.4, 7.3, 1.1 Hz, 1H), 7.27 (d, J = 8.3 Hz, 2H), 7.05 (d, J = 8.2 Hz, 2H), 5.93 (s, 2H), 4.32 (s, 2H), 3.67 – 3.59 (m, 8H), 3.59 – 3.54 (m, 2H), 3.49 (t, J = 6.1 Hz, 2H), 3.22 (t, J = 7.0 Hz, 2H), 3.08 (t, J = 6.4 Hz, 2H), 3.02 – 2.96 (m, 2H), 2.21 (dt, J = 21.1, 7.6 Hz, 4H), 1.94 – 1.80 (m, 6H), 1.73 (dd, J = 13.4, 6.5 Hz, 2H), 1.45 (dd, J = 15.0, 7.5 Hz, 2H), 0.94 (t, J = 7.4 Hz, 3H). 13C NMR (126 MHz, MeOD) δ 175.35, 175.26, 159.05, 150.46, 140.34, 137.61, 135.34, 135.23, 130.95, 129.50, 126.84, 126.42, 125.88, 122.97, 119.60, 114.22, 71.39, 71.09, 71.05, 71.00, 70.39, 69.65, 49.83, 43.54, 40.17, 37.66, 36.31, 36.20, 30.50, 30.34, 28.05, 27.76, 23.32, 23.28, 14.10. MS (ESI-TOF) for $C_{37}H_{53}N_7O_5$ [M + H]$^+$ found 676.4270, calculated m/z 676.4181; [M + 2H]$^{+2}$ found 338.7178, calculated 338.7127.

Synthesis of Compound 5

To a solution of compound **4** (140 mg, 0.19 mmol) in anhydrous dichloromethane, were added carbon disulfide (143 mg, 1.89 mmol) and triethylamine (47 mg, 0.469 mmol). The reaction mixture was stirred for an hour. Di-*tert*-butyl dicarbonate (41 mg, 0.19 mmol) and a catalytic amount of DMAP were added to the reaction mixture. The reaction mixture was stirred for 18 hours and then the solvent was removed under vacuum. The residue was purified using column chromatography (20% MeOH/CH$_2$Cl$_2$) to obtain the compound **5** (*N*1-(4-((4-amino-2-butyl-1*H*-imidazo[4,5-*c*]quinolin-1-yl)methyl)benzyl)-*N*5-(3-(2-(2-(3-isothiocyanatopropoxy)ethoxy)ethoxy)propyl)glutaramide) (55 mg, 40 %). MS (ESI-TOF) for $C_{38}H_{51}N_7O_5S$ [M + H]$^+$ found 718.3578, calculated 718.3745.

Synthesis of Compound 6 (PAM₂CS)

Compound 6 ((R)-3-(((R)-2-amino-3-(((S)-3-hydroxy-1-methoxy-1-oxopropan-2-yl)amino)-3-oxopropyl)thio)propane-1,2-diyl dipalmitate) was synthesized as described previously.[89]

Synthesis of Compound 7 (Hybrid-1)

To a solution of compound **5** (50 mg, 0.07 mmol) in anhydrous pyridine was added compound **6** (54 mg, 0.07 mmol). The reaction mixture was heated at 45 ℃ for 24 hours, followed by removal of the solvent under vacuum. The residue was then purified using column chromatography (12% MeOH/CH₂Cl₂) to obtain compound **7** ((25S,29R)-1-(4-((4-amino-2-butyl-1H-imidazo[4,5-c]quinolin-1-yl)methyl)phenyl)-25-(((S)-3-hydroxy-1-methoxy-1-oxopropan-2-yl)carbamoyl)-3,7-dioxo-23-thioxo-12,15,18-trioxa-27-thia-2,8,22,24-tetraazatriacontane-29,30-diyl dipalmitate, 55 mg, 53%). ^{1}H NMR (500 MHz, MeOD) δ 7.84 (d, J = 8.2 Hz, 1H), 7.68 (d, J = 8.0 Hz, 1H), 7.48 – 7.44 (m, 1H), 7.26 (d, J = 8.2 Hz, 2H), 7.18 – 7.14 (m, 1H), 7.04 (d, J = 8.2 Hz, 2H), 5.87 (s, 2H), 5.23 (bs, 2H), 4.53 (t, J = 4.4 Hz, 1H), 4.38 (dd, J = 11.9, 3.0 Hz, 1H), 4.33 (s, 2H), 4.14 (dd, J = 12.0, 6.5 Hz, 1H), 3.91 (dd, J = 11.3, 4.6 Hz, 1H), 3.80 (dd, J = 11.3, 4.1 Hz, 1H), 3.73 (s, 3H), 3.61 (dd, J = 5.9, 3.0 Hz, 4H), 3.56 (dd, J = 5.7, 2.7 Hz, 4H), 3.53 – 3.47 (m, 4H), 3.22 (t, J = 6.8 Hz, 2H), 3.14 – 3.07 (m, 1H), 3.04 – 2.92 (m, 3H), 2.88 (dd, J = 14.1, 6.1 Hz, 1H), 2.80 (dd, J = 14.2, 7.3 Hz, 1H), 2.35 – 2.28 (m, 4H), 2.21 (dt, J = 21.8, 7.4 Hz, 4H), 1.91 – 1.76 (m, 6H), 1.72 (p, J = 6.5 Hz, 2H), 1.64 – 1.53 (m, 4H), 1.44 (dt, J = 14.7, 7.4 Hz, 2H), 1.27 (s, 50H), 0.94 (t, J = 7.4 Hz, 3H), 0.89 (t, J = 7.0 Hz, 6H). 13C NMR (126 MHz, MeOD) δ 175.24, 174.95, 174.76, 171.98, 156.76, 152.19, 140.07, 136.02, 135.90, 129.48, 129.10, 126.94, 126.79, 124.11, 121.90, 115.50, 79.56, 79.30, 79.04, 71.97, 71.54, 71.52, 71.20, 71.15, 69.97, 65.02, 62.83,

56.34, 56.29, 52.95, 49.72, 43.66, 37.92, 36.34, 36.21, 35.26, 35.02, 33.72, 33.13, 30.88, 30.84, 30.81, 30.73, 30.71, 30.55, 30.52, 30.33, 30.26, 30.24, 27.89, 26.12, 26.09, 23.80, 23.47, 23.28, 14.55, 14.21. MS (ESI-TOF) for $C_{80}H_{131}N_9O_{13}S_2$, $[M + H]^+$ found 1490.9570, calculated 1490.9381.

Synthesis of Compound 9 (Hybrid-2)

Compound **9** was synthesized in three steps involving the synthesis of a tri-lysine synthon, coupling of the tri-lysine to the serine carboxyl group of PAM$_2$CS-OH, followed by coupling of the isothiocyanate-bearing imidazoquinoline derivative **5**.

First, a tri-lysine synthon was synthesized as follows (Fig. S1). To a solution of Fmoc-L-Lys(Boc)-OH (1.6 g, 3.37 mmol, Bachem, Bubendorf, Switzerland) in 1:1 solvent mixture of anhydrous DMF and pyridine were added, HBTU (1.9 g, 5.05 mmol) and H-L-Lys(Boc)-OMe (1 g, 3.37 mmol, Bachem). The reaction mixture was stirred for 1 hour followed by removal of the solvent under vacuum to obtain the crude residue which was dissolved in ethyl acetate, washed sequentially with water and brine, and concentrated under vacuum to obtain the intermediate *N*-Fmoc-protected *bis*-lysine compound (2.46 g). The *N*-Fmoc group was then removed by dissolving the compound in neat piperidine (2.3 mL) and stirring for 5 minutes, followed by quenching the reaction using excess of water and extracting the compound in ethyl acetate. The ethyl acetate fraction was then washed several times with water and dried over sodium sulfate and purified by column chromatography (8% MeOH/CH$_2$Cl$_2$) to obtain compound **K2** (1.3 g, 79%). The third lysine unit was coupled by adding **K2** (1.3 g, 2.66 mmol) to a solution of compound Fmoc-L-Lys(Boc)-OH (791 mg, 2.66 mmol) in a 1:1 solvent mixture of anhydrous DMF and pyridine

containing HBTU (1.5 g, 3.99 mmol). The reaction mixture was stirred for 1 hour, followed by removal of the solvent under vacuum to obtain the crude residue which was dissolved in ethyl acetate, washed with water and brine and concentrated under vacuum to obtain the intermediate *N*-Fmoc protected tri-lysine compound. The *N*-Fmoc group was then removed by dissolving the compound in neat piperidine and stirring for 5 minutes, followed by quenching the reaction using excess of water, and extracting the compound in ethyl acetate. The ethyl acetate fraction was washed several times with water and dried over sodium sulfate and purified by column chromatography (8% MeOH/CH_2Cl_2) to obtain the tri-lysine synthon **K3** (1.6 g, 84%). ^{1}H NMR (500 MHz, $CDCl_3$) δ 7.78 (d, J = 6.3 Hz, 1H), 6.82 (d, J = 7.7 Hz, 1H), 4.80 (s, 3H), 4.53 (d, J = 4.8 Hz, 1H), 4.37 (d, J = 6.5 Hz, 1H), 3.74 (s, 3H), 3.38 (dd, J = 7.9, 4.4 Hz, 1H), 3.18 – 3.00 (m, 6H), 1.96 – 1.77 (m, 3H), 1.70 (dd, J = 15.1, 7.5 Hz, 5H), 1.62 – 1.28 (m, 39H). 13C NMR (126 MHz, CDCl3) δ 175.59, 172.62, 171.57, 156.17, 156.11, 79.15, 79.05, 54.90, 52.68, 52.44, 52.05, 40.05, 34.56, 31.56, 31.44, 29.86, 29.52, 29.44, 28.44, 22.76, 22.61, 22.44. MS (ESI-TOF) for $C_{34}H_{64}N_6O_{10}$ [M + Na$^+$] found 739.4592, calculated 739.4576.

Second, the tri-lysine synthon was coupled to the PAM$_2$CS moiety as follows. NH-Fmoc-PAM$_2$CS-OH was synthesized as described earlier,[192] and was dissolved (27 mg, 0.028 mol) in a 1:1 solvent mixture of DMF and pyridine to which was added HBTU (16 mg, 0.041 mmol) and compound **K3** (20 mg, 0.028 mmol). The reaction mixture was stirred for 4 hours followed by removal of solvent under vacuum to obtain the *N*-Fmoc protected intermediate (17 mg). The *N*-Fmoc group was then removed by dissolving the compound in neat piperidine and stirring for 5 minutes, followed by quenching the reaction using excess of water and extracting the compound in ethyl acetate (12 mg). The ethyl acetate fraction was washed several times with water and dried

over sodium sulfate to obtain crude intermediate which was purified using column chromatography to obtain compound **8** (12 mg, 0.008 mmol).

Finally, the tri-lysine bearing, water-soluble PAM2CS-IMDQ hybrid adjuvant **9** was synthesized as follows: compound **8** (12 mg, 0.008 mmol) was dissolved in pyridine and compound **5** (6 mg, 0.008 mmol) was added. The reaction mixture was stirred for 4 hours followed by removal of solvent under vacuum to obtain the residue which was purified using column chromatography to obtain *tris*-Boc-protected compound (12 mg). To a solution of *tris*-Boc-protected compound (10 mg, 0.005 mmol) in anhydrous dichloromethane was added SnCl$_4$ (0.137 mmol, 36 mg) and the reaction mixture was stirred for 30 minutes.[216] The solvent was then removed under vacuum to obtain the residue which was purified using semi-preparative reverse phase HPLC to obtain the compound **9** ((25*S*,29*R*)-1-(4-((4-amino-2-butyl-1*H*-imidazo[4,5-*c*]quinolin-1-yl)methyl) phenyl)-3,7-dioxo-23-thioxo-25-(((4*R*,7*R*,10*R*,13*S*)-4,7,10-tris(4-aminobutyl)-14-hydroxy-3,6,9,12-tetraoxo-2-oxa-5,8,11-triazatetradecan-13-yl)carbamoyl)-12,15,18-trioxa-27-thia-2,8,22,24-tetraazatriacontane-29,30-diyl dipalmitate, 6 mg). MS (ESI-TOF) for C$_{98}$H$_{167}$N$_{15}$O$_{16}$S$_2$ [M + H+] found 1875.2112, calculated 1875.2229; [M + Na$^+$] found 1897.1929, calculated 1897.2049; [M + 2H$^+$] found 938.1115, calculated 938.1151; [M + 3H$^+$] found 625.7434, calculated 625.7458; [M + 4H$^+$] found 469.5592, calculated 469.5612.

Biology Reagents

PAM$_2$CSK$_4$ and AddaVax™ (oil (squalene)-in-water nano-emulsion) were purchased from InvivoGen (San Diego, CA). ESAT-6 was obtained from BEI resources (catalog number NR-14868). The following antibodies were purchased: B220-APC-eFluor780, CD11b-APC-

eFluor780, CD11c-APC-eFluor780, CD8α-APC-eFluor780 (eBioscience, San Diego, CA; catalog numbers 47-0452-80, 47-0112-82, 47-0114-82, 47-0081-82, respectively), CD4-BV786, CD90.2-BUV395, Bcl-6-FITC, FoxP3-PerCP-Cy5.5, RORγt-BV421, CXCR5-BV650, and T-bet-PE-Cy7 (Becton Dickinson, Franklin Lakes, NJ.; catalog numbers 563331, 565257, 561525, 563902, 562894, 563981, and 561265, respectively). The following goat-anti-mouse antibodies were purchased for ELISA: anti-IgG1, -IgG2a, -IgG2b, -IgG3, -IgM, and -IgA (Sigma Aldrich, St. Louis, MO; catalog numbers M8770, M4434, M8067, M8270, A8786, A4789, respectively). Goat-anti-rabbit IgG-HRP and rabbit-anti-goat IgG-HRP were also procured from Sigma (catalog numbers AP307P and A8919, respectively). PE- and APC-labeled I-A^b tetramers containing ESAT-6 amino acids 4-17, were graciously provided by Marc Jenkins.[217]

Human TLR2/-7/-8 Reporter Gene Assays (NF-κB induction)

The induction of NF-κB was quantified using human TLR2, TLR7 and TLR8-specific HEK-Blue™ reporter gene assays (InvivoGen, San Diego, CA; cell line catalog numbers hkb-htlr2, hkb-htlr7, and hkb-htlr8, respectively) as previously described by us.[88, 90] The reporter cells were incubated at a density of 10^5 cells/mL in a volume of 80 μL/well, in 384-well, flat-bottomed, cell culture-treated microtiter plates, and subsequently stimulated with graded concentrations of stimuli. Secreted alkaline phosphatase was assayed spectrophotometrically using an alkaline phosphatase-specific chromogen (present in HEK-detection medium as supplied by the vendor) at 620 nm on a SpectraMax M2 (Molecular Devices, Sunnyvale, CA).

Rabbit Immunizations

All rabbit immunization experiments were performed by Envigo (Huntington, UK) in accordance with institutional guidelines (University of Kansas IACUC protocol # 119-06) which specifically approved the studies. Hybrid-1 was not water soluble and required formulation in the squalene-based oil-in-water nano-emulsion, AddaVax™. Cohorts of adult female New Zealand White rabbits (n = 3) were immunized intramuscularly in the flank region with (a) 10 µg of bovine α-lactalbumin plus 100 µg of test compounds in 0.2 mL AddaVax, or (b) 10 µg of bovine α-lactalbumin plus 50 µg of IMDQ and 50 µg of PAM$_2$CS in 0.2 mL AddaVax. Prior to immunization pre-immune test-bleeds were first obtained via venipuncture of the marginal vein of the ear. Animals were immunized on days 1, 15 and 28. Immune sera were harvested on day 25 (Immune 1), and day 38 (Immune 2). Sera were stored at −80°C until used.

Enzyme-linked Immunosorbent Assays (ELISA)

Bovine α-lactalbumin-specific ELISAs were performed in 384-well format using automated liquid handling methods as described by us.[88] A Precision 2000 liquid handler (BioTek, Winooski, VT) was used for all serial dilution and reagent addition steps, and a BioTek ELx405 384-well plate washer was employed for plate washing; 100 mM phosphate-buffered saline (PBS) pH 7.4, containing 0.1% Tween-20 was used as wash buffer. Nunc-Immuno MaxiSorp (384-well) plates were coated with 40 µL of 10 µg/mL α-lactalbumin in 100 µM carbonate buffer, pH 9.0 overnight at 4°C. After 3 washes, the plates were blocked with 3% bovine serum albumin (in PBS, pH 7.4) for 1 hour at room temperature. Serum samples (in quadruplicate) were serially diluted in a separate 384-well plate using the liquid handler. After three additional washes of the assay plate, 40 µL of the serum dilutions were transferred using the liquid handler, and the plate incubated at

37°C for 1 hour. The assay plate was washed three times, and 40 µL of 1:10,000 diluted anti-rabbit immunoglobulin (IgG [γ chain]) conjugated with horseradish peroxidase was added to all wells. Following an incubation step at 37°C for 1 hour, and three washes, 40 µL tetramethylbenzidine substrate was added. The chromogenic reaction was terminated at 30 min by the addition of 2M H_2SO_4. Plates were then read at 450 nm using a SpectraMax M2 device (Molecular Devices, Sunnyvale, CA).

Surface Plasmon Resonance Experiment

Surface plasmon resonance experiments were performed as described earlier.[102] Bovine α-lactalbumin was immobilized onto the CM5 sensor chip of a BIAcore 3000 instrument (GE Healthcare, Little Chalfont, UK) using EDCI/NHS chemistry (~900 response units/channel). Rabbit serum samples at a 1:50 dilution in PBS were injected at 10 µL/min for 5 minutes. HEPES-buffered saline (40 µL/min) was used during the dissociation stage. The binding surface was regenerated with a short pulse of 25 mM NaOH. For sensorgram analyses, data points were taken at 15 seconds and 500 seconds of post-injection, and dissociation rates were calculated as a ratio of late-to-early binding response over 500 seconds.

Linear Epitope Mapping

Linear peptide epitope mapping was performed utilizing PEPperMAP® technology (PEPperPRINT GmbH, Heidelberg, Germany) as described earlier.[96] Immune-2 sera (Day 38, following the second boost) from three animals in each cohort were used. The C- and N-termini of the bovine α-lactalbumin were first elongated by neutral GSGSGSG sequences to avoid truncated peptides. The protein sequence was then translated into 13-mer peptides with a peptide-

peptide overlap of 12 amino acids. Arrays of 129 peptides were printed in duplicate spots; four such arrays were printed on each glass slide. Each array was framed by a fusion tag (Flag) peptide (DYKDDDDKGG, 72 spots) and influenza virus hemagglutinin (HA) epitope tag peptide (YPYDVPDYAG, 72 spots) as controls. After pre-soaking the arrays for 10 min in standard buffer (phosphate-buffered saline [PBS], pH 7.4 + 0.05% Tween 20) and 60 min in Rockland blocking buffer (Rockland Immunochemicals, Inc., Gilbertsville, PA), the peptide microarrays were initially incubated with the secondary goat anti-rabbit IgG (H+L) conjugated with DyLight680 antibody at a dilution of 1:5000 for 60 min at room temperature to verify that no significant background interactions occurred with the peptide arrays. The microarrays were washed twice and incubated for an additional 30 min in standard buffer. The peptide arrays were then incubated overnight at 4°C with rabbit sera diluted to 1:1000. After multiple washes in standard buffer, the slides were incubated for 30 min with the secondary goat anti-rabbit IgG (H+L) conjugated with DyLight680 antibody at a dilution of 1:5000 at room temperature. After two additional washes in standard buffer, the microarrays were rinsed with ultrapure water and dried in a stream of air. Green/red fluorescence intensities were acquired on an Odyssey Imager (Lincoln, NE) at a spatial resolution of 21 µm. Staining of Flag and HA control peptides that frame the arrays gave rise to high and homogeneous spot intensities with a coefficient of variation of <2%. The PEPSlide Analyzer algorithm deconvolutes raw fluorescence intensities of each spot into foreground and background signal. Intensity maps were generated based on corrected foreground intensities (averaged over the double spots) of each peptide.

ESAT-6-specific T Cell and Antibody Isotype Analysis

Six-8 week old C57BL/6 mice were housed in specific-pathogen-free conditions according to the University of Minnesota IACUC protocol #1703-34657A. Cohorts of 3 mice were vaccinated subcutaneously 3 times at two-week intervals with 10 µg ESAT-6 adjuvanted with IMDQ, Hybrid-2, or PAM$_2$CSK$_4$. Monophosphoryl lipid a (MPLA) formulated in dimethyldioctadecyl-ammonium bromide (DDA) liposomes[218] was used as reference adjuvant.[213] Unadjuvanted ESAT-6 in phosphate-buffered saline was used for the control cohort. Mice were sacrificed 4 weeks following the final immunization. Blood was collected by cardiac puncture, and the spleen and axillary lymph nodes were harvested for T cell analysis. ESAT-6-specific antibody isotypes were analyzed by ELISA as mentioned above, using 10 µg/mL ESAT-6 for coating and goat-anti-mouse IgG1, IgG2a, IgG2b, IgG3, IgM, and IgA primary antibodies (Sigma Aldrich, St. Louis, MO). ESAT-6-specific T cells were enriched using PE- and APC-labeled I-A^b tetramers containing ESAT-6 amino acids 4-17.[217] Single cell suspensions were stained at room temperature for 1 hour with PE- and APC- tetramers. Tetramer positive cells were enriched using PE- and APC-specific antibodies with dextran magnetic beads (Stemcell Technologies, Vancouver, Canada) as was previously published by Moon and coworkers.[217] Enriched samples were stained with Fixable viability dye eFluor780 (eBioscience, San Diego, CA) and the following antibodies: B220-APC-eFluor780, CD11b-APC-eFluor780, CD11c-APC-eFluor780, CD8α-APC-eFluor780, CD4-BV786, CD90.2-BUV395, Bcl-6-FITC, FoxP3-PerCP-Cy5.5, RORγt-BV421, CXCR5-BV650, and T-bet-PE-Cy7. Samples were acquired on BD LSRFortessa X-20 (BD Bioscience, Franklin Lake, NJ) and analyzed using FlowJo version 10 (FlowJo, LLC, Ashland, OR).

ESAT-6-specific IFN-γ ELISpot Assays

Five cohorts of five C57BL/6 mice each were vaccinated via the subcutaneous route 3 times at two-week intervals with ESAT-6 (10 μg/dose) admixed with Hybrid-2 (20 μg/dose) or IMDQ (20 μg/dose). Control cohorts received either a single dose of 5×10^4 CFU of BCG Pasteur (positive control), or MPLA DDA liposomes[213] (reference adjuvant), or pyrogen-free saline (negative control). An additional two cohorts received only compound Hybrid-2 or IMDQ (20 μg/dose) as adjuvant-only controls. Each cohort was analyzed for their immune responses to vaccination at 4 weeks post-vaccination by ELISpot assay as was previously published by Brandt and coworkers.[219]

ELISpot was conducted using a MultiScreen 96-well plate (Millipore, Billerica, MA) coated with 10 μg/mL of rat anti-mouse IFN-γ capture antibody (Becton Dickinson, Franklin Lakes, NJ.; Catalog number 554412) and incubated overnight at 4°C. Plates were washed in PBS and blocked with RPMI containing 10% fetal calf serum for 1 hour. Spleen, lung, and lymph node cells were plated at 10^5 cells per well in 100 μL followed by ESAT-6 stimulation at 10 μg/mL with 0.2 ng/mL of interleukin-2 for 48 hours at 37°C. The plates were washed with PBS containing 0.1% Tween and incubated overnight at 4°C with a biotin-conjugated rat anti-mouse IFN-γ secondary antibody at 5 μg/mL in PBS containing 0.1% Tween and 0.5% bovine serum albumin. Vectastain ABC avidin peroxidase conjugate and Vectastain AEC substrate kits (Vector Laboratories, Burlingame, CA.; Catalog number PK6100) were used to develop the filters. The reaction was stopped by washing with deionized water and the plates were dried for spot counting.
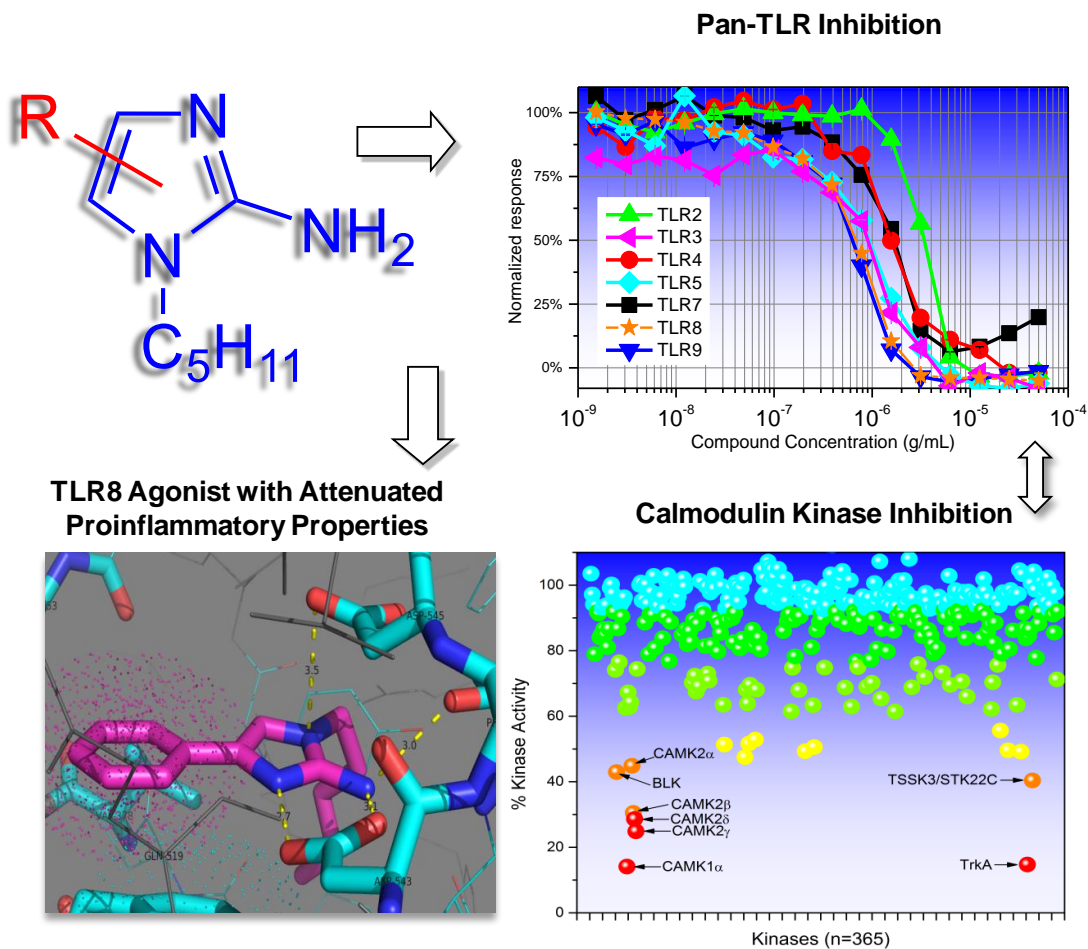
M. tuberculosis Challenge Studies

Five cohorts of five C57BL/6 mice each were vaccinated via the subcutaneous route 3 times at two-week intervals with ESAT-6 (10 µg/dose) admixed with Hybrid-2 (20 µg/dose) or IMDQ (20 µg/dose). Control cohorts received either a single dose of $5x10^4$ CFU of BCG Pasteur (positive control), or MPLA DDA liposomes (reference adjuvant), or pyrogen-free saline (negative control). An additional two cohorts received only compound Hybrid-2 or IMDQ (20 µg/dose) as adjuvant-only controls. *M. tuberculosis* H37Rv were grown from low-passage seed lots in Proskauer-Beck liquid medium containing 0.05% Tween 80 to early log phase. Cultures were stored at −70°C until used. Thawed aliquots were diluted in distilled sterile water to the desired inoculum concentrations. An aerosol generation device (Glas-Col, Terre Haute, Ind.) was used to expose the animals to an aerosol of *M. tuberculosis* and was calibrated to deliver approximately 100 bacilli per mouse.[219] To assess bacterial loads, individual whole-organ homogenates were plated on nutrient Middlebrook 7H11 Bacto agar (Becton Dickinson Microbiology Systems, Cockeysville, Md.). Bacterial colonies were counted after 2 to 3 weeks of incubation at 37°C.

Chapter 5.

# Identification of a Human TLR8-specific Agonist and a Functional Pan-TLR Inhibitor in 2-Aminoimidazoles

Pan-TLR Inhibition

TLR8 Agonist with Attenuated Proinflammatory Properties

Calmodulin Kinase Inhibition

5.1 Introduction

The promising results of the TLR2/7 hybrids (Chapter 4) brought to light the importance of understanding the abilities of various TLR agonists to bias the adaptive immune responses using robust assays. We therefore set out to examine mechanisms of adjuvanticity in individual TLR agonists. We began our efforts by the SAR of the novel TLR8 agonistic 2-aminoimidazoles.

In the context of Th1-biased adaptive immune responses, TLR8 is of particular significance. The engagement of TLR8, which is expressed predominantly in myeloid dendritic cells, monocytes, and monocyte-derived dendritic cells,[194, 220] potently enhances the production of Th1-polarizing cytokines, TNF-α, IL-12, and IL-18 in APCs.[220-223] Our interest in Th1-polarizing small molecule agonists of TLR8 has led to the exploration of a variety of dual TLR7/8-active chemotypes (**1a**-**1c** in Fig. 1),[93, 95, 97, 99] as well as pure TLR8 agonists with no detectable activity at TLR7, including the 2,3-diamino-furo[2,3-*c*]pyridines (**1d**),[98] 4-amino-furo[2,3-*c*]quinolines (**1e**),[25] 3-alkyl-quinoline-2-amines (**1f**),[26] 1-alkyl-2-aminobenzimidazoles (**1g**),[100] and 2-amino-3-pentyl-5-alkylaminoquinolines (**1h**).[113]
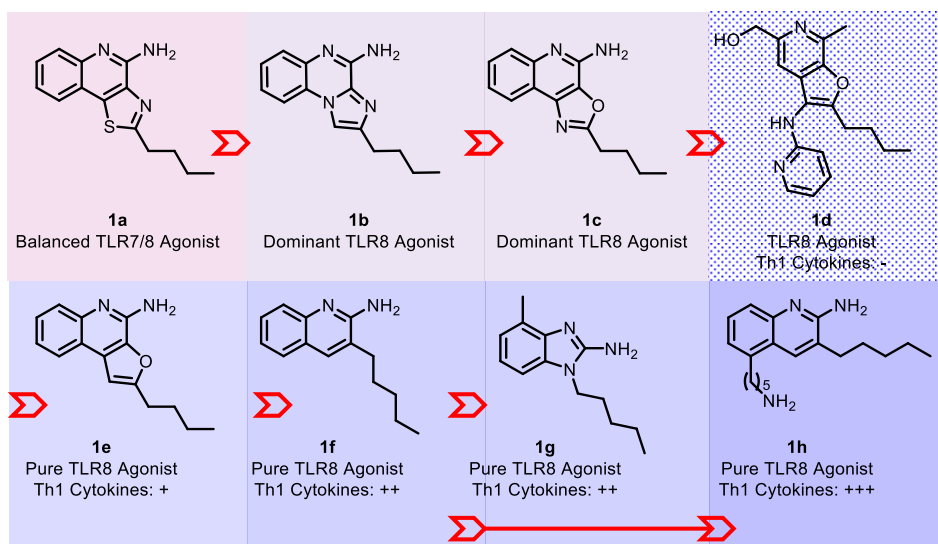
*Figure 1. Structures of the dual TLR7/8-active (**1a-1c**) and pure TLR8-active (**1d-1h**) compounds. Arrows indicate evolution of chemotypes.*
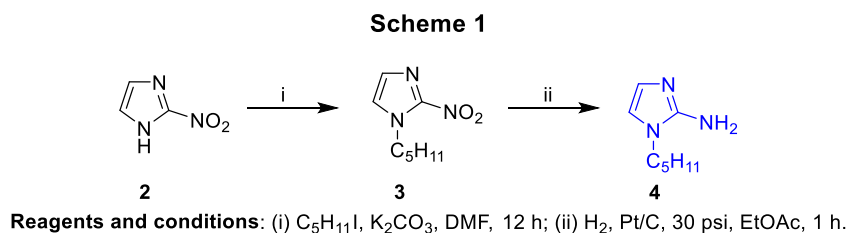
Part-structures of the 2-aminobenzimidazole scaffold were examined with a view to identifying structural requisites corresponding to the smallest possible fragment of the benzimidazole core that would allow for retention of TLR8-agonistic activity, enabling the identification of a TLR8-specific agonist of low proinflammatory potential, and an analogue with functional pan-TLR inhibitory properties, which may prove useful as an anti-inflammatory agent.
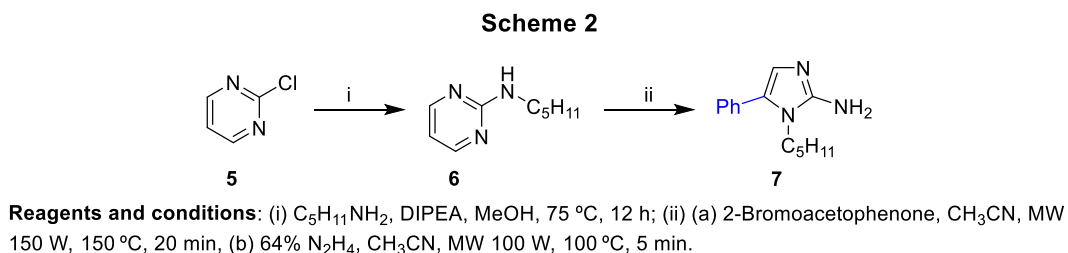
5.2 Results and Discussion

In our earlier exploration of novel TLR8-specific agonists, we had noted distinct differences in potencies in the order: **1h**>**1f**[26] ≈ **1g**[100]>**1e**,[112] with **1d** being TLR8-specific (Fig. 1), but entirely devoid of proinflammatory cytokine-inducing properties. The significant enhancement of potency for TLR8 observed for **1h** was achieved by specifically 'designing in' the 5-pentylamine substituent on to **1f** to yield **1h**, which, based on co-crystal structures, was predicted to afford strong salt-bridge interactions with Asp545 in TLR8.[113] The design of **1e** from **1f** was also arrived at by structure-guided methods derived from co-crystal structures of TLR8 with **1e** showing a hydrophobic pocket enabling optimal binding of C2 alkyl chains.[26] These studies have been instructive, and have provided a strong impetus to explore ligand design for PRRs for which small molecule ligands have not yet been identified, such as TLR3 and TLR9, for which only canonical ligands[224] have been described.

Given the structural homology and highly conserved ligand binding sites within the TLR family,[225-226] one possible approach toward identifying novel small molecule ligands for these innate immune receptors is the *de novo* design of potential ligands[227-228] starting from key

interactions ('hot spots') at the binding site, and then examining hypothesis-driven, focused libraries such as we had successfully undertaken for **1h**.[113] We therefore reverted back to the 2-aminobenzimidazole scaffold of **1g**, and wished to interrogate structural requisites corresponding to the smallest possible part-structure of the benzimidazole core that would allow for retention of agonistic activity, our goal being able to utilize the SAR data in the *de novo* design of ligands.

Scheme 1

Reagents and conditions: (i) $C_5H_{11}I$, K_2CO_3, DMF, 12 h; (ii) H_2, Pt/C, 30 psi, EtOAc, 1 h.

Noting from our previous SAR studies that an appropriately positioned pentyl substituent confers optimal activity, our first target was the synthesis of 1-pentyl-2-aminoimidazole, **4**, obtained from 2-nitroimidazole via *N*-alkylation, followed by reduction of the nitro group (Scheme 1) (synthesis was conducted by Dr. Mallesh Beesu). We noted that, similar to 2-amino-3-alkylindoles,[100] the free base of **4** was unstable in DMSO. The HCl salt, however, was stable and active in TLR8-specific primary screens, with a potency about one-twenty-fifth (EC$_{50}$: 28.4 µM, Table 1) that of the parent compound **1g** (EC$_{50}$: 1.13 µM), likely attributable to loss of π-π interactions with Phe405.[26, 97] In an effort to regain such interactions, we explored aromatic substituents on the unusually diminutive imidazole scaffold.

Scheme 2

Reagents and conditions: (i) $C_5H_{11}NH_2$, DIPEA, MeOH, 75 ºC, 12 h; (ii) (a) 2-Bromoacetophenone, CH_3CN, MW 150 W, 150 ºC, 20 min, (b) 64% N_2H_4, CH_3CN, MW 100 W, 100 ºC, 5 min.

The 5-phenyl substituted analogue **7** was synthesized from *N*-pentylpyrimidin-2-amine and 2-bromoacetophenone under microwave conditions via the elegant, one-pot, two-step protocol developed by Ermolat'ev and colleagues (Scheme 2).[229] Compound **7**, however, was completely inactive, suggesting non-optimal orientation of the 5-phenyl group for adequate π-π interactions. The 4,5-diphenyl substituted analogue **10**, accessed from **3** via sequential dibromination, Suzuki reaction with phenylboronic acid, and reduction of the 2-nitro group (Scheme 3), exhibited very weak TLR-8 agonistic activity (Fig. 2), pointing to out-of-plane orientation of the vicinal phenyl substituents, owing to steric crowding. The 4-phenyl substituted analogue **17a** was synthesized from **3** via mono-bromination at C4, sequential Suzuki reaction with phenylboronic acid, followed by reduction of the 2-nitro group (Scheme 4). A ten-fold gain in TLR8-agonistic activity was observed for **17a** (EC$_{50}$: 2.48 µM; Table 1, Fig. 2) relative to the imidazole **4**, likely indicating restoration of π-π interactions with Phe405 of human TLR8.

Scheme 3
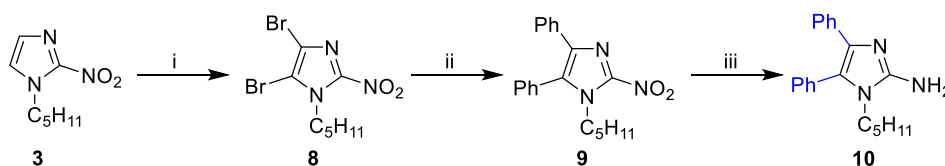
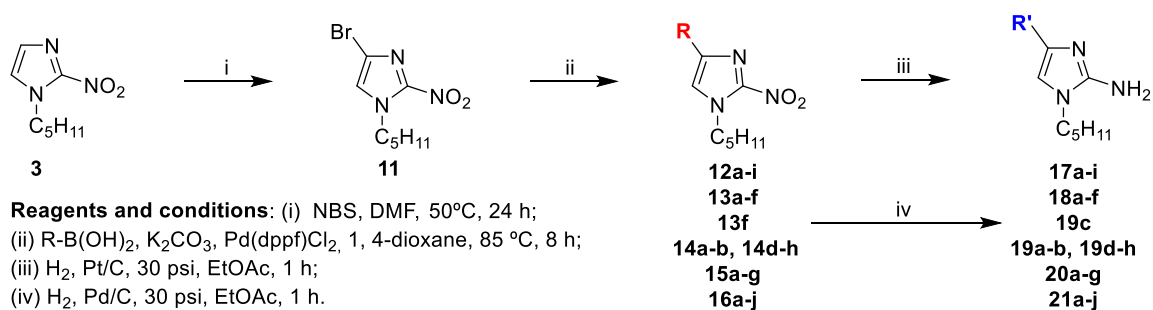**Reagents and conditions**: (i) NBS, DMF, 75 ºC, 12 h; (ii) Ph-B(OH)$_2$, K$_2$CO$_3$, Pd(dppf)Cl$_2$, 1,4-dioxane, 90 ºC, 12 h; (iii) H$_2$, Pt/C, 30 psi, EtOAc, 1 h.

We therefore undertook a detailed exploration of aromatic substituents at C4 (Scheme 4). The majority of analogues in this series showed similar EC$_{50}$ values (1.5-3 µM), but differed substantially in the maximal responses induced in the human TLR8-specific reporter gene assays (Fig. 2) in a manner similar to what we had observed previously with the 2,3-diamino-furo[2,3-*c*]pyridine (**1d**) class of TLR8 agonists,[98] and it should be noted that a discussion of relative potency in primary screens is therefore based on maximal responses (shown in Table 1). Optimal

compounds identified possess both potent EC_{50} and high AUCs. The 4-*o*-tolyl analogue **17b** was marginally less active in primary, TLR8-specific reporter gene assays (EC_{50}: 2.5 μM; Table 1, Fig. 2) than **17a**, while the homologated 4-(2-ethylphenyl) analogue **17c** was significantly weaker, signaling poor tolerance of steric bulk at that position. The regioisomeric analogues **17d** (4-*m*-tolyl), **17e** (4-*p*-tolyl), also showed some attenuation in activity relative to **17b**, and the congeners **17f**-**17i**, bearing 2,3-, 2,4-, 2,5-, and 2,6-dimethylphenyl substituents at C4, respectively (Scheme 4), showed lowered maximal responses (Fig. 2). Replacing the C4-phenyl with a benzyl group (**18a**), or further homologation to a phenethyl substituent (**18b**) led to progressive loss in activity as evidenced by lowering of TLR8 maximal responses (Fig. 2). Naphthyl (**18c**, **18d**), biphenyl (**18e**), or benzyloxyphenyl (**18f**) substituents also were deleterious. Compound **19a**, with a 3-pyridyl group at C4 showed a marked shift-to-the-right in its dose-response profile, and the dimethylisoxazole-bearing **19b** was weaker still (Fig. 2, Table 1). These data, taken together, indicated that neither steric bulk, nor the presence of heteroatoms in the aromatic group at C4 were well-tolerated.

We specifically examined whether the presence of H-bond-donating or -accepting functional groups on the C4-phenyl substituent would enhance activity but found that all such analogues, including the 2-phenolic (1**9c**), 2-hydroxymethyl (**19d**), 4-aminophenyl (**19e**), 4-benazamide (**19f**), 4-methylbenzoate (**19g**), 2-methylbenzoate (**19h**) were weaker than **17a** (Fig. 2, Table 1). Encouraged by the observation that the 2-methoxyphenyl analogue **20a** showed an activity profile comparable to that of **17a** (Fig. 2, Table 1), we synthesized its regioisomeric compounds **20b**-**20c**, the di- and trimethoxyphenyl compounds (**20f** and **20g**, respectively), as well as the methoxymethylphenyl congeners **20d** and **20e**, none of which were more potent than **20a**. We also evaluated analogues with electron-deficient phenyl groups. The chlorophenyl analogues **21a**-**21c**

Scheme 4

Reagents and conditions: (i) NBS, DMF, 50ºC, 24 h;
(ii) R-B(OH)$_2$, K$_2$CO$_3$, Pd(dppf)Cl$_2$, 1, 4-dioxane, 85 ºC, 8 h;
(iii) H$_2$, Pt/C, 30 psi, EtOAc, 1 h;
(iv) H$_2$, Pd/C, 30 psi, EtOAc, 1 h.
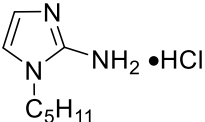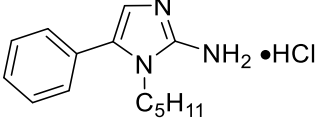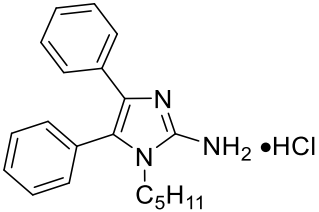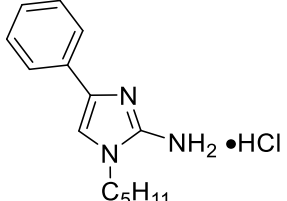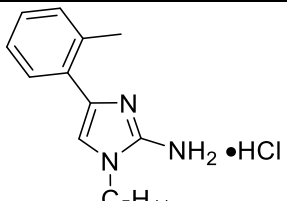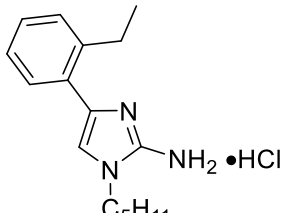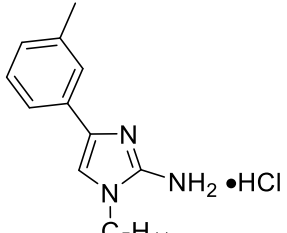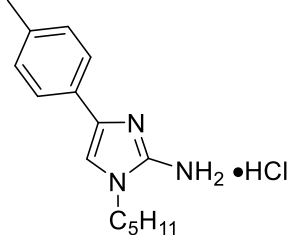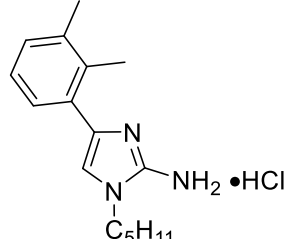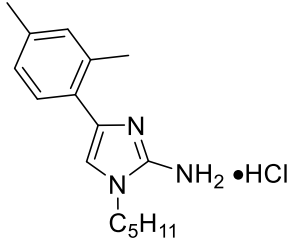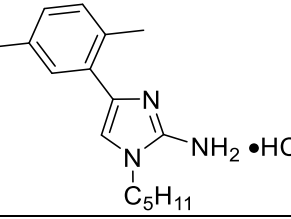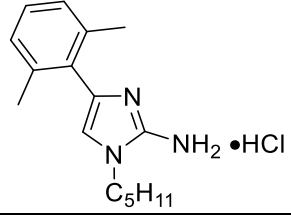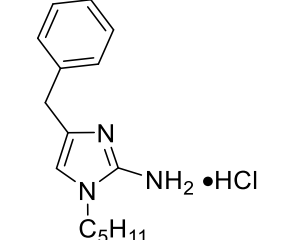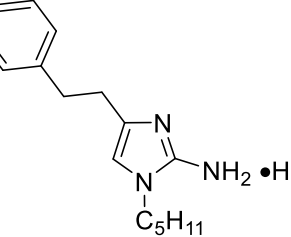
R = **R'** for: **12a-i/17a-i**; **13a/18a**; **13c-f/18c-f**;
14a-b/19a-b; **14f-h/19f-h**;
15a-g/20a-g; **16a-j/21a-j**.

R =

13b	**14d** CHO	**14e**
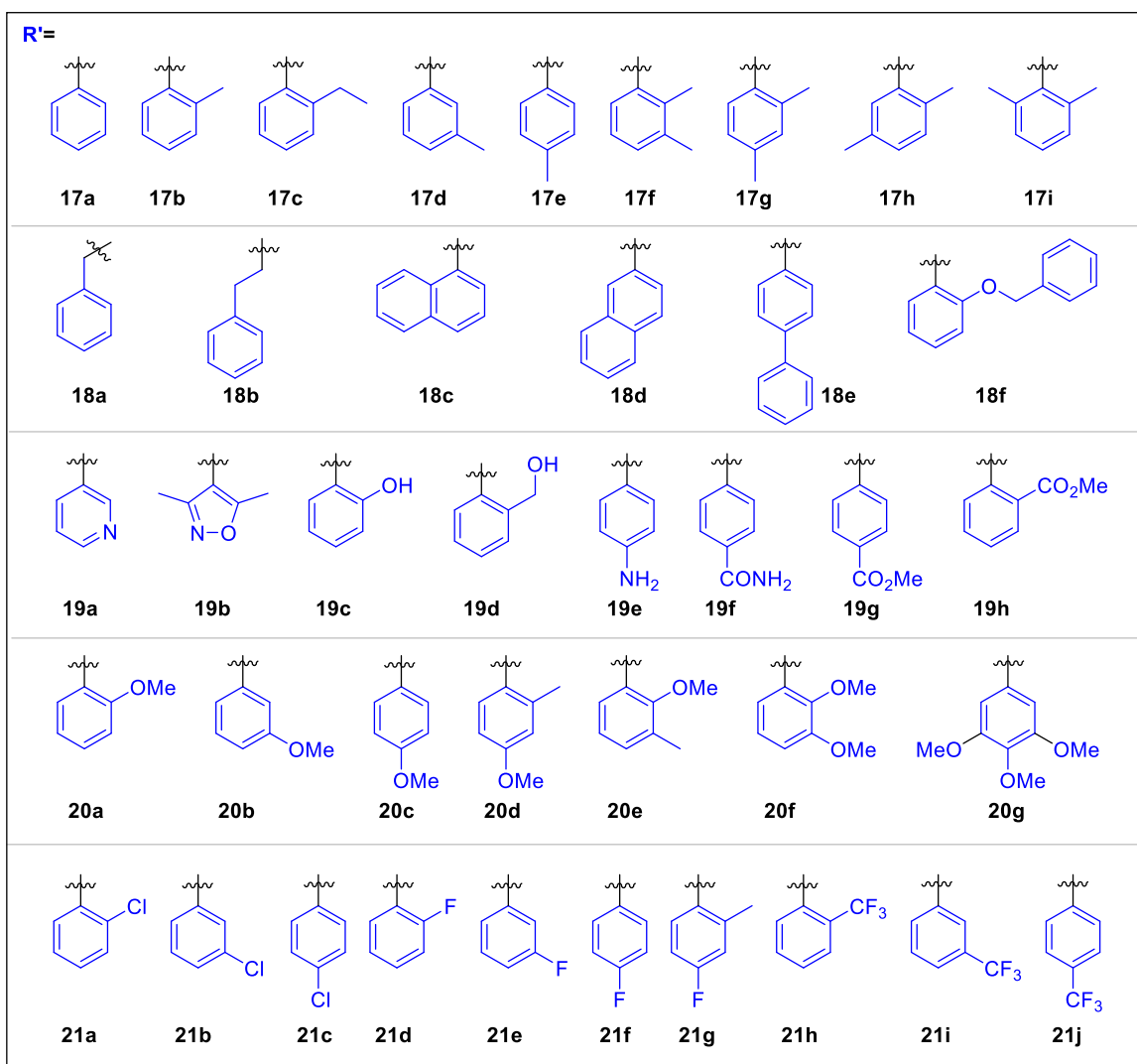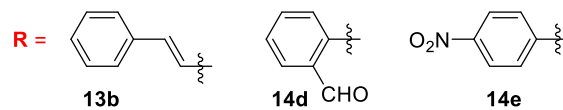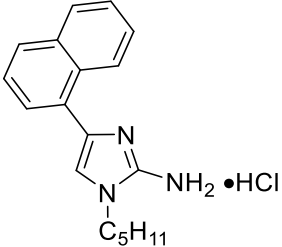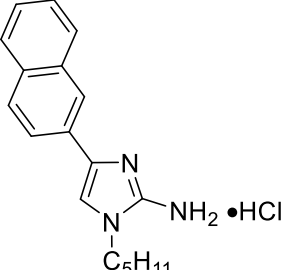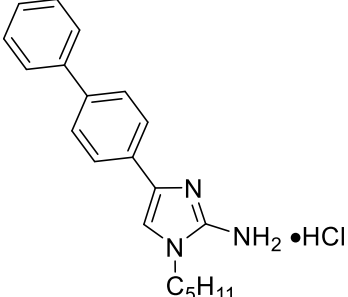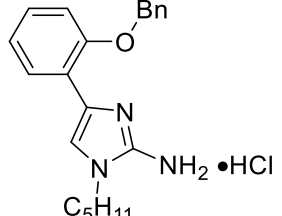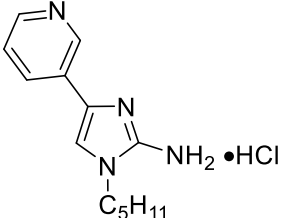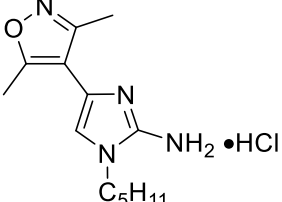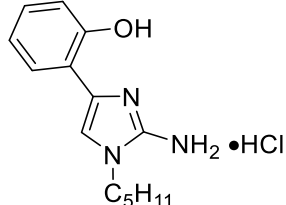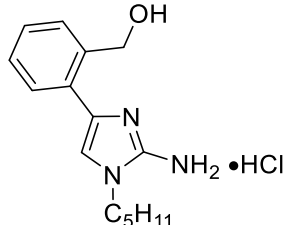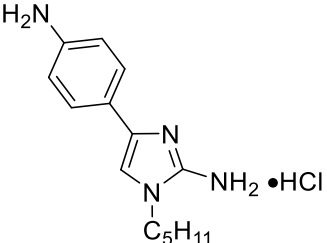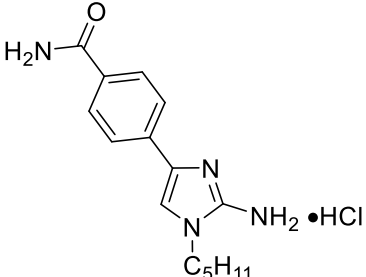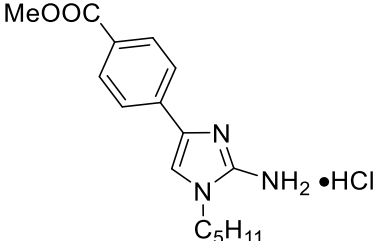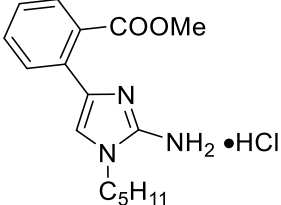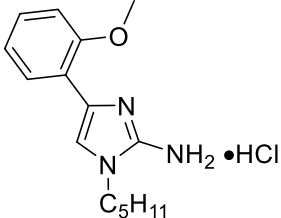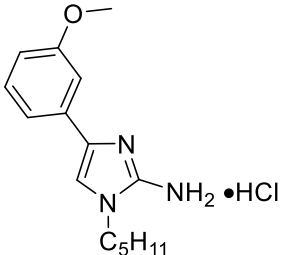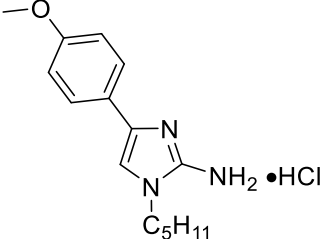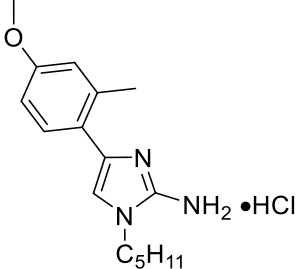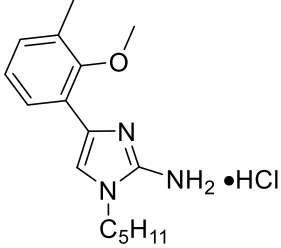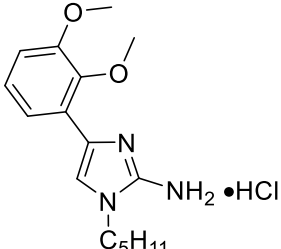
Table 1. EC$_{50}$ values of compounds in human TLR 8-specific reporter gene assays
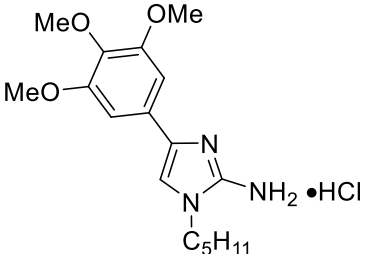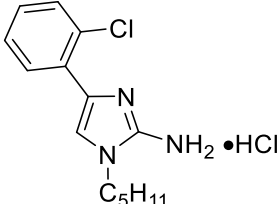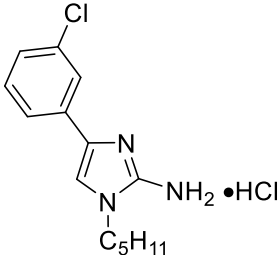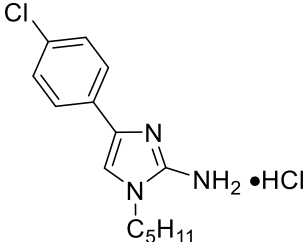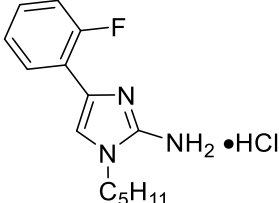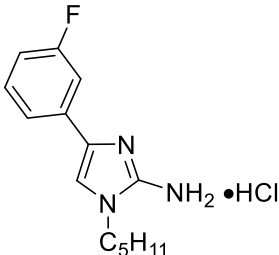
Compound Number	Structure	EC$_{50}$: TLR8 Agonistic Activity(μM)	Maximal Response (Absorbance Units)
4		28.40	1.2
7		Inactive	
10		Very low AUC	0.52
17a		2.48	2.0
17b		2.5	1.4
17c		2.5 Low AUC	0.8
17d		2.0	1.0
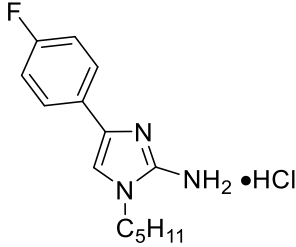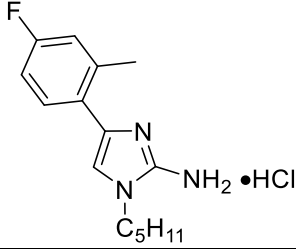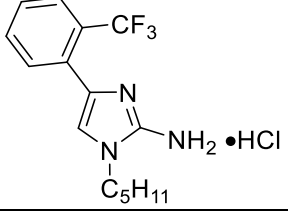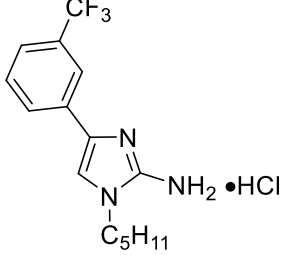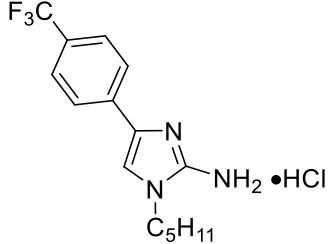
17e		2.5 Low AUC	0.9
17f		1.5	1.3
17g		1.5	1.2
17h		1.5 Low AUC	0.9
17i		2.5	1.2
18a		2.7	1.0
18b		1.8 Low AUC	0.9

18c		1.5 Low AUC	0.9
18d		Very low AUC	0.42
18e		Very low AUC	0.47
18f		Inactive	
19a		21.31	1.8
19b		18.80 Low AUC	0.7

19c		5.10 Low AUC	0.9
19d		8.05	1.6
19e		8.0 Very low AUC	0.6
19f		20.24 Low AUC	0.8
19g		4.04 Low AUC	0.7
19h		11.1	1.2

20a		1.6	1.6
20b		2.2	1.2
20c		2.94 Low AUC	0.7
20d		1.5 Low AUC	0.9
20e		1.5 Low AUC	0.7
20f		2.5 Very low AUC	0.6

20g	MeO, OMe, MeO-substituted phenyl imidazole NH$_2$ •HCl, C$_5$H$_{11}$	3.08 Low AUC	0.8
21a	Cl-substituted phenyl imidazole NH$_2$ •HCl, C$_5$H$_{11}$	1.36	1.0
21b	Cl-substituted phenyl imidazole NH$_2$ •HCl, C$_5$H$_{11}$	1.93 Low AUC	0.9
21c	Cl-substituted phenyl imidazole NH$_2$ •HCl, C$_5$H$_{11}$	6.83 Very low AUC	0.5
21d	F-substituted phenyl imidazole NH$_2$ •HCl, C$_5$H$_{11}$	2.35	1.4
21e	F-substituted phenyl imidazole NH$_2$ •HCl, C$_5$H$_{11}$	2.57	1.6

21f		1.96	2.0
21g		2.01	1.7
21h		1.64 Low AUC	0.9
21i		1.98 Very low AUC	0.6
21j		2.48 Low AUC	0.8

EC_{50} values represent the means obtained on quadruplicate samples using four-parameter logistic fits of dose-response curves. AUC denotes area under dose response curve. Low AUC indicates submaximal activity.
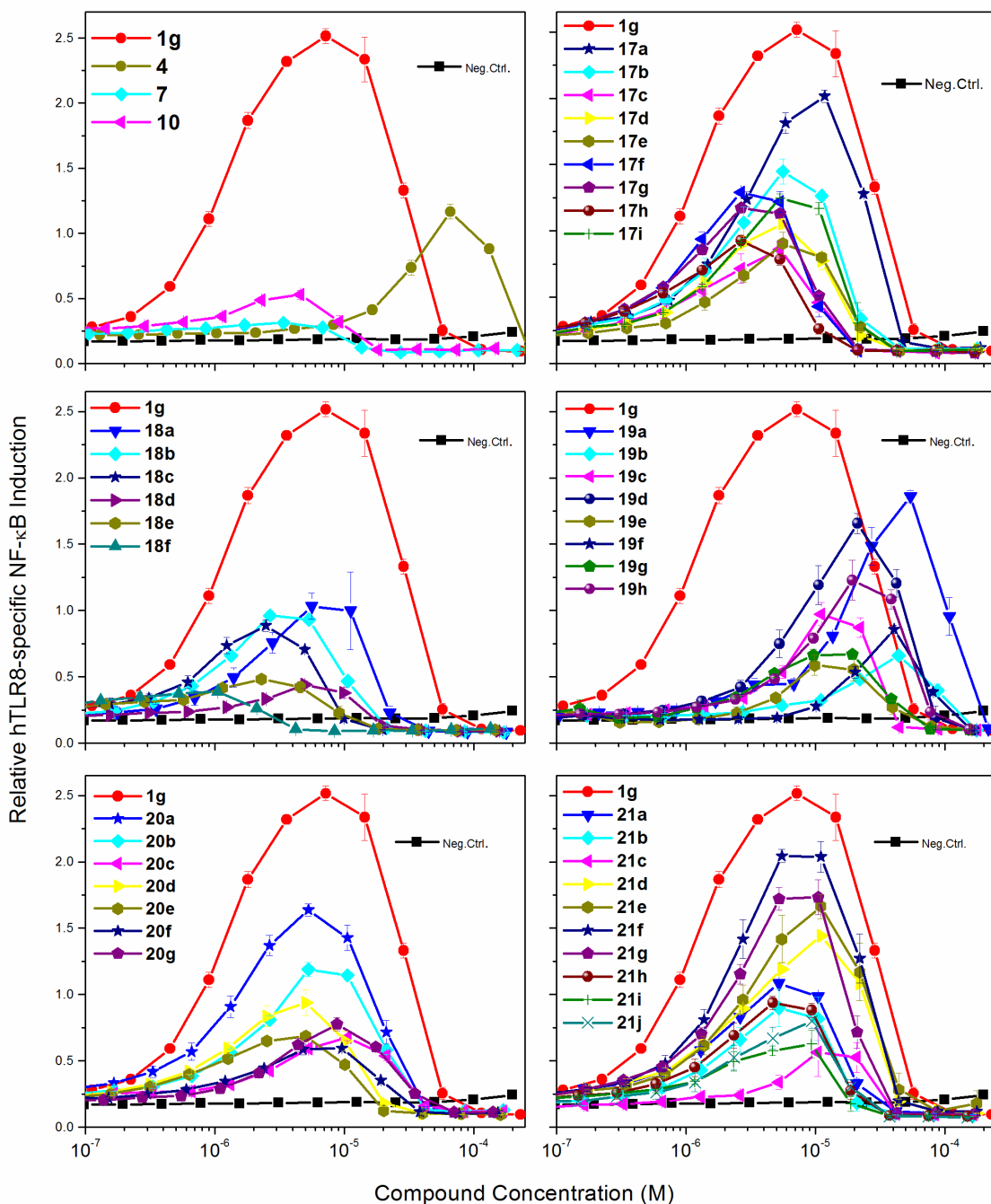
*Figure 2. Agonistic activities of 2-aminoimidazole analogues in human TLR8 reporter gene assays. Means ± SD on quadruplicates are shown. Also included is **1g**, used as a reference TLR8-active compound. The bimodal nature of agonistic responses resulting in apparent inhibition at high ligand concentrations was verified not to be due to cytotoxicity.*

were all considerably weaker, whereas of the fluorophenyl compounds (**21d**-**21g**), the 4-fluorophenyl (**21f**) and 4-fluoro-2-methyl-phenyl (**21g**) analogue were potent, while the trifluoromethylphenyl compounds (**21h**-**21j**) were weak.
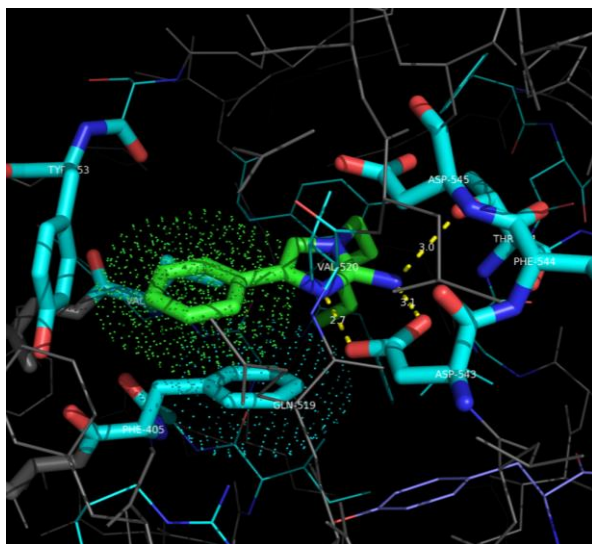
Figure 3. Crystal structure of 17a bound to the ectodomain of human TLR8. *Dashed lines in yellow depict direct hydrogen bonds. Dots indicate van der Waals radii of the aromatic rings of 17a and Phe405.*

A crystal structure of the ectodomain of human TLR8 complexed with **17a** allows the rationalization of several aspects of the SAR that we have observed with this very small (229 Daltons) TLR8-specific agonist. Compound **17a**, similar to other TLR8-binding ligands,[26, 97, 113, 230] occupies the same binding pocket formed by both the TLR8 protomers, with the binding geometry of the ligand and interacting residues being virtually identical; bidentate ionic H-bonds were observed between the side-chain carboxylate of Asp543 of TLR8 and the *N*2 and *N*3 atoms of **17a**. Aromatic stacking with near-perfect coplanarity is observed between the C4-phenyl ring of **17a** and Phe405 in TLR8 (Fig. 3) in a pocket that is tightly circumscribed and delimited by the hydrophobic residues Tyr353, Val378, Val520 and Gln519 (Fig. 3), explaining why the SAR on

the phenyl ring was fastidious and unyielding. An inspection of dihedral angles and inter-atomic distances in the crystal structure also raises the possibility of a halogen bond[231-232] between the fluorine atom in **21f** and the phenolic oxygen of Tyr353.
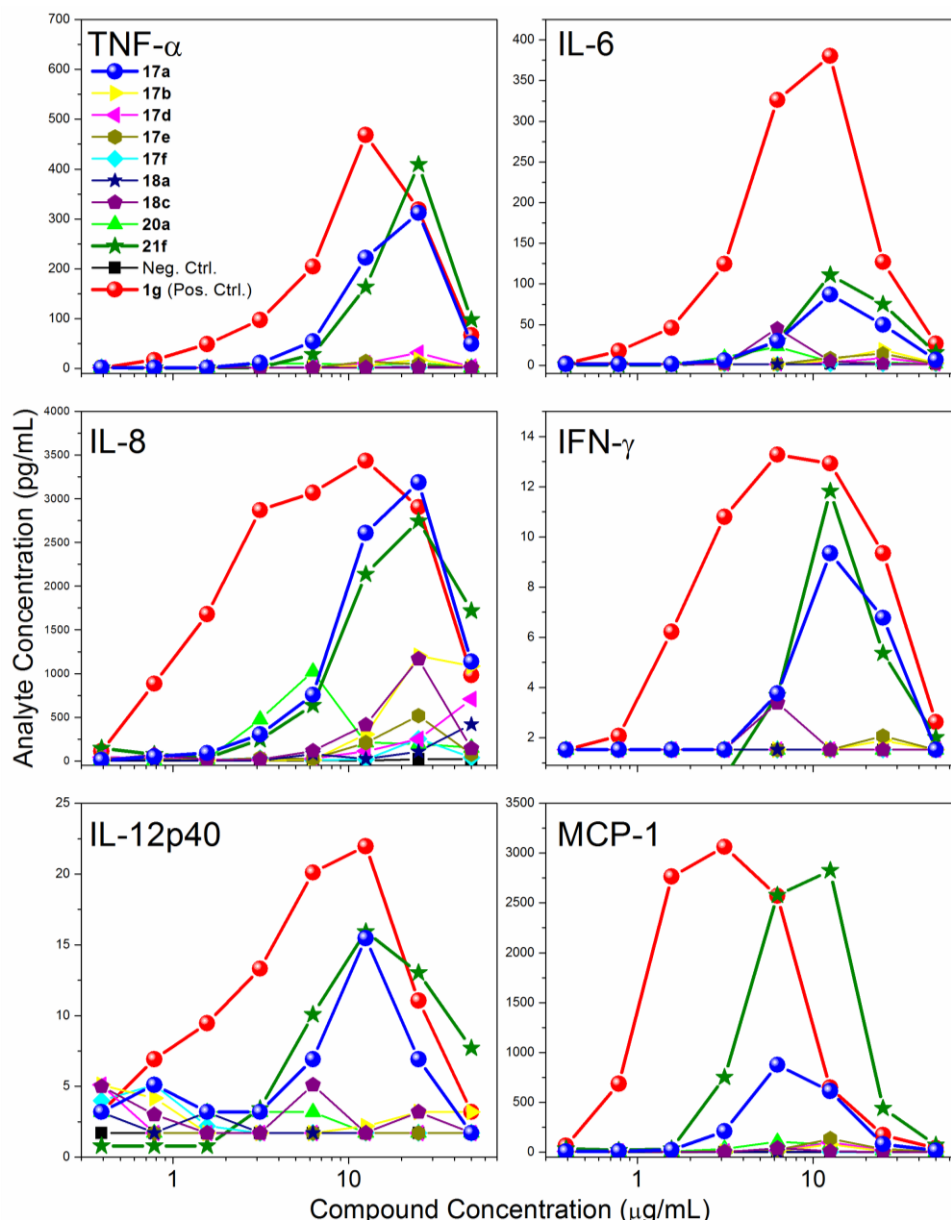
Figure 4. Cytokine induction (excerpted from a 41 cytokine panel) in human PBMCs. Compounds that were found to be active in primary screens were evaluated. Means of a single representative experiment is shown.

Given that the majority of analogues were weak, we examined the TLR8-agonistic properties of all of the compounds for cytokine and chemokine induction in human PBMCs using a 41-analyte multiplexed immunoassay platform. Unexpectedly, only **17a** and **21f** showed cytokine/chemokine profiles (TNF-α, IL-1β, IL-6, IL12p40, IFN-γ, MCP-1, MIP-1α and MIP-1β); a subset of the secondary screen data is shown in Fig. 4. The potencies of both **17a** and **21f** were lower than that of **1g**, used as a comparator (Fig. 4). We attempted to understand the basis of the apparent dissociation of activity in primary cell-based reporter assays and secondary screens in human PBMCs. The proprietary detection medium used in the reporter gene assay contains a chromogenic substrate for alkaline phosphatase in low concentrations of protein (which we verified to be equine albumin by peptide MS/MS fingerprinting), whereas the cytokine assays with human PBMCs are
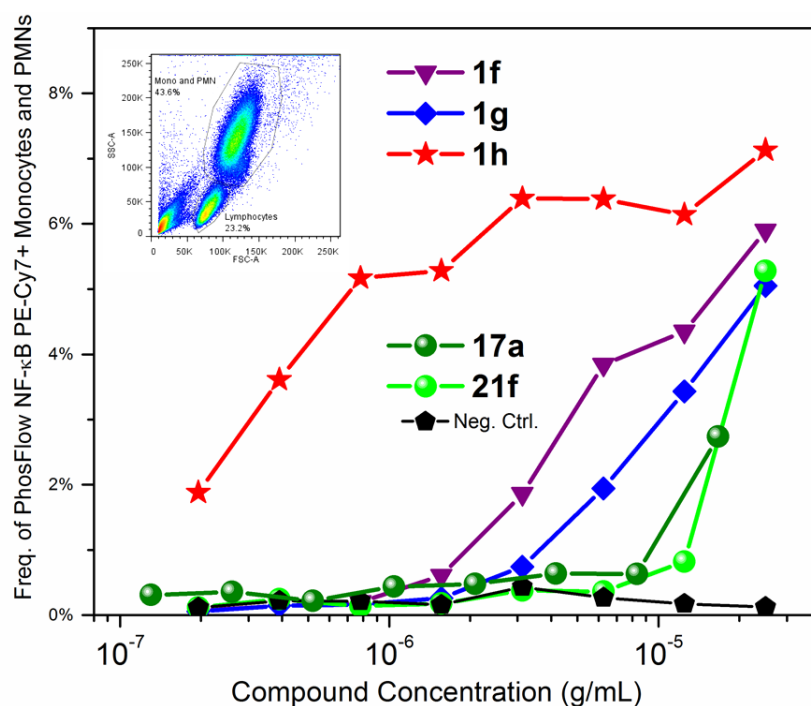
Figure 5. Intracellular PhosFlow™ flow cytometry for quantifying NF-κB phosphorylation in monocytes and polymorphonuclear cells in whole human blood. *Dose-response profile for **17a** and **21f** are shown relative to reference TLR8-active comparators, **1f**, **1g** and **1h**. Inset shows gating strategy.*

performed in medium containing either 10% autologous, decomplemented serum, or 10% fetal bovine serum. Reporter gene assays adapted to include 10% human serum or 10% fetal bovine serum showed no differences in rank-order potencies. Addition of either recombinant human serum albumin[233-234] or human acid 1-glycoprotein[235] (up to concentrations of 1 mg/mL) also did not appreciably attenuate signals in TLR8-specific reporter gene assays (data not shown). The data cannot be explained adequately in terms of differential compartmentalization in the acidic endolysosomal compartment[236] due to pK_a differences, given that highly similar congeneric pairs (**17a**/**17b**, **21f**/**21g**, for instance) show complete dissociation in secondary screens. The reasons for why only **17a** and **21f**, and none of the other analogues retain TLR8-agonistic activity in secondary screens remain enigmatic, and highlights possible shortcomings in strickly using reporter cells for assessing biological activity of novel compounds.
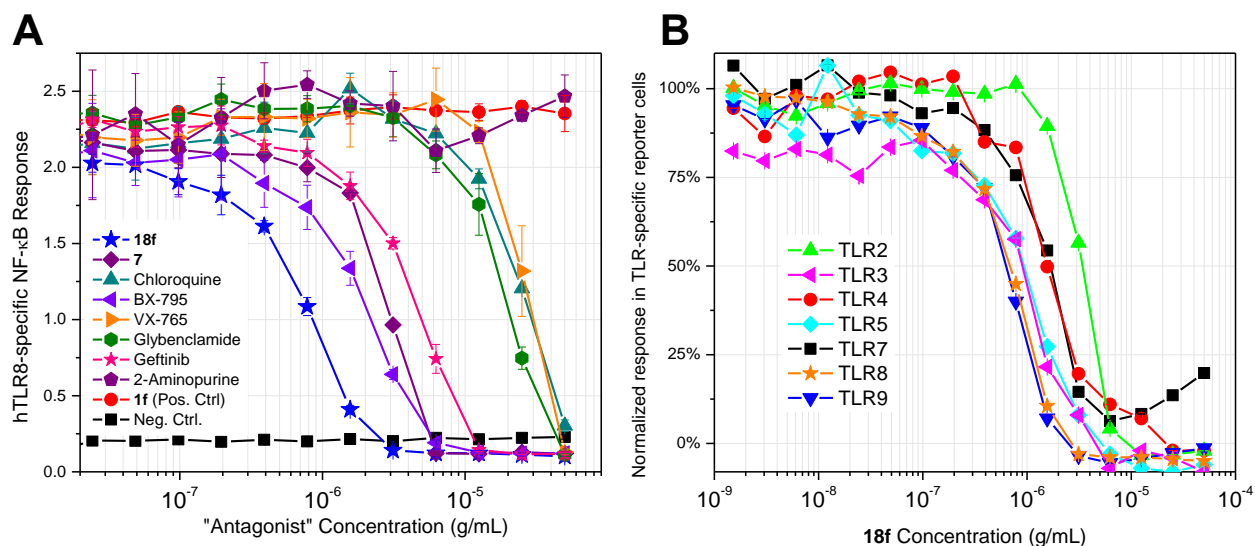
Figure 6. A. Inhibitory activity of 7 and 18f as well as a panel of cell signaling inhibitors in human TLR8 reporter cells. *A 5 µg/mL concentration of **1f** was used as stimulus. TLR inhibitory activities of **18f**. The following stimuli (and reporter cells) were used: PAM2CS (10 ng/mL; TLR2), Poly(I:C) (50 ng/mL; TLR3), LPS (1 µg/mL; TLR4), flagellin from S. typhimurium (1 µg/mL, TLR5), TLR7-specific imidazoquinoline (1 µg/mL, TLR7), **1f** (5µg/mL; TLR8), Oligonucleotide ODN2006 (15 µg/mL; TLR9).*

We had previously reported a clear dependence between antigen-specific IgG titers and *in vitro* TLR8-agonistic potency. In a standardized rabbit model using the diphtheria toxin mutein CRM197[148] as a model antigen and admixed with 100 µg/dose of TLR8-specific agonist, we observed that adjuvantic activity *in vivo* mirrored *in vitro* potency: **1h**>**1f**>**1e**.[113] Because **17a** and **21f** are considerably weaker than **1e**, that these aminoimidazoles would be less adjuvantic than previously-characterized compounds could be reliably predicted, and animal experiments were therefore not warranted.
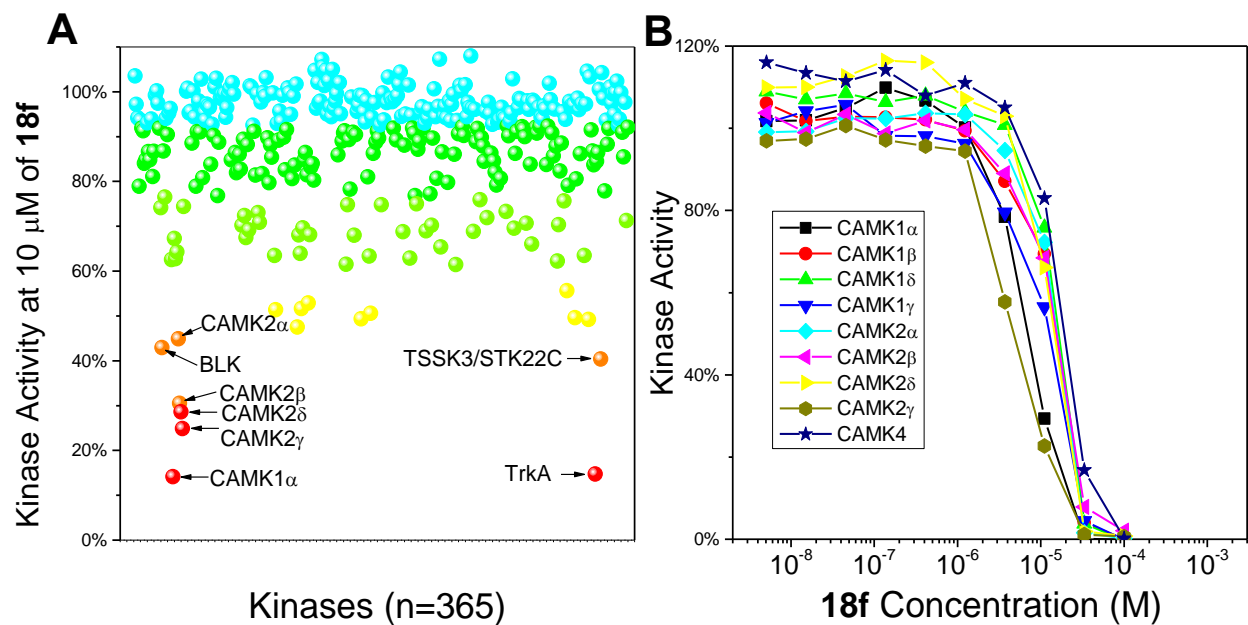
Figure 7. A. Inhibitory screen of 18f against 365 wild-type kinases**. Compound **18f** was used at a single concentration of 10 µM. Mean of duplicates are shown. CAM: calmodulin kinase. TSSK3: testes-specific serine kinase-3; TrkA: tropomyosin kinase. **B**. Dose-response profiles of inhibition of calmodulin kinases by **18f.

Compound **1h**, the most potent TLR8-specific lead adjuvant that we have characterized thus far, displays pronounced proinflammatory properties *in vitro*, and the administration of this water-

soluble compound with properties that predict a high volume of distribution is likely to result in some degree of 'wasted' (systemic) inflammation,[237] and we are currently addressing this potential drawback by devising strategies to target its delivery to secondary lymphoid tissue. Compounds **17a** and **21f** are, conversely, considerably weaker and, consequently, larger doses would become necessary which would likely also increase systemic exposure of the molecule. Indeed, a potential strength of a molecule such as **17a** may well lie in its weakness, and it seemed possible that **17a** could be better suited for other indications such as mucosal immunotherapy for atopic rhinitis. Clinical trials of aqueous formulation of monophosphoryl lipid A (CRX-675; a TLR4 agonist)[238] and methyl2-(3-(((3-(6-amino-2-butoxy-8-oxo-7,8-dihydro-9*H*-purin-9-yl)propyl)(3-morpholinopropyl) amino)methyl)phenyl)acetate (AZD8848; a TLR7 agonist)[239] have proven promising, but have been associated with systemic side effects,[240-242] and it would be desirable and advantageous for these indications to limit systemic exposure. In order to test the premise that **17a** would display significantly lower proinflammatory properties, we sought to directly compare the phosphorylation of p38 mitogen-activated protein kinase (p38MAPK), extracellular-signal-regulated kinase 1/2 (ERK1/2) and NF-κB[243-244] induced by **17a** and **21f** relative to **1f**, **1g**, and **1h**, in whole human blood. Prominent, dose-dependent phosphorylation of NF-κB was evident within 15 min of stimulation in monocytic and polymorphonuclear populations for **1f**, **1g**, and **1h** (Fig. 5), whereas **17a** and **21f** were found to be significantly less potent in inducing phosphorylation of the p65 subunit (transactivation domain) of NF-κB (Fig. 5). Taken together with cytokine induction profiles (Fig. 4), these data strengthen the premise for evaluating the effects of mucosal application of **17a** and **21f**, and experiments designed to probe lamina propria lymphocytic responses in nasal and bronchial mucosa are being planned.
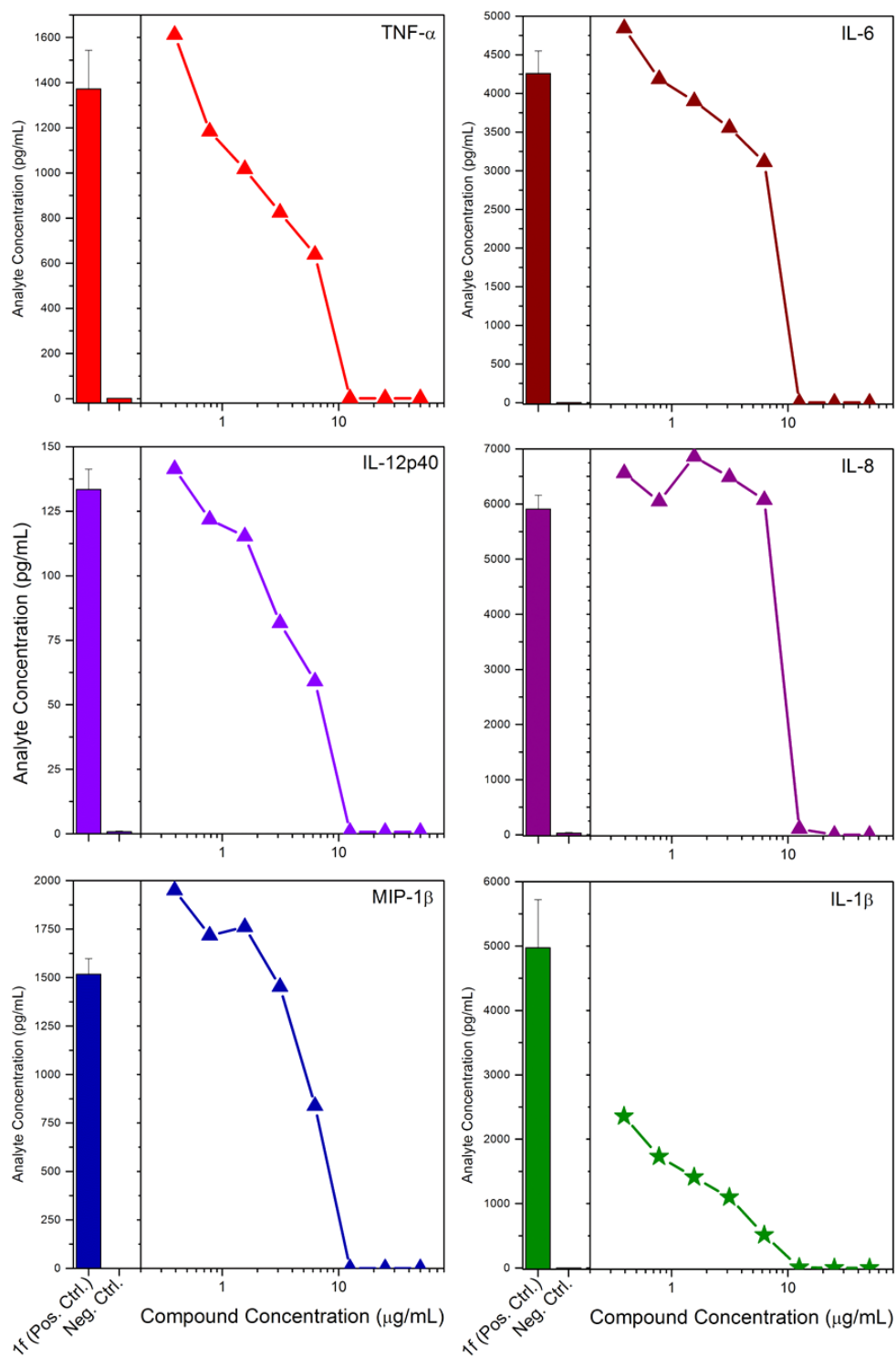
***Figure 8. Dose-dependent inhibition of 1f-stimulated cytokine release in human PBMCs by 18f.** 1f (stimulus) was at a fixed concentration of 10 μg/mL. A subset of cytokine responses are shown highlighting apparent selectivity for IL-1β release. Means of duplicates for one of two independent experiments are shown.*

All compounds were counter-screened for activity in human TLR2, TLR3, TLR4, TLR5, TLR7 and TLR9 reporter gene assays, and were found not to have off-target innate immune receptor-stimulatory activities (data not shown). In addition, we examined all inactive 2-aminoimidazole derivatives for possible receptor antagonistic activity such as we had previously described for TLR7.[90, 94-95] We observed that **7** and **18f** inhibited, in a dose-dependent manner, TLR8 responses induced by **1f** (Fig. 6A). We chose to characterize **18f** in detail due to its greater apparent antagonistic potency (Fig. 6A). We noted that **18f** also inhibited TLR2, TLR3, TLR4, TLR5, TLR7, and TLR9 responses with very similar (0.8-3 μg/mL; 2.4-9 μM) IC_{50} values (Fig. 6B), which suggested a mechanism of inhibition other than by competitive binding at TLR8. We compared the activity of **18f** with a variety of cell signaling inhibitors including chloroquine[245] (endosomal acidification inhibitor), *N*-(3-((5-iodo-4-((3-(thiophene-2-carboxamido)propyl)amino)pyrimidin-2-yl)amino)phenyl)pyrrolidine-1-carboxamide, **22** (BX-795; an inhibitor of 3-phosphoinositide-dependent kinase-1,[246] TANK-binding kinase 1 and IκB kinase-ε),[247] glibenclamide[248] (inhibitor of ATP-sensitive potassium channels), and 2-aminopurine[249] (inhibitor of double-stranded RNA (dsRNA)-activated protein kinase), and gefitinib[250] (epidermal growth factor receptor inhibitor). The inhibitory profile of **18f** closely resembled that of **22** and gefitinib not only in TLR8 screens (Fig. 6A), but also in other reporter cell lines (data not shown), prompting us to explore possible kinase inhibitory activities of **18f**. Compound **18f** was screened at a fixed concentration (10 μM) against 365 wild-type kinases using a commercial screening service (Reaction Biology, Malvern, PA). IC_{50} values for individual kinases were established with either staurosporine or appropriate control compounds (data not shown). Significant inhibition of several calmodulin kinase isoforms, as well as testis-specific serine kinase (TSSKK3), and tropomyosin receptor kinase (TrkA) was observed at 10 μM concentration of **18f** (Fig. 7A). We confirmed the

inhibitory activity of this compound against a panel of calmodulin kinases in follow-up dose-response experiments (Fig. 7B).

Compound **18f** displayed rather weak kinase inhibitory potencies with IC_{50} values ranging from 3-11 µM (Fig. 7B), and it was important to ascertain whether the *in vitro* kinase activities of **18f** would be of any potential pharmacological significance in *ex vivo* assays performed under near-physiological conditions. We first examined dose-dependent cytokine inhibition in human PBMCs stimulated with the TLR8-specific agonist **1f** at 5 µg/mL (23.36 µM) using the 41-analyte multiplexed immunoassay.
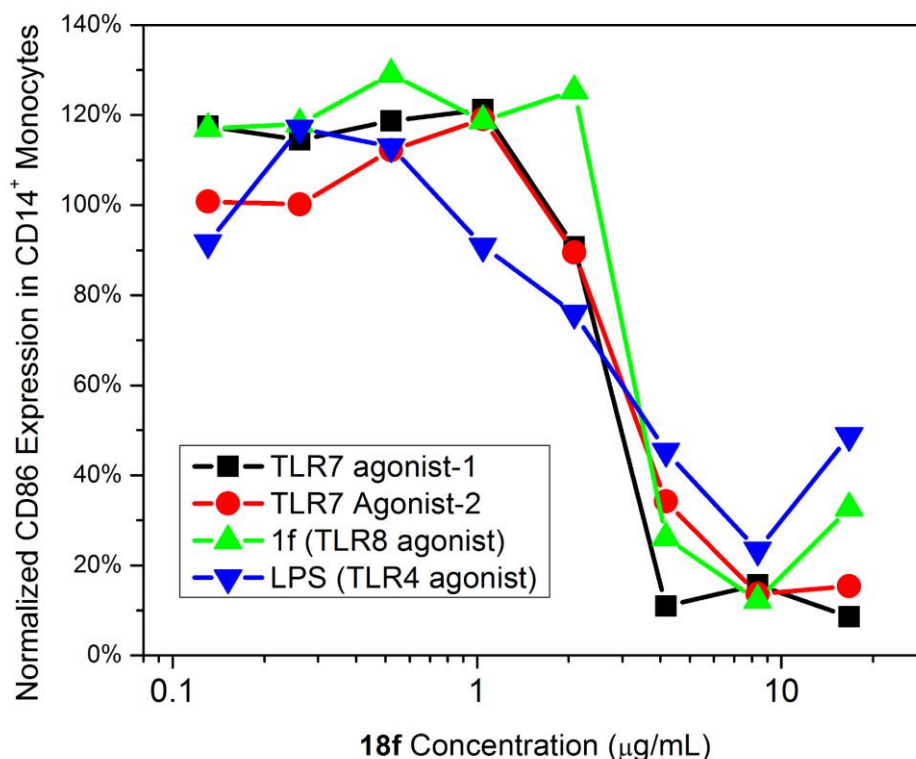
Figure 9. Dose-dependent suppression by 18f of CD86 expression in CD14^{+} monocytic subsets in whole human blood*. A 5 µg/mL concentration of **1f** was used as stimulus.*

We observed a clear, dose-dependent inhibition by **18f** of cytokines and chemokines that were upregulated by the TLR8; the IC_{50} values for the vast majority of analytes were highly concordant (3-5 µg/mL), with the sole exception of IL-1β, which was inhibited substantially at much lower concentrations of **18f** (Fig. 8). Similar profiles were observed with pure TLR4 and TLR7 stimulation (data not shown).

We sought to further confirm inhibition by **18f** of TLR signaling in whole human blood assays. We had recently reported, using multicolor flow cytometry, that TLR8 agonism, in particular, markedly upregulates antigen presentation markers in monocytes.[113] We quantified the effect of **18f** on expression levels of CD80 and CD86 in whole human blood stimulated with **1f**, LPS, and two TLR7-specific agonist that we had previously characterized.[91, 111] Depicted in Fig. 9 is the dose-dependent down-regulation of CD86 by **18f** in CD14$^+$ monocytes. Near-identical responses were also observed for CD80 (data not shown). Compound **18f** also inhibited TLR8, TLR7, and TLR4 stimuli with similar IC_{50} values (2.5 µg/mL; 7.46 µM), suggesting that this compound may be a useful starting point for further evaluation as an anti-inflammatory agent.

5.3 Conclusions

Our exploration of the 2-aminoimidazole scaffold has led us, rather unexpectedly, first to the identification of a TLR8-specific agonist of low potency (and low proinflammatory potential), and then to an analogue with functional pan-TLR inhibitory properties. As mentioned earlier, the highly attenuated proinflammatory properties of **17a** could be useful for indications such as mucosal immunotherapy for atopic rhinitis. A fitting coda for **18f** is yet to be reached, and studies designed to characterize its pharmacology in greater detail are in progress. We do not yet

understand the basis of selective suppression of IL-1β secretion, and the significance of its apparent inhibitory activity on testis-specific serine kinase is being explored.

5.4 Materials and Methods

Chemistry

All compounds were synthesized by Dr. Mallesh Beesu. All of the solvents and reagents used were obtained commercially and used as such unless noted otherwise. Moisture- or air-sensitive reactions were conducted under nitrogen atmosphere in oven-dried (120 ℃) glass apparatus. Solvents were removed under reduced pressure using standard rotary evaporators. Flash column chromatography was carried out using RediSep Rf 'Gold' high performance silica columns on CombiFlash R_f instruments unless otherwise mentioned, while thin-layer chromatography was carried out on silica gel CCM pre-coated aluminum sheets. Purity for all final compounds was confirmed to be greater than 98% by LC-MS using a Zorbax Eclipse Plus 4.6 mm x 150 mm, 5 µm analytical reverse phase C_{18} column with H_2O-CH_3CN and H_2O-MeOH gradients and an Agilent 6520 ESI-QTOF Accurate Mass spectrometer (mass accuracy of 5 ppm) operating in the positive ion acquisition mode.

*2-Nitro-1-pentyl-1H-imidazole (**3**)*

To a solution of 2-nitroimidazole (**2**) (113 mg, 1 mmol) in DMF (5 mL) were added K_2CO_3 (276 mg, 2 mmol) and 1-iodopentane (156.6 μL, 1.2 mmol). The reaction mixture was stirred for 12 h then the solvent was removed under reduced pressure. The reaction mixture was diluted with water and extracted with EtOAc (3 x 10 mL). The combined organic layer was dried over Na_2SO_4, concentrated under reduced pressure, and the crude material was purified by silica gel column chromatography (20% EtOAc/hexanes) to obtain the compound **3** as a pale yellow oil (150 mg,

82%). ^{1}H NMR (500 MHz, CDCl$_3$) δ 7.13 (d, J = 1.1 Hz, 1H), 7.08 (d, J = 1.1 Hz, 1H), 4.39 (t, J = 7.4 Hz, 2H), 1.87 – 1.81 (m, 2H), 1.38 – 1.30 (m, 4H), 0.90 (t, J = 7.1 Hz, 3H). ^{13}C NMR (126 MHz, CDCl$_3$) δ 144.88, 128.41, 125.96, 50.49, 30.35, 28.58, 22.23, 13.96. MS (ESI-TOF) for C$_8$H$_{13}$N$_3$O$_2$[M + H]$^+$ calculated 184.1081, found 184.1076.

1-Pentyl-1H-imidazol-2-amine hydrochloride (4)

To a solution of compound **3** (18.3 mg, 0.1 mmol) in anhydrous EtOAc (10 mL) was added a catalytic amount of Pt/C, and the reaction mixture was subjected to hydrogenation at 30 psi for 1 h. The reaction mixture was filtered, and the filtrate concentrated under reduced pressure. The crude material was purified using silica gel column chromatography (10% MeOH/CH$_2$Cl$_2$) then treated with 2N HCl/Et$_2$O to obtain **4** as white solid (15 mg, 79%). ^{1}H NMR (500 MHz, MeOD) δ 6.89 (d, J = 2.5 Hz, 1H), 6.84 (d, J = 2.4 Hz, 1H), 3.85 (t, J = 7.3 Hz, 2H), 1.79 – 1.72 (m, 2H), 1.42 – 1.31 (m, 4H), 0.94 (t, J = 7.1 Hz, 3H). ^{13}C NMR (126 MHz, MeOD) δ 147.64, 117.47, 113.68, 46.41, 29.55, 29.52, 23.29, 14.24. MS (ESI-TOF) for C$_8$H$_{15}$N$_3$ [M + H]$^+$ calculated 154.1339, found 154.1318.

N-Pentylpyrimidin-2-amine (6)

To a solution of 2-chloropyrimidine (115 mg, 1 mmol) in MeOH (2 mL), was added DIPEA (174 μL, 1 mmol) and amyl amine (116 μL, 1 mmol). The reaction mixture was stirred for 12 h at 75 ºC. The reaction mixture was cooled to room temperature and the solvent was removed under reduced pressure. The reaction mixture was diluted with water and extracted with EtOAc (3 x 20 mL). The combined organic layer was dried over Na$_2$SO$_4$ and concentrated under reduced pressure, and the crude material was purified by flash chromatography (10% MeOH/CH$_2$Cl$_2$) to afford the

compound **6** as a pale oil (125 mg, 75%). ^{1}H NMR (500 MHz, CDCl$_3$) δ 8.26 (d, J = 4.8 Hz, 2H), 6.49 (t, J = 4.8 Hz, 1H), 5.17 (s, 1H), 3.38 (td, J = 5.7, 7.2 Hz, 2H), 1.64 – 1.57 (m, 2H), 1.38 – 1.34 (m, 4H), 0.90 (t, J = 7.1 Hz, 3H). ^{13}C NMR (126 MHz, CDCl$_3$) δ 162.56, 158.15, 110.42, 41.62, 29.41, 29.26, 22.59, 14.17. MS (ESI-TOF) for C$_9$H$_{15}$N$_3$ [M + H]$^+$ calculated 166.1339, found 166.1436.

*1-Pentyl-5-phenyl-1H-imidazol-2-amine hydrochloride (**7**)*

To a solution of compound **6** (66 mg, 0.4 mmol) in anhydrous acetonitrile (2 mL) was added 2-bromoacetophenone (107.4 mg, 0.54 mmol). The reaction mixture was then heated under microwave conditions (150 W, 150 ℃) in a sealed vial for 20 min. The reaction mixture was cooled to room temperature, hydrazine hydrate (0.1 mL, 64% solution) was added, and heated under microwave conditions (100 W, 100 ℃) for another 5 min. The reaction mixture was diluted with water and extracted with dichloromethane (3 x 20 mL). The combined organic layer was dried over Na$_2$SO$_4$ and concentrated under reduced pressure, crude material was purified by flash chromatography (10% MeOH/CH$_2$Cl$_2$) then treated with 2N HCl/Et$_2$O to obtain the compound **7** as a white solid (74 mg, 70%). ^{1}H NMR (500 MHz, MeOD) δ 7.53 – 7.52 (m, 3H), 7.47 – 7.45 (m, 2H), 6.90 (s, 1H), 3.90 (t, J = 7.6 Hz, 2H), 1.56 – 1.50 (m, 2H), 1.19 – 1.08 (m, 4H), 0.78 (t, J = 7.1 Hz, 3H). ^{13}C NMR (126 MHz, MeOD) δ 148.27, 130.81, 130.79, 130.70, 130.22, 128.55, 111.70, 44.03, 29.23, 28.86, 22.95, 14.07. MS (ESI-TOF) for C$_{14}$H$_{19}$N$_3$ [M + H]$^+$ calculated 230.1652, found 230.1669.

*4,5-Dibromo-2-nitro-1-pentyl-1H-imidazole (**8**)*

To a solution of compound **3** (91.6 mg, 0.5 mmol) in anhydrous DMF (5 mL) was added NBS (180 mg, 1 mmol), and the reaction mixture was stirred for 12 h at 75 ℃. The reaction mixture

was cooled to room temperature and the solvent was removed under reduced pressure. The reaction mixture was diluted with water and extracted with EtOAc (3 x 10 mL). The combined organic layer was dried over Na_2SO_4, concentrated under reduced pressure, and the crude material was purified by flash chromatography (10% EtOAc/hexanes) to obtain the compound **8** as a pale yellow solid (102 mg, 60 %). ^{1}H NMR (500 MHz, CDCl$_3$) δ 4.50 (t, J = 7.8 Hz, 2H), 1.84 – 1.78 (m, 2H), 1.40 – 1.36 (m, 4H), 0.93 (t, J = 7.0 Hz, 3H). ^{13}C NMR (126 MHz, CDCl$_3$) δ 143.92, 118.01, 112.75, 50.65, 29.59, 28.54, 22.24, 13.96. MS (ESI-TOF) for $C_8H_{11}Br_2N_3O_2$ [M + H]$^+$ calculated 339.9291, found 339.9252.

*2-Nitro-1-pentyl-4,5-diphenyl-1H-imidazole (**9**)*

To a stirred solution of compound **8** (68.2 mg, 0.2 mmol) in 1,4-dioxane (3 mL) were added phenylboronic acid (97.6 mg, 0.8 mmol), Pd(dppf)Cl$_2$ (29.2 mg, 0.04 mmol) and K_2CO_3 (221 mg, 1.6 mmol). The resulting reaction mixture was stirred at 90 ºC under nitrogen atmosphere for 12 h. The reaction mixture was diluted with water and extracted with EtOAc (3 x 20 mL). The combined organic layer was dried over Na_2SO_4 and concentrated under reduced pressure, crude material was purified by flash chromatography (20% EtOAc/hexanes) to obtain the compound **9** as a yellow solid (37 mg, 55%). ^{1}H NMR (500 MHz, CDCl$_3$) δ 7.59 – 7.51 (m, 3H), 7.46 – 7.44 (m, 2H), 7.39 – 7.37 (m, 2H), 7.22 – 7.21 (m, 3H), 4.20 (t, J = 7.9 Hz, 2H), 1.73 – 1.67 (m, 2H), 1.21 – 1.14 (m, 4H), 0.80 (t, J = 6.9 Hz, 3H). ^{13}C NMR (126 MHz, CDCl$_3$) δ 144.75, 138.33, 134.33, 132.19, 130.95, 130.38, 129.64, 128.64, 128.42, 128.02, 127.35, 47.56, 30.39, 28.61, 21.99, 13.88. MS (ESI-TOF) for $C_{20}H_{21}N_3O_2$ [M + H]$^+$ calculated 336.1707, found 336.1814.

Compound 10 was synthesized similarly as compound 4.

1-Pentyl-4,5-diphenyl-1H-imidazol-2-amine hydrochloride (10)

Compound **9** was used as reagent. Off-white solid (28 mg, 82%). ^{1}H NMR (500 MHz, MeOD) δ 7.57 – 7.52 (m, 3H), 7.45 – 7.42 (m, 2H), 7.30 – 7.28 (m, 3H), 7.24 – 7.21 (m, 2H), 3.77 (t, J = 7.7 Hz, 2H), 1.57 – 1.50 (m, 2H), 1.18 – 1.11 (m, 4H), 0.79 (t, J = 6.7 Hz, 3H). ^{13}C NMR (126 MHz, MeOD) δ 147.79, 132.53, 131.31, 130.57, 129.86, 129.67, 128.85, 128.43, 127.93, 125.65, 124.70, 44.09, 29.28, 28.97, 22.93, 14.06. MS (ESI-TOF) for $C_{20}H_{23}N_3$ [M + H]$^+$ calculated 306.1965, found 306.1971.

4-Bromo-2-nitro-1-pentyl-1H-imidazole (11)

To a solution of compound **3** (183 mg, 1 mmol) in anhydrous DMF (10 mL) was added NBS (178 mg, 1 mmol), and the reaction mixture was stirred for 24 h at 50 ºC. The reaction mixture was cooled to room temperature and the solvent was removed under reduced pressure. The reaction mixture was diluted with water and extracted with EtOAc (3 x 10 mL). The combined organic layer was dried over Na$_2$SO$_4$, concentrated under reduced pressure, and the crude material was purified by silica gel column chromatography (10% EtOAc/hexanes) to obtain the compound **11** as a yellow oil (196 mg, 75%). ^{1}H NMR (500 MHz, CDCl$_3$) δ 7.08 (s, 1H), 4.39 (t, J = 7.4 Hz, 2H), 1.88 – 1.82 (m, 2H), 1.39 – 1.31 (m, 4H), 0.91 (t, J = 7.0 Hz, 3H). ^{13}C NMR (126 MHz, CDCl$_3$) δ 143.45, 125.44, 115.13, 50.95, 30.27, 28.55, 22.23, 13.95. MS (ESI-TOF) for $C_8H_{12}BrN_3O_2$ [M + H]$^+$ calculated 262.0186, found 262.0149.

*2-Nitro-1-pentyl-4-phenyl-1H-imidazole (**12a**)*

To a stirred solution of compound **11** (52 mg, 0.2 mmol) in 1,4-dioxane (2 mL) were added

phenylboronic acid (48.8 mg, 0.4 mmol), Pd(dppf)Cl$_2$ (14.6 mg, 0.02 mmol) and K$_2$CO$_3$ (110 mg,

0.8 mmol). The resulting reaction mixture was stirred at 85 ºC under nitrogen atmosphere for 8 h.

The reaction mixture was diluted with water and extracted with EtOAc (3 x 20 mL). The combined

organic layer was dried over Na$_2$SO$_4$ and concentrated under reduced pressure, crude material was

purified by flash chromatography (15% EtOAc/hexanes) to obtain the compound **12a** as a yellow

oil (45 mg, 87%). ^{1}H NMR (500 MHz, CDCl$_3$) δ 7.83 – 7.80 (m, 2H), 7.43 – 7.40 (m, 2H), 7.36 –

7.32 (m, 2H), 4.44 (t, J = 7.4 Hz, 2H),1.94 – 1.87 (m, 2H), 1.40 – 1.36 (m, 4H), 0.92 (t, J = 6.9

Hz, 3H). ^{13}C NMR (126 MHz, CDCl$_3$) δ 144.61, 140.85, 131.68, 128.94, 128.64, 125.46, 121.49,

50.84, 30.41, 28.68, 22.31, 14.01. MS (ESI-TOF) for C$_{14}$H$_{17}$N$_3$O$_2$ [M + H]$^+$ calculated 260.1394,

found 260.1470.

*Compounds **12b-i**, **13a-f**, **14a-b**, **14d-h**, **15a-g**,and **16a-j** were synthesized similarly as compound*

12a.

*2-Nitro-1-pentyl-4-(o-tolyl)-1H-imidazole (**12b**)*

o-Tolylboronic acid was used as reagent. Yellow solid (42 mg, 77%). ^{1}H NMR (500 MHz, CDCl$_3$)

δ 7.76 – 7.73 (m, 1H), 7.25 – 7.23 (m, 3H), 7.19 (s, 1H), 4.44 (t, J = 7.4 Hz, 2H), 2.49 (s, 3H),

1.93 – 1.87 (m, 2H), 1.40 – 1.34 (m, 4H), 0.91 (t, J = 6.9 Hz, 3H). ^{13}C NMR (126 MHz, CDCl$_3$) δ

144.08, 140.56, 135.53, 131.20, 131.09, 129.10, 128.50, 126.30, 124.00, 50.66, 30.44, 28.69,

22.30, 21.64, 14.02. MS (ESI-TOF) for C$_{15}$H$_{19}$N$_3$O$_2$ [M + H]$^+$ calculated 274.1550, found

274.1581.

*4-(2-Ethylphenyl)-2-nitro-1-pentyl-1H-imidazole (**12c**)*

2-Ethylphenylboronic acid was used as reagent. Yellow oil (50 mg, 87%). ^{1}H NMR (500 MHz, CDCl$_3$) δ 7.60 (dd, J = 1.2, 7.5 Hz, 1H), 7.34 – 7.28 (m, 2H), 7.25 – 7.22 (m, 1H), 7.16 (s, 1H), 4.46 (t, J = 7.3 Hz, 2H), 2.85 (q, J = 7.5 Hz, 2H), 1.95 – 1.88 (m, 2H), 1.41 – 1.36 (m, 4H), 1.22 (t, J = 7.5 Hz, 3H), 0.93 (t, J = 6.9 Hz, 3H). ^{13}C NMR (126 MHz, CDCl$_3$) δ 144.10, 142.11, 140.69, 130.82, 129.74, 129.16, 128.84, 126.12, 123.78, 50.63, 30.41, 28.69, 26.75, 22.31, 15.43, 14.04. MS (ESI-TOF) for C$_{16}$H$_{21}$N$_3$O$_2$ [M + H]$^+$ calculated 288.1707, found 288.1700.

*2-Nitro-1-pentyl-4-(m-tolyl)-1H-imidazole (**12d**)*

m-Tolylboronic acid was used as reagent. Yellow solid (46 mg, 84%). ^{1}H NMR (500 MHz, CDCl$_3$) δ 7.69 (s, 1H), 7.57 (d, J = 7.8 Hz, 1H), 7.35 (s, 1H), 7.30 (t, J = 7.6 Hz, 1H), 7.16 (d, J = 7.5 Hz, 1H), 4.44 (t, J = 7.5 Hz, 2H), 2.39 (s, 3H), 1.94 – 1.87 (m, 2H), 1.40 – 1.35 (m, 4H), 0.92 (t, J = 6.9 Hz, 3H). ^{13}C NMR (126 MHz, CDCl$_3$) δ 144.55, 141.00, 138.76, 131.53, 129.45, 128.81, 126.16, 122.50, 121.52, 50.84, 30.41, 28.68, 22.31, 21.53, 14.02. MS (ESI-TOF) for C$_{15}$H$_{19}$N$_3$O$_2$ [M + H]$^+$ calculated 274.1550, found 274.1578.

*2-Nitro-1-pentyl-4-(p-tolyl)-1H-imidazole (**12e**)*

p-Tolylboronic acid was used as reagent. Yellow solid (44 mg, 80%). ^{1}H NMR (500 MHz, CDCl$_3$) δ 7.70 (d, J = 8.0 Hz, 2H), 7.31 (s, 1H), 7.22 (d, J = 8.0 Hz, 2H), 4.43 (t, J = 7.4 Hz, 2H), 2.37 (s, 3H), 1.93 – 1.85 (m, 2H), 1.42 – 1.33 (m, 4H), 0.92 (t, J = 6.9 Hz, 3H). ^{13}C NMR (126 MHz, CDCl$_3$) δ 144.49, 141.02, 138.60, 129.62, 128.87, 125.37, 121.20, 50.80, 30.40, 28.68, 22.30, 21.45, 14.01. MS (ESI-TOF) for C$_{15}$H$_{19}$N$_3$O$_2$ [M + H]$^+$ calculated 274.1550, found 274.1579.

*4-(2,3-Dimethylphenyl)-2-nitro-1-pentyl-1H-imidazole (**12f**)*

2,3-Dimethylphenylboronic acid was used as reagent. Yellow oil (50 mg, 87%). ^{1}H NMR (500 MHz, CDCl$_3$) δ 7.42 (dd, J = 1.7, 7.4 Hz, 1H), 7.20 – 7.12 (m, 3H), 4.46 (t, J = 7.4 Hz, 2H), 2.37 (s, 3H), 2.34 (s, 3H), 1.95 – 1.88 (m, 2H), 1.42 – 1.36 (m, 4H), 0.93 (t, J = 7.0 Hz, 3H). ^{13}C NMR (126 MHz, CDCl$_3$) δ 143.98, 141.38, 137.60, 134.68, 131.71, 130.27, 127.63, 125.70, 124.21, 50.62, 30.42, 28.71, 22.30, 20.89, 17.07, 14.03. MS (ESI-TOF) for C$_{16}$H$_{21}$N$_3$O$_2$ [M + H]$^+$ calculated 288.1707, found 288.1802.

*4-(2,4-Dimethylphenyl)-2-nitro-1-pentyl-1H-imidazole (**12g**)*

2,4-Dimethylphenylboronic acid was used as reagent. Yellow oil (45 mg, 78%). ^{1}H NMR (500 MHz, CDCl$_3$) δ 7.65 (d, J = 7.7 Hz, 1H), 7.17 (s, 1H), 7.10 – 7.04 (m, 2H), 4.45 (t, J = 7.4 Hz, 2H), 2.46 (s, 3H), 2.34 (s, 3H), 1.94 – 1.87 (m, 2H), 1.40 – 1.36 (m, 4H), 0.92 (t, J = 7.0 Hz, 3H). ^{13}C NMR (126 MHz, CDCl$_3$) δ 144.01, 140.70, 138.35, 135.29, 131.86, 129.02, 128.35, 127.06, 123.79, 50.63, 30.44, 28.70, 22.30, 21.58, 21.27, 14.03. MS (ESI-TOF) for C$_{16}$H$_{21}$N$_3$O$_2$ [M + H]$^+$ calculated 288.1707, found 288.1771.

*4-(2,5-Dimethylphenyl)-2-nitro-1-pentyl-1H-imidazole (**12h**)*

2,5-Dimethylphenylboronic acid was used as reagent. Yellow solid (50 mg, 87%). ^{1}H NMR (500 MHz, CDCl$_3$) δ 7.61 (s, 1H), 7.19 (s, 1H), 7.13 (d, J = 7.7 Hz, 1H), 7.07 (dd, J = 1.9, 7.7 Hz, 1H), 4.45 (t, J = 7.4 Hz, 2H), 2.45 (s, 3H), 2.35 (s, 3H), 1.95 – 1.87 (m, 2H), 1.40 – 1.35 (m, 4H), 0.93 (t, J = 6.9 Hz, 3H). ^{13}C NMR (126 MHz, CDCl$_3$) δ 144.05, 140.61, 135.90, 132.24, 131.05, 130.89, 129.56, 129.28, 124.06, 50.67, 30.44, 28.69, 22.30, 21.25, 21.03, 14.03. MS (ESI-TOF) for C$_{16}$H$_{21}$N$_3$O$_2$ [M + H]$^+$ calculated 288.1707, found 288.1677.

4-(2,6-Dimethylphenyl)-2-nitro-1-pentyl-1H-imidazole (12i)

2,6-Dimethylphenylboronic acid was used as reagent. Yellow oil (48 mg, 84%). ^{1}H NMR (500 MHz, CDCl$_3$) δ 7.20 – 7.16 (m, 1H), 7.11 – 7.05 (m, 2H), 6.98 (s, 1H), 4.48 (t, J = 7.2 Hz, 2H), 2.17 (s, 6H), 1.96 – 1.89 (m, 2H), 1.42 – 1.33 (m, 4H), 0.92 (t, J = 7.0 Hz, 3H). ^{13}C NMR (126 MHz, CDCl$_3$) δ 144.33, 139.57, 137.88, 131.75, 128.69, 127.63, 124.74, 50.56, 30.31, 28.65, 22.28, 20.89, 14.05. MS (ESI-TOF) for C$_{16}$H$_{21}$N$_3$O$_2$ [M + H]$^+$ calculated 288.1707, found 288.1735.

4-Benzyl-2-nitro-1-pentyl-1H-imidazole (13a)

Benzylboronic acid pinacol ester was used as reagent. Yellow oil (30 mg, 55%). ^{1}H NMR (500 MHz, CDCl$_3$) δ 7.34 – 7.30 (m, 2H), 7.27 – 7.23 (m, 3H), 6.65 (s, 1H), 4.29 (t, J = 7.5 Hz, 2H), 3.96 (s, 2H), 1.83 – 1.75 (m, 2H), 1.38 – 1.23 (m, 4H), 0.89 (t, J = 7.1 Hz, 3H). ^{13}C NMR (126 MHz, CDCl$_3$) δ 143.87, 142.16, 138.41, 129.04, 128.86, 126.85, 123.40, 50.43, 35.14, 30.37, 28.64, 22.24, 13.99. MS (ESI-TOF) for C$_{15}$H$_{19}$N$_3$O$_2$ [M + H]$^+$ calculated 274.1550, found 274.1587.

(E)-2-Nitro-1-pentyl-4-styryl-1H-imidazole (13b)

Trans-2-Phenylvinylboronic acid was used as reagent. Yellow solid (40 mg, 70%). ^{1}H NMR (500 MHz, CDCl$_3$) δ 7.50 – 7.48 (m, 2H), 7.41 – 7.34 (m, 3H), 7.29 – 7.27 (m, 1H), 7.12 (s, 1H), 6.92 (d, J = 16.2 Hz, 1H), 4.40 (t, J = 7.3 Hz, 2H), 1.92 – 1.84 (m, 2H), 1.40 – 1.32 (m, 4H), 0.92 (t, J = 6.9 Hz, 3H). ^{13}C NMR (126 MHz, CDCl$_3$) δ 144.41, 139.45, 136.61, 131.35, 128.89, 128.29, 126.76, 123.19, 117.99, 50.74, 30.36, 28.66, 22.30, 14.01. MS (ESI-TOF) for C$_{16}$H$_{19}$N$_3$O$_2$ [M + H]$^+$ calculated 286.1550, found 286.1584.

*4-(Naphthalen-1-yl)-2-nitro-1-pentyl-1H-imidazole (**13c**)*

1-Naphthylboronic acid was used as reagent. Yellow oil (55 mg, 89%). ^{1}H NMR (500 MHz, CDCl$_3$) δ 8.43 – 8.39 (m, 1H), 7.91 – 7.88 (m, 2H), 7.74 (dd, *J* = 1.2, 7.1 Hz, 1H), 7.59 – 7.48 (m, 3H), 7.38 (s, 1H), 4.52 (t, *J* = 7.4 Hz, 2H), 2.02 – 1.92 (m, 2H), 1.45 – 1.39 (m, 4H), 0.95 (t, *J* = 7.0 Hz, 3H). ^{13}C NMR (126 MHz, CDCl$_3$) δ 144.44, 140.33, 134.02, 131.00, 129.38, 129.32, 128.74, 127.49, 126.99, 126.18, 125.44, 125.21, 124.52, 50.79, 30.50, 28.77, 22.33, 14.05. MS (ESI-TOF) for C$_{18}$H$_{19}$N$_3$O$_2$ [M + H]$^+$ calculated 310.1550, found 310.1611.

*4-(Naphthalen-2-yl)-2-nitro-1-pentyl-1H-imidazole (**13d**)*

2-Naphthylboronic acid was used as reagent. Yellow solid (45 mg, 73%). ^{1}H NMR (400 MHz, CDCl$_3$) δ 8.36 (s, 1H), 7.91 – 7.82 (m, 4H), 7.53 – 7.46 (m, 3H), 4.47 (t, *J* = 7.4 Hz, 2H), 1.97 – 1.90 (m, 2H), 1.41 – 1.38 (m, 4H), 0.94 (t, *J* = 6.7 Hz, 3H). ^{13}C NMR (126 MHz, CDCl$_3$) δ 144.73, 140.87, 133.60, 133.41, 128.95, 128.68, 128.42, 127.90, 126.72, 126.50, 124.44, 123.24, 121.84, 50.92, 30.45, 28.72, 22.33, 14.03. MS (ESI-TOF) for C$_{18}$H$_{19}$N$_3$O$_2$ [M + H]$^+$ calculated 310.1550, found 310.1627.

*4-([1,1'-Biphenyl]-4-yl)-2-nitro-1-pentyl-1H-imidazole (**13e**)*

4-Biphenylboronic acid was used as reagent. Yellow solid (56 mg, 83%). ^{1}H NMR (500 MHz, CDCl$_3$) δ 7.90 – 7.83 (m, 2H), 7.67 – 7.62 (m, 4H), 7.48 – 7.43 (m, 2H), 7.39 (s, 1H), 7.38 – 7.33 (m, 1H), 4.46 (t, *J* = 7.4 Hz, 2H), 1.95 – 1.89 (m, 2H), 1.40 – 1.38 (m, 4H), 0.93 (t, *J* = 7.0 Hz, 3H). ^{13}C NMR (126 MHz, CDCl$_3$) δ 144.66, 141.38, 140.55, 130.63, 128.98, 127.68, 127.60, 127.12, 125.86, 121.56, 115.78, 50.89, 30.42, 28.69, 22.32, 14.02. MS (ESI-TOF) for C$_{20}$H$_{21}$N$_3$O$_2$ [M + H]$^+$ calculated 336.1707, found 336.1764.

*4-(2-(Benzyloxy)phenyl)-2-nitro-1-pentyl-1H-imidazole (**13f**)*

2-(Benzyloxy)phenylboronic acid was used as reagent. Yellow solid (55 mg, 75%). ^{1}H NMR (500 MHz, CDCl$_3$) δ 8.27 (dd, J = 1.8, 7.7 Hz, 1H), 7.55 (s, 1H), 7.50 – 7.46 (m, 2H), 7.45 – 7.38 (m, 3H), 7.33 – 7.28 (m, 1H), 7.11 – 7.02 (m, 2H), 5.18 (s, 2H), 4.28 (t, J = 7.3 Hz, 2H), 1.78 – 1.71 (m, 2H), 1.35 – 1.21 (m, 4H), 0.89 (t, J = 7.2 Hz, 3H). ^{13}C NMR (126 MHz, CDCl$_3$) δ 155.92, 143.84, 136.74, 136.70, 129.33, 128.88, 128.57, 128.27, 128.16, 126.26, 121.51, 120.72, 112.00, 70.81, 50.47, 29.97, 28.52, 22.23, 14.01. MS (ESI-TOF) for C$_{21}$H$_{23}$N$_3$O$_3$ [M + H]$^+$ calculated 366.1812, found 366.1814.

*3-(2-Nitro-1-pentyl-1H-imidazol-4-yl)pyridine (**14a**)*

3-Pyridinylboronic acid was used as reagent. Gray solid (30 mg, 58%). ^{1}H NMR (500 MHz, CDCl$_3$) δ 8.98 (d, J = 1.4 Hz, 1H), 8.58 (dd, J = 1.6, 4.8 Hz, 1H), 8.19 – 8.17 (m, 1H), 7.43 (s, 1H), 7.40 – 7.30 (m, 1H), 4.47 (t, J = 7.5 Hz, 2H), 1.95 – 1.89 (m, 2H), 1.40 – 1.38 (m, 4H), 0.93 (t, J = 7.0 Hz, 3H). ^{13}C NMR (126 MHz, CDCl$_3$) δ 149.62, 146.77, 144.93, 137.80, 132.95, 127.86, 123.89, 121.73, 50.98, 30.43, 28.67, 22.29, 14.00. MS (ESI-TOF) for C$_{13}$H$_{16}$N$_4$O$_2$ [M + H]$^+$ calculated 261.1346, found 261.1390.

*3,5-Dimethyl-4-(2-nitro-1-pentyl-1H-imidazol-4-yl)isoxazole (**14b**)*

3,5-Dimethylisoxazol-4-yl-4-boronic acid was used as reagent. Yellow solid (42 mg, 75%). ^{1}H NMR (500 MHz, CDCl$_3$) δ 7.08 (s, 1H), 4.44 (t, J = 7.5 Hz, 2H), 2.61 (s, 3H), 2.42 (s, 3H), 1.94 – 1.87 (m, 2H), 1.42 – 1.33 (m, 4H), 0.93 (t, J = 7.0 Hz, 3H). ^{13}C NMR (126 MHz, CDCl$_3$) δ 167.32, 158.23, 132.07, 128.46, 122.33, 108.50, 50.72, 30.47, 28.69, 22.28, 14.02, 12.58, 11.67. MS (ESI-TOF) for C$_{13}$H$_{18}$N$_4$O$_3$ [M + H]$^+$ calculated 279.1452, found 279.1423.

*2-(2-Nitro-1-pentyl-1H-imidazol-4-yl)benzaldehyde (**14d**)*

2-Formylphenylboronic acid was used as reagent. Yellow solid (42 mg, 73%). ^{1}H NMR (500 MHz, CDCl$_3$) δ 10.40 (s, 1H), 7.98 (dd, J = 1.4, 7.7 Hz, 1H), 7.75 (dd, J = 1.2, 7.7 Hz, 1H), 7.66 – 7.63 (m, 1H), 7.53 – 7.49 (m, 1H), 7.40 (s, 1H), 4.48 (t, J = 7.4 Hz, 2H), 1.97 – 1.89 (m, 2H), 1.41 – 1.37 (m, 4H), 0.93 (t, J = 7.0 Hz, 3H). ^{13}C NMR (126 MHz, CDCl$_3$) δ 192.29, 144.63, 137.56, 134.35, 133.95, 133.89, 130.18, 129.48, 128.94, 125.30, 50.88, 30.42, 28.67, 22.27, 14.00. MS (ESI-TOF) for C$_{15}$H$_{17}$N$_3$O$_3$ [M + H]$^+$ calculated 288.1343, found 288.1349.

*2-Nitro-4-(4-nitrophenyl)-1-pentyl-1H-imidazole (**14e**)*

4-Nitrophenylboronic acid was used as reagent. Red solid (43 mg, 71%). ^{1}H NMR (500 MHz, CDCl$_3$) δ 8.28 (d, J = 8.9 Hz, 2H), 7.98 (d, J = 9.0 Hz, 2H), 7.50 (s, 1H), 4.48 (t, J = 7.5 Hz, 2H), 1.96 – 1.89 (m, 2H), 1.42 – 1.37 (m, 4H), 0.93 (t, J = 6.9 Hz, 3H). ^{13}C NMR (126 MHz, CDCl$_3$) δ 147.63, 145.04, 138.25, 137.89, 125.96, 124.43, 122.88, 51.11, 30.43, 28.67, 22.29, 14.00. MS (ESI-TOF) for C$_{14}$H$_{16}$N$_4$O$_4$ [M + H]$^+$ calculated 305.1244, found 305.1260.

*4-(2-Nitro-1-pentyl-1H-imidazol-4-yl)benzamide (**14f**)*

4-Aminocarbonylphenylboronic acid was used as reagent. Yellow solid (52 mg, 86%). ^{1}H NMR (500 MHz, DMSO-d_6) δ 8.34 (s, 1H), 8.01 (s, 1H), 7.95 (d, J = 8.5 Hz, 2H), 7.90 (d, J = 8.5 Hz, 2H), 7.39 (s, 1H), 4.40 (t, J = 7.4 Hz, 2H), 1.88 – 1.81 (m, 2H), 1.36 – 1.28 (m, 4H), 0.88 (t, J = 6.9 Hz, 3H). ^{13}C NMR (126 MHz, DMSO-d_6) δ 167.40, 144.56, 137.95, 134.56, 133.52, 128.19, 124.77, 124.40, 49.95, 29.25, 28.02, 21.66, 13.82. MS (ESI-TOF) for C$_{15}$H$_{18}$N$_4$O$_3$ [M + H]$^+$ calculated 303.1452, found 303.1446.

*Methyl 4-(2-nitro-1-pentyl-1H-imidazol-4-yl)benzoate (**14g**)*

4-Methoxycarbonylphenylboronic acid was used as reagent. Yellow solid (50 mg, 79%). ^{1}H NMR (500 MHz, CDCl$_3$) δ 8.09 (d, J = 8.7 Hz, 2H), 7.89 (d, J = 8.5 Hz, 2H), 7.45 (s, 1H), 4.46 (t, J = 7.6 Hz, 2H), 3.94 (s, 3H), 1.96 – 1.87 (m, 2H), 1.42 – 1.36 (m, 4H), 0.93 (t, J = 7.0 Hz, 3H). ^{13}C NMR (126 MHz, CDCl$_3$) δ 166.85, 144.82, 139.59, 135.94, 130.31, 129.98, 125.26, 122.36, 52.35, 50.98, 30.43, 28.67, 22.30, 14.00. MS (ESI-TOF) for C$_{16}$H$_{19}$N$_3$O$_4$ [M + H]$^+$ calculated 318.1448, found 318.1430.

*Methyl 2-(2-nitro-1-pentyl-1H-imidazol-4-yl)benzoate (**14h**)*

2-Methoxycarbonylphenylboronic acid was used as reagent. Yellow oil (55 mg, 87%). ^{1}H NMR (500 MHz, CDCl$_3$) δ 7.78 – 7.74 (m, 2H), 7.55 – 7.52 (m, 1H), 7.42 (dd, J = 1.3, 7.6 Hz, 1H), 7.39 (s, 1H), 4.44 (t, J = 7.4 Hz, 2H), 3.86 (s, 3H), 1.94 – 1.86 (m, 2H), 1.41 – 1.35 (m, 4H), 0.93 (t, J = 6.9 Hz, 3H). ^{13}C NMR (126 MHz, CDCl$_3$) δ 169.03, 144.02, 138.79, 131.70, 131.50, 130.46, 130.13, 129.70, 128.36, 124.70, 52.58, 50.74, 30.41, 28.66, 22.31, 14.03. MS (ESI-TOF) for C$_{16}$H$_{19}$N$_3$O$_4$ [M + H]$^+$ calculated 318.1448, found 318.1544.

*4-(2-Methoxyphenyl)-2-nitro-1-pentyl-1H-imidazole (**15a**)*

2-Methoxyphenylboronic acid was used as reagent. Yellow solid (45 mg, 78%). ^{1}H NMR (500 MHz, CDCl$_3$) δ 8.24 (dd, J = 1.8, 7.7 Hz, 1H), 7.66 (s, 1H), 7.36 – 7.27 (m, 1H), 7.07 – 7.04 (m, 1H), 6.97 (dd, J = 1.0, 8.3 Hz, 1H), 4.43 (t, J = 7.4 Hz, 2H), 3.97 (s, 3H), 1.93 – 1.86 (m, 2H), 1.41 – 1.36 (m, 4H), 0.92 (t, J = 7.0 Hz, 3H). ^{13}C NMR (126 MHz, CDCl$_3$) δ 156.67, 143.84, 136.90, 129.38, 128.27, 126.07, 121.20, 120.38, 110.85, 55.54, 50.60, 30.46, 28.66, 22.31, 14.03. MS (ESI-TOF) for C$_{15}$H$_{19}$N$_3$O$_3$ [M + H]$^+$ calculated 290.1499, found 290.1494.

*4-(3-Methoxyphenyl)-2-nitro-1-pentyl-1H-imidazole (**15b**)*

3-Methoxyphenylboronic acid was used as reagent. Yellow solid (48 mg, 83%). ^{1}H NMR (500 MHz, CDCl$_3$) δ 7.38 (dd, J = 1.5, 2.6 Hz, 1H), 7.37 – 7.33 (m, 2H), 7.31 (t, J = 7.8 Hz, 1H), 6.91 – 6.86 (m, 1H), 4.43 (t, J = 7.4 Hz, 2H), 3.87 (s, 3H), 1.93 – 1.85 (m, 2H), 1.41 – 1.33 (m, 4H), 0.92 (t, J = 6.9 Hz, 3H). ^{13}C NMR (126 MHz, CDCl$_3$) δ 160.21, 144.50, 140.71, 133.06, 129.95, 121.75, 117.83, 114.70, 110.57, 55.58, 50.85, 30.39, 28.66, 22.30, 14.00. MS (ESI-TOF) for C$_{15}$H$_{19}$N$_3$O$_3$ [M + H]$^+$ calculated 290.1499, found 290.1503.

*4-(4-Methoxyphenyl)-2-nitro-1-pentyl-1H-imidazole (**15c**)*

4-Methoxyphenylboronic acid was used as reagent. Yellow oil (44 mg, 76%). ^{1}H NMR (500 MHz, CDCl$_3$) δ 7.74 (d, J = 8.9 Hz, 2H), 7.26 (s, 1H), 6.94 (d, J = 8.8 Hz, 2H), 4.43 (t, J = 7.3 Hz, 2H), 3.84 (s, 3H), 1.93 – 1.85 (m, 2H), 1.41 – 1.34 (m, 4H), 0.92 (t, J = 7.0 Hz, 3H). ^{13}C NMR (126 MHz, CDCl$_3$) δ 160.06, 144.46, 140.93, 126.86, 124.41, 120.72, 114.33, 55.50, 50.79, 30.42, 28.69, 22.32, 14.02. MS (ESI-TOF) for C$_{15}$H$_{19}$N$_3$O$_3$ [M + H]$^+$ calculated 290.1499, found 290.1505.

*4-(4-Methoxy-2-methylphenyl)-2-nitro-1-pentyl-1H-imidazole (**15d**)*

4-Methoxy-2-methylphenylboronic acid was used as reagent. Yellow solid (45 mg, 74%). ^{1}H NMR (500 MHz, CDCl$_3$) δ 7.68 (d, J = 8.4 Hz, 1H), 7.13 (s, 1H), 6.82 – 6.77 (m, 2H), 4.44 (t, J = 7.4 Hz, 2H), 3.82 (s, 3H), 2.47 (s, 3H), 1.95 – 1.86 (m, 2H), 1.41 – 1.36 (m, 4H), 0.92 (t, J = 6.9 Hz, 3H). ^{13}C NMR (126 MHz, CDCl$_3$) δ 159.63, 143.96, 140.56, 137.14, 130.47, 124.00, 123.45, 116.45, 111.57, 55.39, 50.61, 30.44, 28.70, 22.31, 21.86, 14.03. MS (ESI-TOF) for C$_{16}$H$_{21}$N$_3$O$_3$ [M + H]$^+$ calculated 304.1656, found 304.1655.

4-(2-Methoxy-3-methylphenyl)-2-nitro-1-pentyl-1H-imidazole (15e)

(2-Methoxy-3-methylphenyl)boronic acid was used as reagent. Yellow solid (42 mg, 69%). ^{1}H NMR (500 MHz, CDCl$_3$) δ 7.97 (dd, J = 1.3, 7.5 Hz, 1H), 7.69 (s, 1H), 7.17 (dd, J = 1.2, 7.4 Hz, 1H), 7.11 (t, J = 7.6 Hz, 1H), 4.46 (t, J = 7.3 Hz, 2H), 3.69 (s, 3H), 2.35 (s, 3H), 1.94 – 1.86 (m, 2H), 1.40 – 1.36 (m, 4H), 0.92 (t, J = 6.9 Hz, 3H). ^{13}C NMR (126 MHz, CDCl$_3$) δ 156.01, 144.04, 137.13, 131.58, 131.45, 126.53, 125.56, 124.97, 124.78, 59.68, 50.70, 30.37, 28.67, 22.31, 16.14, 14.03. MS (ESI-TOF) for C$_{16}$H$_{21}$N$_3$O$_3$ [M + H]$^+$ calculated 304.1656, found 304.1651.

4-(2,3-Dimethoxyphenyl)-2-nitro-1-pentyl-1H-imidazole (15f)

2,3-Dimethoxyphenylboronic acid was used as reagent. Yellow solid (50 mg, 78%). ^{1}H NMR (500 MHz, CDCl$_3$) δ 7.75 (dd, J = 1.5, 8.0 Hz, 1H), 7.70 (s, 1H), 7.13 (t, J = 8.1 Hz, 1H), 6.90 (dd, J = 1.5, 8.1 Hz, 1H), 4.45 (t, J = 7.3 Hz, 2H), 3.91 (s, 3H), 3.85 (s, 3H), 1.93 – 1.86 (m, 2H), 1.41 – 1.33 (m, 4H), 0.91 (t, J = 6.9 Hz, 3H). ^{13}C NMR (126 MHz, CDCl$_3$) δ 152.96, 146.62, 143.99, 136.75, 125.93, 125.65, 124.66, 120.01, 112.32, 59.98, 56.02, 50.68, 30.37, 28.64, 22.30, 14.03. MS (ESI-TOF) for C$_{16}$H$_{21}$N$_3$O$_4$ [M + H]$^+$ calculated 320.1605, found 320.1597.

2-Nitro-1-pentyl-4-(3,4,5-trimethoxyphenyl)-1H-imidazole (15g)

3,4,5-Trimethoxyphenyl-boronic acid was used as reagent. Yellow solid (60 mg, 86%). ^{1}H NMR (500 MHz, CDCl$_3$) δ 7.32 (s, 1H), 7.02 (s, 2H), 4.45 (t, J = 7.4 Hz, 2H), 3.94 (s, 6H), 3.88 (s, 3H), 1.94 – 1.87 (m, 2H), 1.41 – 1.35 (m, 4H), 0.93 (t, J = 6.9 Hz, 3H). ^{13}C NMR (126 MHz, CDCl$_3$) δ 153.79, 144.44, 140.83, 138.66, 127.39, 121.35, 102.71, 61.13, 56.49, 50.89, 30.45, 28.69, 22.32, 14.02. MS (ESI-TOF) for C$_{17}$H$_{23}$N$_3$O$_5$ [M + H]$^+$ calculated 350.1710, found 350.1685.

*4-(2-Chlorophenyl)-2-nitro-1-pentyl-1H-imidazole (**16a**)*

2-Chlorophenylboronic acid was used as reagent. Yellow oil (42 mg, 72%). ^{1}H NMR (500 MHz, CDCl$_3$) δ 8.16 (dd, J = 1.7, 7.9 Hz, 1H), 7.81 (s, 1H), 7.43 (dd, J = 1.3, 8.0 Hz, 1H), 7.38 – 7.34 (m, 1H), 7.29 – 7.25 (m, 1H), 4.47 (t, J = 7.4 Hz, 2H), 1.95 – 1.89 (m, 2H), 1.42 – 1.36 (m, 4H), 0.93 (t, J = 7.0 Hz, 3H). ^{13}C NMR (126 MHz, CDCl$_3$) δ 144.00, 137.05, 131.36, 130.40, 130.34, 130.24, 129.37, 127.37, 125.78, 50.82, 30.42, 28.64, 22.29, 14.02. MS (ESI-TOF) for C$_{14}$H$_{16}$ClN$_3$O$_2$ [M + H]$^+$ calculated 294.1004, found 294.0970.

*4-(3-Chlorophenyl)-2-nitro-1-pentyl-1H-imidazole (**16b**)*

3-Chlorophenylboronic acid was used as reagent. Yellow oil (42 mg, 72%). ^{1}H NMR (500 MHz, CDCl$_3$) δ 7.82 (t, J = 1.7 Hz, 1H), 7.69 (dt, J = 1.5, 7.5 Hz, 1H), 7.36 (s, 1H), 7.34 – 7.29 (m, 2H), 4.45 (t, J = 7.4 Hz, 2H), 1.94 – 1.87 (m, 2H), 1.41 – 1.36 (m, 4H), 0.93 (t, J = 7.0 Hz, 3H). ^{13}C NMR (126 MHz, CDCl$_3$) δ 144.68, 139.41, 135.05, 133.48, 130.23, 128.61, 125.54, 123.52, 121.76, 50.94, 30.40, 28.67, 22.30, 14.01. MS (ESI-TOF) for C$_{14}$H$_{16}$ClN$_3$O$_2$ [M + H]$^+$ calculated 294.1004, found 294.0961.

*4-(4-Chlorophenyl)-2-nitro-1-pentyl-1H-imidazole (**16c**)*

4-Chlorophenylboronic acid was used as reagent. Yellow solid (49 mg, 84%). ^{1}H NMR (500 MHz, CDCl$_3$) δ 7.74 (d, J = 8.7 Hz, 2H), 7.38 (d, J = 8.6 Hz, 2H), 7.34 (s, 1H), 4.44 (t, J = 7.4 Hz, 2H), 1.93 – 1.86 (m, 2H), 1.41 – 1.35 (m, 4H), 0.92 (t, J = 6.9 Hz, 3H). ^{13}C NMR (126 MHz, CDCl$_3$) δ 144.61, 139.73, 134.45, 130.22, 129.15, 126.72, 121.46, 50.89, 30.41, 28.67, 22.30, 14.00. MS (ESI-TOF) for C$_{14}$H$_{16}$ClN$_3$O$_2$ [M + H]$^+$ calculated 294.1004, found 294.0981.

4-(2-Fluorophenyl)-2-nitro-1-pentyl-1H-imidazole (16d)

2-Fluorophenylboronic acid was used as reagent. Yellow solid (38 mg, 68%). ^{1}H NMR (500 MHz, CDCl$_3$) δ 8.20 (td, J = 1.9, 7.8 Hz, 1H), 7.53 (d, J = 3.5 Hz, 1H), 7.33 – 7.28 (m, 1H), 7.25 – 7.22 (m, 1H), 7.15 – 7.10 (m, 1H), 4.45 (t, J = 7.4 Hz, 2H), 1.94 – 1.88 (m, 2H), 1.42 – 1.35 (m, 4H), 0.93 (t, J = 6.9 Hz, 3H). ^{13}C NMR (126 MHz, CDCl$_3$) δ 160.26 (d, J = 248.4 Hz), 144.28, 134.78 (d, J = 1.7 Hz), 129.73 (d, J = 8.5 Hz), 128.30 (d, J = 3.4 Hz), 125.39 (d, J = 14.9 Hz), 124.77 (d, J = 3.2 Hz), 119.63 (d, J = 12.2 Hz), 115.76 (d, J = 21.6 Hz), 50.81, 30.41, 28.64, 22.29, 14.00. MS (ESI-TOF) for C$_{14}$H$_{16}$FN$_3$O$_2$ [M + H]$^+$ calculated 278.1299, found 278.1256.

4-(3-Fluorophenyl)-2-nitro-1-pentyl-1H-imidazole (16e)

3-Fluorophenylboronic acid was used as reagent. Yellow oil (42 mg, 76%). ^{1}H NMR (500 MHz, CDCl$_3$) δ 7.59 – 7.56 (m, 1H), 7.55 – 7.50 (m, 1H), 7.40 – 7.35 (m, 2H), 7.05 – 7.00 (m, 1H), 4.45 (t, J = 7.4 Hz, 2H), 1.94 – 1.87 (m, 2H), 1.42 – 1.34 (m, 4H), 0.93 (t, J = 6.9 Hz, 3H). ^{13}C NMR (126 MHz, CDCl$_3$) δ 163.34 (d, J = 246.0 Hz), 144.61, 139.62 (d, J = 2.8 Hz), 133.92 (d, J = 8.3 Hz), 130.54 (d, J = 8.4 Hz), 121.75, 121.04 (d, J = 2.9 Hz), 115.47 (d, J = 21.2 Hz), 112.47 (d, J = 23.1 Hz), 50.92, 30.41, 28.67, 22.30, 14.00. MS (ESI-TOF) for C$_{14}$H$_{16}$FN$_3$O$_2$ [M + H]$^+$ calculated 278.1299, found 278.1251.

4-(4-Fluorophenyl)-2-nitro-1-pentyl-1H-imidazole (16f)

4-Fluorophenylboronic acid was used as reagent. Yellow oil (44 mg, 79%). ^{1}H NMR (500 MHz, CDCl$_3$) δ 7.79 (dd, J = 5.3, 8.9 Hz, 2H), 7.30 (s, 1H), 7.12 – 7.08 (m, 2H), 4.44 (t, J = 7.4 Hz, 2H), 1.94 – 1.87 (m, 2H), 1.40 – 1.36 (m, 4H), 0.93 (t, J = 6.9 Hz, 3H). ^{13}C NMR (126 MHz, CDCl$_3$) δ 163.04 (d, J = 248.0 Hz), 144.56, 140.01, 127.94 (d, J = 3.2 Hz), 127.28 (d, J = 8.2 Hz), 121.10,

115.96 (d, $J = 21.8$ Hz), 50.85, 30.42, 28.68, 22.31, 14.01. MS (ESI-TOF) for $C_{14}H_{16}FN_3O_2$ [M + H]$^+$ calculated 278.1299, found 278.1252.

*4-(4-Fluoro-2-methylphenyl)-2-nitro-1-pentyl-1H-imidazole (**16g**)*

4-Fluoro-2-methyl-phenylboronic acid was used as reagent. Yellow oil (50 mg, 86%). ^{1}H NMR (500 MHz, CDCl$_3$) δ 7.70 (dd, $J = 5.9, 9.4$ Hz, 1H), 7.16 (s, 1H), 7.00 – 6.90 (m, 2H), 4.45 (t, $J = 7.4$ Hz, 2H), 2.48 (s, 3H), 1.95 – 1.88 (m, 2H), 1.41 – 1.35 (m, 4H), 0.93 (t, $J = 6.9$ Hz, 3H). ^{13}C NMR (126 MHz, CDCl$_3$) δ 162.47 (d, $J = 247.5$ Hz), 143.93, 139.59, 137.98 (d, $J = 7.7$ Hz), 130.84 (d, $J = 8.6$ Hz), 127.30 (d, $J = 3.2$ Hz), 123.55, 117.49 (d, $J = 21.3$ Hz), 113.12 (d, $J = 21.3$ Hz), 50.54, 30.30, 28.56, 22.16, 21.47, 13.88. MS (ESI-TOF) for $C_{15}H_{18}FN_3O_2$ [M + H]$^+$ calculated 292.1456, found 292.1463.

*2-Nitro-1-pentyl-4-(2-(trifluoromethyl)phenyl)-1H-imidazole (**16h**)*

2-(Trifluoromethyl) phenylboronic acid was used as reagent. Yellow oil (50 mg, 76%). ^{1}H NMR (500 MHz, CDCl$_3$) δ 7.92 (d, $J = 7.8$ Hz, 1H), 7.74 (d, $J = 7.9$ Hz, 1H), 7.62 (t, $J = 7.9$ Hz, 1H), 7.48 (t, $J = 7.7$ Hz, 1H), 7.32 (s, 1H), 4.47 (t, $J = 7.3$ Hz, 2H), 1.95 – 1.87 (m, 2H), 1.43 – 1.33 (m, 4H), 0.93 (t, $J = 7.0$ Hz, 3H). ^{13}C NMR (126 MHz, CDCl$_3$) δ 144.20, 137.26, 132.20, 132.11, 130.97, 128.57, 127.38 (q, $J = 30.4$ Hz), 126.25 (q, $J = 5.8$ Hz), 124.91 (q, $J = 5.8$ Hz), 124.18 (q, $J = 273.4$ Hz), 50.80, 30.31, 28.52, 22.27, 13.98. MS (ESI-TOF) for $C_{15}H_{16}F_3N_3O_2$ [M + H]$^+$ calculated 328.1267, found 328.1227.

2-Nitro-1-pentyl-4-(3-(trifluoromethyl)phenyl)-1H-imidazole (16i)

3-(Trifluoromethyl) phenylboronic acid was used as reagent. Yellow solid (45 mg, 69%). ^{1}H NMR (500 MHz, CDCl$_3$) δ 8.04 (s, 1H), 8.02 (d, J = 7.7 Hz, 1H), 7.59 (d, J = 7.9 Hz, 1H), 7.54 (t, J = 7.7 Hz, 1H), 7.43 (s, 1H), 4.46 (t, J = 7.5 Hz, 2H), 1.96 – 1.88 (m, 2H), 1.41 – 1.36 (m, 4H), 0.93 (t, J = 6.9 Hz, 3H). ^{13}C NMR (126 MHz, CDCl$_3$) δ 144.74, 139.32, 132.56, 131.43 (q, J = 32.4 Hz), 129.50, 128.65, 125.17 (q, J = 3.8 Hz), 124.07 (q, J = 301.9 Hz), 122.21 (q, J = 3.9 Hz), 121.85, 50.99, 30.43, 28.68, 22.30, 14.00. MS (ESI-TOF) for C$_{15}$H$_{16}$F$_3$N$_3$O$_2$ [M + H]$^+$ calculated 328.1267, found 328.1230.

2-Nitro-1-pentyl-4-(4-(trifluoromethyl)phenyl)-1H-imidazole (16j)

4-(Trifluoromethyl) phenylboronic acid was used as reagent. Yellow oil (52 mg, 79%). ^{1}H NMR (500 MHz, CDCl$_3$) δ 7.93 (d, J = 7.9 Hz, 2H), 7.67 (d, J = 7.9 Hz, 2H), 7.43 (s, 1H), 4.46 (t, J = 7.4 Hz, 2H), 1.96 – 1.87 (m, 2H), 1.41 – 1.36 (m, 4H), 0.93 (t, J = 6.9 Hz, 3H). ^{13}C NMR (126 MHz, CDCl$_3$) δ 144.80, 139.23, 135.10, 130.41 (q, J = 32.6 Hz), 125.96 (q, J = 3.7 Hz), 125.61, 124.03 (q, J = 272.1 Hz), 122.14, 50.99, 30.43, 28.68, 22.30, 14.01. MS (ESI-TOF) for C$_{15}$H$_{16}$F$_3$N$_3$O$_2$ [M + H]$^+$ calculated 328.1267, found 328.1223.

Compounds 17a-i, 18a-f, 19a-h, 20a-g, and 21a-j were synthesized similarly as compound 4.

1-Pentyl-4-phenyl-1H-imidazol-2-amine hydrochloride (17a)

Compound **12a** was used as reagent. White solid (22 mg, 83%). ^{1}H NMR (500 MHz, MeOD) δ 7.60 – 7.54 (m, 2H), 7.47 – 7.43 (m, 2H), 7.39 – 7.36 (m, 1H), 7.29 (s, 1H), 3.90 (t, J = 7.4 Hz, 2H), 1.85 – 1.79 (m, 2H), 1.45 – 1.35 (m, 4H), 0.95 (t, J = 7.0 Hz, 3H). ^{13}C NMR (126 MHz,

MeOD) δ 148.22, 130.26, 129.77, 128.69, 128.40, 125.56, 113.18, 46.64, 29.59, 29.57, 23.32, 14.26. MS (ESI-TOF) for $C_{14}H_{19}N_3$ [M + H]$^+$ calculated 230.1652, found 230.1677.

*1-Pentyl-4-(o-tolyl)-1H-imidazol-2-amine hydrochloride (**17b**)*

Compound **12b** was used as reagent. White solid (20 mg, 71%). ^{1}H NMR (400 MHz, MeOD) δ 7.39 – 7.37 (m, 1H), 7.36 – 7.25 (m, 3H), 7.02 (s, 1H), 3.92 (t, *J* = 7.3 Hz, 2H), 2.41 (s, 3H), 1.85 – 1.79 (m, 2H), 1.47 – 1.38 (m, 4H), 0.96 (t, *J* = 6.9 Hz, 3H). ^{13}C NMR (126 MHz, MeOD) δ 147.68, 137.43, 132.15, 130.22, 129.46, 128.12, 127.41, 127.04, 115.45, 46.55, 29.62, 29.61, 23.33, 20.91, 14.29. MS (ESI-TOF) for $C_{15}H_{21}N_3$ [M + H]$^+$ calculated 244.1808, found 244.1836.

*4-(2-Ethylphenyl)-1-pentyl-1H-imidazol-2-amine hydrochloride (**17c**)*

Compound **12c** was used as reagent. White solid (20 mg, 68%). ^{1}H NMR (500 MHz, MeOD) δ 7.41 – 7.33 (m, 3H), 7.31 – 7.26 (m, 1H), 6.97 (s, 1H), 3.92 (t, *J* = 7.3 Hz, 2H), 2.74 (q, *J* = 7.6 Hz, 2H), 1.86 – 1.78 (m, 2H), 1.45 – 1.36 (m, 4H), 1.19 (t, *J* = 7.6 Hz, 3H), 0.96 (t, *J* = 7.1 Hz, 3H). ^{13}C NMR (126 MHz, MeOD) δ 147.63, 144.12, 130.77, 130.72, 130.27, 127.64, 127.31, 126.86, 115.12, 46.50, 29.59, 29.57, 27.38, 23.32, 15.64, 14.29. MS (ESI-TOF) for $C_{16}H_{23}N_3$ [M + H]$^+$ calculated 258.1965, found 258.1959.

*1-Pentyl-4-(m-tolyl)-1H-imidazol-2-amine hydrochloride (**17d**)*

Compound **12d** was used as reagent. White solid (22 mg, 79%). ^{1}H NMR (500 MHz, MeOD) δ 7.41 (s, 1H), 7.37 – 7.31 (m, 2H), 7.27 (s, 1H), 7.20 (d, *J* = 7.4 Hz, 1H), 3.89 (t, *J* = 7.3 Hz, 2H), 2.39 (s, 3H), 1.85 – 1.77 (m, 2H), 1.45 – 1.35 (m, 4H), 0.95 (t, *J* = 7.0 Hz, 3H). ^{13}C NMR (126 MHz, MeOD) δ 148.13, 140.26, 130.48, 130.18, 128.58, 128.51, 126.06, 122.67, 113.02, 46.61,

29.60, 29.59, 23.33, 21.41, 14.27. MS (ESI-TOF) for $C_{15}H_{21}N_3$ [M + H]$^+$ calculated 244.1808, found 244.1837.

*1-Pentyl-4-(p-tolyl)-1H-imidazol-2-amine hydrochloride (**17e**)*

Compound **12e** was used as reagent. White solid (20 mg, 71%). ^{1}H NMR (500 MHz, MeOD) δ 7.45 (d, *J* = 8.3 Hz, 2H), 7.27 (d, *J* = 7.7 Hz, 2H), 7.22 (s, 1H), 3.88 (t, *J* = 7.4 Hz, 2H), 2.37 (s, 3H), 1.84 – 1.77 (m, 2H), 1.45 – 1.35 (m, 4H), 0.95 (t, *J* = 7.0 Hz, 3H). ^{13}C NMR (126 MHz, MeOD) δ 148.05, 140.09, 130.84, 128.54, 125.86, 125.53, 112.54, 46.57, 29.60, 29.59, 23.33, 21.25, 14.27. MS (ESI-TOF) for $C_{15}H_{21}N_3$ [M + H]$^+$ calculated 244.1808, found 244.1839.

*4-(2,3-Dimethylphenyl)-1-pentyl-1H-imidazol-2-amine hydrochloride (**17f**)*

Compound **12f** was used as reagent. White solid (22 mg, 75%). ^{1}H NMR (500 MHz, MeOD) δ 7.27 – 7.24 (m, 1H), 7.20 – 7.15 (m, 2H), 6.93 (s, 1H), 3.91 (t, *J* = 7.4 Hz, 2H), 2.35 (s, 3H), 2.29 (s, 3H), 1.86 – 1.79 (m, 2H), 1.45 – 1.37 (m, 4H), 0.96 (t, *J* = 7.0 Hz, 3H). ^{13}C NMR (126 MHz, MeOD) δ 147.52, 139.06, 136.38, 131.99, 128.48, 128.37, 127.73, 126.93, 115.21, 46.50, 29.61, 29.60, 23.32, 20.65, 16.92, 14.28. MS (ESI-TOF) for $C_{16}H_{23}N_3$ [M + H]$^+$ calculated 258.1965, found 258.1932.

*4-(2,4-Dimethylphenyl)-1-pentyl-1H-imidazol-2-amine hydrochloride (**17g**)*

Compound **12g** was used as reagent. White solid (22 mg, 75%). ^{1}H NMR (500 MHz, MeOD) δ 7.26 (d, *J* = 7.8 Hz, 1H), 7.16 (s, 1H), 7.11 (d, *J* = 7.6 Hz, 1H), 6.96 (s, 1H), 3.91 (t, *J* = 7.3 Hz, 2H), 2.37 (s, 3H), 2.34 (s, 3H), 1.85 – 1.78 (m, 2H), 1.44 – 1.36 (m, 4H), 0.96 (t, *J* = 7.0 Hz, 3H). ^{13}C NMR (126 MHz, MeOD) δ 147.54, 140.42, 137.20, 132.82, 129.36, 128.03, 127.16, 125.23,

115.05, 46.51, 29.62, 29.60, 23.33, 21.17, 20.85, 14.29. MS (ESI-TOF) for $C_{16}H_{23}N_3$ $[M + H]^+$ calculated 258.1965, found 258.1959.

*4-(2,5-Dimethylphenyl)-1-pentyl-1H-imidazol-2-amine hydrochloride (**17h**)*

Compound **12h** was used as reagent. White solid (20 mg, 68%). ^{1}H NMR (500 MHz, MeOD) δ 7.23 – 7.18 (m, 2H), 7.14 (dd, *J* = 1.5, 8.3 Hz, 1H), 6.99 (s, 1H), 3.91 (t, *J* = 7.4 Hz, 2H), 2.36 (s, 3H), 2.35 (s, 3H), 1.85 – 1.78 (m, 2H), 1.45 – 1.36 (m, 4H), 0.96 (t, *J* = 7.0 Hz, 3H). ^{13}C NMR (126 MHz, MeOD) δ 147.61, 137.15, 134.18, 132.14, 130.86, 129.83, 127.87, 127.23, 115.32, 46.53, 29.62, 29.60, 23.32, 20.89, 20.46, 14.28. MS (ESI-TOF) for $C_{16}H_{23}N_3$ $[M + H]^+$ calculated 258.1965, found 258.1939.

*4-(2,6-Dimethylphenyl)-1-pentyl-1H-imidazol-2-amine hydrochloride (**17i**)*

Compound **12i** was used as reagent. White solid (22 mg, 75%). ^{1}H NMR (500 MHz, MeOD) δ 7.25 (t, *J* = 7.9 Hz, 1H), 7.15 (d, *J* = 7.6 Hz, 2H), 6.84 (s, 1H), 3.93 (t, *J* = 7.2 Hz, 2H), 2.22 (s, 6H), 1.86 – 1.80 (m, 2H), 1.47 – 1.34 (m, 4H), 0.96 (t, *J* = 7.1 Hz, 3H). ^{13}C NMR (126 MHz, MeOD) δ 147.67, 139.85, 130.84, 128.74, 128.13, 125.18, 115.58, 46.42, 29.58, 29.53, 23.30, 20.47, 14.31. MS (ESI-TOF) for $C_{16}H_{23}N_3$ $[M + H]^+$ calculated 258.1965, found 258.1967.

*4-Benzyl-1-pentyl-1H-imidazol-2-amine hydrochloride (**18a**)*

Compound **13a** was used as reagent. White solid (18 mg, 64%). ^{1}H NMR (500 MHz, MeOD) δ 7.33 (t, *J* = 7.5 Hz, 2H), 7.27 – 7.24 (m, 3H), 6.59 (s, 1H), 3.83 (s, 2H), 3.78 (t, *J* = 7.2 Hz, 2H), 1.77 – 1.68 (m, 2H), 1.42 – 1.26 (m, 4H), 0.93 (t, *J* = 7.1 Hz, 3H). ^{13}C NMR (126 MHz, MeOD) δ 147.67, 138.25, 129.84, 129.60, 128.12, 127.73, 114.16, 46.27, 31.59, 29.55, 29.53, 23.28, 14.26. MS (ESI-TOF) for $C_{15}H_{21}N_3$ $[M + H]^+$ calculated 244.1808, found 244.1789.

*1-Pentyl-4-phenethyl-1H-imidazol-2-amine hydrochloride (**18b**)*

Compound **13b** was used as reagent. White solid (19 mg, 65%). ^{1}H NMR (500 MHz, MeOD) δ
7.29 – 7.25 (m, 2H), 7.20 – 7.17 (m, 3H), 6.48 (s, 1H), 3.74 (t, *J* = 7.2 Hz, 2H), 2.90 (t, *J* = 7.5 Hz,
2H), 2.81 – 2.77 (m, 2H), 1.70 – 1.64 (m, 2H), 1.38 – 1.32 (m, 2H), 1.29 – 1.20 (m, 2H), 0.92 (t,
J = 7.3 Hz, 3H). ^{13}C NMR (126 MHz, MeOD) δ 147.25, 141.53, 129.52, 129.44, 127.64, 127.42,
113.57, 46.12, 35.33, 29.53, 29.44, 27.46, 23.28, 14.24. MS (ESI-TOF) for $C_{16}H_{23}N_3$ [M + H]$^+$
calculated 258.1965, found 258.1917.

*4-(Naphthalen-1-yl)-1-pentyl-1H-imidazol-2-amine hydrochloride (**18c**)*

Compound **13c** was used as reagent. White solid (25 mg, 79%). ^{1}H NMR (500 MHz, MeOD) δ
8.09 – 8.07 (m, 1H), 8.02 – 7.95 (m, 2H), 7.61 – 7.55 (m, 4H), 7.20 (s, 1H), 3.98 (t, *J* = 7.4 Hz,
2H), 1.93 – 1.84 (m, 2H), 1.48 – 1.41 (m, 4H), 0.98 (t, *J* = 7.1 Hz, 3H). ^{13}C NMR (126 MHz,
MeOD) δ 147.96, 135.35, 132.33, 131.03, 129.83, 128.70, 128.31, 127.61, 126.36, 126.24, 125.47,
115.97, 46.65, 29.66, 29.64, 23.36, 14.31. MS (ESI-TOF) for $C_{18}H_{21}N_3$ [M + H]$^+$ calculated
280.1808, found 280.1830.

*4-(Naphthalen-2-yl)-1-pentyl-1H-imidazol-2-amine hydrochloride (**18d**)*

Compound **13d** was used as reagent. White solid (22 mg, 70%). ^{1}H NMR (500 MHz, MeOD) δ
8.04 (s, 1H), 7.95 – 7.87 (m, 3H), 7.68 (dd, *J* = 1.8, 8.6 Hz, 1H), 7.57 – 7.50 (m, 2H), 7.43 (s, 1H),
3.93 (t, *J* = 7.4 Hz, 2H), 1.88 – 1.82 (m, 2H), 1.46 – 1.39 (m, 4H), 0.97 (t, *J* = 6.9 Hz, 3H). [13]C
NMR (126 MHz, MeOD) δ 148.38, 134.78, 134.55, 130.13, 129.07, 128.87, 128.45, 128.10,

127.84, 125.99, 123.97, 123.36, 113.74, 46.70, 29.61, 29.60, 23.34, 14.28. MS (ESI-TOF) for $C_{18}H_{21}N_3$ [M + H]$^+$ calculated 280.1808, found 280.1790.

*4-([1,1'-Biphenyl]-4-yl)-1-pentyl-1H-imidazol-2-amine hydrochloride (**18e**)*

Compound **13e** was used as reagent. White solid (25 mg, 73%). ^{1}H NMR (500 MHz, MeOD) δ 7.72 (d, *J* = 8.3 Hz, 2H), 7.67 – 7.65 (m, 4H), 7.46 (t, *J* = 7.6 Hz, 2H), 7.38 – 7.35 (m, 1H), 7.34 (s, 1H), 3.91 (t, *J* = 7.4 Hz, 2H), 1.85 – 1.80 (m, 2H), 1.46 – 1.36 (m, 4H), 0.96 (t, *J* = 6.9 Hz, 3H). ^{13}C NMR (126 MHz, MeOD) δ 148.26, 142.70, 141.28, 130.02, 128.84, 128.67, 128.11, 127.83, 127.58, 126.00, 113.26, 46.67, 29.60, 29.58, 23.33, 14.27. MS (ESI-TOF) for $C_{20}H_{23}N_3$ [M + H]$^+$ calculated 306.1965, found 306.1963.

*4-(2-(Benzyloxy)phenyl)-1-pentyl-1H-imidazol-2-amine hydrochloride (**18f**)*

Compound **13f** was used as reagent. White solid (24 mg, 64%). ^{1}H NMR (500 MHz, MeOD) δ 7.52 (dd, *J* = 1.6, 7.8 Hz, 1H), 7.49 – 7.46 (m, 2H), 7.44 – 7.39 (m, 2H), 7.37 – 7.32 (m, 2H), 7.20 (dd, *J* = 1.0, 8.4 Hz, 1H), 7.15 (s, 1H), 7.09 – 7.01 (m, 1H), 5.27 (s, 2H), 3.81 (t, *J* = 7.3 Hz, 2H), 1.75 – 1.67 (m, 2H), 1.40 – 1.28 (m, 4H), 0.93 (t, *J* = 7.1 Hz, 3H). ^{13}C NMR (126 MHz, MeOD) δ 156.56, 147.42, 138.08, 130.78, 129.77, 129.35, 128.95, 126.90, 124.50, 122.32, 117.41, 115.94, 114.29, 71.78, 46.41, 29.52, 29.40, 23.26, 14.26. MS (ESI-TOF) for $C_{21}H_{25}N_3O$[M + H]$^+$ calculated 336.2070, found 336.2019.

*1-Pentyl-4-(pyridin-3-yl)-1H-imidazol-2-amine hydrochloride (**19a**)*

Compound **14a** was used as reagent. White solid (18 mg, 68%). ^{1}H NMR (500 MHz, MeOD) δ 8.80 (s, 1H), 8.45 – 8.44 (m, 1H), 8.06 – 8.02 (m, 1H), 7.49 – 7.46 (m, 1H), 7.37 (s, 1H), 3.87 (t,

J = 7.3 Hz, 2H), 1.84 – 1.78 (m, 2H), 1.44 – 1.36 (m, 4H), 0.95 (t, J = 7.0 Hz, 3H). ^{13}C NMR (126 MHz, MeOD) δ 149.89, 148.71, 146.10, 133.66, 128.52, 128.31, 125.46, 114.45, 46.43, 29.93, 29.67, 23.35, 14.29. MS (ESI-TOF) for $C_{13}H_{18}N_4$ [M + H]$^+$ calculated 231.1604, found 231.1570.

*4-(3,5-Dimethylisoxazol-4-yl)-1-pentyl-1H-imidazol-2-amine hydrochloride (**19b**)*

Compound **14b** was used as reagent. White solid (20 mg, 70%). ^{1}H NMR (500 MHz, MeOD) δ 7.06 (s, 1H), 3.90 (t, J = 7.4 Hz, 2H), 2.45 (s, 3H), 2.27 (s, 3H), 1.86 – 1.76 (m, 2H), 1.45 – 1.36 (m, 4H), 0.96 (t, J = 7.0 Hz, 3H). ^{13}C NMR (126 MHz, MeOD) δ 169.82, 160.07, 148.33, 116.89, 116.51, 105.77, 46.66, 29.59, 29.49, 23.30, 14.27, 11.48, 10.32. MS (ESI-TOF) for $C_{13}H_{20}N_4O$[M + H]$^+$ calculated 249.1710, found 249.1689.

*2-(2-Amino-1-pentyl-1H-imidazol-4-yl)phenol hydrochloride (**19c**)*

Compound **13f** and 5% Pd/C were used as reagents. White solid (18 mg, 64%). ^{1}H NMR (500 MHz, MeOD) δ 7.48 (dd, J = 1.6, 7.8 Hz, 1H), 7.31 (s, 1H), 7.19 (ddd, J = 1.6, 7.3, 8.2 Hz, 1H), 6.96 – 6.85 (m, 2H), 3.90 (t, J = 7.4 Hz, 2H), 1.85 – 1.77 (m, 2H), 1.45 – 1.35 (m, 4H), 0.95 (t, J = 7.0 Hz, 3H). ^{13}C NMR (126 MHz, MeOD) δ 155.26, 147.12, 130.63, 126.79, 125.65, 121.06, 117.11, 115.09, 114.34, 46.51, 29.64, 29.58, 23.32, 14.26. MS (ESI-TOF) for $C_{14}H_{19}N_3O$[M + H]$^+$ calculated 246.1601, found 246.1550.

*(2-(2-Amino-1-pentyl-1H-imidazol-4-yl)phenyl)methanol hydrochloride (**19d**)*

Compound **14d** was used as reagent. White solid (21 mg, 71%). ^{1}H NMR (500 MHz, MeOD) δ 7.55 – 7.48 (m, 2H), 7.46 – 7.38 (m, 2H), 7.20 (s, 1H), 4.61 (s, 2H), 3.92 (t, J = 7.4 Hz, 2H), 1.87 – 1.80 (m, 2H), 1.45 – 1.37 (m, 4H), 0.96 (t, J = 7.0 Hz, 3H). ^{13}C NMR (126 MHz, MeOD) δ

147.79, 139.28, 131.40, 130.22, 129.59, 129.46, 128.60, 126.90, 115.18, 63.86, 46.61, 29.61, 29.59, 23.32, 14.27. MS (ESI-TOF) for $C_{15}H_{21}N_3O[M + H]^+$ calculated 260.1757, found 260.1748.

*4-(4-Aminophenyl)-1-pentyl-1H-imidazol-2-amine hydrochloride (**19e**)*

Compound **14e** was used as reagent. White solid (19 mg, 68%). ^1H NMR (500 MHz, MeOD) δ 7.73 (d, J = 8.6 Hz, 2H), 7.44 (d, J = 8.5 Hz, 2H), 7.40 (s, 1H), 3.91 (t, J = 7.4 Hz, 2H), 1.86 – 1.78 (m, 2H), 1.45 – 1.35 (m, 4H), 0.95 (t, J = 7.0 Hz, 3H). ^{13}C NMR (126 MHz, MeOD) δ 148.50, 133.58, 128.73, 127.21, 127.02, 124.32, 114.20, 46.74, 29.57, 29.56, 23.32, 14.26. MS (ESI-TOF) for $C_{14}H_{20}N_4$ $[M + H]^+$ calculated 245.1761, found 245.1762.

*4-(2-Amino-1-pentyl-1H-imidazol-4-yl)benzamide hydrochloride (**19f**)*

Compound **14f** was used as reagent. White solid (20 mg, 65%). ^1H NMR (500 MHz, MeOD) δ 7.96 (d, J = 8.5 Hz, 2H), 7.68 (d, J = 8.5 Hz, 2H), 7.46 (s, 1H), 3.91 (t, J = 7.4 Hz, 2H), 1.86 – 1.79 (m, 2H), 1.45 – 1.35 (m, 4H), 0.96 (t, J = 7.0 Hz, 3H). ^{13}C NMR (126 MHz, MeOD) δ 171.28, 148.58, 134.74, 131.93, 129.62, 127.40, 125.36, 114.71, 46.76, 29.58, 29.57, 23.33, 14.27. MS (ESI-TOF) for $C_{15}H_{20}N_4O$ $[M + H]^+$ calculated 273.1710, found 273.1707.

*Methyl 4-(2-amino-1-pentyl-1H-imidazol-4-yl)benzoate hydrochloride (**19g**)*

Compound **14g** was used as reagent. White solid (22 mg, 68%). ^1H NMR (500 MHz, MeOD) δ 8.09 (d, J = 8.8 Hz, 2H), 7.69 (d, J = 8.8 Hz, 2H), 7.49 (s, 1H), 3.93 – 3.90 (m, 5H), 1.87 – 1.79 (m, 2H), 1.46 – 1.35 (m, 4H), 0.96 (t, J = 7.0 Hz, 3H). ^{13}C NMR (126 MHz, MeOD) δ 167.73, 148.71, 133.16, 131.37, 131.05, 127.33, 125.36, 115.15, 52.78, 46.79, 29.58, 29.55, 23.32, 14.25. MS (ESI-TOF) for $C_{16}H_{21}N_3O_2$ $[M + H]^+$ calculated 288.1707, found 288.1703.

*Methyl 2-(2-amino-1-pentyl-1H-imidazol-4-yl)benzoate hydrochloride (**19h**)*

Compound **14h** was used as reagent. White solid (24 mg, 74%). ^{1}H NMR (500 MHz, MeOD) δ 8.03 – 8.01 (m, 1H), 7.73 – 7.63 (m, 1H), 7.62 – 7.55 (m, 1H), 7.54 – 7.52 (m, 1H), 6.99 (s, 1H), 3.91 (t, *J* = 7.3 Hz, 2H), 3.86 (s, 3H), 1.86 – 1.78 (m, 2H), 1.46 – 1.37 (m, 4H), 0.96 (t, *J* = 7.0 Hz, 3H). ^{13}C NMR (126 MHz, MeOD) δ 168.33, 147.51, 133.61, 132.50, 131.97, 131.37, 130.75, 129.25, 127.23, 115.14, 52.93, 46.51, 29.62, 29.52, 23.33, 14.28. MS (ESI-TOF) for $C_{16}H_{21}N_3O_2$ $[M + H]^+$ calculated 288.1707, found 288.1705.

*4-(2-Methoxyphenyl)-1-pentyl-1H-imidazol-2-amine hydrochloride (**20a**)*

Compound **15a** was used as reagent. White solid (20 mg, 67%). ^{1}H NMR (500 MHz, MeOD) δ 7.52 (dd, *J* = 1.7, 7.7 Hz, 1H), 7.39 – 7.34 (m, 1H), 7.30 (s, 1H), 7.14 (dd, *J* = 1.0, 8.5 Hz, 1H), 7.05 – 7.03 (m, 1H), 3.97 (s, 3H), 3.91 (t, *J* = 7.4 Hz, 2H), 1.86 – 1.77 (m, 2H), 1.45 – 1.36 (m, 4H), 0.95 (t, *J* = 7.0 Hz, 3H). ^{13}C NMR (126 MHz, MeOD) δ 157.33, 147.32, 131.00, 127.10, 124.94, 122.12, 116.87, 115.30, 112.74, 56.12, 46.55, 29.64, 29.58, 23.32, 14.27. MS (ESI-TOF) for $C_{15}H_{21}N_3O[M + H]^+$ calculated 260.1757, found 260.1729.

*4-(3-Methoxyphenyl)-1-pentyl-1H-imidazol-2-amine hydrochloride (**20b**)*

Compound **15b** was used as reagent. White solid (23 mg, 78%). ^{1}H NMR (500 MHz, MeOD) δ 7.36 (t, *J* = 8.3 Hz, 1H), 7.32 (s, 1H), 7.16 – 7.12 (m, 2H), 6.96 – 6.93 (m, 1H), 3.89 (t, *J* = 7.4 Hz, 2H), 3.85 (s, 3H), 1.85 – 1.78 (m, 2H), 1.45 – 1.34 (m, 4H), 0.96 (t, *J* = 7.0 Hz, 3H). ^{13}C NMR (126 MHz, MeOD) δ 161.78, 148.16, 131.41, 129.89, 128.30, 117.77, 115.22, 113.41, 111.11, 55.86, 46.63, 29.60, 29.59, 23.33, 14.27. MS (ESI-TOF) for $C_{15}H_{21}N_3O[M + H]^+$ calculated 260.1757, found 260.1770.

4-(4-Methoxyphenyl)-1-pentyl-1H-imidazol-2-amine hydrochloride (20c)

Compound **15c** was used as reagent. White solid (25 mg, 85%). ^{1}H NMR (500 MHz, MeOD) δ 7.49 (d, *J* = 8.8 Hz, 2H), 7.11 (s, 1H), 6.99 (d, *J* = 8.9 Hz, 2H), 3.86 (t, *J* = 7.3 Hz, 2H), 3.83 (s, 3H), 1.84 – 1.76 (m, 2H), 1.46 – 1.33 (m, 4H), 0.95 (t, *J* = 7.0 Hz, 3H). ^{13}C NMR (126 MHz, MeOD) δ 161.41, 148.16, 128.59, 127.08, 121.85, 115.55, 111.66, 55.84, 46.44, 29.71, 29.62, 23.34, 14.28. MS (ESI-TOF) for $C_{15}H_{21}N_3O[M + H]^+$ calculated 260.1757, found 260.1785.

4-(4-Methoxy-2-methylphenyl)-1-pentyl-1H-imidazol-2-amine hydrochloride (20d)

Compound **15d** was used as reagent. White solid (20 mg, 65%). ^{1}H NMR (500 MHz, MeOD) δ 7.29 (d, *J* = 8.5 Hz, 1H), 6.91 (s, 1H), 6.89 (d, *J* = 2.6 Hz, 1H), 6.85 (dd, *J* = 2.7, 8.5 Hz, 1H), 3.90 (t, *J* = 7.4 Hz, 2H), 3.82 (s, 3H), 2.37 (s, 3H), 1.85 – 1.77 (m, 2H), 1.44 – 1.35 (m, 4H), 0.96 (t, *J* = 7.0 Hz, 3H). ^{13}C NMR (126 MHz, MeOD) δ 161.72, 147.44, 139.27, 131.05, 127.11, 120.53, 117.39, 114.65, 112.70, 55.75, 46.47, 29.62, 29.61, 23.32, 21.00, 14.28. MS (ESI-TOF) for $C_{16}H_{23}N_3O[M + H]^+$ calculated 274.1914, found 274.1901.

4-(2-Methoxy-3-methylphenyl)-1-pentyl-1H-imidazol-2-amine hydrochloride (20e)

Compound **15e** was used as reagent. White solid (19 mg, 61%). ^{1}H NMR (500 MHz, MeOD) δ 7.35 (dd, *J* = 1.6, 7.8 Hz, 1H), 7.31 (s, 1H), 7.24 (dd, *J* = 1.3, 7.5 Hz, 1H), 7.11 (t, *J* = 7.7 Hz, 1H), 3.93 (t, *J* = 7.3 Hz, 2H), 3.69 (s, 3H), 2.35 (s, 3H), 1.86 – 1.78 (m, 2H), 1.45 – 1.36 (m, 4H), 0.95 (t, *J* = 7.0 Hz, 3H). ^{13}C NMR (126 MHz, MeOD) δ 156.64, 147.70, 133.62, 133.02, 125.83, 125.74, 124.85, 121.70, 115.43, 60.34, 46.59, 29.62, 29.59, 23.32, 16.07, 14.28. MS (ESI-TOF) for $C_{16}H_{23}N_3O[M + H]^+$ calculated 274.1914, found 274.1872.

*4-(2,3-Dimethoxyphenyl)-1-pentyl-1H-imidazol-2-amine hydrochloride (**20f**)*

Compound **15f** was used as reagent. White solid (23 mg, 71%). ^{1}H NMR (500 MHz, MeOD) δ 7.33 (s, 1H), 7.18 – 7.09 (m, 2H), 7.06 (dd, J = 1.6, 7.9 Hz, 1H), 3.95 – 3.88 (m, 5H), 3.85 (s, 3H), 1.85 – 1.77 (m, 2H), 1.45 – 1.35 (m, 4H), 0.95 (t, J = 7.0 Hz, 3H). ^{13}C NMR (126 MHz, MeOD) δ 154.73, 147.59, 147.13, 125.92, 124.62, 121.92, 118.77, 115.67, 114.06, 60.66, 56.42, 46.60, 29.61, 29.58, 23.32, 14.28. MS (ESI-TOF) for $C_{16}H_{23}N_3O_2$ [M + H]$^+$ calculated 290.1863, found 290.1807.

*1-Pentyl-4-(3,4,5-trimethoxyphenyl)-1H-imidazol-2-amine hydrochloride (**20g**)*

Compound **15g** was used as reagent. White solid (26 mg, 73%). ^{1}H NMR (500 MHz, MeOD) δ 7.32 (s, 1H), 6.89 (s, 2H), 3.90 – 3.87 (m, 8H), 3.78 (s, 3H), 1.86 – 1.79 (m, 2H), 1.46 – 1.35 (m, 4H), 0.96 (t, J = 7.0 Hz, 3H). ^{13}C NMR (126 MHz, MeOD) δ 155.21, 148.05, 139.60, 128.43, 124.46, 113.07, 103.20, 61.19, 56.80, 46.62, 29.59, 29.57, 23.33, 14.26. MS (ESI-TOF) for $C_{17}H_{25}N_3O_3$ [M + H]$^+$ calculated 320.1969, found 320.1957.

*4-(2-Chlorophenyl)-1-pentyl-1H-imidazol-2-amine hydrochloride (**21a**)*

Compound **16a** was used as reagent. White solid (18 mg, 60%). ^{1}H NMR (500 MHz, MeOD) δ 7.58 – 7.53 (m, 2H), 7.45 – 7.40 (m, 2H), 7.31 (s, 1H), 3.93 (t, J = 7.3 Hz, 2H), 1.86 – 1.78 (m, 2H), 1.45 – 1.36 (m, 4H), 0.96 (t, J = 7.0 Hz, 3H). ^{13}C NMR (126 MHz, MeOD) δ 147.88, 133.14, 131.78, 131.44, 130.76, 128.68, 127.51, 124.74, 116.99, 46.68, 29.60, 29.56, 23.32, 14.28. MS (ESI-TOF) for $C_{14}H_{18}ClN_3$ [M + H]$^+$ calculated 264.1262, found 264.1238.

*4-(3-Chlorophenyl)-1-pentyl-1H-imidazol-2-amine hydrochloride (**21b**)*

Compound **16b** was used as reagent. White solid (20 mg, 67%). ^{1}H NMR (500 MHz, MeOD) δ 7.64 (t, J = 1.9 Hz, 1H), 7.52 – 7.50 (m, 1H), 7.44 (t, J = 7.9 Hz, 1H), 7.40 (s, 1H), 7.39 – 7.36 (m, 1H), 3.90 (t, J = 7.4 Hz, 2H), 1.86 – 1.78 (m, 2H), 1.46 – 1.35 (m, 4H), 0.95 (t, J = 7.0 Hz, 3H). ^{13}C NMR (126 MHz, MeOD) δ 148.47, 136.24, 131.85, 130.69, 129.55, 126.97, 125.45, 123.86, 114.34, 46.72, 29.57, 29.55, 23.32, 14.26. MS (ESI-TOF) for $C_{14}H_{18}ClN_3$ [M + H]$^+$ calculated 264.1262, found 264.1271.

*4-(4-Chlorophenyl)-1-pentyl-1H-imidazol-2-amine hydrochloride (**21c**)*

Compound **16c** was used as reagent. White solid (23 mg, 77%). ^{1}H NMR (500 MHz, MeOD) δ 7.57 (d, J = 8.6 Hz, 2H), 7.28 (d, J = 8.6 Hz, 2H), 7.00 (s, 1H), 3.77 (t, J = 7.3 Hz, 2H), 1.79 – 1.73 (m, 2H), 1.42 – 1.32 (m, 4H), 0.93 (t, J = 7.0 Hz, 3H). ^{13}C NMR (126 MHz, MeOD) δ 150.99, 135.85, 134.46, 132.40, 129.47, 126.58, 112.58, 45.77, 30.57, 29.85, 23.40, 14.34. MS (ESI-TOF) for $C_{14}H_{18}ClN_3$ [M + H]$^+$ calculated 264.1262, found 264.1296.

*4-(2-Fluorophenyl)-1-pentyl-1H-imidazol-2-amine hydrochloride (**21d**)*

Compound **16d** was used as reagent. White solid (20 mg, 70%). ^{1}H NMR (500 MHz, MeOD) δ 7.64 – 7.60 (m, 1H), 7.46 – 7.39 (m, 1H), 7.32 – 7.24 (m, 3H), 3.93 (t, J = 7.4 Hz, 2H), 1.85 – 1.78 (m, 2H), 1.46 – 1.35 (m, 4H), 0.95 (t, J = 7.1 Hz, 3H). ^{13}C NMR (126 MHz, MeOD) δ 160.46 (d, J = 249.0 Hz), 148.16, 131.41 (d, J = 8.6 Hz), 127.60 (d, J = 2.7 Hz), 126.13 (d, J = 3.5 Hz), 122.27 (d, J = 1.4 Hz), 117.32 (d, J = 21.6 Hz), 116.72 (d, J = 12.7 Hz), 116.42 (d, J = 10.8 Hz), 46.71, 29.59, 29.56, 23.33, 14.27. MS (ESI-TOF) for $C_{14}H_{18}FN_3$ [M + H]$^+$ calculated 248.1558, found 248.1572.

*4-(3-Fluorophenyl)-1-pentyl-1H-imidazol-2-amine hydrochloride (**21e**)*

Compound **16e** was used as reagent. White solid (18 mg, 63%). ^{1}H NMR (500 MHz, MeOD) δ 7.50 – 7.45 (m, 1H), 7.41 – 7.33 (m, 3H), 7.16 – 7.07 (m, 1H), 3.90 (t, *J* = 7.4 Hz, 2H), 1.85 – 1.78 (m, 2H), 1.45 – 1.34 (m, 4H), 0.96 (t, *J* = 7.1 Hz, 3H). ^{13}C NMR (126 MHz, MeOD) δ 164.61 (d, *J* = 245.2 Hz), 148.44, 132.27 (d, *J* = 8.6 Hz), 130.97 (d, *J* = 8.7 Hz), 127.22 (d, *J* = 2.8 Hz), 121.39 (d, *J* = 3.1 Hz), 116.33 (d, *J* = 21.4 Hz), 114.28, 112.37 (d, *J* = 24.2 Hz), 46.71, 29.57, 29.56, 23.33, 14.26. MS (ESI-TOF) for $C_{14}H_{18}FN_3$ [M + H]$^+$ calculated 248.1558, found 248.1564.

*4-(4-Fluorophenyl)-1-pentyl-1H-imidazol-2-amine hydrochloride (**21f**)*

Compound **16f** was used as reagent. White solid (20 mg, 70%). ^{1}H NMR (500 MHz, MeOD) δ 7.60 (dd, *J* = 5.1, 8.9 Hz, 2H), 7.26 (s, 1H), 7.23 – 7.17 (m, 2H), 3.89 (t, *J* = 7.4 Hz, 2H), 1.85 – 1.78 (m, 2H), 1.45 – 1.34 (m, 4H), 0.95 (t, *J* = 7.1 Hz, 3H). ^{13}C NMR (126 MHz, MeOD) δ 164.19 (d, *J* = 247.6 Hz), 148.25, 127.84 (d, *J* = 8.4 Hz), 127.54, 125.20 (d, *J* = 3.5 Hz), 117.18 (d, *J* = 22.3 Hz), 113.12, 46.63, 29.58, 29.56, 23.33, 14.26. MS (ESI-TOF) for $C_{14}H_{18}FN_3$ [M + H]$^+$ calculated 248.1558, found 248.1564.

*4-(4-Fluoro-2-methylphenyl)-1-pentyl-1H-imidazol-2-amine hydrochloride (**21g**)*

Compound **16g** was used as reagent. White solid (20 mg, 67%). ^{1}H NMR (500 MHz, MeOD) δ 7.39 (dd, *J* = 5.7, 8.6 Hz, 1H), 7.13 – 7.10 (m, 1H), 7.07 – 7.02 (m, 1H), 7.00 (s, 1H), 3.91 (t, *J* = 7.3 Hz, 2H), 2.40 (s, 3H), 1.85 – 1.79 (m, 2H), 1.44 – 1.37 (m, 4H), 0.96 (t, *J* = 7.0 Hz, 3H). ^{13}C NMR (126 MHz, MeOD) δ 164.30 (d, *J* = 247.8 Hz), 147.71, 140.78 (d, *J* = 8.2 Hz), 131.89 (d, *J* = 8.8 Hz), 126.13, 124.58 (d, *J* = 3.2 Hz), 118.62 (d, *J* = 21.9 Hz), 115.52, 114.19 (d, *J* = 21.9 Hz), 46.55, 29.60, 23.33, 20.80, 20.79, 14.29. MS (ESI-TOF) for $C_{15}H_{20}FN_3$ [M + H]$^+$ calculated 262.1714, found 262.1724.

*1-Pentyl-4-(2-(trifluoromethyl)phenyl)-1H-imidazol-2-amine hydrochloride (**21h**)*

Compound **16h** was used as reagent. White solid (24 mg, 72%). ^{1}H NMR (500 MHz, MeOD) δ 7.87 (d, J = 6.6 Hz, 1H), 7.76 (t, J = 7.6 Hz, 1H), 7.69 (t, J = 7.7 Hz, 1H), 7.62 (d, J = 7.8 Hz, 1H), 7.02 (s, 1H), 3.93 (t, J = 7.2 Hz, 2H), 1.84 – 1.77 (m, 2H), 1.45 – 1.35 (m, 4H), 0.96 (t, J = 7.1 Hz, 3H). ^{13}C NMR (126 MHz, MeOD) δ 147.84, 133.60, 131.23, 130.28 (q, J = 30.3 Hz), 127.68 (q, J = 5.4 Hz), 127.37 (q, J = 272.6 Hz), 127.35, 124.10, 121.93, 116.65 (q, J = 3.0 Hz), 46.55, 29.50, 29.42, 23.27, 14.23. MS (ESI-TOF) for $C_{15}H_{18}F_3N_3$ [M + H]$^+$ calculated 298.1526, found 298.1538.

*1-Pentyl-4-(3-(trifluoromethyl)phenyl)-1H-imidazol-2-amine hydrochloride (**21i**)*

Compound **16i** was used as reagent. White solid (22 mg, 66%). ^{1}H NMR (500 MHz, MeOD) δ 7.92 (s, 1H), 7.85 (d, J = 4.9 Hz, 1H), 7.70 – 7.63 (m, 2H), 7.49 (s, 1H), 3.91 (t, J = 7.3 Hz, 2H), 1.87 – 1.78 (m, 2H), 1.46 – 1.35 (m, 4H), 0.95 (t, J = 6.9 Hz, 3H). ^{13}C NMR (126 MHz, MeOD) δ 148.61, 132.64 (q, J = 32.4 Hz), 131.23, 129.89, 129.10, 126.90, 126.11 (q, J = 4.1 Hz), 125.37 (q, J = 271.6 Hz), 122.10 (q, J = 3.7 Hz), 114.72, 46.78, 29.57, 29.55, 23.33, 14.26. MS (ESI-TOF) for $C_{15}H_{18}F_3N_3$ [M + H]$^+$ calculated 298.1526, found 298.1550

*1-Pentyl-4-(4-(trifluoromethyl)phenyl)-1H-imidazol-2-amine hydrochloride (**21j**)*

Compound **16j** was used as reagent. White solid (24 mg, 72%). ^{1}H NMR (500 MHz, MeOD) δ 7.76 (d, J = 8.3 Hz, 2H), 7.72 (d, J = 8.4 Hz, 2H), 7.43 (s, 1H), 3.89 (t, J = 7.4 Hz, 2H), 1.85 – 1.78 (m, 2H), 1.45 – 1.36 (m, 4H), 0.95 (t, J = 7.0 Hz, 3H). ^{13}C NMR (126 MHz, MeOD) δ 149.26, 133.99, 130.64 (q, J= 32.5 Hz), 128.67, 127.02 (q, J = 3.8 Hz), 125.82, 125.54 (q, J = 271.1 Hz),

114.94, 46.60, 29.76, 29.63, 23.34, 14.28. MS (ESI-TOF) for $C_{15}H_{18}F_3N_3$ $[M + H]^+$ calculated 298.1526, found 298.1562.

Human TLR8 ectodomain expression, purification and crystallization

The extracellular domain of human TLR8 (TLR8, residues 27–827) was prepared as described previously,[230] and was concentrated to 16 mg/mL in 10 mMMES (pH 5.5), 50 mM NaCl. The protein solutions for the crystallization of human TLR8/**17a** complex contained TLR8 (8.0 mg/mL) and saturated **17a**. Crystallization experiments were performed with sitting-drop vapor-diffusion methods at 293 K. Crystals of TLR8/**17a** were obtained with reservoir solutions containing 12.5% (v/v) PEG 3350, 0.2 M potassium formate, and 0.1 M sodium citrate pH 4.9.

Data collection and structure determination

Diffraction datasets were collected on beamlines SPring-8 BL41XU (Hyogo, Japan) under cryogenic conditions at 100 K. Crystals of hTLR8/**17a** were soaked into a cryoprotectant solution containing 7% (v/v) PEG 3350, 0.1 M potassium formate, 50mM sodium citrate pH 4.9, 5mM MES pH 5.5, 75mM NaCl, and 20% glycerol before flash-cooling.

Datasets were processed using the HKL2000 package.[251] Human TLR8/**17a** were determined by the molecular replacement method using the Molrep program[252] with the hTLR8/CL097 structure (PDB ID: 3W3J) as a search model. The model was further refined with stepwise cycles of manual model building using the COOT program[253] and restrained refinement using REFMAC[254] until convergence of the R factor was achieved. Compound, *N*-glycans, and water molecules were modeled into the electron density maps at the latter cycles of the refinement. The quality of the final structure was evaluated with PROCHECK.[255] The statistics of the data collection and

refinement are also summarized in Table S1. The figures representing structures were prepared with PyMOL (Schrödinger, New York, NY).

Human TLR8-specific reporter gene assays (NF-κB induction), and TLR-2/-3/-4/-5/-7/-9 counter-screens

The induction of NF-κB was quantified using human TLR-2/-3/-4/-5/-7/-8/-9-specific, rapid-throughput, liquid handler-assisted reporter gene assays as previously described by us.[31, 91, 101-102] HEK293 cells stably co-transfected with the appropriate hTLR and sAP were maintained in HEK-Blue™ Selection medium. Stable expression of sAP under control of NF-κB/AP-1 promoters is inducible by appropriate TLR agonists, and extracellular sAP in the supernatant is proportional to NF-κB induction. Reporter cells were incubated at a density of $\sim 10^5$ cells/ml in a volume of 80 μl/well, in 384-well, flat-bottomed, cell culture-treated microtiter plates in the presence of graded concentrations of stimuli. sAP was assayed spectrophotometrically using an alkaline phosphatase-specific chromogen (present in HEK-detection medium as supplied by InvivoGen) at 620 nm.

Immunoassays for cytokines

Fresh human PBMCs were isolated from human blood obtained by venipuncture in Cell Preparation Tubes (CPT, Beckton-Dickinson) with informed consent and as per guidelines approved by the University of Minnesota Human Subjects Experimentation Committee. Aliquots of PBMCs (10^5 cells in 100 μL/well) were stimulated for 16 h with graded concentrations of test compounds. Supernatants were isolated by centrifugation, and were assayed in duplicates using analyte-specific multiplexed cytokine/chemokine bead array assays (HCYTMAG-60K-PX29 MILLIPLEX MAP Human Cytokine/Chemokine Magnetic Bead Panel, EMD Millipore, Billerica,

MA) as reported by us previously.[100] The following analytes were quantified: sCD40L, VEGF, TNF-β, TNF-α, TGF-α, RANTES, PDGF-AB/BB, PDGF-AA, MIP-1β, MIP-1α, MDC (CCL22), MCP-3, MCP-1, IP-10, IL-17A, IL-15, IL-13, IL-12 (p70), IL-12 (p40), IL-10, IL-9, IL-8, IL-7, IL-6, IL-5, IL-4, IL-3, IL-2, IL-1ra, IL-1β, IL-1α, IFN-γ, IFN-α2, GRO, GM-CSF, G-CSF, fractalkine, Flt-3 ligand, FGF-2, eotaxin, EGF.

Intracellular PhosFlow™ flow cytometry for quantifying p38MAPK, ERK1/2, and NF-κB phosphorylation

Heparin-anticoagulated whole blood samples were obtained by venipuncture from healthy human volunteers with informed consent and as per guidelines approved by the University of Minnesota Human Subjects Experimentation Committee. Serial dilutions of compounds in RPMI medium supplemented with 10% fetal bovine serum (fRPMI) were performed using a Bio-Tek Precision 2000 XS liquid handler in sterile 96-well polypropylene plates, to which were added 100 μL aliquots of anticoagulated whole human blood. The plates were incubated at 37 °C for 15 min. Following incubation, the blood was transferred to a 96-well deep well plate containing 800 μL of pre-warmed Lyse/Fix buffer (BD Biosciences, San Jose, CA), incubated at 37° C for 15 min, then centrifuged at 300 g for 10 min. The supernatant was discarded, and the Lyse/Fix process was repeated twice. Cell pellets were washed once in fRPMI, and once in ice-cold methanol, resuspended in 800 μL ice-cold methanol and permeabilized for 30 min. After two washes in fRPMI, 2.5 μg (in 30 μL) of anti-human NF-κB (p65)-PECy7, p38MAPK-PE, and ERK1/2-AlexaFluor 647 antibodies (BD Biosciences, San Jose, CA) were added to each well, and incubated on ice for 60 min. After two washes in fRPMI, cells were resuspended in 200 μL of fRPMI. Flow cytometry was performed using a FACSVerse (Becton-Dickinson Biosciences, San Jose, CA)

instrument for acquisition on 100,000 gated events. Compensation for spillover was computed for each experiment on singly-stained Comp Beads (Becton-Dickinson Biosciences, San Jose, CA). Flow cytometric data were analyzed and quantified using FlowJo v 7.0 software (Treestar, Ashland, OR).

Flow-cytometric immunostimulation experiments

Cell surface marker upregulation was determined by flow cytometry using protocols published by us previously,[150] and modified for rapid-throughput. Briefly, heparin-anticoagulated whole blood samples were obtained by venipuncture from healthy human volunteers with informed consent and as per guidelines approved by the University of Minnesota Human Subjects Experimentation Committee. Serial dilutions of selected compounds were performed using a Bio-Tek Precision 2000 XS liquid handler in sterile 96-well polypropylene plates, to which were added 100 µL aliquots of anticoagulated whole human blood. The plates were incubated at 37°C for 16 h. Negative (endotoxin free water) controls were included in each experiment. The following fluorochrome-conjugated antibodies were used: CD3-PE, CD19-FITC, CD56-APC (eBioscience, San Diego, CA), CD14-V500, CD28 PE-Cy7, CD40 V450, CD80 APC-H7, CD86 PerCP-Cy5.5 (Becton-Dickinson Biosciences, San Jose, CA). Following incubation, 2.5 µg of each antibody was added to wells with a liquid handler, and incubated at 4°C in the dark for 60 min. Following staining, erythrocytes were lysed and leukocytes fixed by mixing 200 µL of the samples in 800 µL pre-warmed Whole Blood Lyse/Fix Buffer (Becton-Dickinson Biosciences, San Jose, CA) in 96 deep-well plates. After washing the cells twice at 300 g for 10 minutes in RPMI, the cells were transferred to a 96-well plate. Flow cytometry was performed using a BD FACSVerse instrument for acquisition on 100,000 gated events. Compensation for spillover was computed for each

experiment on singly-stained Comp Beads (Becton-Dickinson Biosciences, San Jose, CA).

Kinase inhibitions screens

Kinase inhibition studies were performed at Reaction Biology (Malvern, PA). Compound **18f** was tested against 365 wild-type kinases in single dose duplicate mode at a concentration of 10 µM. The following kinase panel was used for re-screening in 10-dose IC_{50} mode with three-fold serial dilutions starting at 100 µM: calmodulin kinase (CAMK) CAMK1α, CAMK1β, CAMK1δ, CAMK1γ, CAMK2α, CAMK2β, CAMK2δ, CAMK2γ, CAMK4, CAMKK1, CAMKK2. Staurosporine (positive control) was tested in 10-dose IC_{50} mode with four-fold serial dilution starting at 20 µM. IC_{50} values were determined using four-parameter logistic fits.

Chapter 6.

Selective Induction of Pyroptosis-like Cell Death in Monocytes by Toll-like Receptor 8 Agonists, Leading to Antigen-loaded Extracellular Vesicles
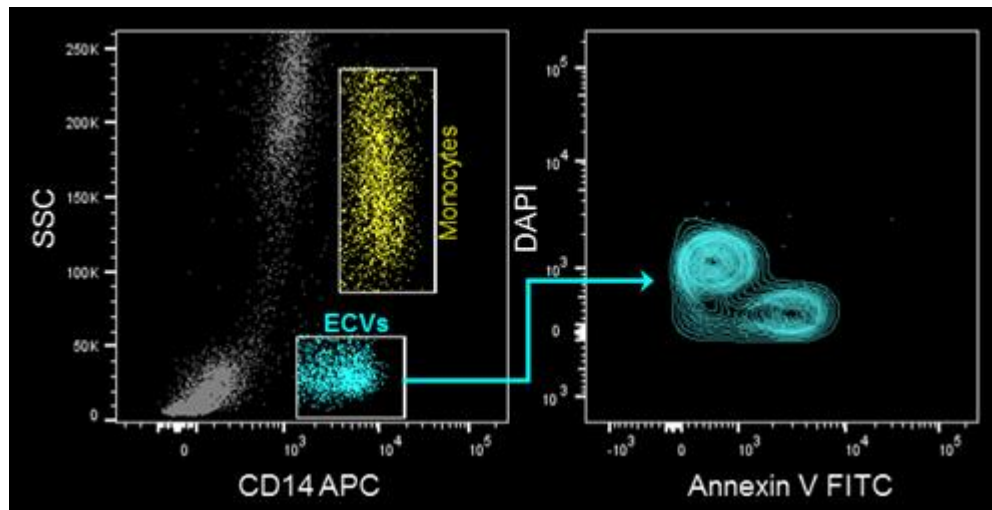
6.1 Introduction

Following the successful SAR campaign on the 2-aminoimidazoles (Chapter 5), we sought to further examine the mechanisms of adjuvanticity of TLR8 agonists. The mechanisms of adjuvanticity for TLR8 agonists are less well understood than many of the other TLRs due to the inability of canonical TLR8 agonists to stimulate mouse TLR8.[256] We therefore turned to the human system to examine the mechanistic basis of the adjuvantic activity of TLR8 agonists, with particular attention to their potential use in neonatal vaccines.

Infants have a heightened susceptibility to infection[257] and respond poorly to vaccination.[258-260] Although the mechanistic basis for the immunological differences between adults and neonates is yet to be understood clearly, it is thought that anti-inflammatory rather than pro-inflammatory responses to innate immune stimuli, as well as feeble plasma cell and germinal center T follicular helper and B cell induction and Th2-biased responses, contribute to the poor immunological responses in the very young.[258] Vaccine adjuvants currently in use lack the ability to stimulate neonatal immune systems effectively and, consequently, may be suboptimal.[261-264] It has been demonstrated that TLR8 agonists are unique in their ability to activate neonatal APCs by the induction of the proinflammatory cytokines, TNF-α and IL-12p40/70, upregulation of the co-stimulatory molecule CD40, and phosphorylation of p38MAPK.[222, 265]

The effects of TLR8 agonists on innate immune function suggest that these compounds could be potentially useful as vaccine adjuvants in neonatal vaccines. The consequences of TLR8 engagement on downstream adaptive immune responses are largely unknown, especially given that murine TLR8 is not responsive to canonical, small-molecule TLR8 agonists.[266]

We examined how TLR8 agonists influence processing of soluble antigens by APCs. TLR8-active compounds were unique in inducing pyroptosis-like death in monocytes, leading to the formation of CD14$^+$ Annexin V$^+$ extracellular vesicles (ECV) of 100-400 nm diameter. This process was dependent on myeloid differentiation primary response gene 88 (MyD88), interleukin-1 receptor-associated kinases (IRAK) 1 and 4, and p38MAPK. The monocyte-derived ECVs contain near-intact soluble antigens, and were capable of stimulating antigen-specific recall responses in autologous CD4$^+$ T lymphocytes. The formation of antigen-loaded, monocyte-derived ECVs may contribute to the adjuvantic effects of TLR8 agonists.

6.2 Results

TLR8 agonists induce ECV formation in monocytes

Our initial goal was to explore antigen internalization in APCs (monocytes and dendritic cell subsets) by flow cytometry. In examining a panel of TLR agonists (Fig. 1), dramatic changes in the CD14$^+$ monocytes were observed in samples that were stimulated with either pure TLR8, or dual TLR7/8 agonists: we noted a dose-dependent reduction in frequency of side scatter (SSC)^{high}/ forward scatter (FSC)^{high} CD14$^+$ monocyte population, which was accompanied by the appearance of a new, SSC^{low}/ FSC^{low} CD14$^+$ population (Fig. 2). The new population was dimorphic with respect to staining with DAPI and Annexin V, with approximately equal numbers of events being DAPI$^+$/Annexin$^-$, and DAPI$^-$/Annexin$^+$ (Fig. 3). The new CD14$^+$ population was also human leukocyte antigen (HLA)-DR$^+$ (data not shown). The apparent loss of the conventional monocytic population, and the concomitant appearance of CD14$^+$, HLA-DR$^+$ bodies with attenuated forward- and side-scatter properties with dimorphic DAPI and Annexin V staining properties suggested that these were monocyte-derived, possessing mixed apoptotic and pyroptotic properties. Isolation of

these bodies and examination by transmission electron microscopy confirmed that these were extracellular vesicles (ECVs) with a diameter ranging from 100 nm to 400 nm (Fig. 3).
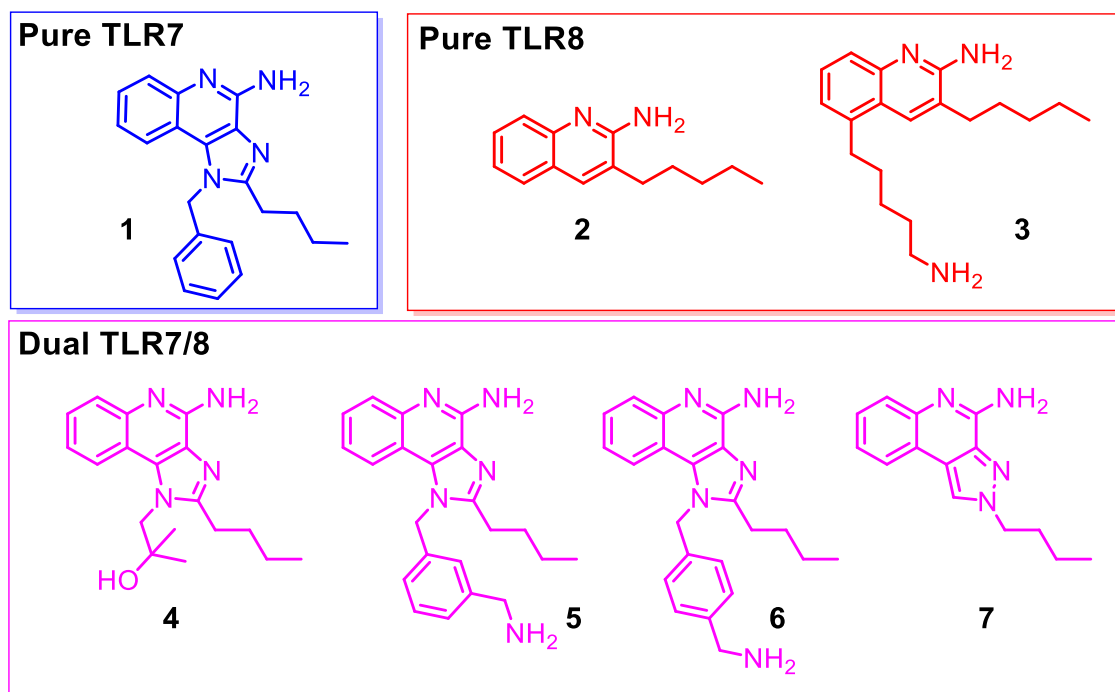
Figure 1: Structures of TLR agonists. *The TLR7 agonist is shown in blue, the TLR8 agonists are shown in red, and the dual TLR7/8 agonists are shown in purple.*

As noted earlier, only TLR8 or dual TLR7/8 agonists induced ECV formation, and neither the pure TLR7 agonist compound **1**, nor agonists of TLR2, -3, -4, -5, or -9 elicited vesicles. The phenomenon appeared specific to TLR8 or TLR7/8 ligands themselves, and not to secondary, autocrine, or paracrine cytokine induction because incubation of PBMCs with TNF-α, IL-18, IL-12, IL-6, IL-4, IL-2, IFN-α, and IFN-γ were unable to induce the formation of ECVs even up to concentrations of 1000 U/mL (data not shown).
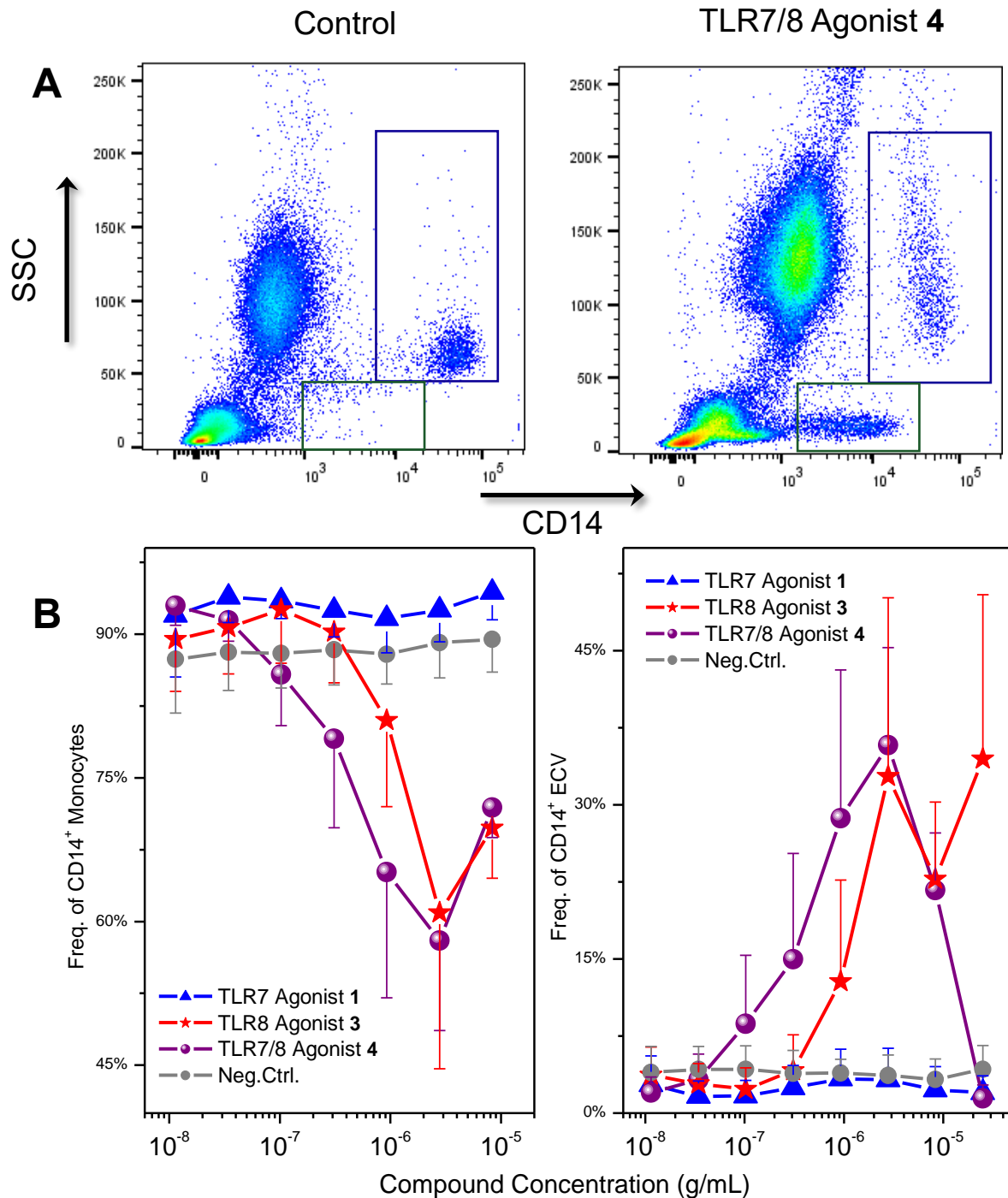
Figure 2: Whole human blood stimulated with various TLR agonists. A. *SSC^{high}/ FSC^{high} CD14^{+} monocytes were observed in mock-stimulated samples, but a new SSC^{low}/ FSC^{low} CD14^{+} population was observed following stimulation with either TLR8 or dual TLR7/8 agonists.* ***B.*** *Dose-dependent formation of the SSC^{low}/ FSC^{low} CD14^{+} population was accompanied by concomitant reductions in the SSC^{high}/ FSC^{high} CD14^{+} monocytes.*
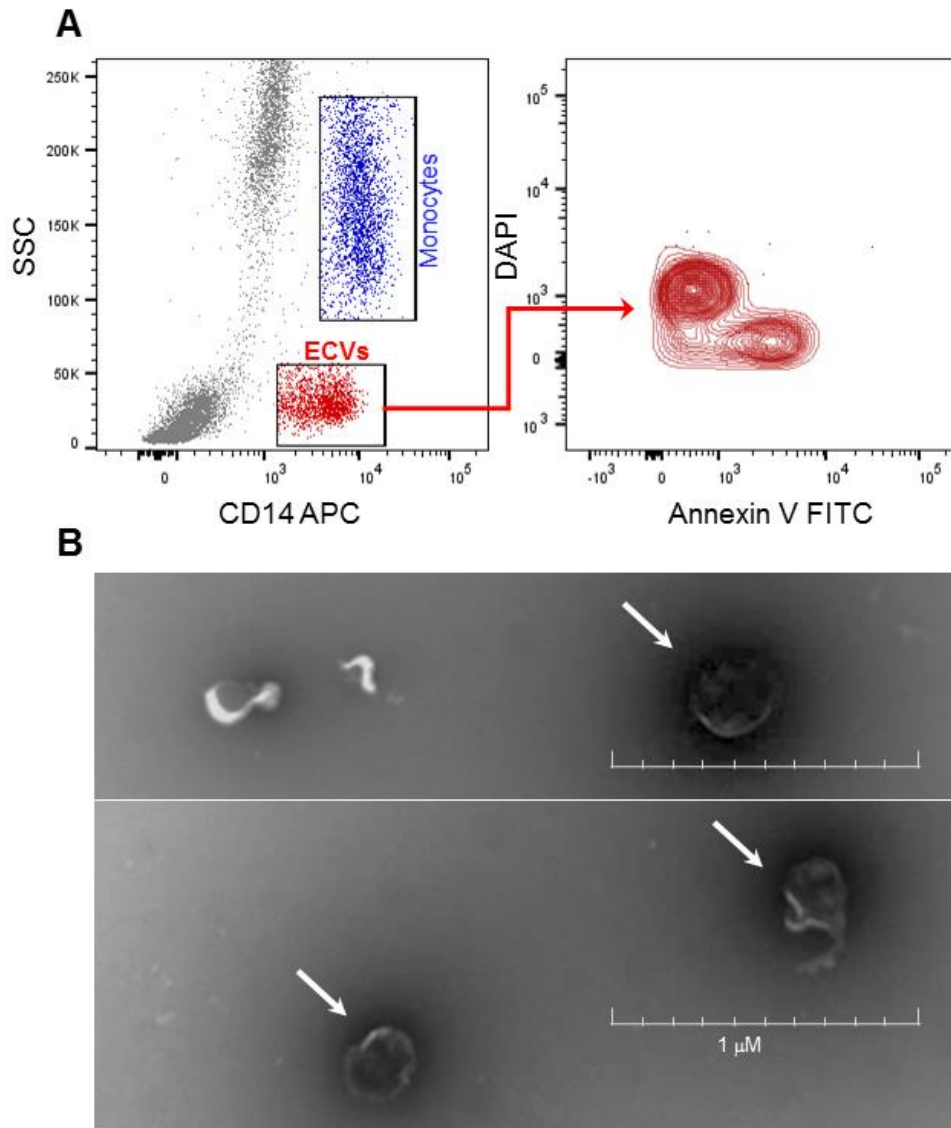
Figure 3: Phenotypic characterization of the SSC^{low}/ FSC^{low} CD14$^+$ population. A. The SSC^{low}/ FSC^{low} CD14$^+$ population was composed of Annexin V$^+$/DAPI$^-$ and Annexin V$^-$/DAPI$^+$ subpopulations. **B.** Transmission electron microscopy (negative stain with phosphotungstate) of isolated SSC^{low}/ FSC^{low} CD14$^+$ population showed that these were vesicles with a diameter of 100-400 nm.

ECV generation is dependent on p38 MAPK, MyD88, and IRAK1/4

Our observations indicated that ECV formation was dependent exclusively on TLR8 and not on TLR7. We sought to determine whether there was divergence in the signaling pathways distal to TLR7 and TLR8 engagement, and whether any signaling events were uniquely associated with TLR8 activation. Using a variety of inhibitors of the TLR signaling pathway, including a MyD88 inhibitor,[267] we examined if any of the inhibitors 'rescued' monocytes and reduced ECV formation induced by the TLR8 and TLR7/8 agonists. The MyD88 inhibitor 4210, IRAK 1/4 Inhibitor I, and SB20358 caused significant inhibition of monocytic loss and consequent ECV formation, implicating MyD88, IRAK 1 and 4, and p38MAPK (Fig. 4). The inhibitors for the caspases, P2X7 extracellular ATP sensor, NF-κB, c-Jun N-terminal kinase (JNK), TANK binding kinase (TBK) 1/inhibitor of NF- κB (IKKε), and the NLRP3 inflammasome were ineffective.

Activation of p38MAPK in monocytes

Signaling in both TLR7 and TLR8 are MyD88-dependent,[268-269] and IRAK-4 acts as a kinase downstream from MyD88 and upstream from IRAK-1.[270] Our attention therefore turned to p38MAPK which has been recently shown to be involved in TLR8-dependent priming of NADPH oxidase activation in human neutrophils.[271] We compared p38MAPK activation in monocytes by TLR7, TLR8, and dual TLR7/8 agonists, using anisomycin [272] as a positive control. Kinetic experiments showed that measurable monocytic loss could be observed at 4 h following stimulation. In order to examine intact monocytes, PBMCs were treated with the TLR agonists for 2 h. Both the dual TLR7/8 agonists and the TLR8 agonists induced significant, dose-dependent p38MAPK activation in CD14$^+$ monocytes, comparable to that observed with anisomycin, whereas the TLR7 agonist compound **1** induced much lower levels of p38MAPK activation (Fig. 5).
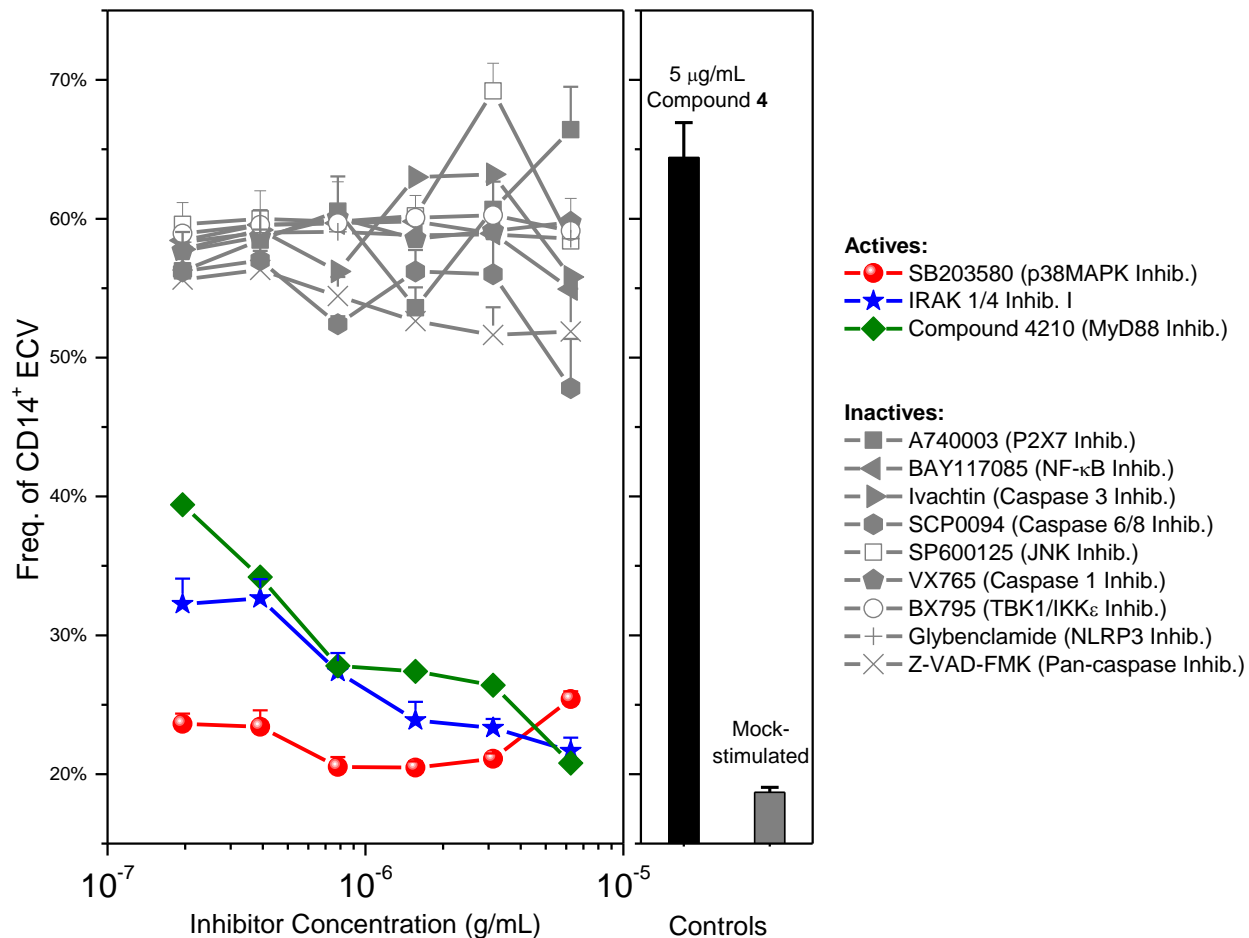
Figure 4: Inhibition assay to determine the signaling pathways leading to ECV formation. *Compound 4210, IRAK 1/4 Inhibitor I, and SB203580 reduced ECV formation and 'rescued' monocytes, which indicated MyD88, IRAK 1 and 4, and p38MAPK, respectively, were critical to ECV development.*

Antigen packaging in ECVs

Reverting back to the question of how TLR8 agonists influence antigen internalization in APCs, we interrogated if exogenous, soluble antigens would be present in the monocyte-derived ECVs. PBMCs were cultured in the presence of 5 μg/mL of compound **4**, and 100 μg/mL of either a 54.1 kDa antigenic construct of Zika virus E-glycoprotein fused to mannose binding protein (MBP-
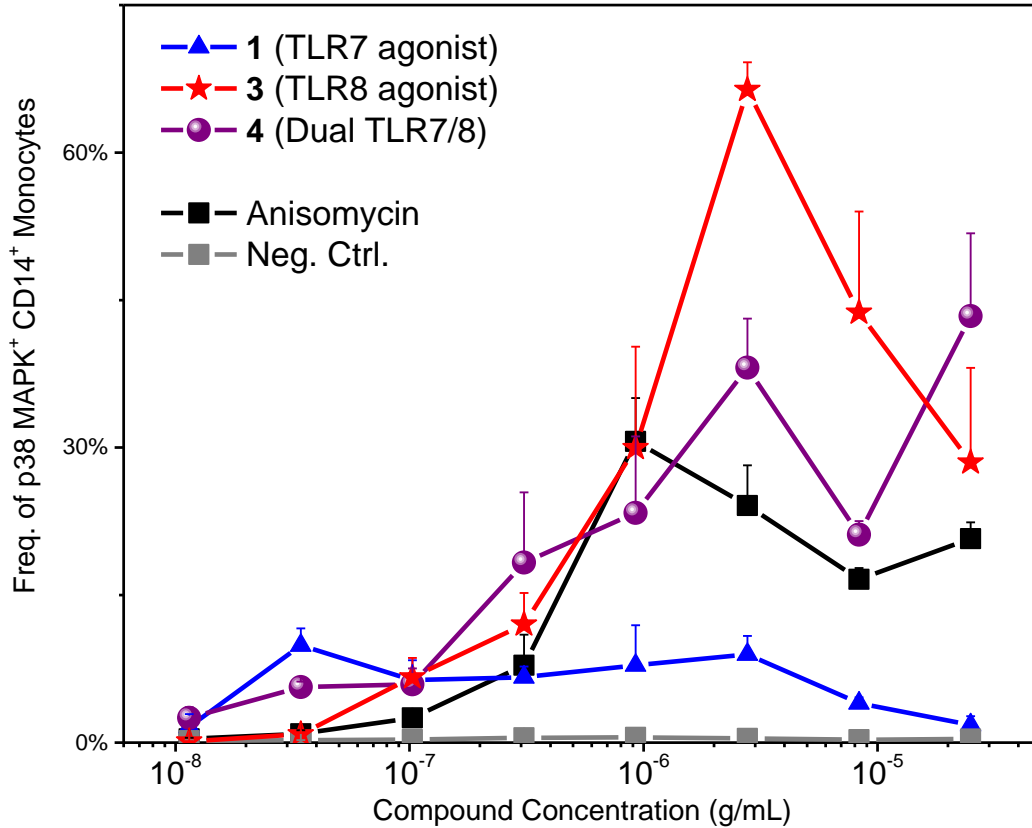
Figure 5: Induction of p38MAPK by TLR7 and TLR8 agonists. *TLR8 and dual TLR7/8 agonists, but not the TLR7 agonist, induced dose-dependent activation of p38MAPK in CD14$^+$ monocytes in a manner similar to the positive control anisomycin.*

ZIKV) which we are currently evaluating as an immunogen in animal models, or the 58 kDa non-toxic diphtheria toxin mutein, CRM197,[147] which we have previously used as a model immunogen in animal immunization studies.[24, 88] Monocyte-derived ECVs were isolated from the PBMC cultures by centrifugation, and washed at least three times in complete RPMI to ensure removal of extravesicular antigen. The washed ECVs were lysed using a two-step procedure using 1 N sodium hydroxide with sonication, followed by 1 N hydrochloric acid. Western blots with appropriate rabbit immune sera were performed not only to test whether antigens were present in the ECVs, but also to determine integrity (immunoreactivity) and the relative size of the antigens recovered from ECVs. Both MBP-ZIKV, and CRM197 were readily observed in the ECV lysates with

dominant bands corresponding to 54 and 58 kDa, respectively (Fig. 6). In PBMC culture supernatants, as well as in ECVs, accessory bands of lower molecular weights were observed signifying a degree of proteolysis (Fig. 6). It is noteworthy that the degree of proteolytic degradation was significantly higher for CRM197, with prominent bands of approximately 40 and 23 kDa (Fig. 6), which is likely a consequence of the cleavage of A and B fragments.[273] The molecular weight profiles of antigens recovered from the culture supernatants appeared to match the antigen recovered from the ECVs suggesting that proteolysis occurs during incubation with PBMCs, and not within the ECVs. These results indicated that exogenous, soluble antigens were internalized in TLR8-activated monocytes, packaged, and then released as extracellular vesicles.
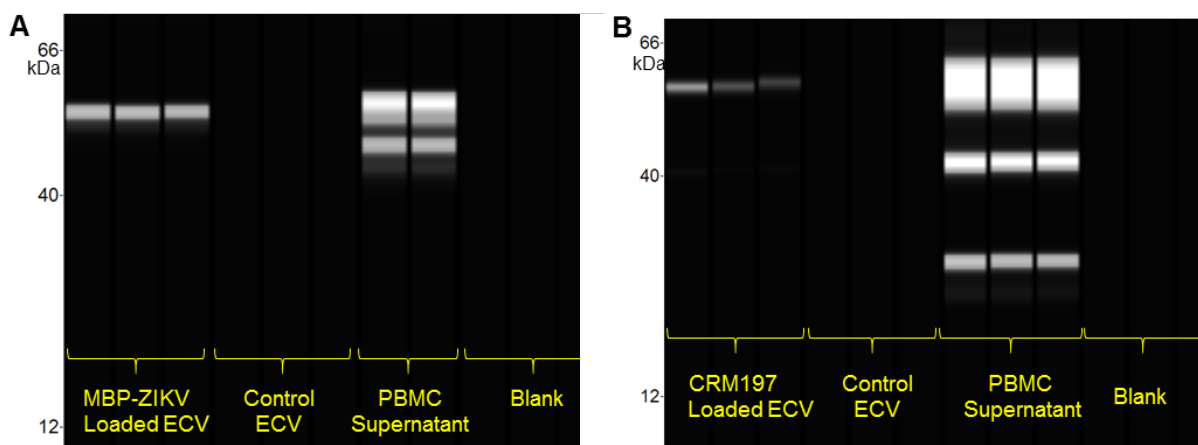
Figure 6: Antigen loading in ECVs. A. Lysates from ECVs loaded with the a 54 kDa MBP-ZIKV antigen were examined by Western blots. Intact MBP-ZIKV antigen was readily detectable in the ECV lysates. B. Intact antigen was also detectable from the lysates of ECVs loaded with CRM197. CRM197 showed degradation in the culture, which likely corresponded to cleavage of the A and B fragments.

Antigen-loaded ECVs stimulate recall in CD4+ Th cells

Given that the ECVs were positive for HLA-DR and Annexin V, it was unclear if the antigen-loaded vesicles would be immunostimulatory (as has been documented, for instance, for dendritic

cell-derived vesicles[274]), or tolerogenic, (as has been observed in human polymorphonuclear cell-derived vesicles[275]). We sought to determine whether ECVs loaded with CMV tegument protein pp65 (pp65) were capable of stimulating autologous CD4$^+$ lymphocytes. ECVs were generated as mentioned earlier from PBMCs cultured with 100 µg/mL pp65 and stimulated with 5 µg/mL of compound **4**. ECVs were cultured with freshly-isolated autologous PBMCs from either CMV seropositive (n = 4) or seronegative (n = 3) donors. Recall responses in CD4$^+$ Th population were measured by quantifying bifunctional IL-2$^+$ and IFN-γ$^+$ populations. CD3/CD28 Dynabeads, used as a positive control, induced significant numbers of double positive T cells (Fig 7), while negative control samples lacking either antigen, or antigen and TLR7/8 stimulus showed sparse IL-2$^+$/IFN-γ$^+$ double positive events. The assay was benchmarked using PBMCs from seropositive individuals stimulated with soluble pp65 alone, which elicited significantly higher numbers of IL-2$^+$/IFN-γ$^+$ events relative to unstimulated controls. ECVs loaded with pp65 were found to induce similar numbers of activated CD4$^+$ cells, indicating that the ECVs were functional, and were causing pp65-specific recall responses in CD4$^+$ lymphocytes (Fig. 7).

Antigen-loaded ECVs are unable to directly stimulate isolated CD3$^+$ T cells

The finding that pp65 packed ECVs were able to elicit antigen-specific CD4$^+$ T cell responses in autologous PBMCs, coupled with the observation that the ECVs were positive for HLA-DR prompted us to examine if antigen-loaded ECVs could directly present antigen to T cells. CD3$^+$ T cells were isolated using magnetic microbeads and stimulated with autologous ECVs loaded with pp65. Both soluble pp65 as well as ECVs loaded with pp65 failed to activate isolated T cells (Fig. 8); PBMCs incubated with soluble pp65 showed similar responses to previous experiments and, as expected, CD3/CD28 Dynabeads also activated isolated T cells. These results suggested that

ECVs were not capable of directly stimulating T cells, despite the expression of MHC II molecules on their surface.

ECVs are taken up by CD14$^+$ monocytes in PBMC culture

In light of the fact that direct activation of T cells by the ECVs was not observed, we examined if accessory cells (such as APCs) present in PBMCs were internalizing the antigen-bearing ECVs and secondarily causing antigen-specific T cell responses. ECVs loaded with pp65 were cultured with PBMCs, which was followed by fixation, permeabilization, and staining with anti-CMV pp65 antibodies. The antibody signal was enriched using tyramide signal amplification[168-169] to enhance the pp65 signal to such levels as are required for reliable detection by flow cytometry. Signals from both soluble pp65 and ECVs loaded with pp65 were detected in CD14$^+$ monocytes to comparable levels (Fig. 8), indicating that antigen-packed ECVs were internalized primarily by monocytes, thereby possibly contributing to the activation of T cells observed *ex vivo*.

6.3 Discussion

We have been investigating TLR agonists for their potential utility as vaccine adjuvants. TLR8 agonists were of particular interest to us because of their strong proinflammatory cytokine profile, including IL-1β, TNF-α, and IFN-γ, and their ability to directly act upon monocytes, macrophages, and CD1c$^+$ dendritic cells to significantly upregulate co-stimulatory molecules, including CD40, CD80 and CD86.[39, 276-277] We aimed to build upon the existing APC activation profiles and explore how TLR8 agonists impacted APC internalization of soluble antigen to better understand mechanisms of adjuvanticity.
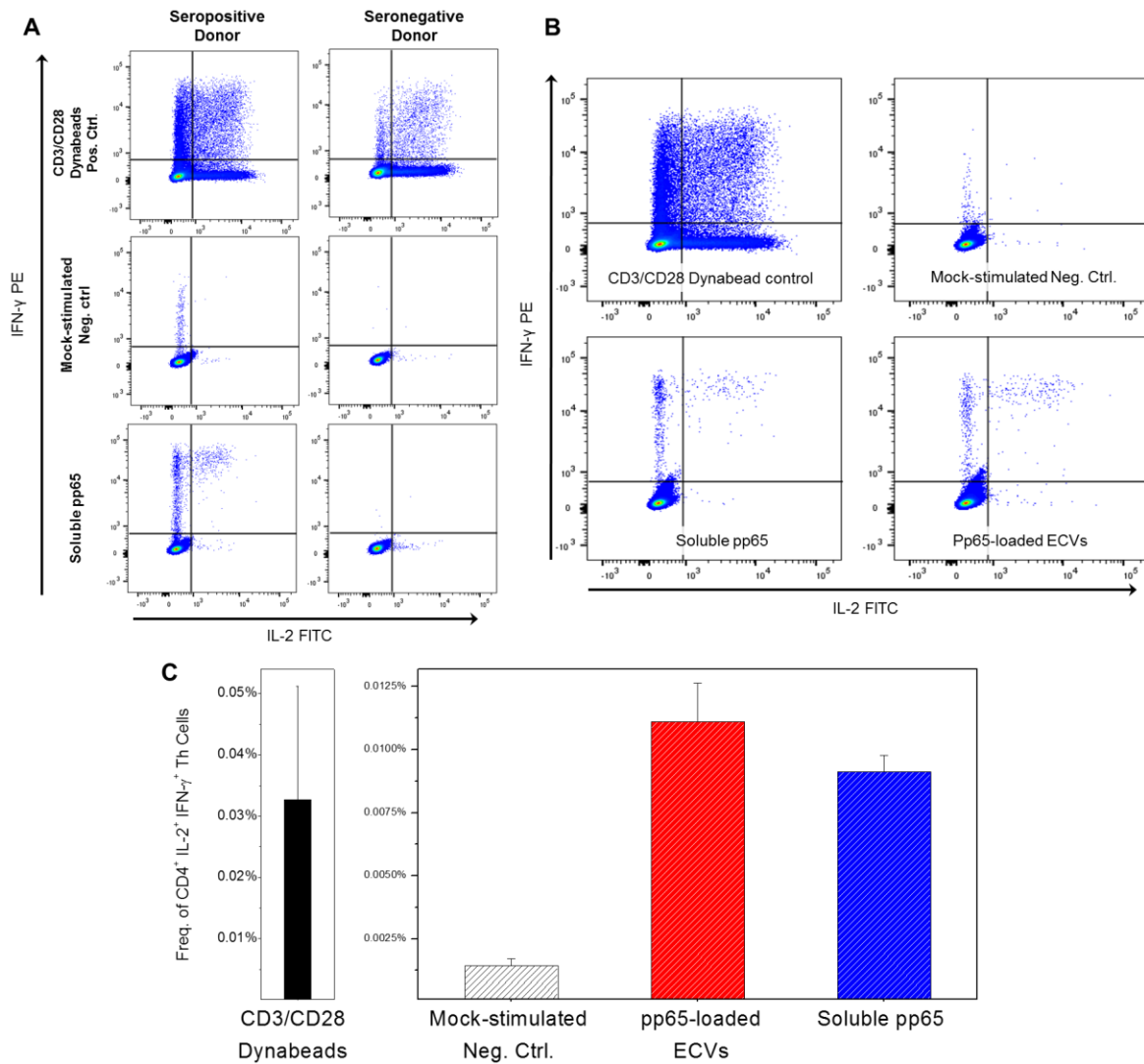
Figure 7: Functional recall responses in PBMCs to CMV pp65-loaded ECVs. A. *CMV seronegative (n = 3) and seropositive (n = 4) donors were examined for soluble CMV protein pp65-specific recall responses in bifunctional IL-2$^+$/IFN-γ^+ CD4$^+$ T cells. Only CMV seropositive donors responded to soluble pp65.* ***B.*** *CMV pp65-loaded ECVs generated from PBMCs of seropositive donors elicited increases in the number of bifunctional IL-2$^+$/IFN-γ^+ CD4$^+$ T cells in autologous PBMCs. The increases were comparable to samples stimulated with only soluble pp65. Autologous PBMCs mock-stimulated with ECVs not loaded with pp65 failed to show any responses.* ***C.*** *Quantitation of antigen-specific bifunctional IL-2$^+$/IFN-γ^+ CD4$^+$ recall responses to either soluble pp65, or autologous ECVs loaded with pp65. Mock-stimulated PBMCs did not induced T cells responses.*

TLR7 and TLR8 both recognize single-stranded RNA,[2] but they differ dramatically in their innate immune activation signatures. TLR7 engagement is characterized by strong induction of Type I interferons, upregulation of the early activation marker CD69 in B cells, natural killer cells, and cytokine-induced killer cells, and upregulation of the co-stimulatory molecules CD40 and CD80 in monocytes, plasmacytoid dendritic cells, CD1c^{+} conventional dendritic cells, and CD141^{+} conventional dendritic cells.[27, 29, 39, 111] TLR8 activation, on the other hand, is distinguished by strong Type II interferon induction, and upregulation of the co-stimulatory molecules CD40 and CD80 in only monocytes and CD141^{+} conventional dendritic cells.[24, 39, 278] The downstream
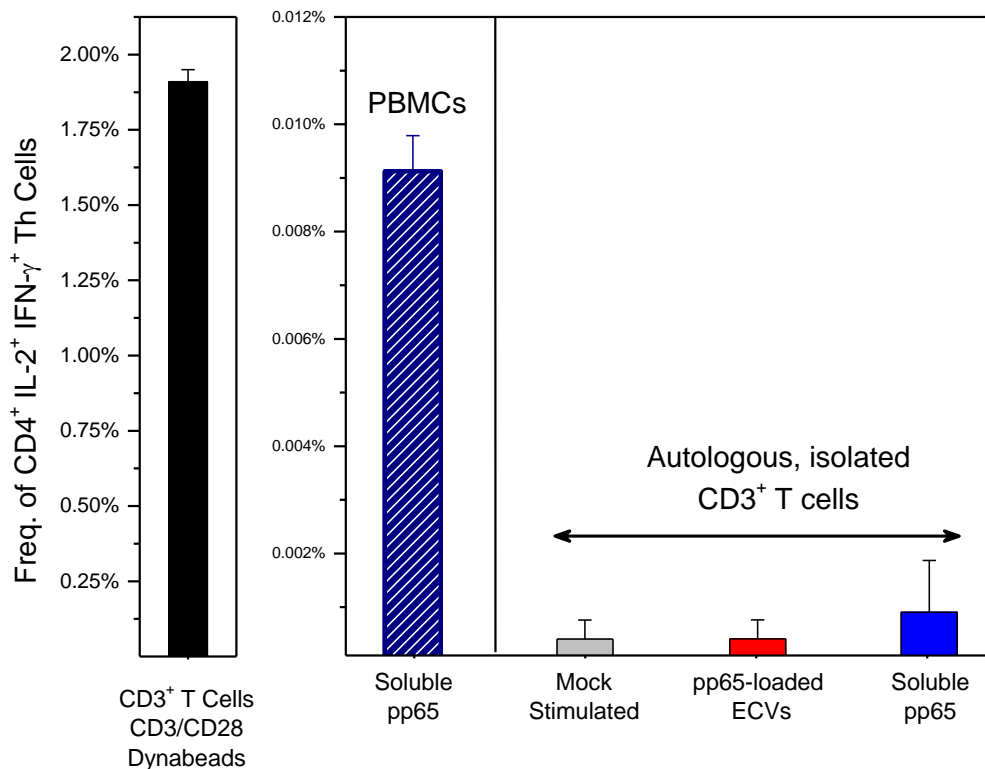
Figure 8: Failure to induce recall responses in isolated CD3^{+} T cells by pp65-loaded ECVs. *Neither soluble pp65, nor ECVs loaded with pp65 activated T cells in autologous, isolated CD3^{+} T cells from CMV-seropositive donors. CD3^{+} T cells stimulated with CD3/CD28 Dynabeads as well as PBMCs stimulated with soluble pp65 induced bifunctional IL-2^{+}/IFN-γ^{+} CD4^{+} T cell responses as expected.*

responses to TLR7 and TLR8 signaling are therefore distinct, which holds true in the present study demonstrating the apparent loss of CD14^{+} monocytes and consequent formation of ECVs, which occurred only following stimulation with TLR8-active compounds (Fig. 2).
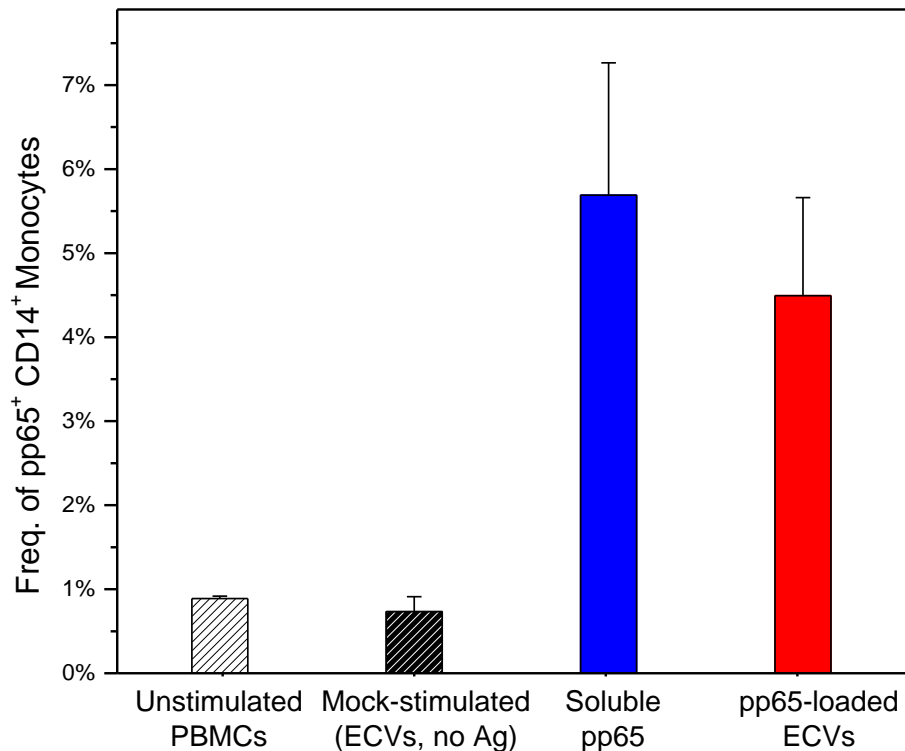
Figure 9: CMV pp65-loaded ECVs and soluble pp65 internalization in monocytes. ECVs loaded with pp65, as well as soluble pp65, were internalized by CD14^{+} monocytes in fresh, autologous PBMCs. Detection of the antigen was enhanced using tyramide signal amplification.

The loss of the monocytes bear similarities to inflammatory cell death observed during pyroptosis. Pyroptotic cells undergo DNA cleavage, swelling, and lysis that result in ECVs that are considerably smaller (<500 nm) than those occurring due to apoptosis (1-4 μm). Both pyroptotic and apoptotic bodies, however, expose phosphatidylserine on the outer leaflet of the ECV [279]. The monocyte-derived ECVs described here were predominantly anuclear, possessed exposed phosphatidylserine, and were much smaller than the reported size of apoptotic bodies (Fig. 3).[279]

While similarities with pyroptotic outcomes were observed, it was not possible to determine with certainty that pyroptosis was the cause of monocyte loss. Caspase 1 activation is one of the defining characteristics of pyroptosis,[279] but inhibition of caspase 1 did not inhibit ECV formation (Fig 4). The role of caspases in TLR8 induced monocyte death requires further investigation to determine the extent of their involvement in this form of cell death.

The exact cellular processes leading to ECV formation remain elusive. The requirement for p38MAPK activation in ECV formation offered an interesting point of comparison to NETosis in neutrophils. NETosis, a form of cell death in neutrophils that centers on the release of chromatin structures loaded with antimicrobial molecules called neutrophil extracellular traps, was shown to be dependent on the activation of p38MAPK by reactive oxygen species.[280] Recent reports of NETosis induction by the TLR7/8 agonist R848[281] and our observations of TLR8 agonist-induced p38MAPK-dependent cell death (Fig. 5) show a possible link between p38MAPK driven cell death induced by TLR8 agonists across multiple leukocyte populations.[282]

Much of the early work involving cell death and the clearance of ECVs did not distinguish between the various forms of cell death and showed them to be either immunoquiescent or immunostimulatory.[283-284] It was shown more recently that the activation state of the cell at death and type of cell death can greatly influence how the immune system reacts with the dying cell and resulting ECVs.[285-286] Furthermore ECVs, such as exosomes, were shown to possess the ability to present antigen via major histocompatibility complex class II to cognate T cells.[287] It was with this in mind that we sought to determine if the ECVs we observed were able to present antigen to T

cells. These studies show that ECVs contained exogenous, soluble antigens from the culture using two distinct antigens: MBP-ZIKV and CRM197 (Fig. 6). We utilized the prevalence of CMV seropositivity in the population to explore antigen-specific recall in T cells to CMV antigen pp65 using intracellular IL-2 and IFN-γ as markers for T cell activation. The strong responses in CD4$^+$ T cells with ECVs loaded with CMV pp65 indicated that the internalized antigen was available for adaptive immune responses (Fig. 7).

We next examined if the ECVs could directly present antigen to T cells. The failure of isolated CD3$^+$ T cells to respond to pp65 loaded ECVs indicates that the antigen is likely not being presented on the surface of the ECVs, but rather retained within as near-intact protein requiring processing and presentation from additional APCs (Fig. 8). We demonstrate that monocytes from fresh PBMC culture internalize both the soluble pp65 antigen, as well as pp65-loaded ECVs (Fig. 9), which is consistent with the known trafficking of antigen-laden exosomes of monocytes, macrophages and dendritic cells.[288-290] No pp65 was detected in the lymphocyte populations indicating that the B cells were likely not contributing to the T cell responses observed.

The induction of cell death and antigen packing we have described here are consistent with the reported mechanisms of adjuvanticity of other immunostimulants. Several groups have found correlations between vaccine adjuvant-induced cell death and antigen internalization in APCs that points to cell death and the release of danger associated molecular patterns as being central to adjuvant-induced immunostimulation.[291-292] This is true, for example, of the adjuvantic extract of *Q. saponaria* (QS-21), which functions through the induction of the NLRP3 inflammasome to facilitate IL-1β and IL-18 release, and induces caspase-1 and -11 independent cell death of

dendritic cells.[293-294] Furthermore, alum, the most widely used FDA-approved vaccine adjuvant, has been shown to induce cell death at the site of injection, leading to the release of danger signals from dying cells, which ultimately contributes to NLRP3 inflammasome activation and adjuvant effects.[295]

6.4 Conclusions

The unique immunostimulatory properties of TLR8 agonists, including inflammatory cell death, make them interesting candidates for vaccine adjuvants. The induction of pyroptosis-like cell death in monocytes and attendant cytokine responses are likely only part of the adjuvantic mechanisms at play with the TLR8 agonists and, as such, warrant further exploration into mechanisms of adjuvanticity.

6.5 Materials and Methods

TLR agonists

The pure TLR7 agonist **1** (1-benzyl-2-butyl-1*H*-imidazo[4,5-*c*]quinolin-4-amine) [91], the pure 8 agonists **2** (3-pentylquinolin-2-amine),[26] **3** (5-(5-aminopentyl)-3-pentylquinolin-2-amine),[24] and the dual TLR7/8 agonists **4** (1-(4-amino-2-butyl-1*H*-imidazo[4,5-*c*]quinolin-1-yl)-2-methylpropan-2-ol),[91] **5** (1-(3-(amino-methyl)benzyl)-2-butyl-1*H*-imidazo[4,5-*c*]quinolin-4-amine), **6** (1-(4-(aminomethyl)benzyl)-2-butyl-1*H*-imidazo[4,5-*c*]quinolin-4-amine),[92] **7** (2-butyl-2*H*-pyrazolo[3,4-*c*]quinolin-4-amine)[97] were synthesized as reported earlier by us (Fig. 1). Synthetic PAM$_2$CSK$_4$ (TLR2 agonist), Poly(I:C) (TLR3 agonist), ultrapure LPS from *E. coli* K12 (TLR4 agonist), flagellin from *S. typhimurium* (TLR5 agonist), and ODN-2006 (TLR9 agonist) were procured from InvivoGen (San Diego, CA).

Synthesis of MyD88 inhibitor

The precursor moiety ((*S*)-4-methyl-3-((3-phenylpropyl)amino)-1-(pyrrolidin-1-yl)pentan-2-one) was synthesized as reported by Bartfai and colleagues.[296] The MyD88 inhibitor 4210 (N^1,N^4-*bis*((*S*)-4-methyl-2-oxo-1-(pyrrolidin-1-yl)pentan-3-yl)-N^1,N^4-*bis*(3-phenylpropyl)cyclohexane-1,4-dicarboxamide, Fig. 1)[267] was synthesized as reported by Alam and colleagues with modifications as follows: *trans*-cyclohexane-1,4-dicarboxylic acid (3.0 mmol) was dissolved in ethyl acetate (3 mL) with *N,N*-diisopropylethylamine (15 mmol), compound **8** (7.5 mmol), and 1-[*bis*(dimethylamino)methylene]-1*H*-1,2,3-triazolo[4,5-*b*]pyridinium 3-oxide hexafluoro-phosphate (HATU, 7.5 mmol) followed by stirring for 96 h at 40°C. The solvent was evaporated under vacuum. The oil was dissolved with ethyl acetate (150 mL), extracted with 1 M NaOH (50 mL), 1.2 M HCl (50 mL), and saturated $NaHCO_3$ (50 mL), followed by drying over Na_2SO_4. The organic layer was evaporated and the residue was purified by silica gel flash chromatography with a CombiFlash® Rf (Teledyne Isco Inc., Lincoln, NE; methanol/DCM: 0→6%) instrument, followed by basic alumina flash chromatography (ethyl acetate/hexane 0→40%). An overall yield of 35% was obtained for Compound 4210.

Antigens and antisera

Diphtheria toxin mutant CRM197[147-148] was purchased from List Biologicals (Campbell, CA), and Cytomegalovirus (CMV) pp65 antigen was purchased from Abcam (Cambridge, UK., catalog number ab43031). A 54.1 kilo Dalton antigenic construct consisting of an N-terminal mannose binding-protein fused to a Zika virus E-glycoprotein derived antigen (MBP-ZIKV) was expressed and purified by KanPro Research Corp., (Lawrence, KS). Rabbit immune sera to CRM197 and MBP-ZIKV were generated by us as previously described.[171]

Reagents

The following antibodies were purchased from commercial sources as noted: CD14-APC, HLA-DR-APC and Annexin V-FITC (eBioscience, San Diego, CA., catalog numbers 17-0149-42, 17-9956-42, and 88-8005-74, respectively), CD14-BV421, CD4-V450, CD8-V500, Phosflow™ p38 MAPK-PE, anti-IL-2-FITC, anti-IFN-γ-PE (BD Bioscience, Becton Dickinson Franklin Lakes, NJ., catalog numbers 563743, 560345, 560774, 612565, 555431, and 554701, respectively). TLR pathway inhibitors SP600125, BAY 11-7085, IRAK1/4 Inhibitor, A740003, SCP0094, and cytochalasin D were purchased from Sigma Aldrich (St. Louis, MO). SB203580, VX-765, Glybenclamide, VAD-FMK, BX795, and Gefitinib were purchased from InvivoGen (San Diego, CA). TNF-α, IL-18, IL-12, IL-6, IL-4, IL-2, IFN-α, and IFN-γ were purchased from R&D Biosystems (Minneapolis, MN).

Ex vivo human whole blood stimulation

Whole human blood was collected in heparinized Vacutainer™ tubes, and PBMCs were collected and isolated in CPT™ tubes (Becton Dickinson, Franklin Lakes, NJ) from healthy volunteers providing written informed consent in accordance with the University of Minnesota Institutional Review Board (IRB Protocol 1506M74641). All experiments were replicated using a minimum of three individual donors. Whole heparinized blood was 1:2 diluted in RPMI 1640 supplemented with 10% fetal bovine serum, 100 U/mL penicillin, and 100 μg/mL streptomycin (complete RPMI). Cells were cultured in either polypropylene U bottom 96-well plates or 5 mL polypropylene capped tubes at 37ºC for 4 to 16 h, as indicated for each experiment. Whole blood was incubated with graded concentrations of TLR agonists for 16 h.

Flow cytometry

Samples were pre-cooled to 4ºC for 1 h, and then stained with combinations of 2.5 µg/well surface markers, Annexin V-FITC and/or DAPI. Erythrocytes were lysed and leukocytes fixed by transferring 200 µL of diluted blood to 800 µL of pre-warmed Lyse/Fix buffer (Becton Dickinson, Franklin Lakes, NJ) in a 96-deep well plate by liquid handler and incubated for 10 min at 37ºC. The Lyse/Fix process was carried out one additional time before washing with 800 µL complete RPMI. Samples were resuspended in 200 µL complete RPMI for acquisition on a BD FACSVerse flow cytometer (Becton Dickinson, Franklin Lakes, NJ) for 250,000 gated events. Monocytes were gated as $CD14^+$ SSC^{high} while extracellular vesicles (ECVs) were gated as $CD14^+$ SSC^{low}. ECVs were evaluated for DAPI, Annexin V, and frequencies with FlowJo 10 (FlowJo LLC, Ashland, OR). For intracellular p38MAPK staining, cells were resuspended in 800 µL Perm Buffer III (Becton Dickinson Franklin Lakes, NJ) for 30 min on ice, and washed twice in 800 µL of complete RPMI before resuspension in 200 µL complete RPMI with Phosflow™ p38MAPK-PE overnight at 4ºC. Cells were washed twice in complete RPMI and acquired on a FACSVerse for 250,000 gated events

Inhibition of formation of monocyte-derived extracellular vesicles

Fresh human whole blood was preincubated with graded concentrations of inhibitors or vehicle-alone control (DMSO) for 30 min at 37ºC. The inhibitors used were: SP600125 (JNK inhibitor), BAY 11-7085 (irreversible inhibitor of IκBα phosphorylation), IRAK1/4 Inhibitor I, SCP0094 (inhibitor of Group III caspases), cytochalasin D (inhibitor of actin polymerization), SB203580 (inhibitor of p38 MAPK and MAPKAP kinase-2), A740003 (competitive P2X7 receptor antagonist), VX-765 (inhibitor of caspase-1 and -4), Glybenclamide (NLRP3 inflammasome

inhibitor), VAD-FMK (pan-caspase inhibitor), BX795 (inhibitor of TBK1/IKKε phosphorylation), and gefitinib (EGFR tyrosine kinase inhibitor). Then dual TLR7/8 agonists were added to the samples in a volume of 30 µL at a final concentration of 5 µg/mL, and the plates were incubated at 37ºC for 4 h. ECV formation was measured by flow cytometry as described above.

Transmission electron microscopy for ECVs

The ECVs were separated from intact cells by gentle agitation of the culture tubes followed by low speed centrifugation at 300 g. The supernatants were pelleted at 20,000 g in complete RPMI containing 15 mM $CaCl_2$, and washed three times with the same medium. ECV samples were used either undiluted, diluted 1:10, or 1:100 in PBS. 30 µL droplets of ECV suspensions were placed on a piece of Parafilm M® in a glass Petri dish containing pre-moistened filter paper. Formvar/Carbon on 200 Mesh copper grids (Electron Microscopy Sciences, Hatfield, PA) were placed on the ECV drops for 30 min, rinsed three times with PBS, and fixed in 2% glutaraldehyde in PBS for 10 min. The grids were rinsed with ultrapure water (NANOpure Infinity®; Barnstead/ThermoFisher Scientific; Waltham, Maryland), stained with 30 µL of 1% phosphotungstic acid (pH 7) for 10 min, then blotted dry on filter paper. Samples were examined with an FEI Philips CM 12 transmission electron microscope operating at 60 kV. Images were recorded with a Maxim DL digital capture system.

Isolation of ECVs and evaluation of antigen packing

Plasma was decomplemented in a water bath at 56ºC for 1 h and clarified by centrifugation. PBMCs were isolated using CPT™ tubes and cultured in 5 mL tubes with RPMI supplemented with 15% decomplemented, autologous plasma. Protein antigen, either 54.1 kDa Zika virus

antigen, or CRM197 were added to PBMCs at 100 µg/mL. ECVs were generated using a fixed concentration of compound **4** at 5 µg/mL (determined to be optimal in dose-response experiments) for 16 h. The ECVs were separated from intact cells by gentle agitation of the culture tubes followed by low speed centrifugation at 300 g. The supernatants were pelleted at 20,000 g in complete RPMI containing 15 mM CaCl$_2$, and washed three times with the same medium. ECVs were lysed by resuspension in 25 µL 1N NaOH with sonication for 15 minutes, and the pH was neutralized by the addition of 25 µL 1N HCl and 25 µL of RIPA buffer. The antigen packed within the ECVs was evaluated using Wes 12-230 kDa anti-rabbit kit (Protein Simple, San Jose, CA., catalog number SM-W004-1). Primary antibody was 1:5000 rabbit polyclonal immune sera generated to the specific antigen as mentioned above. Control antigen was treated in an identical manner to the ECV lysis to ensure protein integrity.

Induction of recall responses with ECV

PBMCs were cultured overnight as mentioned above with the antigen CMV pp65 at 100 µg/mL and compound **4** at 5 µg/mL, and the ECVs were isolated and washed as mentioned above. Following the final wash, the ECVs were resuspended in 100 µL RPMI supplemented with 15% decomplemented autologous plasma, and transferred to a 5 mL tube of either autologous PBMCs or autologous, autoMACS pro (Miltenyi Biotec, Bergisch Gladbach, Germany, Catalog number 130-050-101) isolated CD3$^+$ T cells. ECVs generated in the absence of CMV pp65, compound **4** alone, and CD3/28 Dynabeads™ (Gibco, Gaithersburg, MD., catalog number 11161D) were used as controls. Stimulated cells were incubated for 2 h at 37ºC, followed by the addition of 10 µg/mL Brefeldin A (Sigma Aldrich, St. Louis, MO) and 12 additional hours of incubation. Cells were then stained with CD4-V450 and CD8-V500 for 30 min at 4ºC. Samples were fixed and permeabilized using Cytofix/Cytoperm kits (Becton Dickinson, Franklin Lakes, NJ). Fixed samples were stained

overnight in perm/wash buffer (supplied with Cytofix/Cytoperm kit) with anti-IL2-FITC and anti-IFN-γ-PE. Samples were washed 3 times in perm/wash buffer then resuspended in complete RPMI. Samples were acquired on a FACSVerse for 3,000,000 events. CD4^{+} Th and CD8^{+} CTLs were evaluated for dual functional IL-2 and IFN-γ positive cells.

Tyramide signal amplification

PBMCs were co-cultured with ECVs loaded with CMV pp65 for 12 h. Following the incubation, cells were stained with CD14-BV421 and permeabilized as mentioned above with Cytofix/Cytoperm kits. Each sample was blocked with 10% goat serum in PBS (recommended blocking buffer for the Tyramide Superboost kit, described below) for 1 h at room temperature. Anti-CMV pp65 antibody (Abcam, Cambridge, UK., Catalog number ab53489) was utilized at 1:100 dilutions in 100 μL blocking buffer to stain cells for 1 h at room temperature, followed by 1 h of incubation with goat-anti-rabbit-HRP antibody conjugate. Tyramide signal amplification was carried out for 5 min according to the Tyramide SuperBoost kit's manufacturer (Invitrogen, Carlsbad, CA., Catalog number B40922). Samples were acquired on a FACSVerse for 250,000 gated samples. CD14^{+} Monocytes were evaluated for uptake of ECVs loaded with CMV pp65 and soluble CMV pp65.

References

1.   Brubaker, S. W.; Bonham, K. S.; Zanoni, I.; Kagan, J. C., Innate Immune Pattern Recognition: A Cell Biological Perspective. *Annu. Rev. Immunol.* **2015,** *33*, 257-290.

2.   Takeda, K.; Kaisho, T.; Akira, S., Toll-like Receptors. *Annu. Rev. Immunol.* **2003,** *21*, 335-376.

3.   Takeuchi, O.; Kawai, T.; Sanjo, H.; Copeland, N. G.; Gilbert, D. J.; Jenkins, N. A.; Takeda, K.; Akira, S., TLR6: A Novel Member Of An Expanding Toll-Like Receptor Family. *Gene.* **1999,** *231* (1-2), 59-65.

4.   Buwitt-Beckmann, U.; Heine, H.; Wiesmuller, K. H.; Jung, G.; Brock, R.; Akira, S.; Ulmer, A. J., Toll-Like Receptor 6-Independent Signaling By Diacylated Lipopeptides. *Eur. J. Immunol.* **2005,** *35* (1), 282-289.

5.   Triantafilou, M.; Gamper, F. G.; Haston, R. M.; Mouratis, M. A.; Morath, S.; Hartung, T.; Triantafilou, K., Membrane Sorting Of Toll-Like Receptor (TLR)-2/6 And TLR2/1 Heterodimers At The Cell Surface Determines Heterotypic Associations With CD36 And Intracellular Targeting. *J. Biol. Chem.* **2006,** *281* (41), 31002-310011.

6.   Horng, T.; Barton, G. M.; Flavell, R. A.; Medzhitov, R., The Adaptor Molecule TIRAP Provides Signalling Specificity For Toll-Like Receptors. *Nature.* **2002,** *420* (6913), 329-333.

7.   Yamamoto, M.; Sato, S.; Hemmi, H.; Sanjo, H.; Uematsu, S.; Kaisho, T.; Hoshino, K.; Takeuchi, O.; Kobayashi, M.; Fujita, T.; Takeda, K.; Akira, S., Essential Role For TIRAP In Activation Of The Signalling Cascade Shared By TLR2 And TLR4. *Nature.* **2002,** *420* (6913), 324-329.

8.   Kang, J. Y.; Nan, X.; Jin, M. S.; Youn, S. J.; Ryu, Y. H.; Mah, S.; Han, S. H.; Lee, H.; Paik, S. G.; Lee, J. O., Recognition Of Lipopeptide Patterns By Toll-Like Receptor 2-Toll-Like Receptor 6 Heterodimer. *Immunity.* **2009,** *31* (6), 873-884.

9.   Hantke, K.; Braun, V., Covalent Binding Of Lipid To Protein. Diglyceride And Amide-Linked Fatty Acid At The N-Terminal End Of The Murein-Lipoprotein Of The *Escherichia coli* Outer Membrane. *Eur. J. Biochem.* **1973,** *34* (2), 284-296.

10.   Takeuchi, O.; Sato, S.; Horiuchi, T.; Hoshino, K.; Takeda, K.; Dong, Z.; Modlin, R. L.; Akira, S., Cutting Edge: Role Of Toll-Like Receptor 1 In Mediating Immune Response To Microbial Lipoproteins. *J. Immunol.* **2002,** *169* (1), 10-14.

11.   Dillon, S.; Agrawal, A.; Van Dyke, T.; Landreth, G.; McCauley, L.; Koh, A.; Maliszewski, C.; Akira, S.; Pulendran, B., A Toll-Like Receptor 2 Ligand Stimulates Th2 Responses In Vivo, Via Induction Of Extracellular Signal-Regulated Kinase Mitogen-Activated Protein Kinase And C-Fos In Dendritic Cells. *J. Immunol.* **2004,** *172* (8), 4733-4743.

12.   Halliday, A.; Turner, J. D.; Guimaraes, A.; Bates, P. A.; Taylor, M. J., The TLR2/6 Ligand PAM2CSK4 Is A Th2 Polarizing Adjuvant In *Leishmania major* And *Brugia malayi* Murine Vaccine Models. *Parasit. Vectors.* **2016,** *9*, 96. doi: 10.1186/s13071-016-1381-0.

13.   Pulendran, B.; Kumar, P.; Cutler, C. W.; Mohamadzadeh, M.; Van Dyke, T.; Banchereau, J., Lipopolysaccharides From Distinct Pathogens Induce Different Classes Of Immune Responses In Vivo. *J. Immunol.* **2001,** *167* (9), 5067-5076.

14.   Gautier, G.; Humbert, M.; Deauvieau, F.; Scuiller, M.; Hiscott, J.; Bates, E. E.; Trinchieri, G.; Caux, C.; Garrone, P., A Type I Interferon Autocrine-Paracrine Loop Is Involved In Toll-Like Receptor-Induced Interleukin-12p70 Secretion By Dendritic Cells. *J. Exp. Med.* **2005,** *201* (9), 1435-1446.

15.   Zhu, X.; Ramos, T. V.; Gras-Masse, H.; Kaplan, B. E.; BenMohamed, L., Lipopeptide Epitopes Extended By An Nepsilon-Palmitoyl-Lysine Moiety Increase Uptake And Maturation Of Dendritic Cells Through A Toll-Like Receptor-2 Pathway And Trigger A Th1-Dependent Protective Immunity. *Eur. J. Immunol.* **2004,** *34* (11), 3102-3114.

16.   Agrawal, S.; Agrawal, A.; Doughty, B.; Gerwitz, A.; Blenis, J.; Van Dyke, T.; Pulendran, B., Cutting Edge: Different Toll-Like Receptor Agonists Instruct Dendritic Cells To Induce Distinct Th Responses Via Differential Modulation Of Extracellular Signal-Regulated Kinase-Mitogen-Activated Protein Kinase And C-Fos. *J. Immunol.* **2003,** *171* (10), 4984-4989.

17.   Korsholm, K. S.; Petersen, R. V.; Agger, E. M.; Andersen, P., T-Helper 1 And T-Helper 2 Adjuvants Induce Distinct Differences In The Magnitude, Quality And Kinetics Of The Early Inflammatory Response At The Site Of Injection. *Immunology.* **2010,** *129* (1), 75-86.

18.   Thoma-Uszynski, S.; Kiertscher, S. M.; Ochoa, M. T.; Bouis, D. A.; Norgard, M. V.; Miyake, K.; Godowski, P. J.; Roth, M. D.; Modlin, R. L., Activation Of Toll-Like Receptor 2 On Human Dendritic Cells Triggers Induction Of IL-12, But Not IL-10. *J. Immunol.* **2000,** *165* (7), 3804-3810.

19.   Du, X.; Poltorak, A.; Wei, Y.; Beutler, B., Three Novel Mammalian Toll-Like Receptors: Gene Structure, Expression, And Evolution. *Eur. Cytokine Netw*. **2000,** *11* (3), 362-371.

20.   Chuang, T. H.; Ulevitch, R. J., Cloning And Characterization Of A Sub-Family Of Human Toll-Like Receptors: hTLR7, hTLR8 And hTLR9. *Eur. Cytokine Netw*. **2000,** *11* (3), 372-378.

21.   Baumann, C. L.; Aspalter, I. M.; Sharif, O.; Pichlmair, A.; Bluml, S.; Grebien, F.; Bruckner, M.; Pasierbek, P.; Aumayr, K.; Planyavsky, M.; Bennett, K. L.; Colinge, J.; Knapp, S.;

Superti-Furga, G., CD14 Is A Coreceptor Of Toll-Like Receptors 7 And 9. *J. Exp. Med.* **2010,** *207* (12), 2689-2701.

22.   Tomai, M. A.; Gibson, S. J.; Imbertson, L. M.; Miller, R. L.; Myhre, P. E.; Reiter, M. J.; Wagner, T. L.; Tamulinas, C. B.; Beaurline, J. M.; Gerster, J. F.; et al., Immunomodulating And Antiviral Activities Of The Imidazoquinoline S-28463. *Antiviral Res.* **1995,** *28* (3), 253-264.

23.   Kokatla, H. P.; Yoo, E.; Salunke, D. B.; Sil, D.; Ng, C. F.; Balakrishna, R.; Malladi, S. S.; Fox, L. M.; David, S. A., Toll-Like Receptor-8 Agonistic Activities In C2, C4, And C8 Modified Thiazolo[4,5-*c*]Quinolines. *Org. Biomol. Chem.* **2013,** *11* (7), 1179-1198.

24.   Beesu, M.; Caruso, G.; Salyer, A. C.; Khetani, K. K.; Sil, D.; Weerasinghe, M.; Tanji, H.; Ohto, U.; Shimizu, T.; David, S. A., Structure-Based Design Of Human TLR8-Specific Agonists With Augmented Potency And Adjuvanticity. *J. Med. Chem.* **2015,** *58* (19), 7833-7849.

25.   Kokatla, H. P.; Sil, D.; Malladi, S. S.; Balakrishna, R.; Hermanson, A. R.; Fox, L. M.; Wang, X.; Dixit, A.; David, S. A., Exquisite Selectivity For Human Toll-Like Receptor 8 In Substituted Furo[2,3-*c*]Quinolines. *J. Med. Chem.* **2013,** *56* (17), 6871-6885.

26.   Kokatla, H. P.; Sil, D.; Tanji, H.; Ohto, U.; Malladi, S. S.; Fox, L. M.; Shimizu, T.; David, S. A., Structure-Based Design Of Novel Human Toll-Like Receptor 8 Agonists. *ChemMedChem.* **2014,** *9* (4), 719-723.

27.   Shukla, N. M.; Malladi, S. S.; Mutz, C. A.; Balakrishna, R.; David, S. A., Structure-Activity Relationships In Human Toll-Like Receptor 7-Active Imidazoquinoline Analogues. *J. Med. Chem.* **2010,** *53* (11), 4450-4465.

28.   Yoo, E.; Crall, B. M.; Balakrishna, R.; Malladi, S. S.; Fox, L. M.; Hermanson, A. R.; David, S. A., Structure-Activity Relationships In Toll-Like Receptor 7 Agonistic 1*H*-Imidazo[4,5-*c*]Pyridines. *Org. Biomol. Chem.* **2013,** *11* (38), 6526-6545.

29.   Shukla, N. M.; Mutz, C. A.; Malladi, S. S.; Warshakoon, H. J.; Balakrishna, R.; David, S. A., Toll-Like Receptor (TLR)-7 And -8 Modulatory Activities Of Dimeric Imidazoquinolines. *J. Med. Chem.* **2012,** *55* (3), 1106-1116.

30.   Honda, K.; Taniguchi, T., IRFs: Master Regulators Of Signalling By Toll-Like Receptors And Cytosolic Pattern-Recognition Receptors. *Nat. Rev. Immunol.* **2006,** *6* (9), 644-658.

31.   Yarilina, A.; Park-Min, K. H.; Antoniv, T.; Hu, X.; Ivashkiv, L. B., TNF Activates An IRF1-Dependent Autocrine Loop Leading To Sustained Expression Of Chemokines And STAT1-Dependent Type I Interferon-Response Genes. *Nat. Immunol.* **2008,** *9* (4), 378-387.

32.   Krieg, M. A., Therapeutic Potential Of Toll-Like Receptor 9 Activation. *Nat. Rev.* **2006,** *5* (6), 471-484.

33.   Vollmer, J.; Weeratna, R.; Payette, P.; Jurk, M.; Schetter, C.; Laucht, M.; Wader, T.; Tluk, S.; Liu, M.; Davis, H. L.; Krieg, A. M., Characterization Of Three CpG Oligodeoxynucleotide Classes With Distinct Immunostimulatory Activities. *Eur. J. Immunol.* **2004,** *34* (1), 251-262.

34.   Hartmann, G.; Weeratna, R. D.; Ballas, Z. K.; Payette, P.; Blackwell, S.; Suparto, I.; Rasmussen, W. L.; Waldschmidt, M.; Sajuthi, D.; Purcell, R. H.; Davis, H. L.; Krieg, A. M., Delineation Of A CpG Phosphorothioate Oligodeoxynucleotide For Activating Primate Immune Responses In Vitro And In Vivo. *J. Immunol.* **2000,** *164* (3), 1617-1624.

35.   Ballas, Z. K.; Rasmussen, W. L.; Krieg, A. M., Induction Of NK Activity In Murine And Human Cells By CpG Motifs In Oligodeoxynucleotides And Bacterial DNA. *J. Immunol.* **1996,** *157* (5), 1840-1845.

36.   Rissoan, M. C.; Soumelis, V.; Kadowaki, N.; Grouard, G.; Briere, F.; de Waal Malefyt, R.; Liu, Y. J., Reciprocal Control Of T Helper Cell And Dendritic Cell Differentiation. *Science.* **1999,** *283* (5405), 1183-1186.

37.   Liu, Y. J.; Kanzler, H.; Soumelis, V.; Gilliet, M., Dendritic Cell Lineage, Plasticity And Cross-Regulation. *Nat. Immunol.* **2001,** *2* (7), 585-589.

38.   Krug, A.; Towarowski, A.; Britsch, S.; Rothenfusser, S.; Hornung, V.; Bals, R.; Giese, T.; Engelmann, H.; Endres, S.; Krieg, A. M.; Hartmann, G., Toll-Like Receptor Expression Reveals CpG DNA As A Unique Microbial Stimulus For Plasmacytoid Dendritic Cells Which Synergizes With CD40 Ligand To Induce High Amounts Of IL-12. *Eur. J. Immunol.* **2001,** *31* (10), 3026-3037.

39.   Beesu, M.; Salyer, A. C.; Brush, M. J.; Trautman, K. L.; Hill, J. K.; David, S. A., Identification of High-Potency Human TLR8 and Dual TLR7/TLR8 Agonists in Pyrimidine-2,4-diamines. *J. Med. Chem.* **2017,** *60* (5), 2084-2098.

40.   Souza-Fonseca-Guimaraes, F.; Parlato, M.; Philippart, F.; Misset, B.; Cavaillon, J. M.; Adib-Conquy, M.; Captain study, g., Toll-Like Receptors Expression And Interferon-Gamma Production By NK Cells In Human Sepsis. *Crit. Care.* **2012,** *16* (5), R206. doi: 10.1186/cc11838.

41.   Sivori, S.; Carlomagno, S.; Pesce, S.; Moretta, A.; Vitale, M.; Marcenaro, E., TLR/NCR/KIR: Which One To Use And When? *Front. Immunol.* **2014,** *5*, 105. doi: 10.3389/fimmu.2014.00105.

42.   Bekeredjian-Ding, I.; Jego, G., Toll-Like Receptors--Sentries In The B-Cell Response. *Immunology.* **2009,** *128* (3), 311-323.

43.   Hammond, T.; Lee, S.; Watson, M. W.; Flexman, J. P.; Cheng, W.; Fernandez, S.; Price, P., Toll-Like Receptor (TLR) Expression On CD4+ And CD8+ T-Cells In Patients Chronically Infected With Hepatitis C Virus. *Cell. Immunol.* **2010,** *264* (2), 150-155.

44.   McClure, R.; Massari, P., TLR-Dependent Human Mucosal Epithelial Cell Responses To Microbial Pathogens. *Front. Immunol.* **2014,** *5*, 386. doi: 10.3389/fimmu.2014.00386.

45.   Sha, Q.; Truong-Tran, A. Q.; Plitt, J. R.; Beck, L. A.; Schleimer, R. P., Activation Of Airway Epithelial Cells By Toll-Like Receptor Agonists. *Am. J. Respir. Cell. Mol. Biol.* **2004,** *31* (3), 358-364.

46.   Dong, Z.; Yang, Z.; Wang, C., Expression Of TLR2 And TLR4 Messenger RNA In The Epithelial Cells Of The Nasal Airway. *Am. J. Rhinol.* **2005,** *19* (3), 236-239.

47.   Bautista, M. V.; Chen, Y.; Ivanova, V. S.; Rahimi, M. K.; Watson, A. M.; Rose, M. C., IL-8 Regulates Mucin Gene Expression At The Posttranscriptional Level In Lung Epithelial Cells. *J. Immunol.* **2009,** *183* (3), 2159-2166.

48.   Ryu, J. H.; Yoo, J. Y.; Kim, M. J.; Hwang, S. G.; Ahn, K. C.; Ryu, J. C.; Choi, M. K.; Joo, J. H.; Kim, C. H.; Lee, S. N.; Lee, W. J.; Kim, J.; Shin, D. M.; Kweon, M. N.; Bae, Y. S.; Yoon, J. H., Distinct TLR-Mediated Pathways Regulate House Dust Mite-Induced Allergic Disease In The Upper And Lower Airways. *J. Allergy Clin. Immunol.* **2013,** *131* (2), 549-561.

49.   Ohkuni, T.; Kojima, T.; Ogasawara, N.; Masaki, T.; Fuchimoto, J.; Kamekura, R.; Koizumi, J.; Ichimiya, S.; Murata, M.; Tanaka, S.; Himi, T.; Sawada, N., Poly(I:C) Reduces Expression Of JAM-A And Induces Secretion Of IL-8 And TNF-Alpha Via Distinct NF-κB Pathways In Human Nasal Epithelial Cells. *Toxicol. Appl. Pharmacol.* **2011,** *250* (1), 29-38.

50.   Wu, C. A.; Peluso, J. J.; Zhu, L.; Lingenheld, E. G.; Walker, S. T.; Puddington, L., Bronchial Epithelial Cells Produce IL-5: Implications For Local Immune Responses In The Airways. *Cell. Immunol.* **2010,** *264* (1), 32-41.

51.   MacRedmond, R. E.; Greene, C. M.; Dorscheid, D. R.; McElvaney, N. G.; O'Neill, S. J., Epithelial Expression Of TLR4 Is Modulated In COPD And By Steroids, Salmeterol And Cigarette Smoke. *Respir. Res.* **2007,** *8*, 84.

52.   Andre, F. E.; Booy, R.; Bock, H. L.; Clemens, J.; Datta, S. K.; John, T. J.; Lee, B. W.; Lolekha, S.; Peltola, H.; Ruff, T. A.; Santosham, M.; Schmitt, H. J., Vaccination Greatly Reduces Disease, Disability, Death And Inequity Worldwide. *Bull. World Health Organ.* **2008,** *86* (2), 140-146.

53.   Levine, M. M.; Robins-Browne, R., Vaccines, Global Health And Social Equity. *Immunol. Cell. Biol.* **2009,** *87* (4), 274-278.

54.   Fine, P. E., Herd Immunity: History, Theory, Practice. *Epidemiol. Rev.* **1993,** *15* (2), 265-302.

55.   Noh, J. Y.; Kim, W. J., Influenza Vaccines: Unmet Needs And Recent Developments. *Infect. Chemother.* **2013,** *45* (4), 375-386.

56.   Leroux-Roels, G., Unmet Needs In Modern Vaccinology: Adjuvants To Improve The Immune Response. *Vaccine.* **2010,** *28. doi: 10.1016/j.vaccine.2010.07.021.*

57.   Bandyopadhyay, A. S.; Garon, J.; Seib, K.; Orenstein, W. A., Polio Vaccination: Past, Present And Future. *Future. Microbiol.* **2015,** *10* (5), 791-808.

58.   Sabin, A. B., Oral Poliovirus Vaccine: History Of Its Development And Use And Current Challenge To Eliminate Poliomyelitis From The World. *J. Infect. Dis.* **1985,** *151* (3), 420-436.

59.   Minor, P., Vaccine-Derived Poliovirus (VDPV): Impact On Poliomyelitis Eradication. *Vaccine.* **2009,** *27* (20), 2649-2652.

60.   Platt, L. R.; Estivariz, C. F.; Sutter, R. W., Vaccine-Associated Paralytic Poliomyelitis: A Review Of The Epidemiology And Estimation Of The Global Burden. *J. Infect. Dis.* **2014,** *210* *doi: 10.1093/infdis/jiu184.*

61.   Laassri, M.; Lottenbach, K.; Belshe, R.; Wolff, M.; Rennels, M.; Plotkin, S.; Chumakov, K., Effect Of Different Vaccination Schedules On Excretion Of Oral Poliovirus Vaccine Strains. *J. Infect. Dis.* **2005,** *192* (12), 2092-2098.

62.   Moyle, P. M.; Toth, I., Modern Subunit Vaccines: Development, Components, And Research Opportunities. *ChemMedChem.* **2013,** *8* (3), 360-376.

63.   Reed, S. G.; Orr, M. T.; Fox, C. B., Key Roles Of Adjuvants In Modern Vaccines. *Nat. Med.* **2013,** *19* (12), 1597-608.

64.   Janeway, C. A., Jr., Approaching The Asymptote? Evolution And Revolution In Immunology. *Cold Spring Harb. Symp. Quant. Biol.* **1989,** *54 Pt 1*, 1-13.

65.   Glenny, A. T., Buttle G. A. H., Stevens, M. F. , Rate Of Disappearance Of Diphtheria Toxoid Injected Into Rabbits And Guinea-Pigs: Toxoid Precipitated With Alum. *J. Pathol.* **1931,** *34* (2), 267-275.

66.   De Gregorio, E.; Tritto, E.; Rappuoli, R., Alum Adjuvanticity: Unraveling A Century Old Mystery. *Eur. J. Immunol.* **2008,** *38* (8), 2068-2071.

67.   Martinon, F.; Petrilli, V.; Mayor, A.; Tardivel, A.; Tschopp, J., Gout-Associated Uric Acid Crystals Activate The NALP3 Inflammasome. *Nature.* **2006,** *440* (7081), 237-241.

68.   Kool, M.; Soullie, T.; van Nimwegen, M.; Willart, M. A.; Muskens, F.; Jung, S.; Hoogsteden, H. C.; Hammad, H.; Lambrecht, B. N., Alum Adjuvant Boosts Adaptive Immunity

By Inducing Uric Acid And Activating Inflammatory Dendritic Cells. *J. Exp. Med.* **2008,** *205* (4), 869-882.

69.   Wang, H. B.; Weller, P. F., Pivotal Advance: Eosinophils Mediate Early Alum Adjuvant-Elicited B Cell Priming And IgM Production. *J. Leukoc. Biol.* **2008,** *83* (4), 817-821.

70.   Lindblad, E. B., Aluminium Compounds For Use In Vaccines. *Immunol. Cell Biol.* **2004,** *82* (5), 497-505.

71.   Warfel, J. M.; Zimmerman, L. I.; Merkel, T. J., Acellular Pertussis Vaccines Protect Against Disease But Fail To Prevent Infection And Transmission In A Nonhuman Primate Model. *Proc. Natl. Acad. Sci. U.S.A.* **2014,** *111* (2), 787-792.

72.   Descamps, D.; Hardt, K.; Spiessens, B.; Izurieta, P.; Verstraeten, T.; Breuer, T.; Dubin, G., Safety Of Human Papillomavirus (HPV)-16/18 AS04-Adjuvanted Vaccine For Cervical Cancer Prevention: A Pooled Analysis Of 11 Clinical Trials. *Hum. Vaccin.* **2009,** *5* (5), 332-340.

73.   Garcon, N.; Wettendorff, M.; Van Mechelen, M., Role Of AS04 In Human Papillomavirus Vaccine: Mode Of Action And Clinical Profile. *Expert. Opin. Biol. Ther.* **2011,** *11* (5), 667-677.

74.   Didierlaurent, A. M.; Morel, S.; Lockman, L.; Giannini, S. L.; Bisteau, M.; Carlsen, H.; Kielland, A.; Vosters, O.; Vanderheyde, N.; Schiavetti, F.; Larocque, D.; Van Mechelen, M.; Garcon, N., AS04, An Aluminum Salt- And TLR4 Agonist-Based Adjuvant System, Induces A Transient Localized Innate Immune Response Leading To Enhanced Adaptive Immunity. *J. Immunol.* **2009,** *183* (10), 6186-6197.

75.   Dupuis, M.; McDonald, D. M.; Ott, G., Distribution Of Adjuvant MF59 And Antigen gD2 After Intramuscular Injection In Mice. *Vaccine.* **1999,** *18* (5-6), 434-439.

76.   Marrack, P.; McKee, A. S.; Munks, M. W., Towards An Understanding Of The Adjuvant Action Of Aluminium. *Nat. Rev. Immunol.* **2009,** *9* (4), 287-293.

77.   Seubert, A.; Calabro, S.; Santini, L.; Galli, B.; Genovese, A.; Valentini, S.; Aprea, S.; Colaprico, A.; D'Oro, U.; Giuliani, M. M.; Pallaoro, M.; Pizza, M.; O'Hagan, D. T.; Wack, A.; Rappuoli, R.; De Gregorio, E., Adjuvanticity Of The Oil-In-Water Emulsion MF59 Is Independent Of NLRP3 Inflammasome But Requires The Adaptor Protein Myd88. *Proc. Natl. Acad. Sci. U.S.A.* **2011,** *108* (27), 11169-11174.

78.   Calabro, S.; Tortoli, M.; Baudner, B. C.; Pacitto, A.; Cortese, M.; O'Hagan, D. T.; De Gregorio, E.; Seubert, A.; Wack, A., Vaccine Adjuvants Alum And MF59 Induce Rapid Recruitment Of Neutrophils And Monocytes That Participate In Antigen Transport To Draining Lymph Nodes. *Vaccine.* **2011,** *29* (9), 1812-1823.

79.   Morel, S.; Didierlaurent, A.; Bourguignon, P.; Delhaye, S.; Baras, B.; Jacob, V.; Planty, C.; Elouahabi, A.; Harvengt, P.; Carlsen, H.; Kielland, A.; Chomez, P.; Garcon, N.; Van Mechelen, M., Adjuvant System AS03 Containing Alpha-Tocopherol Modulates Innate Immune Response And Leads To Improved Adaptive Immunity. *Vaccine.* **2011,** *29* (13), 2461-2473.

80.   Dowling, J. K.; Mansell, A., Toll-Like Receptors: The Swiss Army Knife Of Immunity And Vaccine Development. *Clin. Transl. Immunology.* **2016,** *5* (5), doi: 10.1038/cti.2016.22.

81.   Levine, M. M.; Robins-Browne, R., Vaccines, Global Health And Social Equity. *Immunol. Cell Biol.* **2009,** *87* (4), 274-278.

82.   Grant, J. P., The Children's Vaccine Initiative...And Other Promises To Keep. *J. Trop. Pediatr.* **1991,** *37* (6), 272-274.

83.   Robbins, A., The Children's Vaccine Initiative. *Am. J. Dis. Child.* **1993,** *147* (2), 152-153.

84.   Birmingham, K., The Sun Sets On The CVI. Children's Vaccine Initiative. *Nat. Med.* **1999,** *5* (5), 469-470.

85.   Hajj Hussein, I.; Chams, N.; Chams, S.; El Sayegh, S.; Badran, R.; Raad, M.; Gerges-Geagea, A.; Leone, A.; Jurjus, A., Vaccines Through Centuries: Major Cornerstones of Global Health. *Front. Public Health.* **2015,** *3*, 269 doi: 10.3389/fpubh.2015.00269.

86.   Plotkin, S. A., Vaccines: The Fourth Century. *Clin.Vaccine Immunol.* **2009,** *16* (12), 1709-1719.

87.   Salunke, D. B.; Shukla, N. M.; Yoo, E.; Crall, B. M.; Balakrishna, R.; Malladi, S. S.; David, S. A., Structure-Activity Relationships In Human Toll-Like Receptor 2-Specific Monoacyl Lipopeptides. *J. Med. Chem.* **2012,** *55* (7), 3353-3363.

88.   Salunke, D. B.; Connelly, S. W.; Shukla, N. M.; Hermanson, A. R.; Fox, L. M.; David, S. A., Design And Development Of Stable, Water-Soluble, Human Toll-Like Receptor 2 Specific Monoacyl Lipopeptides As Candidate Vaccine Adjuvants. *J. Med. Chem.* **2013,** *56* (14), 5885-5900.

89.   Wu, W.; Li, R.; Malladi, S. S.; Warshakoon, H. J.; Kimbrell, M. R.; Amolins, M. W.; Ukani, R.; Datta, A.; David, S. A., Structure-Activity Relationships In Toll-Like Receptor-2 Agonistic Diacylthioglycerol Lipopeptides. *J. Med. Chem.* **2010,** *53* (8), 3198-3213.

90.   Shukla, N. M.; Kimbrell, M. R.; Malladi, S. S.; David, S. A., Regioisomerism-Dependent TLR7 Agonism And Antagonism In An Imidazoquinoline. *Bioorg. Med. Chem. Lett.* **2009,** *19* (8), 2211-2214.

91.   Shukla, N. M.; Malladi, S. S.; Mutz, C. A.; Balakrishna, R.; David, S. A., Structure-Activity Relationships In Human Toll-Like Receptor 7-Active Imidazoquinoline Analogues. *J. Med. Chem.* **2010,** *53* (11), 4450-4465.

92.   Shukla, N. M.; Mutz, C. A.; Ukani, R.; Warshakoon, H. J.; Moore, D. S.; David, S. A., Syntheses Of Fluorescent Imidazoquinoline Conjugates As Probes Of Toll-Like Receptor 7. *Bioorg. Med. Chem. Lett.* **2010,** *20* (22), 6384-6386.

93.   Shukla, N. M.; Lewis, T. C.; Day, T. P.; Mutz, C. A.; Ukani, R.; Hamilton, C. D.; Balakrishna, R.; David, S. A., Toward Self-Adjuvanting Subunit Vaccines: Model Peptide And Protein Antigens Incorporating Covalently Bound Toll-Like Receptor-7 Agonistic Imidazoquinolines. *Bioorg. Med. Chem. Lett.* **2011,** *21* (11), 3232-3236.

94.   Shukla, N. M.; Malladi, S. S.; Day, V.; David, S. A., Preliminary Evaluation Of A 3*H* Imidazoquinoline Library As Dual TLR7/TLR8 Antagonists. *Bioorg. Med. Chem.* **2011,** *19* (12), 3801-3811.

95.   Shukla, N. M.; Mutz, C. A.; Malladi, S. S.; Warshakoon, H. J.; Balakrishna, R.; David, S. A., Toll-Like Receptor (TLR)-7 And -8 Modulatory Activities Of Dimeric Imidazoquinolines. *J. Med. Chem.* **2012,** *55* (3), 1106-1116.

96.   Shukla, N. M.; Salunke, D. B.; Balakrishna, R.; Mutz, C. A.; Malladi, S. S.; David, S. A., Potent Adjuvanticity Of A Pure TLR7-Agonistic Imidazoquinoline Dendrimer. *PloS One.* **2012,** *7* (8), doi: 10.1371/journal.pone.0043612.

97.   Yoo, E.; Salunke, D. B.; Sil, D.; Guo, X.; Salyer, A. C.; Hermanson, A. R.; Kumar, M.; Malladi, S. S.; Balakrishna, R.; Thompson, W. H.; Tanji, H.; Ohto, U.; Shimizu, T.; David, S. A., Determinants Of Activity At Human Toll-Like Receptors 7 And 8: Quantitative Structure-Activity Relationship (QSAR) Of Diverse Heterocyclic Scaffolds. *J. Med. Chem.* **2014,** *57* (19), 7955-7970.

98.   Salunke, D. B.; Yoo, E.; Shukla, N. M.; Balakrishna, R.; Malladi, S. S.; Serafin, K. J.; Day, V. W.; Wang, X.; David, S. A., Structure-Activity Relationships In Human Toll-Like Receptor 8-Active 2,3-Diamino-Furo[2,3-*c*]Pyridines. *J. Med. Chem.* **2012,** *55* (18), 8137-8151.

99.   Kokatla, H. P.; Yoo, E.; Salunke, D. B.; Sil, D.; Ng, C. F.; Balakrishna, R.; Malladi, S. S.; Fox, L. M.; David, S. A., Toll-Like Receptor-8 Agonistic Activities In C2, C4, And C8 Modified Thiazolo[4,5-*c*]Quinolines. *Org. Biol. Chem.* **2013,** *11* (7), 1179-1198.

100.   Beesu, M.; Malladi, S. S.; Fox, L. M.; Jones, C. D.; Dixit, A.; David, S. A., Human Toll-Like Receptor 8-Selective Agonistic Activities In 1-Alkyl-1*H*-Benzimidazol-2-Amines. *J. Med. Chem.* **2014,** *57* (17), 7325-7341.

101.   Agnihotri, G.; Ukani, R.; Malladi, S. S.; Warshakoon, H. J.; Balakrishna, R.; Wang, X.; David, S. A., Structure-Activity Relationships In Nucleotide Oligomerization Domain 1 (NOD1) Agonistic Gamma-Glutamyldiaminopimelic Acid Derivatives. *J. Med. Chem.* **2011,** *54* (5), 1490-1510.

102.   Ukani, R.; Lewis, T. C.; Day, T. P.; Wu, W.; Malladi, S. S.; Warshakoon, H. J.; David, S. A., Potent Adjuvantic Activity Of A CCR1-Agonistic *Bis*-Quinoline. *Bioorg. Med. Chem. Lett.* **2012,** *22* (1), 293-295.

103.   Miller, R. L.; Gerster, J. F.; Owens, M. L.; Slade, H. B.; Tomai, M. A., Imiquimod Applied Topically: A Novel Immune Response Modifier And New Class Of Drug. *Int. J. Immunopharmacol.* **1999,** *21* (1), 1-14.

104.   Gerster, J. F.; Lindstrom, K. J.; Miller, R. L.; Tomai, M. A.; Birmachu, W.; Bomersine, S. N.; Gibson, S. J.; Imbertson, L. M.; Jacobson, J. R.; Knafla, R. T.; Maye, P. V.; Nikolaides, N.; Oneyemi, F. Y.; Parkhurst, G. J.; Pecore, S. E.; Reiter, M. J.; Scribner, L. S.; Testerman, T. L.; Thompson, N. J.; Wagner, T. L.; Weeks, C. E.; Andre, J. D.; Lagain, D.; Bastard, Y.; Lupu,

M., Synthesis And Structure-Activity-Relationships Of 1*H*-Imidazo[4,5-*c*]Quinolines That Induce Interferon Production. *J. Med. Chem.* **2005,** *48* (10), 3481-3491.

105.   Schiaffo, C. E.; Shi, C.; Xiong, Z.; Olin, M.; Ohlfest, J. R.; Aldrich, C. C.; Ferguson, D. M., Structure-Activity Relationship Analysis Of Imidazoquinolines With Toll-Like Receptors 7 And 8 Selectivity And Enhanced Cytokine Induction. *J. Med. Chem.* **2014,** *57* (2), 339-347.

106.   Roethle, P. A.; McFadden, R. M.; Yang, H.; Hrvatin, P.; Hui, H.; Graupe, M.; Gallagher, B.; Chao, J.; Hesselgesser, J.; Duatschek, P.; Zheng, J.; Lu, B.; Tumas, D. B.; Perry, J.; Halcomb, R. L., Identification And Optimization Of Pteridinone Toll-Like Receptor 7 (TLR7) Agonists For The Oral Treatment Of Viral Hepatitis. *J. Med. Chem.* **2013,** *56* (18), 7324-7333.

107.   Nakamura, T.; Wada, H.; Kurebayashi, H.; McInally, T.; Bonnert, R.; Isobe, Y., Synthesis And Evaluation Of 8-Oxoadenine Derivatives As Potent Toll-Like Receptor 7 Agonists With High Water Solubility. *Bioorg. Med. Chem. Lett.* **2013,** *23* (3), 669-672.

108.   Lan, T.; Dai, M.; Wang, D.; Zhu, F. G.; Kandimalla, E. R.; Agrawal, S., Toll-Like Receptor 7 Selective Synthetic Oligoribonucleotide Agonists: Synthesis And Structure-Activity Relationship Studies. *J. Med. Chem.* **2009,** *52* (21), 6871-6879.

109.   Kurimoto, A.; Hashimoto, K.; Nakamura, T.; Norimura, K.; Ogita, H.; Takaku, H.; Bonnert, R.; McInally, T.; Wada, H.; Isobe, Y., Synthesis And Biological Evaluation Of 8-Oxoadenine Derivatives As Toll-Like Receptor 7 Agonists Introducing The Antedrug Concept. *J. Med. Chem.* **2010,** *53* (7), 2964-2972.

110.   Bazin, H. G.; Li, Y.; Khalaf, J. K.; Mwakwari, S.; Livesay, M. T.; Evans, J. T.; Johnson, D. A., Structural Requirements For TLR7-Selective Signaling By 9-(4-Piperidinylalkyl)-8-Oxoadenine Derivatives. *Bioorg. Med. Chem. Lett.* **2015,** *25* (6), 1318-1323.

111. Yoo, E.; Crall, B. M.; Balakrishna, R.; Malladi, S. S.; Fox, L. M.; Hermanson, A. R.; David, S. A., Structure-Activity Relationships In Toll-Like Receptor 7 Agonistic 1*H*-Imidazo[4,5-*c*]Pyridines. *Org. Biomol. Chem.* **2013**, *11* (38), 6526-6545.

112. Kokatla, H. P.; Sil, D.; Malladi, S. S.; Balakrishna, R.; Hermanson, A. R.; Fox, L. M.; Wang, X.; Dixit, A.; David, S. A., Exquisite Selectivity For Human Toll-Like Receptor 8 In Substituted Furo[2,3-*c*]Quinolines. *J. Med. Chem.* **2013,** *56* (17), 6871-6885.

113. Beesu, M.; Caruso, G.; Salyer, A. C.; Khetani, K. K.; Sil, D.; Weerasinghe, M.; Tanji, H.; Ohto, U.; Shimizu, T.; David, S. A., Structure-Based Design Of Human TLR8-Specific Agonists With Augmented Potency And Adjuvanticity. *J. Med. Chem.* **2015,** *58* (19), 7833-7849.

114. Nour, A.; Hayashi, T.; Chan, M.; Yao, S.; Tawatao, R. I.; Crain, B.; Tsigelny, I. F.; Kouznetsova, V. L.; Ahmadiiveli, A.; Messer, K.; Pu, M.; Corr, M.; Carson, D. A.; Cottam, H. B., Discovery Of Substituted 4-Aminoquinazolines As Selective Toll-Like Receptor 4 Ligands. *Bioorg. Med. Chem. Lett.* **2014,** *24* (21), 4931-4938.

115. Hayashi, T.; Crain, B.; Yao, S.; Caneda, C. D.; Cottam, H. B.; Chan, M.; Corr, M.; Carson, D. A., Novel Synthetic Toll-Like Receptor 4/MD2 Ligands Attenuate Sterile Inflammation. *J. Pharmacol. Exp. Ther.* **2014,** *350* (2), 330-340.

116. Chan, M.; Hayashi, T.; Mathewson, R. D.; Nour, A.; Hayashi, Y.; Yao, S.; Tawatao, R. I.; Crain, B.; Tsigelny, I. F.; Kouznetsova, V. L.; Messer, K.; Pu, M.; Corr, M.; Carson, D. A.; Cottam, H. B., Identification Of Substituted Pyrimido[5,4-*b*]Indoles As Selective Toll-Like Receptor 4 Ligands. *J. Med. Chem.* **2013,** *56* (11), 4206-4223.

117. Goff, P. H.; Hayashi, T.; Martinez-Gil, L.; Corr, M.; Crain, B.; Yao, S.; Cottam, H. B.; Chan, M.; Ramos, I.; Eggink, D.; Heshmati, M.; Krammer, F.; Messer, K.; Pu, M.; Fernandez-Sesma, A.; Palese, P.; Carson, D. A., Synthetic Toll-Like Receptor 4 (TLR4) And TLR7 Ligands

As Influenza Virus Vaccine Adjuvants Induce Rapid, Sustained, And Broadly Protective Responses. *J. Virol.* **2015,** *89* (6), 3221-3235.

118.   Cheng, K.; Gao, M.; Godfroy, J. I.; Brown, P. N.; Kastelowitz, N.; Yin, H., Specific Activation Of The TLR1-TLR2 Heterodimer By Small-Molecule Agonists. *Sci. Adv.* **2015,** *1* (3) pii: e1400139.

119.   Guan, Y.; Omueti-Ayoade, K.; Mutha, S. K.; Hergenrother, P. J.; Tapping, R. I., Identification Of Novel Synthetic Toll-Like Receptor 2 Agonists By High Throughput Screening. *J. Biol. Chem.* **2010,** *285* (31), 23755-23762.

120.   Zhang, J. H.; Chung, T. D.; Oldenburg, K. R., A Simple Statistical Parameter For Use In Evaluation And Validation Of High Throughput Screening Assays. *J. Biomol. Screen.* **1999,** *4* (2), 67-73.

121.   Li, K.; Chen, Z.; Kato, N.; Gale, M., Jr.; Lemon, S. M., Distinct Poly(I:C) And Virus-Activated Signaling Pathways Leading To Interferon-Beta Production In Hepatocytes. *J. Biol. Chem.* **2005,** *280* (17), 16739-16747.

122.   Loo, Y. M.; Gale, M., Jr., Immune Signaling By RIG-I-Like Receptors. *Immunity.* **2011,** *34* (5), 680-692.

123.   Rodriguez, K. R.; Bruns, A. M.; Horvath, C. M., MDA5 And LGP2: Accomplices And Antagonists Of Antiviral Signal Transduction. *J. Virol.* **2014,** *88* (15), 8194-8200.

124.   Jin, M. S.; Kim, S. E.; Heo, J. Y.; Lee, M. E.; Kim, H. M.; Paik, S. G.; Lee, H.; Lee, J. O., Crystal Structure Of The TLR1-TLR2 Heterodimer Induced By Binding Of A Tri-Acylated Lipopeptide. *Cell.* **2007,** *130* (6), 1071-1082.

125.   Irvine, K. L.; Hopkins, L. J.; Gangloff, M.; Bryant, C. E., The Molecular Basis For Recognition Of Bacterial Ligands At Equine TLR2, TLR1 And TLR6. *Vet. Res.* **2013,** *44*, 50. doi: 10.1186/1297-9716-44-50.

126.   Matusiak, M.; Van Opdenbosch, N.; Vande Walle, L.; Sirard, J. C.; Kanneganti, T. D.; Lamkanfi, M., Flagellin-Induced NLRC4 Phosphorylation Primes The Inflammasome For Activation By NAIP5. *Proc. Natl. Acad. Sci. U.S.A.* **2015,** *112* (5), 1541-1546.

127.   Lightfield, K. L.; Persson, J.; Brubaker, S. W.; Witte, C. E.; von Moltke, J.; Dunipace, E. A.; Henry, T.; Sun, Y. H.; Cado, D.; Dietrich, W. F.; Monack, D. M.; Tsolis, R. M.; Vance, R. E., Critical Function For Naip5 In Inflammasome Activation By A Conserved Carboxy-Terminal Domain Of Flagellin. *Nat. Immunol.* **2008,** *9* (10), 1171-1178.

128.   Sau, K.; Mambula, S. S.; Latz, E.; Henneke, P.; Golenbock, D. T.; Levitz, S. M., The Antifungal Drug Amphotericin B Promotes Inflammatory Cytokine Release By A Toll-Like Receptor- And CD14-Dependent Mechanism. *J. Biol. Chem.* **2003,** *278* (39), 37561-37568.

129.   Razonable, R. R.; Henault, M.; Lee, L. N.; Laethem, C.; Johnston, P. A.; Watson, H. L.; Paya, C. V., Secretion Of Proinflammatory Cytokines And Chemokines During Amphotericin B Exposure Is Mediated By Coactivation Of Toll-Like Receptors 1 And 2. *Antimicrob. Agents Chemother.* **2005,** *49* (4), 1617-1621.

130.   Adediran, S. A.; Day, T. P.; Sil, D.; Kimbrell, M. R.; Warshakoon, H. J.; Malladi, S. S.; David, S. A., Synthesis Of A Highly Water-Soluble Derivative Of Amphotericin B With Attenuated Proinflammatory Activity. *Mol. Pharm.* **2009,** *6* (5), 1582-1590.

131.   Gallis, H. A.; Drew, R. H.; Pickard, W. W., Amphotericin B: 30 Years Of Clinical Experience. *Rev. Infect. Dis.* **1990,** *12* (2), 308-329.

132.   Dutcher, J. D., The Discovery And Development Of Amphotericin B. *Dis. Chest.* **1968,** *54:Suppl 1:296-8.*, Suppl-8.

133.   Torrado, J. J.; Espada, R.; Ballesteros, M. P.; Torrado-Santiago, S., Amphotericin B Formulations And Drug Targeting. *J. Pharm. Sci.* **2008,** *97* (7), 2405-2425.

134.   Day, T. P.; Sil, D.; Shukla, N. M.; Anbanandam, A.; Day, V. W.; David, S. A., Imbuing Aqueous Solubility To Amphotericin B And Nystatin With A Vitamin. *Mol. Pharm.* **2011,** *8* (1), 297-301.

135.   Farhat, K.; Riekenberg, S.; Heine, H.; Debarry, J.; Lang, R.; Mages, J.; Buwitt-Beckmann, U.; Roschmann, K.; Jung, G.; Wiesmuller, K. H.; Ulmer, A. J., Heterodimerization Of TLR2 With TLR1 Or TLR6 Expands The Ligand Spectrum But Does Not Lead To Differential Signaling. *J. Leukoc. Biol.* **2008,** *83* (3), 692-701.

136.   Buwitt-Beckmann, U.; Heine, H.; Wiesmuller, K. H.; Jung, G.; Brock, R.; Ulmer, A. J., Lipopeptide Structure Determines TLR2 Dependent Cell Activation Level. *FEBS J.* **2005,** *272* (24), 6354-6364.

137.   Tagliabue, A.; Rappuoli, R., Vaccine Adjuvants: The Dream Becomes Real. *Hum. Vaccin.* **2008,** *4* (5), 347-349.

138.   Esposito, S.; Birlutiu, V.; Jarcuska, P.; Perino, A.; Man, S. C.; Vladareanu, R.; Meric, D.; Dobbelaere, K.; Thomas, F.; Descamps, D., Immunogenicity And Safety Of Human Papillomavirus-16/18 AS04-Adjuvanted Vaccine Administered According To An Alternative Dosing Schedule Compared With The Standard Dosing Schedule In Healthy Women Aged 15 To 25 Years: Results From A Randomized Study. *Pediatr. Infect. Dis. J.* **2011,** *30* (3), e49-e55 doi: 10.1097/INF.0b013e318206c26e.

139.	Garcon, N.; Segal, L.; Tavares, F.; Van Mechelen, M., The Safety Evaluation Of Adjuvants During Vaccine Development: The AS04 Experience. *Vaccine.* **2011,** *29* (27), 4453-4459.

140.	Mata-Haro, V.; Cekic, C.; Martin, M.; Chilton, P. M.; Casella, C. R.; Mitchell, T. C., The Vaccine Adjuvant Monophosphoryl Lipid A As A TRIF-Biased Agonist Of TLR4. *Science.* **2007,** *316* (5831), 1628-1632.

141.	Casella, C. R.; Mitchell, T. C., Putting Endotoxin To Work For Us: Monophosphoryl Lipid A As A Safe And Effective Vaccine Adjuvant. *Cell. Mol. Life Sci.* **2008,** *65* (20), 3231-3240.

142.	Bowen, W. S.; Minns, L. A.; Johnson, D. A.; Mitchell, T. C.; Hutton, M. M.; Evans, J. T., Selective TRIF-Dependent Signaling By A Synthetic Toll-Like Receptor 4 Agonist. *Sci. Signal.* **2012,** *5* (211), ra13. doi: 10.1126/scisignal.2001963.

143.	Khoo, S. H.; Bond, J.; Denning, D. W., Administering Amphotericin B--A Practical Approach. *J. Antimicrob. Chemother.* **1994,** *33* (2), 203-213.

144.	Michie, H. R.; Manogue, K. R.; Spriggs, D. R.; Revhaug, A.; O'Dwyer, S.; Dinarello, C. A.; Cerami, A.; Wolff, S. M.; Wilmore, D. W., Detection Of Circulating Tumor Necrosis Factor After Endotoxin Administration. *N. Engl. J. Med.* **1988,** *318* (23), 1481-1486.

145.	Martich, G. D.; Boujoukos, A. J.; Suffredini, A. F., Response Of Man To Endotoxin. *Immunobiology* **1993,** *187* (3-5), 403-416.

146.	Suffredini, A. F.; Fromm, R. E.; Parker, M. M.; Brenner, M.; Kovacs, J. A.; Wesley, R. A.; Parrillo, J. E., The Cardiovascular Response Of Normal Humans To The Administration Of Endotoxin. *N. Engl. J. Med.* **1989,** *321* (5), 280-287.

147.   Pappenheimer, A. M., Studies On Diphtheria Toxin And Its Reaction With Antitoxin. *J. Bacteriol.* **1942,** *43* (3), 273-289.

148.   Malito, E.; Bursulaya, B.; Chen, C.; Lo, S. P.; Picchianti, M.; Balducci, E.; Biancucci, M.; Brock, A.; Berti, F.; Bottomley, M. J.; Nissum, M.; Costantino, P.; Rappuoli, R.; Spraggon, G., Structural Basis For Lack Of Toxicity Of The Diphtheria Toxin Mutant CRM197. *Proc. Natl. Acad. Sci. U.S.A* **2012,** *109* (14), 5229-5234.

149.   Pappenheimer, A. M., Jr., The Story Of A Toxic Protein, 1888-1992. *Protein Sci.* **1993,** *2* (2), 292-298.

150.   Hood, J. D.; Warshakoon, H. J.; Kimbrell, M. R.; Shukla, N. M.; Malladi, S.; Wang, X.; David, S. A., Immunoprofiling Toll-Like Receptor Ligands: Comparison Of Immunostimulatory And Proinflammatory Profiles In Ex Vivo Human Blood Models. *Hum. Vaccin.* **2010,** *6* (4), 1-14.

151.   He, P.; Zou, Y.; Hu, Z., Advances In Aluminum Hydroxide-Based Adjuvant Research And Its Mechanism. *Hum. Vaccin. Immunother.* **2015,** *11* (2), 477-488.

152.   Gupta, R. K., Aluminum Compounds As Vaccine Adjuvants. *Adv. Drug Deliv. Rev.* **1998,** *32* (3), 155-172.

153.   Khurana, S.; Verma, N.; Yewdell, J. W.; Hilbert, A. K.; Castellino, F.; Lattanzi, M.; Del Giudice, G.; Rappuoli, R.; Golding, H., MF59 Adjuvant Enhances Diversity And Affinity Of Antibody-Mediated Immune Response To Pandemic Influenza Vaccines. *Sci. Transl. Med.* **2011,** *3* (85), 85ra48. doi: 10.1126/scitranslmed.3002336.

154.   El Sahly, H., MF59 As A Vaccine Adjuvant: A Review Of Safety And Immunogenicity. *Expert. Rev. Vaccines.* **2010,** *9* (10), 1135-1141.

155.   Seubert, A.; Monaci, E.; Pizza, M.; O'Hagan, D. T.; Wack, A., The Adjuvants Aluminum Hydroxide And MF59 Induce Monocyte And Granulocyte Chemoattractants And Enhance Monocyte Differentiation Toward Dendritic Cells. *J. Immunol.* **2008,** *180* (8), 5402-5412.

156.   Salunke, D. B.; Connelly, S. W.; Shukla, N. M.; Hermanson, A. R.; Fox, L. M.; David, S. A., Design And Development Of Stable, Water-Soluble, Human Toll-Like Receptor 2 Specific Monoacyl Lipopeptides As Candidate Vaccine Adjuvants. *J. Med. Chem.* **2013**. *56*(14), 5885-5900

157.   Smith, R. S.; Smith, T. J.; Blieden, T. M.; Phipps, R. P., Fibroblasts As Sentinel Cells. Synthesis Of Chemokines And Regulation Of Inflammation. *Am. J. Pathol.* **1997,** *151* (2), 317-322.

158.   Silzle, T.; Randolph, G. J.; Kreutz, M.; Kunz-Schughart, L. A., The Fibroblast: Sentinel Cell And Local Immune Modulator In Tumor Tissue. *Int. J. Cancer.* **2004,** *108* (2), 173-180.

159.   Witowski, J.; Thiel, A.; Dechend, R.; Dunkel, K.; Fouquet, N.; Bender, T. O.; Langrehr, J. M.; Gahl, G. M.; Frei, U.; Jorres, A., Synthesis Of C-X-C And C-C Chemokines By Human Peritoneal Fibroblasts: Induction By Macrophage-Derived Cytokines. *Am. J. Pathol.* **2001,** *158* (4), 1441-1450.

160.   Servais, C.; Erez, N., From Sentinel Cells To Inflammatory Culprits: Cancer-Associated Fibroblasts In Tumour-Related Inflammation. *J. Pathol.* **2013,** *229* (2), 198-207.

161.   Ritchlin, C., Fibroblast Biology. Effector Signals Released By The Synovial Fibroblast In Arthritis. *Arthritis Res.* **2000,** *2* (5), 356-360.

162.   Hosokawa, Y.; Hosokawa, I.; Ozaki, K.; Nakae, H.; Murakami, K.; Miyake, Y.; Matsuo, T., CXCL12 And CXCR4 Expression By Human Gingival Fibroblasts In Periodontal Disease. *Clin. Exp. Immunol.* **2005,** *141* (3), 467-474.

163.   Diaz-Araya, G.; Vivar, R.; Humeres, C.; Boza, P.; Bolivar, S.; Munoz, C., Cardiac Fibroblasts As Sentinel Cells In Cardiac Tissue: Receptors, Signaling Pathways And Cellular Functions. *Pharmacol. Res.* **2015,** *101*, 30-40.

164.   Almine, J. F.; Wise, S. G.; Hiob, M.; Singh, N. K.; Tiwari, K. K.; Vali, S.; Abbasi, T.; Weiss, A. S., Elastin Sequences Trigger Transient Proinflammatory Responses By Human Dermal Fibroblasts. *FASEB J.* **2013,** *27* (9), 3455-3465.

165.   Buwitt-Beckmann, U.; Heine, H.; Wiesmuller, K. H.; Jung, G.; Brock, R.; Ulmer, A. J., Lipopeptide Structure Determines TLR2 Dependent Cell Activation Level. *FEBS J.* **2005,** *272* (24), 6354-6364.

166.   Farhat, K.; Riekenberg, S.; Heine, H.; Debarry, J.; Lang, R.; Mages, J.; Buwitt-Beckmann, U.; Roschmann, K.; Jung, G.; Wiesmuller, K. H.; Ulmer, A. J., Heterodimerization Of TLR2 With TLR1 Or TLR6 Expands The Ligand Spectrum But Does Not Lead To Differential Signaling. *J. Leukoc. Biol.* **2008,** *83* (3), 692-701.

167.   Ioannidis, I.; Ye, F.; McNally, B.; Willette, M.; Flano, E., Toll-Like Receptor Expression And Induction Of Type I And Type III Interferons In Primary Airway Epithelial Cells. *J. Virol.* **2013,** *87* (6), 3261-3270.

168.   Stack, E. C.; Wang, C.; Roman, K. A.; Hoyt, C. C., Multiplexed Immunohistochemistry, Imaging, And Quantitation: A Review, With An Assessment Of Tyramide Signal Amplification, Multispectral Imaging And Multiplex Analysis. *Methods.* **2014,** *70* (1), 46-58.

169.   Chao, J.; DeBiasio, R.; Zhu, Z.; Giuliano, K. A.; Schmidt, B. F., Immunofluorescence Signal Amplification By The Enzyme-Catalyzed Deposition Of A Fluorescent Reporter Substrate (CARD). *Cytometry.* **1996,** *23* (1), 48-53.

170.   Marshall, J. D.; Fearon, K.; Abbate, C.; Subramanian, S.; Yee, P.; Gregorio, J.; Coffman, R. L.; Van Nest, G., Identification Of A Novel Cpg DNA Class And Motif That Optimally Stimulate B Cell And Plasmacytoid Dendritic Cell Functions. *J. Leukoc. Biol.* **2003,** *73* (6), 781-792.

171.   Salunke, D. B.; Shukla, N. M.; Yoo, E.; Crall, B. M.; Balakrishna, R.; Malladi, S. S.; David, S. A., Structure-Activity Relationships In Human Toll-Like Receptor 2-Specific Monoacyl Lipopeptides. *J. Med. Chem.* **2012,** *55*, 3353-3363.

172.   Tran Vdu, T.; Souiai, O.; Romero-Barrios, N.; Crespi, M.; Gautheret, D., Detection Of Generic Differential RNA Processing Events From RNA-Seq Data. *RNA Biol.* **2016,** *13* (1), 59-67.

173.   Li, X.; Brock, G. N.; Rouchka, E. C.; Cooper, N. G. F.; Wu, D.; O'Toole, T. E.; Gill, R. S.; Eteleeb, A. M.; O'Brien, L.; Rai, S. N., A Comparison Of Per Sample Global Scaling And Per Gene Normalization Methods For Differential Expression Analysis Of RNA-Seq Data. *PloS One.* **2017,** *12* (5), e0176185. doi: 10.1371/journal.pone.0176185.

174.   Beesu, M.; Salyer, A. C.; Trautman, K. L.; Hill, J. K.; David, S. A., Human Toll-Like Receptor (TLR) 8-Specific Agonistic Activity In Substituted Pyrimidine-2,4-Diamines. *J. Med. Chem.* **2016,** *59* (17), 8082-8093.

175.   Salyer, A. C.; Caruso, G.; Khetani, K. K.; Fox, L. M.; Malladi, S. S.; David, S. A., Identification Of Adjuvantic Activity Of Amphotericin B In A Novel, Multiplexed, Poly-TLR/NLR High-Throughput Screen. *PloS One.* **2016,** *11* (2), e0149848. doi: 10.1371/journal.pone.0149848.

176.	Ottenhoff, T. H.; Kaufmann, S. H., Vaccines Against Tuberculosis: Where Are We And Where Do We Need To Go? *PLoS Pathog.* **2012,** *8* (5), e1002607. doi: 10.1371/journal.ppat.1002607.

177.	Diacon, A. H.; Pym, A.; Grobusch, M. P.; de los Rios, J. M.; Gotuzzo, E.; Vasilyeva, I.; Leimane, V.; Andries, K.; Bakare, N.; De Marez, T.; Haxaire-Theeuwes, M.; Lounis, N.; Meyvisch, P.; De Paepe, E.; van Heeswijk, R. P.; Dannemann, B.; Group, T. C. S., Multidrug-Resistant Tuberculosis And Culture Conversion With Bedaquiline. *N. Engl. J. Med.* **2014,** *371* (8), 723-732.

178.	Trunz, B. B.; Fine, P.; Dye, C., Effect Of BCG Vaccination On Childhood Tuberculous Meningitis And Miliary Tuberculosis Worldwide: A Meta-Analysis And Assessment Of Cost-Effectiveness. *Lancet.* **2006,** *367* (9517), 1173-1180.

179.	Khandaker, G.; Beard, F. H.; Dey, A.; Coulter, C.; Hendry, A. J.; Macartney, K. K., Evaluation Of Bacille Calmette-Guerin Immunisation Programs In Australia. *Commun. Dis. Intell. Q. Rep.* **2017,** *41* (1), E33-E48.

180.	Zodpey, S. P.; Shrikhande, S. N.; Salodkar, A. D.; Maldhure, B. R.; Kulkarni, S. W., Effectiveness Of Bacillus Calmette-Guerin (BCG) Vaccination In The Prevention Of Leprosy; A Case-Finding Control Study In Nagpur, India. *Int. J. Lepr. Other. Mycobact. Dis.* **1998,** *66* (3), 309-315.

181.	Sterne, J. A.; Rodrigues, L. C.; Guedes, I. N., Does The Efficacy Of BCG Decline With Time Since Vaccination? *Int. J. Tuberc. Lung Dis.* **1998,** *2* (3), 200-207.

182.	Birk, N. M.; Nissen, T. N.; Zingmark, V.; Kjaergaard, J.; Thostesen, L. M.; Kofoed, P. E.; Stensballe, L. G.; Andersen, A.; Nielsen, S. D.; Benn, C. S.; Pryds, O.; Jeppesen, D. L.,

Bacillus Calmette-Guerin Vaccination, Thymic Size, And Thymic Output In Healthy Newborns. *Pediatr. Res.* **2017,** *81* (6), 873-880.

183.   Reed, S. G.; Hsu, F. C.; Carter, D.; Orr, M. T., The Science Of Vaccine Adjuvants: Advances In TLR4 Ligand Adjuvants. *Curr. Opin. Immunol.* **2016,** *41*, 85-90.

184.   McKee, A. S.; Marrack, P., Old And New Adjuvants. *Curr. Opin. Immunol.* **2017,** *47*, 44-51.

185.   Bonam, S. R.; Partidos, C. D.; Halmuthur, S. K. M.; Muller, S., An Overview Of Novel Adjuvants Designed For Improving Vaccine Efficacy. *Trends Pharmacol. Sci.* **2017**. doi: 10.1016/j.tips.2017.06.002.

186.   Cliff, J. M.; Kaufmann, S. H.; McShane, H.; van Helden, P.; O'Garra, A., The Human Immune Response To Tuberculosis And Its Treatment: A View From The Blood. *Immunol. Rev.* **2015,** *264* (1), 88-102.

187.   Bhatt, K.; Verma, S.; Ellner, J. J.; Salgame, P., Quest For Correlates Of Protection Against Tuberculosis. *Clin. Vaccine Immunol.* **2015,** *22* (3), 258-66.

188.   Jouanguy, E.; Lamhamedi-Cherradi, S.; Lammas, D.; Dorman, S. E.; Fondaneche, M. C.; Dupuis, S.; Doffinger, R.; Altare, F.; Girdlestone, J.; Emile, J. F.; Ducoulombier, H.; Edgar, D.; Clarke, J.; Oxelius, V. A.; Brai, M.; Novelli, V.; Heyne, K.; Fischer, A.; Holland, S. M.; Kumararatne, D. S.; Schreiber, R. D.; Casanova, J. L., A Human IFNGR1 Small Deletion Hotspot Associated With Dominant Susceptibility To Mycobacterial Infection. *Nat. Genet.* **1999,** *21* (4), 370-378.

189.   Bustamante, J.; Boisson-Dupuis, S.; Abel, L.; Casanova, J. L., Mendelian Susceptibility To Mycobacterial Disease: Genetic, Immunological, And Clinical Features Of Inborn Errors Of IFN-Gamma Immunity. *Semin. Immunol.* **2014,** *26* (6), 454-470.

190.	Lancioni, C. L.; Li, Q.; Thomas, J. J.; Ding, X.; Thiel, B.; Drage, M. G.; Pecora, N. D.; Ziady, A. G.; Shank, S.; Harding, C. V.; Boom, W. H.; Rojas, R. E., Mycobacterium Tuberculosis Lipoproteins Directly Regulate Human Memory CD4(+) T Cell Activation Via Toll-Like Receptors 1 And 2. *Infect. Immun.* **2011,** *79* (2), 663-673.

191.	Dwivedi, V. P.; Bhattacharya, D.; Chatterjee, S.; Prasad, D. V.; Chattopadhyay, D.; Van Kaer, L.; Bishai, W. R.; Das, G., Mycobacterium Tuberculosis Directs T Helper 2 Cell Differentiation By Inducing Interleukin-1beta Production In Dendritic Cells. *J. Biol. Chem.* **2012,** *287* (40), 33656-33663.

192.	Agnihotri, G.; Crall, B. M.; Lewis, T. C.; Day, T. P.; Balakrishna, R.; Warshakoon, H. J.; Malladi, S. S.; David, S. A., Structure-Activity Relationships In Toll-Like Receptor 2-Agonists Leading To Simplified Monoacyl Lipopeptides. *J. Med. Chem.* **2011,** *54* (23), 8148-8160.

193.	Wu, W.; Li, R.; Malladi, S. S.; Warshakoon, H. J.; Kimbrell, M. R.; Amolins, M. W.; Ukani, R.; Datta, A.; David, S. A., Structure-Activity Relationships In Toll-Like Receptor-2 Agonistic Diacylthioglycerol Lipopeptides. *J. Med. Chem.* **2010,** *53* (8), 3198-3213.

194.	Warshakoon, H. J.; Hood, J. D.; Kimbrell, M. R.; Malladi, S.; Wu, W. Y.; Shukla, N. M.; Agnihotri, G.; Sil, D.; David, S. A., Potential Adjuvantic Properties Of Innate Immune Stimuli. *Hum. Vaccin.* **2009,** *5*, 381-394.

195.	Nuhn, L.; Vanparijs, N.; De Beuckelaer, A.; Lybaert, L.; Verstraete, G.; Deswarte, K.; Lienenklaus, S.; Shukla, N. M.; Salyer, A. C.; Lambrecht, B. N.; Grooten, J.; David, S. A.; De Koker, S.; De Geest, B. G., pH-Degradable Imidazoquinoline-Ligated Nanogels For Lymph Node-Focused Immune Activation. *Proc. Natl. Acad. Sci. U.S.A.* **2016,** *113* (29), 8098-8103.

196.   Mata-Haro, V.; Cekic, C.; Martin, M.; Chilton, P. M.; Casella, C. R.; Mitchell, T. C., The Vaccine Adjuvant Monophosphoryl Lipid A As A TRIF-Biased Agonist Of TLR4. *Science.* **2007,** *316* (5831), 1628-1632.

197.   Kasturi, S. P.; Skountzou, I.; Albrecht, R. A.; Koutsonanos, D.; Hua, T.; Nakaya, H. I.; Ravindran, R.; Stewart, S.; Alam, M.; Kwissa, M.; Villinger, F.; Murthy, N.; Steel, J.; Jacob, J.; Hogan, R. J.; Garcia-Sastre, A.; Compans, R.; Pulendran, B., Programming The Magnitude And Persistence Of Antibody Responses With Innate Immunity. *Nature.* **2011,** *470* (7335), 543-547.

198.   Napolitani, G.; Rinaldi, A.; Bertoni, F.; Sallusto, F.; Lanzavecchia, A., Selected Toll-Like Receptor Agonist Combinations Synergistically Trigger A T Helper Type 1-Polarizing Program In Dendritic Cells. *Nat. Immunol.* **2005,** *6* (8), 769-776.

199.   Tom, J. K.; Dotsey, E. Y.; Wong, H. Y.; Stutts, L.; Moore, T.; Davies, D. H.; Felgner, P. L.; Esser-Kahn, A. P., Modulation Of Innate Immune Responses Via Covalently Linked TLR Agonists. *ACS Cent. Sci.* **2015,** *1* (8), 439-448.

200.   Madan-Lala, R.; Pradhan, P.; Roy, K., Combinatorial Delivery Of Dual And Triple TLR Agonists Via Polymeric Pathogen-Like Particles Synergistically Enhances Innate And Adaptive Immune Responses. *Sci. Rep.* **2017,** *7* (1), 2530. doi: 10.1038/s41598-017-02804-y.

201.   Lynn, G. M.; Laga, R.; Darrah, P. A.; Ishizuka, A. S.; Balaci, A. J.; Dulcey, A. E.; Pechar, M.; Pola, R.; Gerner, M. Y.; Yamamoto, A.; Buechler, C. R.; Quinn, K. M.; Smelkinson, M. G.; Vanek, O.; Cawood, R.; Hills, T.; Vasalatiy, O.; Kastenmuller, K.; Francica, J. R.; Stutts, L.; Tom, J. K.; Ryu, K. A.; Esser-Kahn, A. P.; Etrych, T.; Fisher, K. D.; Seymour, L. W.; Seder, R. A., In Vivo Characterization Of The Physicochemical Properties Of Polymer-Linked TLR Agonists That Enhance Vaccine Immunogenicity. *Nat. Biotechnol.* **2015,** *33* (11), 1201-1210.

202.   Gutjahr, A.; Papagno, L.; Nicoli, F.; Lamoureux, A.; Vernejoul, F.; Lioux, T.; Gostick, E.; Price, D. A.; Tiraby, G.; Perouzel, E.; Appay, V.; Verrier, B.; Paul, S., Cutting Edge: A Dual TLR2 And TLR7 Ligand Induces Highly Potent Humoral And Cell-Mediated Immune Responses. *J. Immunol.* **2017**, 198 (11), 4205-4209.

203.   Nakagawa, M.; Greenfield, W.; Moerman-Herzog, A.; Coleman, H. N., Cross-Reactivity, Epitope Spreading, And De Novo Immune Stimulation Are Possible Mechanisms Of Cross-Protection Of Nonvaccine Human Papillomavirus (HPV) Types In Recipients Of HPV Therapeutic Vaccines. *Clin. Vaccine Immunol.* **2015,** *22* (7), 679-687.

204.   Chung, K. Y.; Coyle, E. M.; Jani, D.; King, L. R.; Bhardwaj, R.; Fries, L.; Smith, G.; Glenn, G.; Golding, H.; Khurana, S., ISCOMATRIX Adjuvant Promotes Epitope Spreading And Antibody Affinity Maturation Of Influenza A H7N9 Virus Like Particle Vaccine That Correlate With Virus Neutralization In Humans. *Vaccine.* **2015,** *33* (32), 3953-3962.

205.   Bothamley, G. H., Epitope-Specific Antibody Levels In Tuberculosis: Biomarkers Of Protection, Disease, And Response To Treatment. *Front. Immunol.* **2014,** *5*, 243. doi: 10.3389/fimmu.2014.00243.

206.   Kawai, T.; Akira, S., The Role Of Pattern-Recognition Receptors In Innate Immunity: Update On Toll-Like Receptors. *Nat. Immunol.* **2010,** *11* (5), 373-384.

207.   Brandt, K. J.; Fickentscher, C.; Kruithof, E. K.; de Moerloose, P., TLR2 Ligands Induce NF-κB Activation From Endosomal Compartments Of Human Monocytes. *PloS One.* **2013,** *8* (12), e80743. doi: 10.1371/journal.pone.0080743.

208.   Shamsul, H. M.; Hasebe, A.; Iyori, M.; Ohtani, M.; Kiura, K.; Zhang, D.; Totsuka, Y.; Shibata, K., The Toll-Like Receptor 2 (TLR2) Ligand FSL-1 Is Internalized Via The Clathrin-

Dependent Endocytic Pathway Triggered By CD14 And CD36 But Not By TLR2. *Immunology.* **2010,** *130* (2), 262-272.

209.   Chai, L. Y.; Kullberg, B. J.; Vonk, A. G.; Warris, A.; Cambi, A.; Latge, J. P.; Joosten, L. A.; van der Meer, J. W.; Netea, M. G., Modulation Of Toll-Like Receptor 2 (TLR2) And TLR4 Responses By Aspergillus Fumigatus. *Infect. Immun.* **2009,** *77* (5), 2184-2192.

210.   Langermans, J. A.; Doherty, T. M.; Vervenne, R. A.; van der Laan, T.; Lyashchenko, K.; Greenwald, R.; Agger, E. M.; Aagaard, C.; Weiler, H.; van Soolingen, D.; Dalemans, W.; Thomas, A. W.; Andersen, P., Protection Of Macaques Against Mycobacterium Tuberculosis Infection By A Subunit Vaccine Based On A Fusion Protein Of Antigen 85B And ESAT-6. *Vaccine.* **2005,** *23* (21), 2740-2750.

211.   Ravindran, R.; Bhowmick, S.; Das, A.; Ali, N., Comparison Of BCG, MPL And Cationic Liposome Adjuvant Systems In Leishmanial Antigen Vaccine Formulations Against Murine Visceral Leishmaniasis. *BMC Microbiol.* **2010,** *10*, 181. doi: 10.1186/1471-2180-10-181.

212.   Alving, C. R.; Rao, M.; Steers, N. J.; Matyas, G. R.; Mayorov, A. V., Liposomes Containing Lipid A: An Effective, Safe, Generic Adjuvant System For Synthetic Vaccines. *Expert Rev. Vaccines.* **2012,** *11* (6), 733-744.

213.   Esparza-Gonzalez, S. C.; Troy, A. R.; Izzo, A. A., Comparative Analysis Of Bacillus Subtilis Spores And Monophosphoryl Lipid A As Adjuvants Of Protein-Based Mycobacterium Tuberculosis-Based Vaccines: Partial Requirement For Interleukin-17a For Induction Of Protective Immunity. *Clin. Vaccine Immunol.* **2014,** *21* (4), 501-508.

214.   Mountford, A. P.; Fisher, A.; Wilson, R. A., The Profile Of IgG1 And IgG2a Antibody Responses In Mice Exposed To Schistosoma Mansoni. *Parasite Immunol.* **1994,** *16* (10), 521-527.

215.   Germann, T.; Bongartz, M.; Dlugonska, H.; Hess, H.; Schmitt, E.; Kolbe, L.; Kolsch, E.; Podlaski, F. J.; Gately, M. K.; Rude, E., Interleukin-12 Profoundly Up-Regulates The Synthesis Of Antigen-Specific Complement-Fixing IgG2a, IgG2b And IgG3 Antibody Subclasses *in vivo*. *Eur. J. Immunol.* **1995,** *25* (3), 823-829.

216.   Frank, R., Schutkowski, M., Extremely Mild Reagent For Boc Deprotection Applicable To The Synthesis Of Peptides With Thioamide Linkages *Chem. Coommun.* **1996**, 2509-2510.

217.   Moon, J. J.; Chu, H. H.; Pepper, M.; McSorley, S. J.; Jameson, S. C.; Kedl, R. M.; Jenkins, M. K., Naive CD4(+) T Cell Frequency Varies For Different Epitopes And Predicts Repertoire Diversity And Response Magnitude. *Immunity.* **2007,** *27* (2), 203-213.

218.   Nordly, P.; Agger, E. M.; Andersen, P.; Nielsen, H. M.; Foged, C., Incorporation Of The TLR4 Agonist Monophosphoryl Lipid A Into The Bilayer Of DDA/TDB Liposomes: Physico-Chemical Characterization And Induction Of CD8+ T-Cell Responses *in vivo*. *Pharm. Res.* **2011,** *28* (3), 553-562.

219.   Brandt, L.; Skeiky, Y. A.; Alderson, M. R.; Lobet, Y.; Dalemans, W.; Turner, O. C.; Basaraba, R. J.; Izzo, A. A.; Lasco, T. M.; Chapman, P. L.; Reed, S. G.; Orme, I. M., The Protective Effect Of The *Mycobacterium bovis* BCG Vaccine Is Increased By Coadministration With The *Mycobacterium tuberculosis* 72-Kilodalton Fusion Polyprotein Mtb72F In *M. tuberculosis*-Infected Guinea Pigs. *Infect. Immun.* **2004,** *72* (11), 6622-6632.

220.   Bekeredjian-Ding, I.; Roth, S. I.; Gilles, S.; Giese, T.; Ablasser, A.; Hornung, V.; Endres, S.; Hartmann, G., T Cell-Independent, TLR-Induced IL-12p70 Production In Primary Human Monocytes. *J. Immunol.* **2006,** *176* (12), 7438-7446.

221.   Bohnenkamp, H. R.; Papazisis, K. T.; Burchell, J. M.; Taylor-Papadimitriou, J., Synergism Of Toll-Like Receptor-Induced Interleukin-12p70 Secretion By Monocyte-Derived

Dendritic Cells Is Mediated Through p38 MAPK And Lowers The Threshold Of T-Helper Cell Type 1 Responses. *Cell. Immunol.* **2007,** *247* (2), 72-84.

222.   Philbin, V. J.; Levy, O., Immunostimulatory Activity Of Toll-Like Receptor 8 Agonists Towards Human Leucocytes: Basic Mechanisms And Translational Opportunities. *Biochem. Soc. Trans.* **2007,** *35*, 1485-1491.

223.   Saruta, M.; Michelsen, K. S.; Thomas, L. S.; Yu, Q. T.; Landers, C. J.; Targan, S. R., TLR8-Mediated Activation Of Human Monocytes Inhibits TL1A Expression. *Eur. J. Immunol.* **2009,** *39* (8), 2195-2202.

224.   Kumagai, Y.; Takeuchi, O.; Akira, S., Pathogen Recognition By Innate Receptors. *J. Infect. Chemother.* **2008,** *14* (2), 86-92.

225.   Kang, J. Y.; Lee, J. O., Structural Biology Of The Toll-Like Receptor Family. *Annu .Rev. Biochem.* **2011,** *80:917-41.*, 917-941.

226.   Botos, I.; Segal, D. M.; Davies, D. R., The Structural Biology of Toll-like Receptors. *Structure.* **2011,** *19* (4), 447-459.

227.   Hatzakis, N. S., Single Molecule Insights On Conformational Selection And Induced Fit Mechanism. *Biophys. Chem.* **2014,** *186*, 46-54.

228.   Amaravadhi, H.; Baek, K.; Yoon, H. S., Revisiting De Novo Drug Design: Receptor Based Pharmacophore Screening. *Curr. Top. Med. Chem.* **2014,** *14* (16), 1890-1898.

229.   Ermolat'ev, D. S.; Babaev, E. V.; Van der Eycken, E. V., Efficient One-Pot, Two-Step, Microwave-Assisted Procedure For The Synthesis Of Polysubstituted 2-Aminoimidazoles. *Org. Lett.* **2006,** *8* (25), 5781-5784.

230.   Tanji, H.; Ohto, U.; Shibata, T.; Miyake, K.; Shimizu, T., Structural reorganization of the Toll-like receptor 8 dimer induced by agonistic ligands. *Science.* **2013,** *339* (6126), 1426-1429.

231.   Scholfield, M. R.; Zanden, C. M.; Carter, M.; Ho, P. S., Halogen bonding (X-bonding): a biological perspective. *Protein Sci.* **2013,** *22* (2), 139-152.

232.   Auffinger, P.; Hays, F. A.; Westhof, E.; Ho, P. S., Halogen Bonds In Biological Molecules. *Pro. Natl. Acad. Sci. U.S.A.* **2004,** *101* (48), 16789-16794.

233.   Merlot, A. M.; Kalinowski, D. S.; Richardson, D. R., Unraveling The Mysteries Of Serum Albumin-More Than Just A Serum Protein. *Front. Physiol.* **2014,** *5*, 299. doi: 10.3389/fphys.2014.00299.

234.   Bohnert, T.; Gan, L. S., Plasma Protein Binding: From Discovery To Development. *J. Pharm. Sci.* **2013,** *102* (9), 2953-2994.

235.   Huang, Z.; Ung, T., Effect Of Alpha-1-Acid Glycoprotein Binding On Pharmacokinetics And Pharmacodynamics. *Curr. Drug Metab.* **2013,** *14* (2), 226-238.

236.   MacIntyre, A. C.; Cutler, D. J., The Potential Role Of Lysosomes In Tissue Distribution Of Weak Bases. *Biopharm. Drug Dispos.* **1988,** *9* (6), 513-526.

237.   Wu, T. Y.; Singh, M.; Miller, A. T.; De Gregorio, E.; Doro, F.; D'Oro, U.; Skibinski, D. A.; Mbow, M. L.; Bufali, S.; Herman, A. E.; Cortez, A.; Li, Y.; Nayak, B. P.; Tritto, E.; Filippi, C. M.; Otten, G. R.; Brito, L. A.; Monaci, E.; Li, C.; Aprea, S.; Valentini, S.; Calabromicron, S.; Laera, D.; Brunelli, B.; Caproni, E.; Malyala, P.; Panchal, R. G.; Warren, T. K.; Bavari, S.; O'Hagan, D. T.; Cooke, M. P.; Valiante, N. M., Rational Design Of Small Molecules As Vaccine Adjuvants. *Sci. Transl. Med.* **2014,** *6* (263), 263ra160. doi: 10.1126/scitranslmed.3009980.

238.   Casale, T. B.; Kessler, J.; Romero, F. A., Safety Of The Intranasal Toll-Like Receptor 4 Agonist CRX-675 In Allergic Rhinitis. *Ann. Allergy Asthma Immunol.* **2006,** *97* (4), 454-456.

239.   Greiff, L.; Cervin, A.; Ahlstrom-Emanuelsson, C.; Almqvist, G.; Andersson, M.; Dolata, J.; Eriksson, L.; Hogestatt, E.; Kallen, A.; Norlen, P.; Sjolin, I. L.; Widegren, H., Repeated

Intranasal TLR7 Stimulation Reduces Allergen Responsiveness In Allergic Rhinitis. *Respir. Res.* **2012,** *13*, 53. doi: 10.1186/1465-9921-13-53.

240.   Matsui, H.; Tomizawa, H.; Eiho, K.; Kashiwazaki, Y.; Edwards, S.; Biffen, M.; Bell, J. P.; Bahl, A.; Leishman, A. J.; Murray, C. M.; Takaku, H.; Ueda, Y., Mechanism Of Action Of Inhibition Of Allergic Immune Responses By A Novel Antedrug TLR7 Agonist. *J. Immunol.* **2012,** *189* (11), 5194-5205.

241.   Kaufman, E. H.; Jacoby, D. B., Upping The Antedrug: Is A Novel Anti-Inflammatory Toll-Like Receptor 7 Agonist Also A Bronchodilator? *Br. J. Pharmacol.* **2012,** *166* (2), 569-572.

242.   Biffen, M.; Matsui, H.; Edwards, S.; Leishman, A. J.; Eiho, K.; Holness, E.; Satterthwaite, G.; Doyle, I.; Wada, H.; Fraser, N. J.; Hawkins, S. L.; Aoki, M.; Tomizawa, H.; Benjamin, A. D.; Takaku, H.; McInally, T.; Murray, C. M., Biological Characterization Of A Novel Class Of Toll-Like Receptor 7 Agonists Designed To Have Reduced Systemic Activity. *Br. J. Pharmacol.* **2012,** *166* (2), 573-586.

243.   Han, J.; Lee, J. D.; Bibbs, L.; Ulevitch, R. J., A MAP Kinase Targeted By Endotoxin And Hyperosmolarity In Mammalian Cells. *Science.* **1994,** *265* (5173), 808-811.

244.   Pearson, G.; Robinson, F.; Beers Gibson, T.; Xu, B. E.; Karandikar, M.; Berman, K.; Cobb, M. H., Mitogen-Activated Protein (MAP) Kinase Pathways: Regulation And Physiological Functions. *Endocr. Rev.* **2001,** *22* (2), 153-183.

245.   Mellman, I.; Fuchs, R.; Helenius, A., Acidification Of The Endocytic And Exocytic Pathways. *Annu. Rev. Biochem.* **1986,** *55*, 663-700.

246.   Feldman, R. I.; Wu, J. M.; Polokoff, M. A.; Kochanny, M. J.; Dinter, H.; Zhu, D.; Biroc, S. L.; Alicke, B.; Bryant, J.; Yuan, S.; Buckman, B. O.; Lentz, D.; Ferrer, M.; Whitlow, M.;

Adler, M.; Finster, S.; Chang, Z.; Arnaiz, D. O., Novel Small Molecule Inhibitors Of 3-Phosphoinositide-Dependent Kinase-1. *J. Bio. Chem.* **2005,** *280* (20), 19867-19874.

247.   Clark, K.; Plater, L.; Peggie, M.; Cohen, P., Use Of The Pharmacological Inhibitor BX795 To Study The Regulation And Physiological Roles Of TBK1 And Ikappab Kinase Epsilon: A Distinct Upstream Kinase Mediates Ser-172 Phosphorylation And Activation. *J. Biol. Chem.* **2009,** *284* (21), 14136-14146.

248.   Serrano-Martin, X.; Payares, G.; Mendoza-Leon, A., Glibenclamide, A Blocker Of K+(ATP) Channels, Shows Antileishmanial Activity In Experimental Murine Cutaneous Leishmaniasis. *Antimicrob. Agents Chemother.* **2006,** *50* (12), 4214-4216.

249.   Sekellick, M. J.; Carra, S. A.; Bowman, A.; Hopkins, D. A.; Marcus, P. I., Transient Resistance Of Influenza Virus To Interferon Action Attributed To Random Multiple Packaging And Activity Of NS Genes. *J. Interferon Cytokine Res.* **2000,** *20* (11), 963-970.

250.   Sordella, R.; Bell, D. W.; Haber, D. A.; Settleman, J., Gefitinib-Sensitizing EGFR Mutations In Lung Cancer Activate Anti-Apoptotic Pathways. *Science.* **2004,** *305* (5687), 1163-1167.

251.   Ostinowski, Z. M., W., Processing Of X-Ray Diffraction Data Collected In Oscillation Mode. *Methods Enzymol.* **1997,** *276*, 307-326.

252.   Vagin, A.; Teplyakov, A., Molecular Replacement With MOLREP. *Acta. crystallogr. D Biol. Crystallogr.* **2010,** *66* (Pt 1), 22-25.

253.   Emsley, P.; Cowtan, K., Coot: Model-Building Tools For Molecular Graphics. *Acta. crystallogr. D Biol. Crystallogr.* **2004,** *60* (Pt 12 Pt 1), 2126-2132.

254. Murshudov, G. N.; Vagin, A. A.; Dodson, E. J., Refinement Of Macromolecular Structures By The Maximum-Likelihood Method. *Acta. crystallogr. D Biol. Crystallogr.* **1997,** *53* (Pt 3), 240-255.

255. Laskowski, R. A. M., M.W.;Moss,D.S.;Thornton,J.M., Procheck – A Program To Check The Stereochemical Quality Of Protein Structures. *J. Appl. Crystallogr.* **1993,** *26*, 283-291.

256. Jurk, M.; Heil, F.; Vollmer, J.; Schetter, C.; Krieg, A. M.; Wagner, H.; Lipford, G.; Bauer, S., Human TLR7 Or TLR8 Independently Confer Responsiveness To The Antiviral Compound R-848. *Nat. Immunol.* **2002,** *3* (6), 499.

257. Lawn, J. E.; Cousens, S.; Zupan, J.; Lancet Neonatal Survival Steering, T., 4 million neonatal deaths: when? Where? Why? *Lancet.* **2005,** *365* (9462), 891-900.

258. Mohr, E.; Siegrist, C. A., Vaccination In Early Life: Standing Up To The Challenges. *Curr. Opin. Immunol.* **2016,** *41*, 1-8.

259. Kollmann, T. R.; Kampmann, B.; Mazmanian, S. K.; Marchant, A.; Levy, O., Protecting The Newborn And Young Infant From Infectious Diseases: Lessons From Immune Ontogeny. *Immunity.* **2017,** *46* (3), 350-363.

260. Hodgins, D. C.; Shewen, P. E., Vaccination Of Neonates: Problem And Issues. *Vaccine.* **2012,** *30* (9), 1541-1559.

261. Saini, V.; MacDonald, S. E.; McNeil, D. A.; McDonald, S. W.; Kellner, J. D.; Edwards, S. A.; Stagg, V.; Tough, S., Timeliness And Completeness Of Routine Childhood Vaccinations In Children By Two Years Of Age In Alberta, Canada. *Can. J. Public Health.* **2017,** *108* (2), e124-e128. doi: 10.17269/cjph.108.5885.

262.   Carazo Perez, S.; De Serres, G.; Bureau, A.; Skowronski, D. M., Reduced Antibody Response To Infant Measles Vaccination: Effects Based On Type And Timing Of The First Vaccine Dose Persist After The Second Dose. *Clin. Infect. Dis.* **2017**. doi: 10.1093/cid/cix510.

263.   Aho, C.; Michael, A.; Yoannes, M.; Greenhill, A.; Jacoby, P.; Reeder, J.; Pomat, W.; Saleu, G.; Namuigi, P.; Phuanukoonnon, S.; Smith-Vaughan, H.; Leach, A. J.; Richmond, P.; Lehmann, D.; Neonatal Pneumococcal Conjugate Vaccine Trial Study, T., Limited Impact Of Neonatal Or Early Infant Schedules Of 7-Valent Pneumococcal Conjugate Vaccination On Nasopharyngeal Carriage Of Streptococcus Pneumoniae In Papua New Guinean Children: A Randomized Controlled Trial. *Vaccine Rep.* **2016,** *6*, 36-43.

264.   Gill, C. J.; Hodsdon, L.; Santosham, M.; O'Brien, K. L., The Unattainable Criteria For New Infant Vaccines. *Hum. Vaccin. Immunother.* **2017**. doi: 10.1080/21645515.2017.1328334.

265.   Levy, O.; Suter, E. E.; Miller, R. L.; Wessels, M. R., Unique Efficacy Of Toll-Like Receptor 8 Agonists In Activating Human Neonatal Antigen-Presenting Cells. *Blood.* **2006,** *108* (4), 1284-1290.

266.   Liu, J.; Xu, C.; Hsu, L. C.; Luo, Y.; Xiang, R.; Chuang, T. H., A Five-Amino-Acid Motif In The Undefined Region Of The TLR8 Ectodomain Is Required For Species-Specific Ligand Recognition. *Mol. Immunol.* **2010,** *47* (5), 1083-1090.

267.   Alam, S.; Javor, S.; Degardin, M.; Ajami, D.; Rebek, M.; Kissner, T. L.; Waag, D. M.; Rebek, J., Jr.; Saikh, K. U., Structure-Based Design And Synthesis Of A Small Molecule That Exhibits Anti-Inflammatory Activity By Inhibition Of Myd88-Mediated Signaling To Bacterial Toxin Exposure. *Chem. Biol. Drug Des.* **2015,** *86* (2), 200-209.

268.   Kawai, T.; Akira, S., Toll-Like Receptor And RIG-I-Like Receptor Signaling. *Ann. N. Y. Acad. Sci.* **2008,** *1143*, 1-20.

269.   Coll, R. C.; O'Neill, L. A., New Insights Into The Regulation Of Signalling By Toll-Like Receptors And Nod-Like Receptors. *J. Innate Immunol.* **2010,** *2* (5), 406-421.

270.   Suzuki, N.; Saito, T., IRAK-4--A Shared NF-κB Activator In Innate And Acquired Immunity. *Treands Immunol.* **2006,** *27* (12), 566-572.

271.   Makni-Maalej, K.; Marzaioli, V.; Boussetta, T.; Belambri, S. A.; Gougerot-Pocidalo, M. A.; Hurtado-Nedelec, M.; Dang, P. M.; El-Benna, J., TLR8, But Not TLR7, Induces The Priming Of The NADPH Oxidase Activation In Human Neutrophils. *J. Leukoc. Biol.* **2015,** *97* (6), 1081-1087.

272.   Zhang, C.; Baumgartner, R. A.; Yamada, K.; Beaven, M. A., Mitogen-Activated Protein (MAP) Kinase Regulates Production Of Tumor Necrosis Factor-Alpha And Release Of Arachidonic Acid In Mast Cells. Indications Of Communication Between p38 And p42 MAP Kinases. *J. Biol. Chem.* **1997,** *272* (20), 13397-13402.

273.   Pappenheimer, A. M., Jr., Diphtheria Toxin. *Ann. Rev. Biochem.* **1977,** *46*, 69-94.

274.   Zitvogel, L.; Regnault, A.; Lozier, A.; Wolfers, J.; Flament, C.; Tenza, D.; Ricciardi-Castagnoli, P.; Raposo, G.; Amigorena, S., Eradication Of Established Murine Tumors Using A Novel Cell-Free Vaccine: Dendritic Cell-Derived Exosomes. *Nat. Med.* **1998,** *4* (5), 594-600.

275.   Eken, C.; Martin, P. J.; Sadallah, S.; Treves, S.; Schaller, M.; Schifferli, J. A., Ectosomes Released By Polymorphonuclear Neutrophils Induce A MerTK-Dependent Anti-Inflammatory Pathway In Macrophages. *J. Biol. Chem.* **2010,** *285* (51), 39914-39921.

276.   Schwarz, H.; Posselt, G.; Wurm, P.; Ulbing, M.; Duschl, A.; Horejs-Hoeck, J., TLR8 And NOD Signaling Synergistically Induce The Production Of IL-1β And IL-23 In Monocyte-Derived DCs And Enhance The Expression Of The Feedback Inhibitor SOCS2. *Immunobiology.* **2013,** *218* (4), 533-542.

277.   Dowling, D. J.; Tan, Z.; Prokopowicz, Z. M.; Palmer, C. D.; Matthews, M. A.; Dietsch, G. N.; Hershberg, R. M.; Levy, O., The Ultra-Potent And Selective TLR8 Agonist VTX-294 Activates Human Newborn And Adult Leukocytes. *PloS One.* **2013,** *8* (3), e58164. doi: 10.1371/journal.pone.0058164.

278.   Beesu, M.; Salyer, A. C.; Trautman, K. L.; Hill, J. K.; David, S. A., Human Toll-Like Receptor (TLR) 8-Specific Agonistic Activity In Substituted Pyrimidine-2,4-Diamines. *J. Med. Chem.* **2016,** *59* (17), 8082-8093.

279.   Fink, S. L.; Cookson, B. T., Apoptosis, Pyroptosis, And Necrosis: Mechanistic Description Of Dead And Dying Eukaryotic Cells. *Infect. Immun.* **2005,** *73* (4), 1907-1916.

280.   Douda, D. N.; Khan, M. A.; Grasemann, H.; Palaniyar, N., SK3 Channel And Mitochondrial ROS Mediate NADPH Oxidase-Independent Netosis Induced By Calcium Influx. *Proc. Natl. Acad. Sci. U.S.A.* **2015,** *112* (9), 2817-2822.

281.   Wu, J. J.; Huang, D. B.; Tyring, S. K., Resiquimod: A New Immune Response Modifier With Potential As A Vaccine Adjuvant For Th1 Immune Responses. *Antiviral Res.* **2004,** *64* (2), 79-83.

282.   Lood, C.; Arve, S.; Ledbetter, J.; Elkon, K. B., TLR7/8 Activation In Neutrophils Impairs Immune Complex Phagocytosis Through Shedding Of FcγRIIA. *J. Exp. Med.* **2017**. doi: 10.1084/jem.20161512.

283.   Ren, G.; Su, J.; Zhao, X.; Zhang, L.; Zhang, J.; Roberts, A. I.; Zhang, H.; Das, G.; Shi, Y., Apoptotic Cells Induce Immunosuppression Through Dendritic Cells: Critical Roles Of IFN-γ And Nitric Oxide. *J. Immunol.* **2008,** *181* (5), 3277-3284.

284.   Erwig L-P, Henson PM. Immunological Consequences Of Apoptotic Cell Phagocytosis. *Am. J. Pathol.*. **2007**, *171*(1). doi:10.2353/ajpath.2007.070135.

285.   Pathak, S. K.; Skold, A. E.; Mohanram, V.; Persson, C.; Johansson, U.; Spetz, A. L., Activated Apoptotic Cells Induce Dendritic Cell Maturation Via Engagement Of Toll-Like Receptor 4 (TLR4), Dendritic Cell-Specific Intercellular Adhesion Molecule 3 (ICAM-3)-Grabbing Nonintegrin (DC-SIGN), And Beta2 Integrins. *J. Biol. Chem.* **2012,** *287* (17), 13731-13742.

286.   Koopman, G.; Beenhakker, N.; Hofman, S.; Walther-Jallow, L.; Makitalo, B.; Mooij, P.; Anderson, J.; Verschoor, E.; Bogers, W. M.; Heeney, J. L.; Spetz, A. L., Immunization With Apoptotic Pseudovirus Transduced Cells Induces Both Cellular And Humoral Responses: A Proof Of Concept Study In Macaques. *Vaccine.* **2012,** *30* (15), 2523-2534.

287.   Pitt, J. M.; Charrier, M.; Viaud, S.; Andre, F.; Besse, B.; Chaput, N.; Zitvogel, L., Dendritic Cell-Derived Exosomes As Immunotherapies In The Fight Against Cancer. *J. Immunol.* **2014,** *193* (3), 1006-1011.

288.   Mulcahy, L. A.; Pink, R. C.; Carter, D. R., Routes And Mechanisms Of Extracellular Vesicle Uptake. *J. Extracell. Vesicles.* **2014,** *3*. doi: 10.3402/jev.v3.24641.

289.   Luketic, L.; Delanghe, J.; Sobol, P. T.; Yang, P.; Frotten, E.; Mossman, K. L.; Gauldie, J.; Bramson, J.; Wan, Y., Antigen Presentation By Exosomes Released From Peptide-Pulsed Dendritic Cells Is Not Suppressed By The Presence Of Active CTL. *J. Immunol.* **2007,** *179* (8), 5024-5032.

290.   Xu, Y.; Liu, Y.; Yang, C.; Kang, L.; Wang, M.; Hu, J.; He, H.; Song, W.; Tang, H., Macrophages Transfer Antigens To Dendritic Cells By Releasing Exosomes Containing Dead-Cell-Associated Antigens Partially Through A Ceramide-Dependent Pathway To Enhance CD4(+) T-Cell Responses. *Immunology.* **2016,** *149* (2), 157-171.

291.   Yang, Y. W.; Wu, C. A.; Morrow, W. J., Cell Death Induced By Vaccine Adjuvants Containing Surfactants. *Vaccine.* **2004,** *22* (11-12), 1524-1536.

292.   Yang, Y. W.; Shen, S. S., Enhanced Antigen Delivery Via Cell Death Induced By The Vaccine Adjuvants. *Vaccine.* **2007,** *25* (45), 7763-7772.

293.   Ng, H. I.; Fernando, G. J.; Depelsenaire, A. C.; Kendall, M. A., Potent Response Of QS-21 As A Vaccine Adjuvant In The Skin When Delivered With The Nanopatch, Resulted In Adjuvant Dose Sparing. *Sci. Rep.* **2016,** *6*, 29368. doi: 10.1038/srep29368.

294.   Marty-Roix, R.; Vladimer, G. I.; Pouliot, K.; Weng, D.; Buglione-Corbett, R.; West, K.; MacMicking, J. D.; Chee, J. D.; Wang, S.; Lu, S.; Lien, E., Identification Of QS-21 As An Inflammasome-Activating Molecular Component Of Saponin Adjuvants. *J. Biol. Chem.* **2016,** *291* (3), 1123-36.

295.   Marichal, T.; Ohata, K.; Bedoret, D.; Mesnil, C.; Sabatel, C.; Kobiyama, K.; Lekeux, P.; Coban, C.; Akira, S.; Ishii, K. J.; Bureau, F.; Desmet, C. J., DNA Released From Dying Host Cells Mediates Aluminum Adjuvant Activity. *Nat. Med.* **2011,** *17* (8), 996-1002.

296.   Bartfai, T.; Behrens, M. M.; Gaidarova, S.; Pemberton, J.; Shivanyuk, A.; Rebek, J., Jr., A low molecular weight mimic of the Toll/IL-1 receptor/resistance domain inhibits IL-1 receptor-mediated responses. *Proc. Natl. Acad. Sci. U.S.A.* **2003,** *100* (13), 7971-7976.